Series in High Energy Physics, Cosmology, and Gravitation

Beyond the Standard Model of Particle Physics

Advanced Theories in Particle Physics

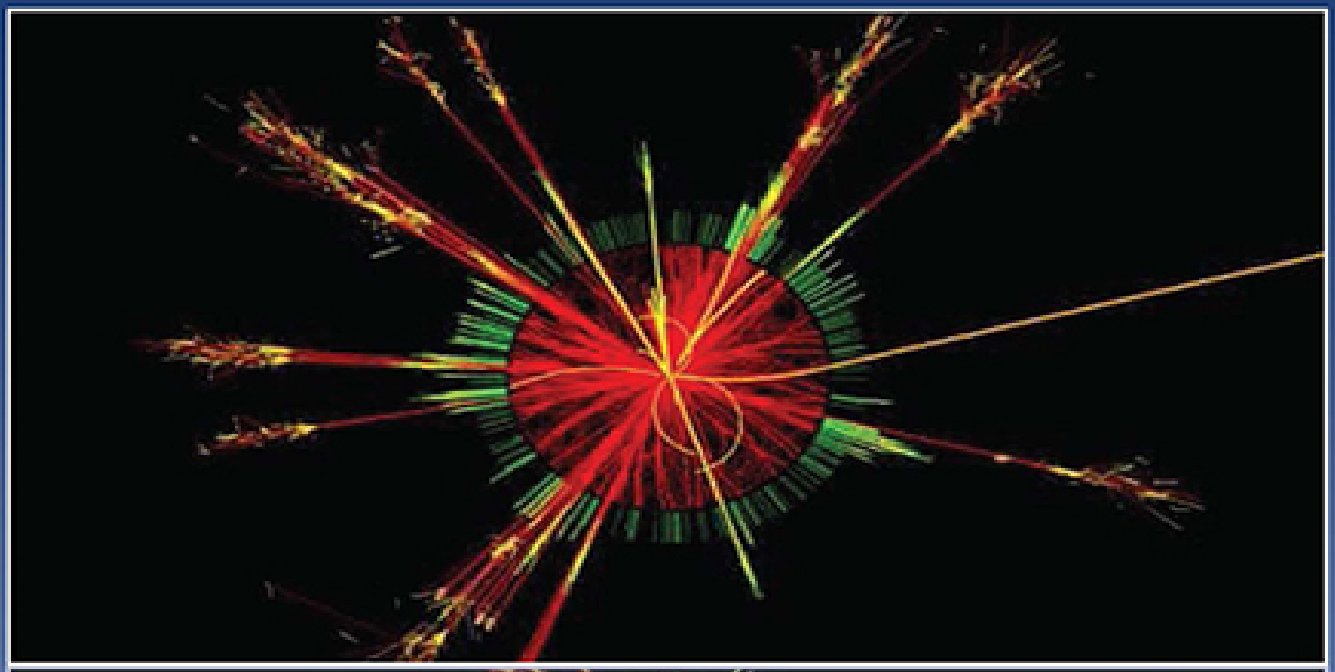

Shaaban Khalil

CRC Press
Taylor & Francis Group

Series in High Energy Physics, Cosmology, and Gravitation

Beyond the Standard Model of Particle Physics

Advanced Theories in Particle Physics

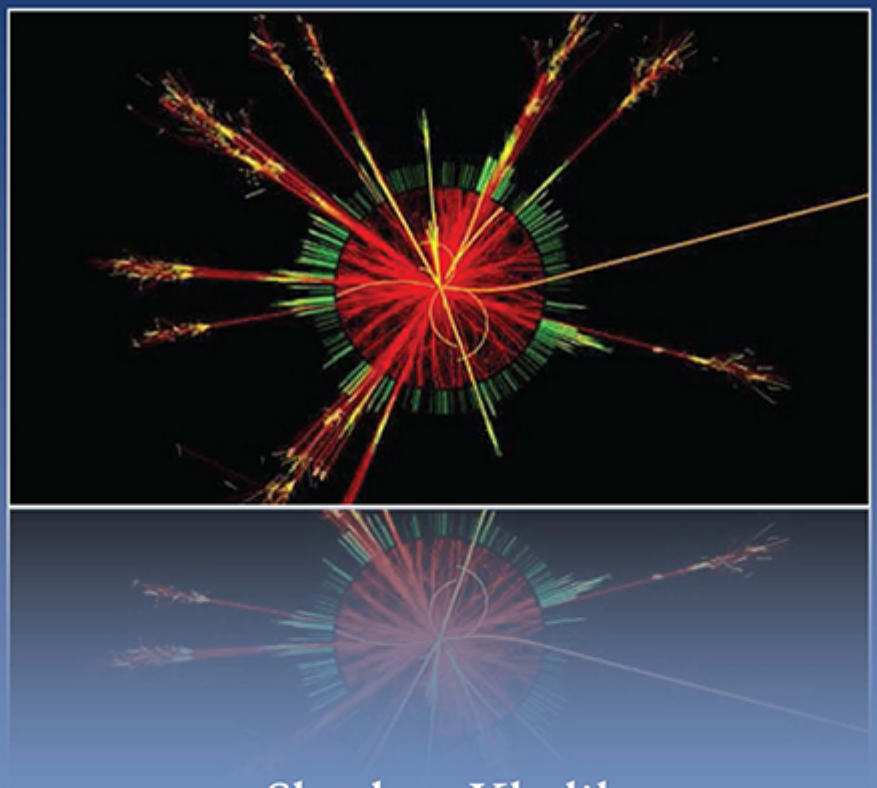

Shaaban Khalil

CRC Press
Taylor & Francis Group

Beyond the Standard Model of Particle Physics

Beyond the Standard Model of Particle Physics provides a comprehensive overview of the current state of research in the field, as well as the theories and models that are being developed to explain the unexplained phenomena in the universe. It also discusses the experiments and observations that are being conducted to test these theories, and the potential implications for our understanding of the universe. The primary advantage of the book is its in-depth examination of theories that go beyond the standard model of particle physics, which has been the dominant framework for understanding particle interactions for several decades. The book assumes a solid understanding of quantum field theory, particle physics, and general relativity before delving into advanced topics in the field. Its extensive coverage includes various topics such as grand unification, supersymmetry, extra dimensions, and others. It also discusses the theoretical and experimental implications of these ideas, providing readers with a comprehensive overview of the current state of the field. Additionally, the book highlights the significance of experimental data in testing new theoretical ideas and refining them based on experimental results. As a result, this resource is invaluable for graduate-level researchers, physicists and students seeking to stay abreast of the most recent developments in the field.

Key Features:

- Provides extensive coverage of theories that transcend the Standard Model of particle physics,
- Connects theoretical concepts with real-world experimental data in a clear and accessible style.
- Written by an expert in the field.

Professor Shaaban Khalil is one of the most prominent High Energy Physicists in the Middle East. He is well known for his outstanding contributions to the understanding of possible new physics beyond the standard model of particle physics. He has been the founding director of the Center for Fundamental Physics at Zewail City of Science and Technology in Egypt, since 2012. Prof. Khalil has published more than 300 scientific papers in renowned scientific journals. His work enabled him to earn a D.Sc. degree in 2006. His research has been widely recognised, and he has received several national and international awards. Prof. Khalil has been a visiting professor at the University of Southampton since 2011. He is the president of the Arab Physical Society and the founding team leader of the Egyptian particle physics group at the CMS experiment at CERN, Geneva, Switzerland.

Series in Particle Physics, Cosmology, and Gravitation

This series of books covers all aspects of theoretical and experimental high energy physics, cosmology and gravitation and the interface between them. In recent years the fields of particle physics and astrophysics have become increasingly interdependent and the aim of this series is to provide a library of books to meet the needs of students and researchers in these fields.

Other recent books in the series:

An Introduction to Beam Physics
Martin Berz, Kyoko Makino, and Weishi Wan

Neutrino Physics, Second Edition
K Zuber

Group Theory for the Standard Model of Particle Physics and Beyond
Ken J Barnes

The Standard Model and Beyond
Paul Langacker

Particle and Astroparticle Physics
Utpal Sakar

Joint Evolution of Black Holes and Galaxies
M Colpi, V Gorini, F Haardt, and U Moschella (Eds)

Gravitation: From the Hubble Length to the Planck Length
I Ciufolini, E Coccia, V Gorini, R Peron, and N Vittorio (Eds)

The Galactic Black Hole: Lectures on General Relativity and Astrophysics
H Falcke, and F Hehl (Eds)

The Mathematical Theory of Cosmic Strings: Cosmic Strings in the Wire Approximation
M R Anderson

Geometry and Physics of Branes

U Bruzzo, V Gorini, and U Moschella (Eds)

Modern Cosmology
S Bonometto, V Gorini, and U Moschella (Eds) Gravitation and Gauge SymmetriesM Blagojevic

Gravitational Waves
I Ciufolini, V Gorini, U Moschella, and P Fré (Eds)

Introduction to Particle Physics and Cosmology
Grant J. Mathews and Guobao Tang

Beyond the Standard Model of Particle Physics
Shaaban Khalil

Beyond the Standard Model of Particle Physics

Advanced Theories in Particle Physics

Shaaban Khalil

CRC Press
Taylor & Francis Group
Boca Raton London New York

CRC Press is an imprint of the
Taylor & Francis Group, an **informa** business

Designed cover image: ATLAS collision event in which a microscopic-black-hole was produced in the collision of two protons. © 2008-2025 CERN

First edition published 2026
by CRC Press
2385 NW Executive Center Drive, Suite 320, Boca Raton FL 33431

and by CRC Press
4 Park Square, Milton Park, Abingdon, Oxon, OX14 4RN

CRC Press is an imprint of Taylor & Francis Group, LLC

ISBN: 978-1-032-59699-0 (hbk)
ISBN: 978-1-032-60137-3 (pbk)
ISBN: 978-1-003-45770-1 (ebk)

DOI: 10.1201/9781003457701

Typeset in Latin Modern font
by KnowledgeWorks Global Ltd.

To my late wife, with love and remembrance

Contents

Preface

The Standard Model (SM) of particle physics stands as one of the most successful scientific theories of the 20th century. It has passed numerous experimental tests with extraordinary precision and has accurately described the electromagnetic, weak, and strong interactions among elementary particles. The discovery of the Higgs boson at the Large Hadron Collider (LHC) in 2012 marked the crowning achievement of the SM, confirming its mechanism of mass generation. Yet, despite these triumphs, the SM leaves many fundamental questions unanswered.

Why do neutrinos have mass? What is the nature of dark matter? How can we resolve the hierarchy problem? What explains the baryon asymmetry of the universe? Is there a deeper symmetry behind the SM gauge structure? These puzzles, and many others, provide strong motivation for the search for physics beyond the SM (BSM).

This book offers a comprehensive introduction to BSM physics, aimed at advanced undergraduate students, graduate students, and researchers with an interest in high-energy theory and phenomenology. The topics covered span a wide range of well-motivated extensions of the SM, including:

- Two Higgs Doublet Models (2HDMs), which provide a richer scalar sector and natural explanations for dark matter and baryogenesis;
- Gauged $U(1)_{B-L}$ models, which accommodate neutrino masses and right-handed neutrinos in a theoretically consistent manner;
- Left-Right Symmetric Models (LRSMs), offering a compelling framework for restoring parity symmetry and generating neutrino masses through seesaw mechanisms;
- Grand Unified Theories (GUTs), such as $SU(5)$, which seek a unified description of the SM forces;
- Supersymmetry (SUSY), a symmetry that links fermions and bosons and addresses the hierarchy problem;

- Theories with extra spatial dimensions, which aim to resolve outstanding theoretical puzzles and may connect particle physics with quantum gravity.

Special emphasis is placed on the phenomenological implications of these models. Chapters examine how BSM physics manifests in collider signatures, flavor observables, neutrino experiments, and cosmological measurements. Particular attention is given to the testability of these models at current and future experiments, including the LHC and proposed next-generation colliders. The interplay between particle physics and cosmology, especially in addressing the nature of dark matter, dark energy, and the matter-antimatter asymmetry, remains a central focus in contemporary particle physics.

The structure of the book reflects a logical progression: from foundational motivations for BSM physics, to detailed presentations of theoretical frameworks, to their testable predictions. Throughout, both theoretical consistency and experimental viability are prioritized.

This book is the result of years of engagement with the open questions at the frontier of fundamental physics. It is intended as both a learning tool and a reference for those aiming to deepen their understanding or contribute to the development of particle physics BSM. Whether used in a classroom setting, during independent study, or as a guide to research, we hope this volume provides readers with both conceptual clarity and inspiration for further exploration of the fundamental laws of nature.

Shaaban Khalil

CHAPTER 1

Introduction to Physics BSM

DOI: 10.1201/9781003457701-1

The Standard Model (SM) of particle physics is a highly successful quantum field theory that describes electromagnetic, weak, and strong interactions among elementary particles. It has provided a remarkably accurate framework for understanding particle dynamics and interactions at accessible energies. This chapter summarizes both the achievements and limitations of the SM, drawing from reference [1].

1.1 SM OVERVIEW AND FEATURES

The SM is based on the gauge symmetry:

$$SU(3)_C \times SU(2)_L \times U(1)_Y,$$

where $SU(3)_C$ corresponds to quantum chromodynamics (QCD), which governs strong interactions, while $SU(2)_L \times U(1)_Y$ describes electroweak interactions.

The model respects gauge invariance and Poincaré symmetry, and it is renormalizable, ensuring well-defined predictions at various energy scales. The matter content of the SM comprises three generations of fermions, each consisting of a left-handed quark doublet and a left-handed lepton doublet transforming under $SU(2)_L$, along with right-handed singlets for the up-type quark, down-type quark, and charged lepton. The gauge sector comprises eight gluons, three weak gauge bosons, and one hypercharge

gauge boson. Electroweak symmetry is spontaneously broken by the Higgs mechanism, which gives masses to the weak bosons and fermions. Table 1.1 summarizes the field content and quantum numbers of the SM.

TABLE 1.1 The SM field content and quantum numbers under the gauge group $SU(3)_C \times SU(2)_L \times U(1)_Y$.

Fields	Components (Spin)	$SU(3)_C$	$SU(2)_L$	$U(1)_Y$
Fermions				
L	$\begin{pmatrix}\nu\\ e\end{pmatrix}_L$ (1/2)	1	2	$-\frac{1}{2}$
E	e_R (1/2)	1	1	-1
Q	$\begin{pmatrix}u\\ d\end{pmatrix}_L$ (1/2)	3	2	$+\frac{1}{6}$
U	u_R (1/2)	3	1	$+\frac{2}{3}$
D	d_R (1/2)	3	1	$-\frac{1}{3}$
Gauge Bosons				
B_μ	B_μ (1)	singlet	singlet	singlet
W_μ	W^+, W^-, W^3 (1)	singlet	triplet	singlet
G_μ	G^a_μ $(a = 1 \dots 8)$ (1)	octet	singlet	singlet
Higgs				
ϕ	$\begin{pmatrix}\phi^+\\ \phi^0\end{pmatrix}$ (0)	1	2	$+\frac{1}{2}$

A key relation in the SM is the Gell-Mann-Nishijima formula, which links the electric charge Q to the third component of the weak isospin T_3 and the hypercharge Y:

$$Q = T_3 + \frac{Y}{2}. \tag{1.1}$$

This equation emerges from electroweak unification, where the symmetry $SU(2)_L \times U(1)_Y$ is spontaneously broken to $U(1)_{\text{EM}}$ via the Higgs

mechanism. The resulting massless photon and massive weak bosons reflect the decomposition of gauge degrees of freedom. The Gell-Mann-Nishijima relation provides a consistent framework for assigning electric charges to all SM particles.

1.1.1 The SM Lagrangian

Having outlined the particle content, gauge symmetries, and charge assignments in the SM, we now present its full Lagrangian formulation. The SM Lagrangian encodes the dynamics and interactions of all fundamental fields, incorporating gauge invariance under the group $SU(3)_C \times SU(2)_L \times U(1)_Y$, spontaneous symmetry breaking via the Higgs mechanism, and the generation of fermion masses through Yukawa interactions [2–7].

The total SM Lagrangian can be written as:

$$\mathscr{L}_{\text{SM}} = \mathscr{L}_{\text{YM}} + \mathscr{L}_{\text{K}} + \mathscr{L}_{\text{Higgs}} + \mathscr{L}_{\text{Y}}, \tag{1.2}$$

where:

- $\mathscr{L}_{\text{YM}}$ describes the gauge fields and their self-interactions.
- $\mathscr{L}_{\text{K}}$ contains the kinetic terms of fermions and their gauge interactions.
- $\mathscr{L}_{\text{Higgs}}$ governs the Higgs field dynamics and potential.
- $\mathscr{L}_{\text{Y}}$ accounts for the Yukawa interactions between fermions and the Higgs field.

Gauge Field Kinetic Terms

The Yang-Mills part of the SM Lagrangian describes the dynamics of the gauge bosons:

$$\mathscr{L}_{\text{YM}} = -\frac{1}{4} G^a_{\mu\nu} G^{\mu\nu a} - \frac{1}{4} W^i_{\mu\nu} W^{\mu\nu i} - \frac{1}{4} B_{\mu\nu} B^{\mu\nu}, \tag{1.3}$$

where the field strength tensors for the $SU(3)_C$, $SU(2)_L$, and $U(1)_Y$ gauge groups are:

$$G^a_{\mu\nu} = \partial_\mu G^a_\nu - \partial_\nu G^a_\mu - g_s f^{abc} G^b_\mu G^c_\nu, \tag{1.4}$$

$$W^i_{\mu\nu} = \partial_\mu W^i_\nu - \partial_\nu W^i_\mu - g\,\epsilon^{ijk} W^j_\mu W^k_\nu, \tag{1.5}$$

$$B_{\mu\nu} = \partial_\mu B_\nu - \partial_\nu B_\mu. \tag{1.6}$$

Here, g_s, g, and g_Y are the gauge couplings for $SU(3)_C$, $SU(2)_L$, and $U(1)_Y$, respectively. The gluons G^a_μ ($a = 1, \ldots, 8$), weak gauge bosons W^i_μ ($i = 1, 2, 3$), and the hypercharge field B_μ correspond to the gauge groups $SU(3)_C$, $SU(2)_L$, and $U(1)_Y$, respectively. The structure constants f^{abc} and ϵ^{ijk} satisfy the commutation relations:

$$[T^\alpha, T^\beta] = i f^{\alpha\beta\gamma} T^\gamma, \qquad [\tau^a, \tau^b] = i\varepsilon^{abc}\tau^c, \tag{1.7}$$

for $SU(3)_C$ and $SU(2)_L$, respectively.

Fermion Kinetic Terms

The kinetic terms for fermions, including their gauge interactions, are given by:

$$\begin{aligned}\mathscr{L}_{\mathrm{K}} = i \sum_{j=1}^{3} \Big(& \overline{L}_j \gamma^\mu D_\mu L_j + \overline{E}_j \gamma^\mu D_\mu E_j + \overline{Q}_j \gamma^\mu D_\mu Q_j \\ & + \overline{U}_j \gamma^\mu D_\mu U_j + \overline{D}_j \gamma^\mu D_\mu D_j \Big),\end{aligned} \tag{1.8}$$

where the covariant derivative is:

$$D_\mu = \partial_\mu - i g_s \Lambda^a G^a_\mu - i g T^i W^i_\mu - i g_Y Y B_\mu. \tag{1.9}$$

This expression depends on the specific gauge representation and hypercharge Y of each fermion, as summarized in Table 1.1. For example:

$$\bar{L}\gamma^\mu D_\mu L \quad = \bar{L}\gamma^\mu \left(\partial_\mu - \frac{ig}{2}\sigma \cdot W_\mu + \frac{ig_Y}{2} B_\mu\right) L,$$

(1.10)

$$\bar{E}\gamma^\mu D_\mu E \quad = \bar{E}\gamma^\mu \left(\partial_\mu + ig_Y B_\mu\right) E,$$

(1.11)

$$\begin{aligned}\bar{Q}^\alpha \gamma^\mu D_\mu Q^\beta \quad &= \bar{Q}^\alpha \gamma^\mu \left[\left(\partial_\mu - \frac{ig}{2}\sigma \cdot W_\mu - \frac{ig_Y}{6} B_\mu\right)\delta_{\alpha\beta} \right. \\ &\left. - \frac{ig_s}{2}\lambda_{\alpha\beta} \cdot G_\mu\right] Q^\beta.\end{aligned}$$

(1.12)

Analogous expressions hold for U and D quarks. Here, σ^i and λ^a are the Pauli and Gell-Mann matrices, and the indices α, β denote color.

Higgs Sector

The Higgs Lagrangian consists of kinetic and potential terms for the scalar doublet field ϕ:

$$\mathscr{L}_{\text{Higgs}} = (D^\mu \phi)^\dagger (D_\mu \phi) - V(\phi),$$

(1.13)

with the covariant derivative:

$$D_\mu \phi = \left(\partial_\mu - \frac{ig}{2}\sigma \cdot W_\mu - \frac{ig_Y}{2} B_\mu\right)\phi.$$

(1.14)

The scalar potential is:

$$V(\phi) = \mu^2 \phi^\dagger \phi + \lambda (\phi^\dagger \phi)^2,$$

(1.15)

where $\lambda > 0$ ensures the potential is bounded from below. Electroweak symmetry breaking occurs when $\mu^2 < 0$, giving rise to the Higgs VEV and generating masses for the weak bosons and fermions [7–9].

Yukawa Interactions

The Yukawa Lagrangian governs the interactions between fermions and the Higgs field, which after electroweak symmetry breaking generate fermion masses:

$$\mathscr{L}_{\mathrm{Y}} = -\sum_{i,j=1}^{3} \left(y^{e}_{ij} \overline{L}_i \phi E_j + y^{u}_{ij} \overline{Q}_i \widetilde{\phi} U_j + y^{d}_{ij} \overline{Q}_i \phi D_j \right) + \mathrm{h.c.}$$

(1.16)

Here, the dual Higgs doublet $\widetilde{\phi}$ is defined as:

$$\widetilde{\phi} \equiv i\sigma^2 \phi^* = \begin{pmatrix} \phi^{0*} \\ -\phi^- \end{pmatrix},$$

(1.17)

and y^e, y^u, y^d are complex 3×3 matrices of Yukawa couplings.

1.1.2 Spontaneous Symmetry Breaking and the Higgs Mechanism

In the SM Lagrangian, all fermions and gauge bosons are initially massless. The Higgs mechanism introduces mass for these particles via spontaneous symmetry breaking. The electroweak symmetry breaking pattern is given by:

$$SU(2)_L \times U(1)_Y \xrightarrow{\langle \phi \rangle} U(1)_{\mathrm{EM}},$$

(1.18)

where $U(1)_{\mathrm{EM}}$ corresponds to the electromagnetic gauge symmetry.

The Higgs field in the SM is a complex scalar doublet under $SU(2)_L$, and is given by:

$$\phi = \begin{pmatrix} \phi^+ \\ \phi^0 \end{pmatrix},$$

(1.19)

with quantum numbers listed in Table 1.1. For $\mu^2 < 0$ in the Higgs potential (1.15), the vacuum is degenerate and spontaneous symmetry breaking occurs, as illustrated in Fig. 1.1. The VEV of the Higgs field satisfies:

$$|\phi|^2 = \frac{v^2}{2}, \quad \text{where} \quad v = \sqrt{\frac{-\mu^2}{\lambda}}.$$

(1.20)

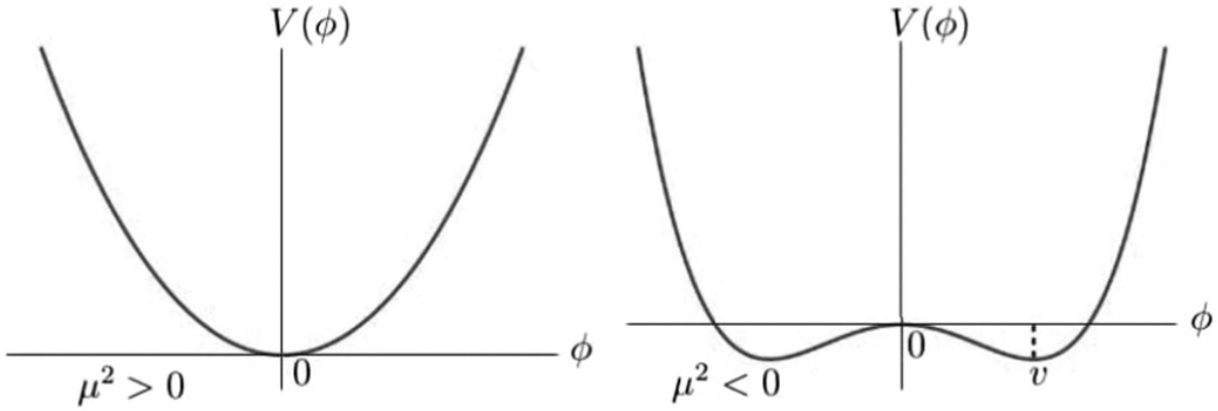

Figure 1.1 The scalar potential $V(\phi)$ for $\mu^2 > 0$ (symmetric phase) and $\mu^2 < 0$ (broken phase), respectively. ⏎

Choosing a specific vacuum, we take:

$$\phi_0 = \begin{pmatrix} 0 \\ \frac{v}{\sqrt{2}} \end{pmatrix}.$$

(1.21)

The action of the electroweak generators on the vacuum state ϕ_0 is:

$$\begin{aligned} \frac{1}{2}\tau^1\phi_0 &= \frac{1}{2}\begin{pmatrix} v/\sqrt{2} \\ 0 \end{pmatrix}, \quad \frac{1}{2}\tau^2\phi_0 = \frac{1}{2}\begin{pmatrix} -iv/\sqrt{2} \\ 0 \end{pmatrix}, \\ \frac{1}{2}\tau^3\phi_0 &= -\frac{1}{2}\phi_0, \quad Y\phi_0 = \phi_0. \end{aligned}$$

(1.22)

Thus, the vacuum is not invariant under $SU(2)_L \times U(1)_Y$, indicating that these symmetries are spontaneously broken. However, the electromagnetic gauge symmetry remains unbroken since:

$$Q\phi_0 = \left(\frac{1}{2}\tau^3 + \frac{1}{2}Y\right)\phi_0 = 0.$$

(1.23)

The Higgs field contains four real degrees of freedom, three of which become the longitudinal components of the $W^{\pm}$ and Z bosons via the Higgs mechanism. These can be parameterized as:

$$\phi(x) = \frac{1}{\sqrt{2}}\, e^{-i\tau^i \eta^i(x)/2v} \begin{pmatrix} 0 \\ v + h(x) \end{pmatrix},$$

(1.24)

where $\eta^i(x)$ (with $i = 1, 2, 3$) are Goldstone bosons and $h(x)$ is the physical Higgs field. In the unitary gauge, where $\phi \to U(\eta)\phi$, the Higgs field simplifies to:

$$\phi(x) = \frac{1}{\sqrt{2}} \begin{pmatrix} 0 \\ v + h(x) \end{pmatrix}.$$

(1.25)

1.1.3 Particle Mass Generation in the SM

Gauge Boson Masses

To derive gauge boson masses, consider the kinetic term of the Higgs doublet:

$$\mathscr{L}_{\text{kin}} = (D_\mu \phi)^\dagger (D^\mu \phi),$$

(1.26)

where the covariant derivative is:

$$D_\mu = \partial_\mu - ig\frac{\tau^a}{2} W_\mu^a - ig'\frac{Y}{2} B_\mu.$$

(1.27)

Substituting $\phi \to \phi_0$, the mass terms for gauge bosons become:

$$\mathscr{L}_{\text{mass}} \supset M_W^2 W_\mu^+ W^{-\mu} + \frac{M_Z^2}{2} Z_\mu Z^\mu,$$

(1.28)

with the physical eigenstates:

$$W_\mu^\pm = \frac{1}{\sqrt{2}}(W_\mu^1 \mp i W_\mu^2), \tag{1.29}$$

$$Z_\mu = \cos\theta_W W_\mu^3 - \sin\theta_W B_\mu, \tag{1.30}$$

$$A_\mu = \sin\theta_W W_\mu^3 + \cos\theta_W B_\mu. \tag{1.31}$$

The corresponding masses are:

$$M_W = \frac{1}{2} g v, \tag{1.32}$$

$$M_Z = \frac{1}{2} v \sqrt{g^2 + g'^2}, \tag{1.33}$$

$$M_A = 0. \tag{1.34}$$

The Weinberg angle θ_W is defined via:

$$\sin\theta_W = \frac{g'}{\sqrt{g^2 + g'^2}}, \tag{1.35}$$

$$\cos\theta_W = \frac{g}{\sqrt{g^2 + g'^2}}. \tag{1.36}$$

Fermion Masses

In the unitary gauge, the Yukawa Lagrangian (1.16) becomes:

$$\mathscr{L}_Y = -\frac{v + h(x)}{\sqrt{2}} \left(y^e_{ij} \overline{e_{Li}} e_{Rj} + y^u_{ij} \overline{u_{Li}} u_{Rj} + y^d_{ij} \overline{d_{Li}} d_{Rj} \right) + \text{h.c.}$$

(1.37)

The corresponding fermion masses are:

$$m_e = \frac{y_e v}{\sqrt{2}}, \quad m_u = \frac{y_u v}{\sqrt{2}}, \quad m_d = \frac{y_d v}{\sqrt{2}}.$$

(1.38)

For three families, the Yukawa matrices y_f (with $f = e, u, d$) are 3×3 complex matrices. These can be diagonalized via unitary transformations:

$$f_L \to V_f f_L, \quad f_R \to U_f f_R, \quad \nu_L \to V_e \nu_L,$$

(1.39)

such that:

$$y_f^{\text{diag}} = V_f^\dagger y_f U_f.$$

(1.40)

The physical masses are then:

$$m_{f_i} = y_{f_i}^{\text{diag}} \frac{v}{\sqrt{2}}.$$

(1.41)

Higgs Mass

The Higgs potential after spontaneous symmetry breaking becomes:

$$V(\phi^\dagger \phi) \quad = -\frac{\mu^2}{2}(v+h)^2 + \frac{\lambda}{4}(v+h)^4$$

(1.42)

$$= \frac{1}{2}(2\lambda v^2)h^2 + \lambda v h^3 + \frac{\lambda}{4}h^4 - \frac{\mu^2 v^2}{4}.$$

(1.43)

From the quadratic term, the Higgs boson mass is:

$$M_h = \sqrt{2\lambda v^2}.$$

(1.44)

The Higgs mass and the self-coupling λ are not predicted within the SM and must be determined experimentally.

1.1.4 SM Interactions

This section provides a systematic overview of the SM interaction structure, beginning with the electroweak and Higgs sectors, and highlighting their implications for fermion masses, gauge boson couplings, and flavor physics.

Electroweak Interactions

The electroweak interactions of leptons and quarks in the SM are derived from the fermionic kinetic terms in the Lagrangian:

$$\begin{aligned}\mathscr{L}_{\mathrm{K}} &= i\sum_{j=1}^{3}\Big(\overline{L}_j\gamma^\mu D_\mu L_j + \overline{E}_j\gamma^\mu D_\mu E_j + \overline{Q}_j\gamma^\mu D_\mu Q_j \\ &\quad + \overline{U}_j\gamma^\mu D_\mu U_j + \overline{D}_j\gamma^\mu D_\mu D_j\Big),\end{aligned}$$

(1.45)

where the covariant derivative D_μ encodes the electroweak gauge fields. The interactions of fermions with the gauge bosons are extracted from the covariant derivatives:

$$\begin{aligned}\overline{\psi} i\gamma^\mu D_\mu \psi &\supset \overline{\psi}\gamma^\mu\Big(\frac{g}{\sqrt{2}}(W_\mu^+ T^+ + W_\mu^- T^-)P_L + eQA_\mu \\ &\quad + \frac{g}{\cos\theta_W}(T^3 P_L - \sin^2\theta_W Q)Z_\mu\Big)\psi,\end{aligned}$$

(1.46)

where $P_L = \frac{1}{2}(1-\gamma_5)$, $T^\pm = T_1 \pm iT_2$, and $e = g\sin\theta_W = g_Y\cos\theta_W$.

The full electroweak interaction Lagrangian can be written in a compact form:

$$\mathscr{L}_{\mathrm{EW}} = \mathscr{L}_{\mathrm{EM}} + \mathscr{L}_{\mathrm{NC}} + \mathscr{L}_{\mathrm{CC}},$$

(1.47)

where

$$\mathscr{L}_{\text{EM}} = eA_\mu J^\mu_A,$$

(1.48)

$$\mathscr{L}_{\text{NC}} = \frac{g}{\cos\theta_W} Z_\mu J^\mu_Z,$$

(1.49)

$$\mathscr{L}_{\text{CC}} = \frac{g}{\sqrt{2}}\left(W^+_\mu J^\mu_W + W^-_\mu J^{\mu\dagger}_W\right).$$

(1.50)

With the currents:

$$J^\mu_A = \bar{\psi}\gamma^\mu Q\psi,$$

(1.51)

$$J^\mu_Z = \bar{\psi}\gamma^\mu(T^3 P_L - \sin^2\theta_W Q)\psi,$$

(1.52)

$$J^\mu_W = \bar{\psi}\gamma^\mu T^+ P_L\psi, \quad J^{\mu\dagger}_W = \bar{\psi}\gamma^\mu T^- P_L\psi.$$

(1.53)

Electromagnetic Interactions

Electromagnetic interactions, mediated by the photon, couple only to electrically charged fermions:

$$\mathscr{L}_{\text{EM}} = eA_\mu J^\mu_A,$$

(1.54)

with the current:

$$J^\mu_A = \sum_i Q^i \bar{f}_i\gamma^\mu f_i = -\bar{e}\gamma^\mu e + \frac{2}{3}\bar{u}\gamma^\mu u - \frac{1}{3}\bar{d}\gamma^\mu d.$$

(1.55)

Neutral Current Interactions

Neutral weak interactions are mediated by the Z-boson:

$$\mathscr{L}_{\rm NC} = \frac{g}{\cos\theta_W} Z_\mu J^\mu_Z,$$

(1.56)

with current:

$$\begin{aligned} J^\mu_Z &= \sum_i \bar{f}_i \gamma^\mu (T^3_i P_L - Q^i \sin^2\theta_W) f_i \\ &= \frac{1}{2}\bar{\nu}_e \gamma^\mu P_L \nu_e + \bar{e}\gamma^\mu(-\frac{1}{2}P_L + \sin^2\theta_W)e \\ &\quad + \bar{u}\gamma^\mu\left(\frac{1}{2}P_L - \frac{2}{3}\sin^2\theta_W\right)u + \bar{d}\gamma^\mu\left(-\frac{1}{2}P_L + \frac{1}{3}\sin^2\theta_W\right)d. \end{aligned}$$

(1.57)

Charged Current Interactions

Charged weak interactions are mediated by the $W^\pm$ bosons:

$$\mathscr{L}_{\rm CC} = \frac{g}{\sqrt{2}}\left(W^+_\mu J^\mu_W + W^-_\mu J^{\mu\dagger}_W\right),$$

(1.58)

with:

$$J^\mu_W = \sum_{i,j} (\bar{\nu}_{Li}\gamma^\mu e_{Lj}\delta_{ij} + \bar{u}_{Li}\gamma^\mu d_{Lj} V_{ij}),$$

(1.59)

$$J^{\mu\dagger}_W = \sum_{i,j}\left(\bar{e}_{Lj}\gamma^\mu \nu_{Li}\delta_{ij} + \bar{d}_{Lj}\gamma^\mu u_{Li} V^\dagger_{ij}\right),$$

(1.60)

where $V \equiv V_{\rm CKM} = V^{u\dagger}V^d$ is the Cabibbo-Kobayashi-Maskawa (CKM) matrix [10, 11].

The CKM matrix parameterizes quark generation mixing:

$$V_{\rm CKM} = \begin{pmatrix} c_{12}c_{13} & s_{12}c_{13} & s_{13}e^{-i\delta} \\ -s_{12}c_{23} - c_{12}s_{23}s_{13}e^{i\delta} & c_{12}c_{23} - s_{12}s_{23}s_{13}e^{i\delta} & s_{23}c_{13} \\ s_{12}s_{23} - c_{12}c_{23}s_{13}e^{i\delta} & -c_{12}s_{23} - s_{12}c_{23}s_{13}e^{i\delta} & c_{23}c_{13} \end{pmatrix},$$

(1.61)

with $s_{ij} = \sin\theta_{ij}$, $c_{ij} = \cos\theta_{ij}$. Experimental values are [12]:

$$\sin\theta_{12} = 0.2229 \pm 0.0022, \tag{1.62}$$

$$\sin\theta_{23} = 0.0412 \pm 0.0002, \tag{1.63}$$

$$\sin\theta_{13} = 0.0036 \pm 0.0007, \tag{1.64}$$

$$\delta = 1.02 \pm 0.22. \tag{1.65}$$

In the SM, neutrinos are massless and right-handed neutrinos are absent. Thus, the lepton mixing matrix can be chosen trivial: $V^{\nu} = V^{e}$, leading to no observable lepton flavor mixing in the charged current sector.

Higgs Interactions in the SM

The kinetic Lagrangian (1.13) of the Higgs field contains the following interaction terms of Higgs field and gauge bosons

$$\mathscr{L}^{\mathrm{K}}_{\mathrm{Higgs}} \supset W^{+}_{\mu}W^{-\mu}(\frac{g^2}{4}h^2 + gM_W h) + Z_{\mu}Z^{\mu}(\frac{g^2}{8\cos^2\theta_{_W}}h^2 + \frac{gM_Z}{2\cos\theta_{_W}}h) \tag{1.66}$$

In the unitary gauge, the Yukawa Lagrangian Eq. (1.37) contains the following interaction terms of the Higgs field with fermions

$$-\mathscr{L}_Y \supset \frac{h}{v}\sum_f m_f\bar{f}f = \frac{h}{v}(m_e\bar{e}e + m_u\bar{u}u + m_d\bar{d}d) \tag{1.67}$$

As the neutrino is massless, it doesn't interact with the Higgs field. The primary Higgs interaction channels in the SM are illustrated in Figs. 1.2 and 1.3.

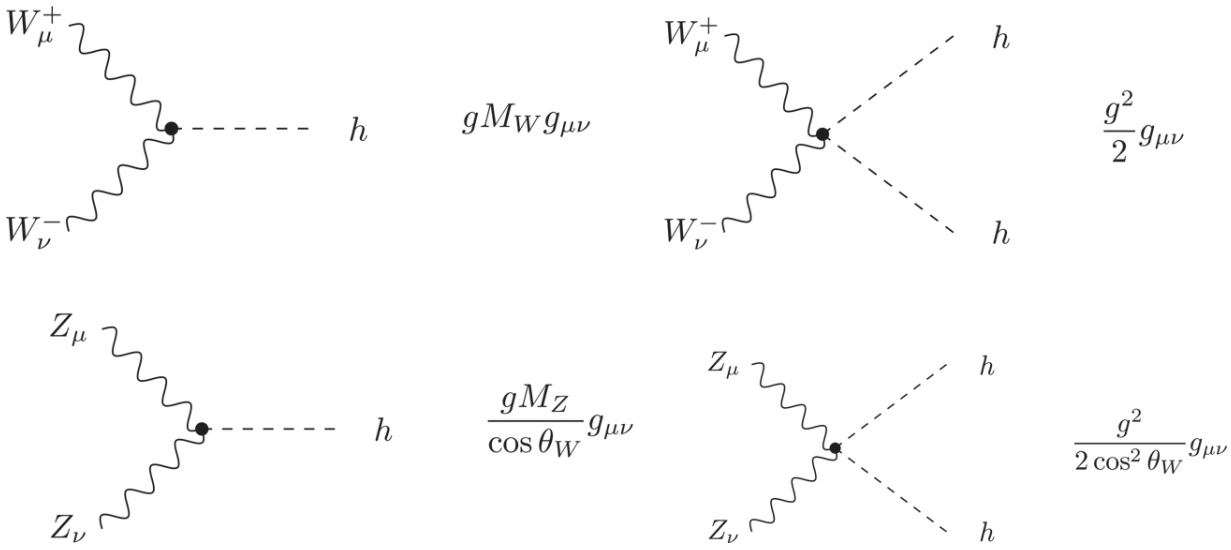

▶ Long Description for Figure 1.2

Figure 1.2 Feynman diagrams and rules of Higgs-gauge interactions in the SM.

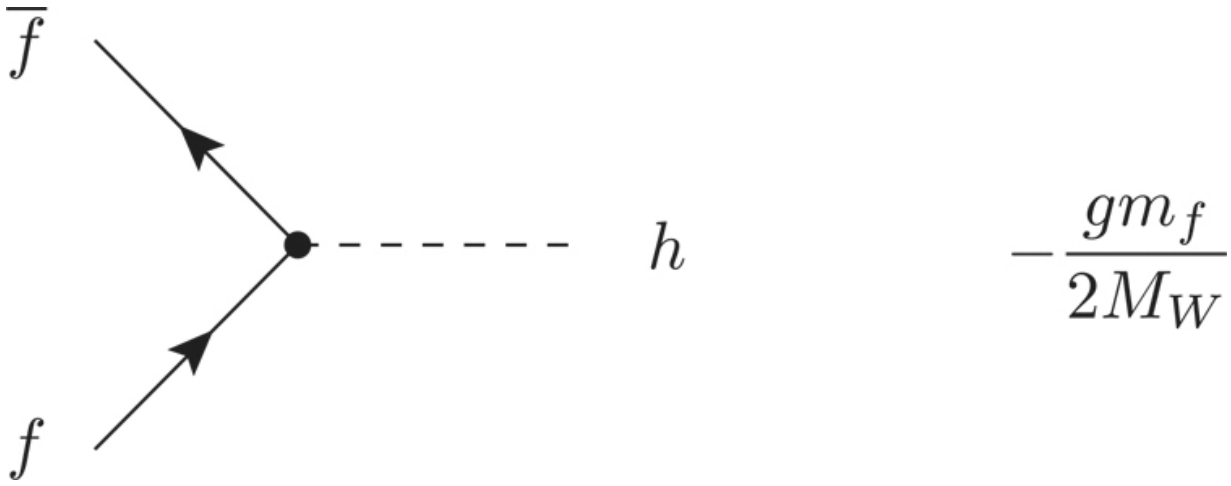

Figure 1.3 Feynman diagram and rule of Higgs-fermion interactions in the SM.

1.2 EVIDENCE FOR PHYSICS BSM

The SM is a four-dimensional quantum field theory invariant under the Poincaré group and based on the local gauge symmetry

$$SU(3)_C \times SU(2)_L \times U(1)_Y.$$

It contains three generations of point-like fermions (quarks and leptons), gauge bosons mediating the fundamental forces, and a single complex scalar Higgs doublet responsible for electroweak symmetry breaking via the Brout-Englert-Higgs mechanism [7, 8].

In its minimal form, the SM does not include right-handed neutrinos, implying that neutrinos are massless. This is in clear contradiction with the experimental observation of neutrino oscillations, which imply nonzero neutrino masses and lepton flavor violation [13, 14].

Despite its tremendous success in describing particle physics phenomena up to the electroweak scale [12], there are several theoretical and experimental indications that the SM is incomplete:

- Neutrino masses: The SM cannot accommodate nonzero neutrino masses without extension.
- Dark matter: Astrophysical and cosmological observations require a stable, non-baryonic component of matter not accounted for in the SM.
- Baryon asymmetry: The observed imbalance between matter and antimatter in the universe cannot be explained by SM CP violation alone.
- Hierarchy problem: The quadratic sensitivity of the Higgs mass to ultraviolet scales suggests the need for a naturalness mechanism.
- Gauge coupling unification: The running of gauge couplings in the SM does not result in unification at a high energy scale.

In addition to these conceptual issues, several experimental anomalies provide further hints of new physics:

- Muon anomalous magnetic moment: The long-standing discrepancy between the measured value of the muon $g-2$ and the SM prediction persists at the level of about 4.2σ [15, 16].
- Flavor anomalies in B-meson decays: Deviations from lepton flavor universality in rare B decays, such as R_D and R_{D^*}, have been observed and interpreted as potential signs of new heavy gauge bosons or leptoquarks [17, 18].

In the following chapters, we will explore well-motivated extensions of the SM that aim to resolve these open questions and anomalies. These

efforts represent the forefront of modern particle physics and may provide critical insights into a more fundamental underlying theory.

1.2.1 Neutrino Masses

One of the most compelling indications for physics beyond the SM is the observation of nonzero neutrino masses. In the SM, fermion masses arise through Yukawa couplings to the Higgs field, but neutrinos were originally assumed to be massless due to the absence of right-handed (RH) neutrino fields. Consequently, the SM predicts lepton flavor conservation and no neutrino mixing.

However, neutrino oscillation experiments have conclusively demonstrated that neutrinos undergo flavor transitions, which can only occur if neutrinos have non-degenerate masses and nontrivial mixing angles. These results were first established by the Super-Kamiokande experiment [13] and later confirmed by multiple independent experiments.

A minimal extension to the SM that accommodates neutrino masses is to introduce RH neutrinos ν_{R_i}, which are gauge singlets. This permits a renormalizable Yukawa interaction:

$$\mathscr{L}_\nu = y_\nu \, \overline{\ell_L} \, \phi \, \nu_R + \text{h.c.}, \tag{1.68}$$

where ℓ_L is the left-handed lepton doublet, ϕ is the Higgs doublet, and y_ν is the neutrino Yukawa coupling. After electroweak symmetry breaking, this yields a Dirac mass term $m_\nu = y_\nu v$, with $v \approx 246\,\text{GeV}$.

To reproduce the sub-eV neutrino masses inferred from oscillation data, one must assume a tiny Yukawa coupling, $y_\nu \sim 10^{-12}$, which is many orders of magnitude smaller than that of the electron. This severe hierarchy is widely regarded as unnatural and has motivated alternative explanations such as the seesaw mechanism [19, 20], which naturally generates small Majorana neutrino masses through the exchange of heavy singlet fermions.

Type I Seesaw Mechanism

The Type I seesaw mechanism provides a compelling explanation for the smallness of neutrino masses within a minimal extension of the SM. It introduces heavy RH neutrinos, denoted by ν_R, which are gauge singlets and therefore do not interact via the SM gauge bosons. However, they do

participate in Yukawa interactions with the SM lepton doublets and the Higgs field [19, 20].

The extended Lagrangian includes the terms:

$$\mathscr{L} \supset -y_\nu \, \overline{\ell_L} \tilde{\phi} \nu_R - \frac{1}{2} \overline{(\nu_R)^c} M_R \nu_R + \text{h.c.},$$

(1.69)

where y_ν is the neutrino Yukawa coupling matrix, $\tilde{\phi} = i\sigma_2 \phi^*$ is the conjugate Higgs doublet, and M_R is a Majorana mass matrix for the RH neutrinos, which can be taken diagonal, real, and positive without loss of generality.

Since M_R is not constrained by SM symmetries, it can naturally lie at a very high scale. Integrating out the heavy RH neutrinos at energies below M_R generates the dimension-five Weinberg operator, yielding an effective Lagrangian:

$$\mathscr{L}^{\nu}_{\text{eff}} = \frac{y_\nu^2}{2M_R} \, \overline{\ell_L} \, \phi \, \phi^T \ell_L^c + \text{h.c.}$$

(1.70)

This results in a Majorana mass for the light neutrinos after electroweak symmetry breaking:

$$m_\nu \simeq -\langle \phi^0 \rangle^2 \, y_\nu \, M_R^{-1} \, y_\nu^T,$$

(1.71)

naturally explaining their smallness for $M_R \gg \langle \phi^0 \rangle$. This mechanism is illustrated in Fig. 1.4.

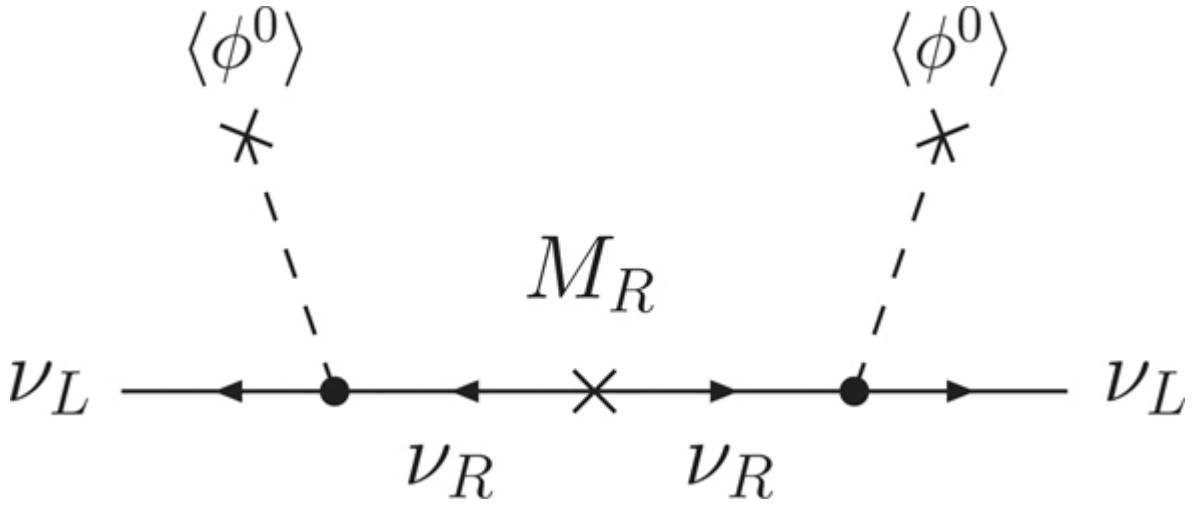

Figure 1.4 Type I seesaw realization of the small Majorana mass for the left-handed neutrino with $m_\nu \simeq -\langle\phi^0\rangle^2\, y_\nu\, M_R^{-1}\, y_\nu^T$. ⏎

After spontaneous symmetry breaking, the neutrino mass terms can be written as:

$$\mathscr{L}_m^\nu = -\overline{\nu_L} m_D \nu_R - \frac{1}{2}\overline{(\nu_R)^c} M_R \nu_R + \text{h.c.},$$

(1.72)

where $m_D = y_\nu \langle\phi^0\rangle$ is the Dirac mass matrix. Combining terms, the full mass matrix becomes:

$$-\mathscr{L}_m^\nu = \begin{pmatrix}\overline{\nu}_L & \overline{(\nu_R)^c}\end{pmatrix} \underbrace{\begin{pmatrix} 0 & m_D \\ m_D^T & M_R \end{pmatrix}}_{M_\nu} \begin{pmatrix}(\nu_L)^c \\ \nu_R\end{pmatrix} + \text{h.c.}$$

(1.73)

Assuming $m_D \ll M_R$, this matrix can be block-diagonalized via a unitary transformation:

$$M_\nu^{\text{diag}} \simeq \begin{pmatrix} -m_D M_R^{-1} m_D^T & 0 \\ 0 & M_R \end{pmatrix},$$

(1.74)

$$V \simeq \begin{pmatrix} -1 & m_D M_R^{-1} \\ m_D^T M_R^{-1} & 1 \end{pmatrix} \begin{pmatrix} i & 0 \\ 0 & -i \end{pmatrix}.$$

(1.75)

Thus, the light neutrino masses are suppressed by the large Majorana scale M_R, while the heavy states acquire masses of order M_R. This framework provides a natural mechanism for understanding the observed neutrino mass hierarchy and is a cornerstone of many Grand Unified Theories (GUTs) and leptogenesis scenarios.

Type II Seesaw Mechanism

In addition to the Type I seesaw mechanism, several extensions of the SM have been proposed to generate small Majorana neutrino masses. One such extension is the *Type II seesaw mechanism* [21, 22]. In this scenario, the SM Higgs sector is augmented by a heavy scalar triplet Δ, which carries hypercharge $Y = -2$ and transforms as a $(1, 3, -2)$ under the SM gauge group.

The triplet scalar field can be conveniently represented by a 2×2 matrix:

$$\Delta = \begin{pmatrix} \Delta^- / \sqrt{2} & \Delta^{--} \\ \Delta^0 & -\Delta^- / \sqrt{2} \end{pmatrix}.$$

(1.76)

In this case, the relevant terms in the Lagrangian are given by:

$$-\mathscr{L}_{\text{type-II}} = \frac{Y_\Delta}{2}\, \overline{\ell_L} i\tau_2\, \Delta\, \ell_L^c + \mu_\Delta\, \phi^T i\tau_2 \Delta\, \phi + M_\Delta^2\, \mathrm{Tr}(\Delta^\dagger \Delta) + \text{h.c.},$$

(1.77)

where Y_Δ is the Yukawa coupling matrix, μ_Δ is a trilinear scalar coupling with mass dimension one, and M_Δ is the mass of the scalar triplet.

After electroweak symmetry breaking, the neutral component of the Higgs doublet acquires a non-vanishing VEV, inducing a small VEV for the neutral component of Δ through the μ_Δ term. This leads to the effective Majorana mass for light neutrinos:

$$m_{\text{eff}}^{II} \simeq \mu_\Delta\, Y_\Delta \frac{\langle \phi^0 \rangle^2}{M_\Delta^2} = \lambda_\Delta\, Y_\Delta \frac{\langle \phi^0 \rangle^2}{M_\Delta},$$

(1.78)

where $\mu_\Delta \equiv \lambda_\Delta M_\Delta$ defines a dimensionless coupling λ_Δ. This expression mirrors the general seesaw formula, where $M_\Delta \gg \langle \phi^0 \rangle$ ensures the smallness of neutrino masses. A diagram representing this process appears in the left panel of Fig. 1.5. This elegant mechanism is referred to as the Type II seesaw.

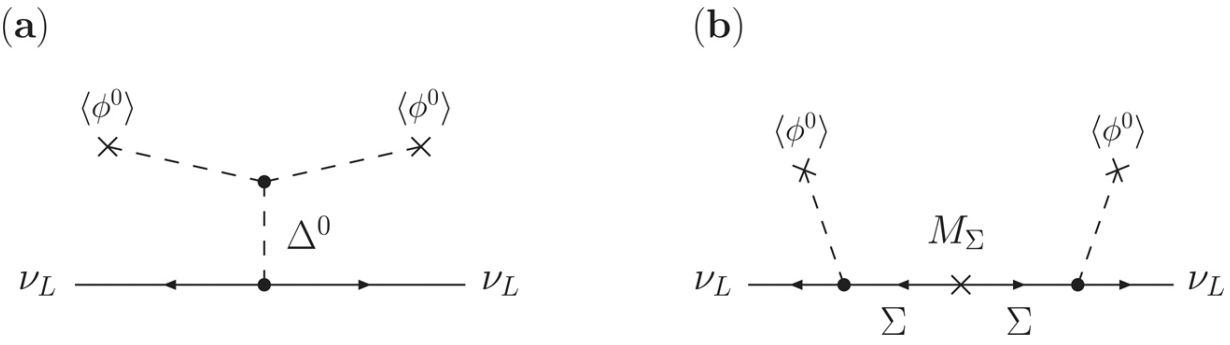

Figure 1.5 (Left) Neutrino mass generation via the Type II seesaw mechanism involving a scalar triplet Δ. (Right) Type III seesaw mechanism mediated by a heavy fermionic triplet Σ. ⏎

Type III Seesaw Mechanism

Another compelling approach to generate neutrino masses is the *Type III seesaw mechanism* [23]. Here, the SM is extended by introducing fermionic triplets Σ with zero hypercharge ($Y = 0$), which couple to the SM lepton and Higgs doublets via Yukawa interactions. In contrast to Type II seesaw, this scenario does not alter the scalar sector.

The $SU(2)_L$ triplet fermion field is self-conjugate and can be written in matrix form as:

$$\Sigma = \begin{pmatrix} \Sigma^0/\sqrt{2} & \Sigma^+ \\ \Sigma^- & -\Sigma^0/\sqrt{2} \end{pmatrix}. \tag{1.79}$$

The relevant Lagrangian terms are:

$$-\mathscr{L}_{\text{type-III}} = Y_\Sigma \, \overline{\ell_L} \, \Sigma \, \tilde{\phi} + \frac{1}{2} M_\Sigma \, \mathrm{Tr}\left(\overline{\Sigma^c} \, \Sigma\right) + \text{h.c.}, \tag{1.80}$$

where Y_Σ is the Yukawa matrix and M_Σ is the mass of the fermion triplet. After electroweak symmetry breaking, integrating out the heavy Σ fields gives an effective neutrino mass matrix:

$$m_{\text{eff}}^{III} \simeq Y_\Sigma \frac{\langle \phi^0 \rangle^2}{M_\Sigma} Y_\Sigma^T.$$

(1.81)

This shows that, much like in the other seesaw variants, light Majorana neutrino masses naturally emerge when $M_\Sigma \gg \langle \phi^0 \rangle$. The process is depicted in the right panel of Fig. 1.5. The Type III mechanism is phenomenologically attractive due to the potential collider signatures of the charged fermion components of Σ.

Linear and Inverse Seesaw Mechanisms

In the standard type I seesaw mechanism, the smallness of neutrino masses is attributed to the exchange of heavy right-handed neutrinos with large Majorana masses $M_R \gg v$, where v is the electroweak VEV. However, this high scale is far beyond experimental reach. Alternative low-scale mechanisms such as the inverse seesaw [24, 25] and linear seesaw [26] offer phenomenologically accessible frameworks where lepton number is only softly broken, allowing $M_R \sim \mathcal{O}(\text{TeV})$.

Both mechanisms introduce two Standard Model (SM) singlet fermions: the conventional right-handed neutrino ν_R and an additional singlet S. These frameworks differ in the nature of lepton number violation and in how small neutrino masses are generated.

Inverse Seesaw

The inverse seesaw extends the neutrino sector by adding a small Majorana mass term μ_S for the singlet fermion S, leading to the Lagrangian:

$$\mathcal{L}_{\text{ISS}}^{\nu} = y_\nu \overline{\ell_L} \tilde{\phi} \nu_R + M_R \overline{(\nu_R)^c} S + \mu_S \overline{S^c} S + \text{h.c.},$$

(1.82)

where y_ν is the neutrino Yukawa coupling, and $\mu_S \ll M_R$ softly breaks lepton number. After electroweak symmetry breaking, with $m_D = y_\nu v$, the light neutrino mass is approximately:

$$m_{\nu_\ell} \approx \frac{m_D^2}{M_R^2}\mu_S.$$

(1.83)

This allows $y_\nu \sim \mathcal{O}(1)$ and $M_R \sim$ TeV, provided $\mu_S \sim \mathcal{O}(10^{-7})$ GeV.

Linear Seesaw

In the linear seesaw, lepton number is broken via a small Dirac-type Yukawa coupling y_S between the SM lepton doublet and the new singlet S, and the Majorana mass term μ_S is absent:

$$\mathscr{L}^{\nu}_{\text{LSS}} = y_\nu \overline{\ell_L}\tilde{\phi}\nu_R + M_R\overline{(\nu_R)^c}S + y_S\overline{\ell_L}\tilde{\phi}S + \text{h.c.},$$

(1.84)

with $y_S \ll 1$. The resulting light neutrino mass is:

$$m_{\nu_\ell} \approx \frac{y_\nu y_S v^2}{M_R},$$

(1.85)

which is linearly suppressed by the small lepton-number-violating parameter y_S. This again allows for a low seesaw scale, potentially within reach of current collider experiments.

Both mechanisms naturally explain the smallness of neutrino masses without invoking ultra-high energy scales and open the door for rich phenomenology at the TeV scale.

1.2.2 Dark Matter

A wide consensus among astronomers, cosmologists, and particle physicists holds that approximately 95% of the matter in the Universe is composed of an invisible, non-luminous component known as Dark Matter (DM) and Dark Energy (DE). The evidence for DM, in particular, emerges from a range of astrophysical observations. One of the earliest and most compelling lines of evidence comes from the rotational dynamics of galaxies. According to Newtonian mechanics, the rotational velocity of stars in a galaxy should follow:

$$v(r) = \sqrt{\frac{GM(r)}{r}},$$

(1.86)

where $v(r)$ is the velocity at radius *r, G* is the gravitational constant, and $M(r)$ is the enclosed mass. However, observations of numerous spiral galaxies reveal that their rotation curves remain flat or even rise with increasing distance from the galactic center, as shown in Fig. 1.6, indicating the presence of additional, unseen mass [27, 28].

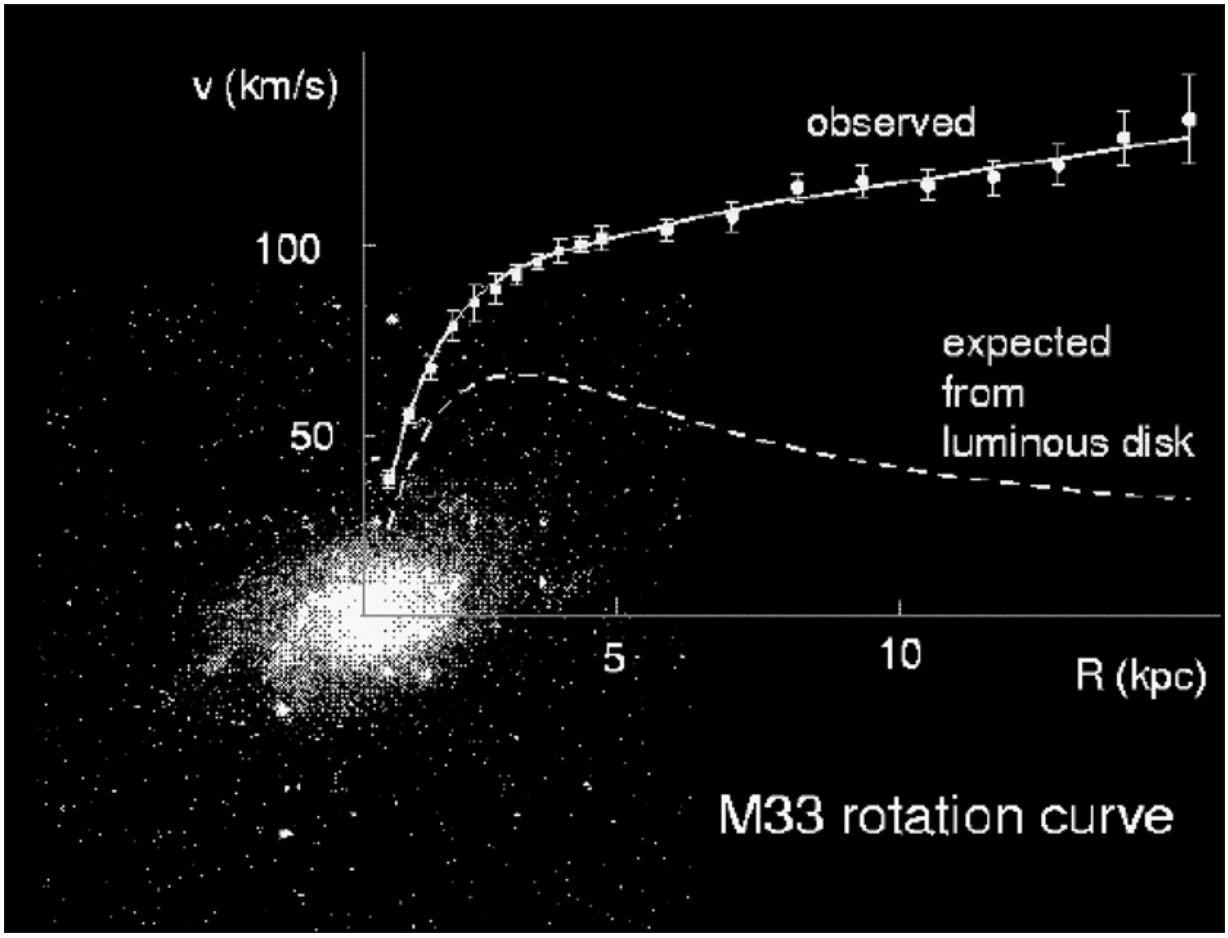

Figure 1.6 The observed rotation curve of the dwarf spiral galaxy M33 overlaid on its optical image [28]. ⏎

Another powerful probe of DM is gravitational lensing, where the deflection of light from distant galaxies by massive foreground objects reveals much more mass than is visible. These lensing measurements

confirm that the gravitational mass far exceeds the luminous matter content [29, 30].

These findings suggest that galaxies reside within massive DM halos, extending far beyond their visible components. Moreover, precise measurements of the cosmic microwave background (CMB), particularly from the Planck satellite, provide strong evidence for the abundance and non-baryonic nature of DM. The 2018 Planck results indicate [31]:

$$\Omega_{\mathrm{m}}h^2 = 0.1430 \pm 0.0011, \quad \Omega_{\mathrm{b}}h^2 = 0.02237 \pm 0.00015, \tag{1.87}$$

where the significant difference between Ω_{m} and Ω_{b} implies that most matter is not composed of baryons. This is consistent with Big Bang nucleosynthesis predictions [32].

As shown in Fig. 1.7, the Universe consists of approximately 4.9% ordinary (baryonic) matter, 26.6% DM, and 68.5% dark energy. Despite the compelling evidence, the particle nature of DM remains unknown.

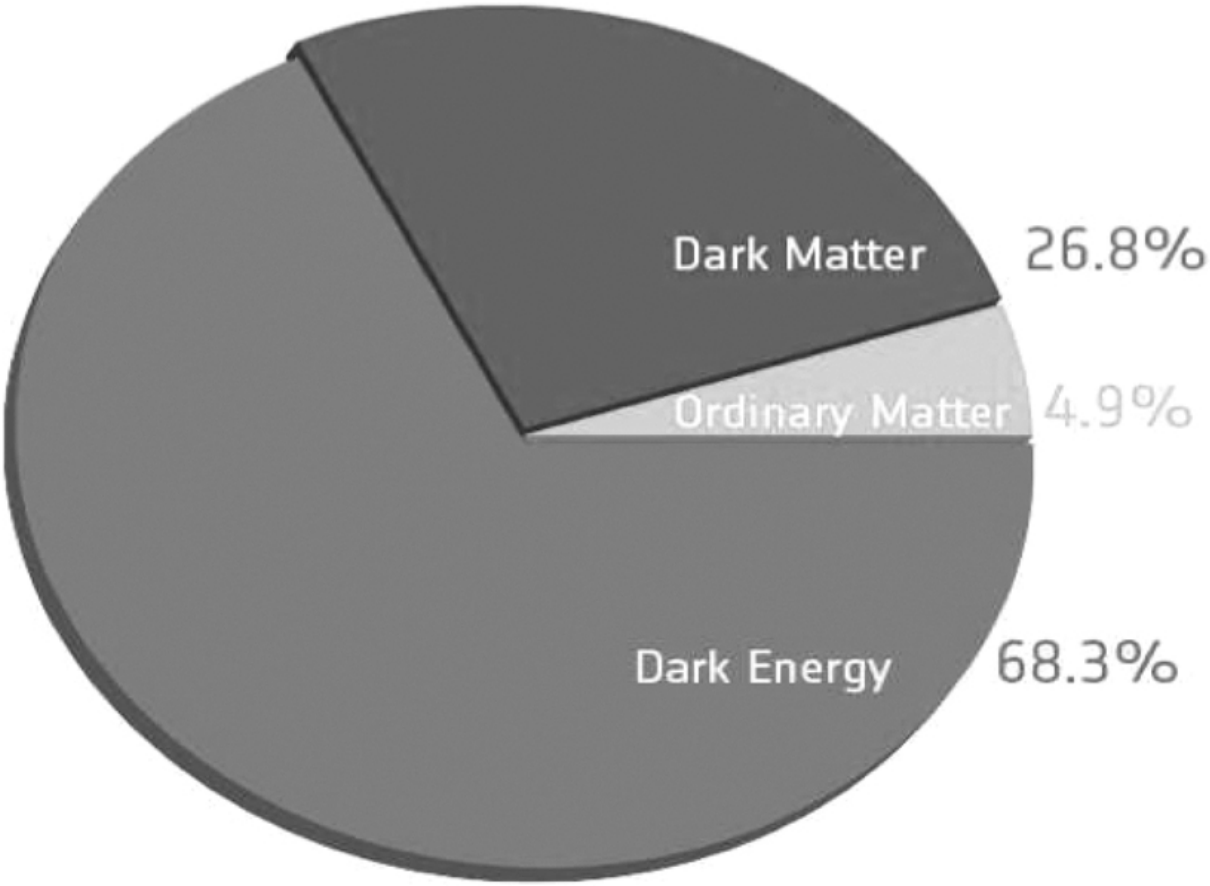

Figure 1.7 Composition of the universe based on Planck 2018 data. ⏎

There are three principal methods to detect DM: direct detection, indirect detection, and collider production. These are diagrammatically represented by a generic Feynman diagram involving DM particles χ and SM particles (Fig. 1.8). Among various DM candidates, Weakly Interacting Massive Particles (WIMPs) are particularly attractive. With masses in the 10 GeV–TeV range and weak-scale interactions, WIMPs naturally lead to the correct DM abundance through the *freeze-out* mechanism [33].

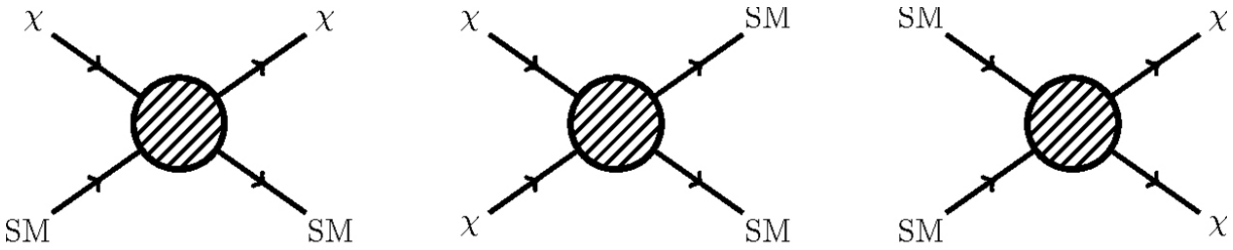

(a) Direct detection (b) Indirect detection (c) Collider production

Figure 1.8 Generic Feynman diagrams for direct detection, indirect detection, and collider production of DM. ⏎

In the early Universe, WIMPs were in thermal equilibrium. As the Universe cooled below $T < m_\chi$, WIMP annihilation could no longer keep up with the expansion, leading to a relic abundance. The Boltzmann equation describing the evolution of WIMP number density n_χ is:

$$\frac{dn_\chi}{dt} + 3Hn_\chi = -\langle \sigma v \rangle (n_\chi^2 - (n_\chi^{\text{eq}})^2),$$

(1.88)

where $\langle \sigma v \rangle$ is the thermally averaged annihilation cross-section times velocity. For non-relativistic DM, this cross-section can be expanded as [34]:

$$\langle \sigma v \rangle \simeq a + \frac{6b}{x}, \quad x \equiv \frac{m_\chi}{T}.$$

(1.89)

The relic density is then given by:

$$\Omega h^2 \simeq \frac{1.07 \times 10^9 \, x_f \, \mathrm{GeV}^{-1}}{\sqrt{g_*} M_{\mathrm{Pl}} (a + \frac{3b}{x_f})},$$

(1.90)

where x_f is the freeze-out parameter, g_* is the effective number of relativistic degrees of freedom, and M_{Pl} is the Planck mass. This expression shows that a weak-scale cross-section yields the observed relic density $\Omega h^2 \approx 0.12$, a phenomenon often referred to as the WIMP miracle.

1.2.3 Higgs Mass Hierarchy

As discussed earlier, electroweak symmetry breaking in the SM is triggered by the Higgs VEV:

$$v^2 = \frac{4M_W^2}{g^2} \simeq 10^4 \, \mathrm{GeV}^2 \ll M_{\mathrm{Pl}}^2 \simeq 10^{38} \, \mathrm{GeV}^2,$$

(1.91)

where M_W is the mass of the W boson, g is the SU(2) gauge coupling, and M_{Pl} is the reduced Planck mass. This enormous disparity between the electroweak scale and the Planck scale, spanning over 16 orders of magnitude, has no natural explanation within the SM and constitutes what is known as the hierarchy problem [35, 36].

The issue becomes more severe at the quantum level, as scalar masses in quantum field theory receive large radiative corrections from higher energy scales. For the Higgs boson, one-loop corrections from fermionic loops (see Fig. 1.9) lead to a quadratically divergent mass correction:

$$\delta m_H^2 = -\frac{|\lambda|^2}{8\pi^2} \left[\Lambda^2 - 2m_f^2 \ln \left(\frac{\Lambda}{m_f} \right) \right],$$

(1.92)

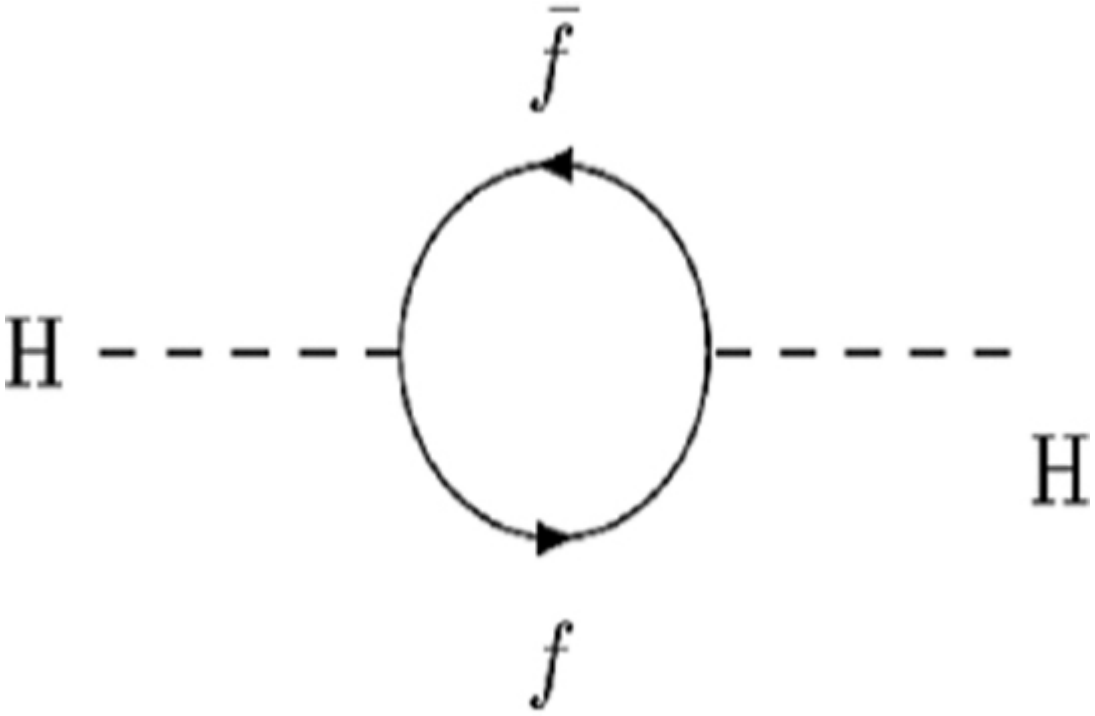

Figure 1.9 One-loop radiative correction to the Higgs boson mass from a fermion loop. ⏎

where λ is the Yukawa coupling between the Higgs field and a fermion f, m_f is the fermion mass, and Λ is the ultraviolet (UV) cutoff scale, which can be as high as the Planck scale. For $\Lambda \sim 10^{19}\,\text{GeV}$, the correction becomes $\delta m_H \sim 10^{30}\,\text{GeV}^2$, vastly exceeding the physical Higgs mass $m_H \approx 125\,\text{GeV}$. Reconciling such corrections with the observed Higgs mass would require extreme fine-tuning of bare parameters, a situation considered highly unnatural [37, 38].

In contrast, fermion masses such as the electron mass receive only logarithmically divergent corrections (see Fig. 1.10):

$$\delta m_e = \frac{2\alpha_{\text{em}}}{\pi} m_e \ln\left(\frac{\Lambda}{m_e}\right),$$

(1.93)

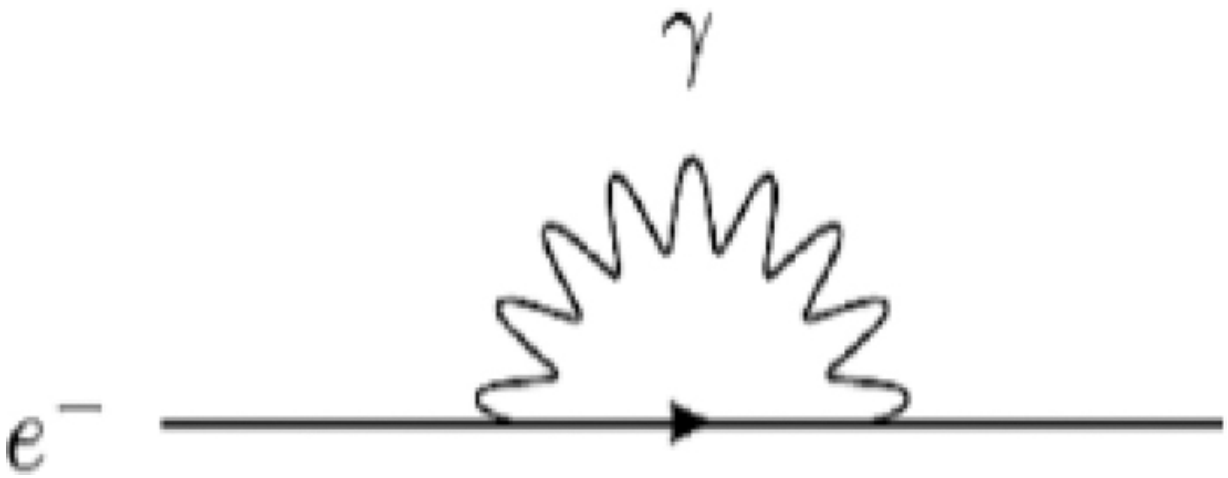

Figure 1.10 One-loop radiative correction to the electron mass. ⏎

where α_{em} is the electromagnetic fine-structure constant. Even for a cutoff $\Lambda \sim 10^{19}$ GeV, the correction remains modest: $\delta m_e \approx 0.24 m_e$. Moreover, in the limit $m_e \to 0$, the correction vanishes due to the restoration of chiral symmetry, which protects fermion masses from large radiative corrections.

To resolve the hierarchy problem, many theoretical frameworks propose new physics at or near the TeV scale. One prominent example is supersymmetry, which introduces superpartners for all SM particles and naturally cancels the quadratic divergences in Higgs mass corrections. Other approaches include models with composite Higgs bosons, extra spatial dimensions, or invoking the anthropic principle in a multiverse framework [39].

These models aim to stabilize the Higgs mass without unnatural fine-tuning, and many of them predict new particles or interactions accessible to current or future experiments, making the hierarchy problem one of the central driving forces in the search for physics beyond the SM.

1.2.4 Baryon Asymmetry

Baryon asymmetry refers to the observed imbalance between baryons—particles composed of three quarks, such as protons and neutrons—and antibaryons, their corresponding antiparticles, in the universe. This discrepancy is one of the most profound puzzles in physics, requiring an explanation that goes beyond the SM of particle physics. The SM, in its present form, lacks a mechanism to account for this asymmetry, known as baryogenesis. According to the SM, the interactions in the early universe should have resulted in equal amounts of matter and antimatter, which

would have led to their mutual annihilation, leaving behind a universe devoid of any baryons.

The enigma of baryon asymmetry, also referred to as the matter-antimatter asymmetry, raises a critical question: why does the universe consist predominantly of matter, with a clear absence of antimatter? Neither the SM of particle physics nor the theory of general relativity can provide a satisfactory explanation for this striking imbalance. In 1967, Andrei Sakharov outlined three necessary conditions for the generation of a net baryon number in the universe [40]:

- *Baryon number violation,*
- *Thermal non-equilibrium,*
- *C (charge conjugation) and CP (charge-parity) violation.*

During the early stages of the universe, all these conditions were likely satisfied. However, our understanding of CP violation in particle interactions and the ability to calculate the baryon asymmetry from first principles remain topics of active research.

The baryon-to-photon ratio, which quantifies the baryon asymmetry of the universe, is given by [41]:

$$\frac{n_B - n_{\bar{B}}}{n_\gamma} = 6.1 \times 10^{-10}, \tag{1.94}$$

indicating a small excess of baryons over antibaryons. Investigating the origin of this asymmetry, particularly the role of CP violation, and deriving it from first principles are central goals in the search for physics beyond the SM.

Several mechanisms have been proposed to explain the baryon asymmetry. One of the most well-known is leptogenesis, which involves the violation of lepton number conservation. In this scenario, the early universe may have seen the decay of heavy particles known as right-handed neutrinos. These decays could have resulted in an excess of quarks over antiquarks, which then generated the observed baryon asymmetry through sphaleron interactions. Other mechanisms beyond the SM have also been suggested, including GUTs, where the three fundamental forces of the SM (strong, weak, and electromagnetic forces) are unified at high energies [42].

1.2.5 Other Unresolved Theoretical Questions

Furthermore, when we look closely at particle physics, we find some really interesting questions that the SM can't fully answer. These questions include:

- Electroweak Symmetry Breaking: We still lack a complete understanding of how particles acquire mass, making this one of the most important questions in modern physics.
- Symmetry Group: The SM is based on a specific gauge symmetry group, $SU(3)_C \times SU(2)_L \times U(1)_Y$, but the reason for this particular choice remains unclear. Understanding its origin could provide deeper insight into the fundamental forces of nature.
- Unification: Can all the known fundamental forces be described within a single, unified framework? Achieving such unification would greatly simplify and deepen our understanding of the universe.
- Three Families of Particles: The Standard Model contains three generations of similar fermions, but the reason for this replication is unknown. Uncovering its origin could offer deeper insight into the structure and behavior of fundamental particles.
- Quantum Gravity: While we have successful quantum theories for three of the four fundamental forces, gravity remains incompatible with quantum mechanics. Developing a consistent theory of quantum gravity is one of the most profound challenges in theoretical physics.
- Cosmological Constant: The cosmological constant in Einstein's equations is vastly smaller than theoretical expectations. Understanding this discrepancy could shed light on the nature of vacuum energy and the universe's accelerated expansion.

These questions highlight the limitations of the SM and underscore the need for new theoretical frameworks to address these unresolved mysteries. The pursuit of physics BSM represents a major endeavor in the scientific community, aimed at achieving a deeper understanding of the fundamental structure and dynamics of the universe.

1.3 POSSIBLE DIRECTIONS FOR BSM

In this section, we will explore a range of avenues and approaches that physicists are actively investigating to expand our comprehension of fundamental particles and forces beyond the SM. These diverse directions encompass various theoretical frameworks and concepts, all geared toward tackling the constraints of the SM and striving for a more encompassing depiction of the universe.

- Extension of Gauge Symmetry: One direction involves extending the gauge symmetry beyond the SM gauge symmetries. This could introduce new particles and interactions that might help explain some of the unanswered questions in particle physics.
- Extension of Higgs Sector: Another avenue is to expand the Higgs sector, which is responsible for giving particles mass. Extending this sector could provide new insights into the origins of mass and the fundamental nature of the Higgs boson.
- Extension of Matter Content: Expanding the matter content involves introducing new types of particles or matter beyond what is currently described in the SM. This can lead to a richer and more diverse particle spectrum.
- Extension with Flavor Symmetry: Flavor symmetry extensions seek to understand the relationships between different types of particles and their properties, such as different flavors of quarks and leptons. This extension may reveal underlying patterns in particle physics.
- Extension of Space-time Dimensions: Some theories propose the existence of extra spatial dimensions beyond the familiar three dimensions of space. These extra dimensions could help address various questions in physics, including the unification of forces.
- Extension of Lorentz Symmetry (Supersymmetry): Supersymmetry extends the concept of spacetime symmetry, known as Lorentz symmetry. It posits a connection between particles with different intrinsic angular momenta (spin), potentially leading to a more unified theory of particles and forces.
- Incorporate Gravity (Supergravity): Incorporating gravity into the framework of particle physics is a significant challenge. Supergravity attempts to merge the principles of general relativity (gravity) with the

concepts of supersymmetry from particle physics. It is a step toward a unified theory of all fundamental forces.

- One-dimensional Object (Superstring): Superstring theory proposes that the fundamental building blocks of the universe are not particles but tiny, vibrating strings. This theory aims to reconcile gravity with quantum mechanics and provide a unified framework for all fundamental forces.

These directions represent the ongoing efforts in theoretical physics to push the boundaries of our knowledge and explore new frameworks that can address the unresolved questions posed by the SM. While each direction has its own set of challenges and complexities, they collectively contribute to the pursuit of a more comprehensive and unified theory of the fundamental forces and particles in the universe.

Throughout the chapters of this book, our objective is to delve into as many potential avenues beyond the SM as we can, providing a comprehensive overview of the ongoing pursuit for a deeper comprehension of the universe.

CHAPTER 2

Two Higgs Doublet Models

DOI: 10.1201/9781003457701-2

The Two Higgs Doublet Model (2HDM) is a well-motivated extension of the SM of particle physics, achieved by introducing a second complex scalar doublet in addition to the one present in the SM [43]. This extension offers a promising framework to address phenomena beyond the SM, such as the baryon asymmetry of the universe and the existence of dark matter candidates. In this chapter, we examine the theoretical structure and phenomenological implications of 2HDMs, highlighting how this framework can resolve some of the SM limitations.

The two complex scalar doublets in a 2HDM are typically denoted as Φ_1 and Φ_2, and are expressed as follows:

$$\Phi_1 = \begin{pmatrix} \phi_1^+ \\ \phi_1^0 \end{pmatrix}, \quad \Phi_2 = \begin{pmatrix} \phi_2^+ \\ \phi_2^0 \end{pmatrix}.$$

Here, ϕ_1^+, ϕ_1^0, ϕ_2^+, and ϕ_2^0 represent the scalar fields associated with the two Higgs doublets. These doublets can acquire VEVs, which break the electroweak symmetry, giving mass to the W and Z bosons and to fermions through Yukawa couplings.

The 2HDM can be classified into several types based on the manner in which fermions (quarks and leptons) couple to the Higgs doublets and the specific Yukawa couplings. The most common types are:

1. Type-I 2HDM: In this model, only one Higgs doublet, Φ_2, couples to the charged fermions (both up-type and down-type quarks as well as

charged leptons), while Φ_1 does not couple to any fermions [44]. This is sometimes referred to as a Fermiophobic 2HDM.

2. Type-II 2HDM: In this configuration, one Higgs doublet, Φ_2, couples to the up-type quarks, while the other, Φ_1, couples to the down-type quarks and leptons [44]. This model is the one most commonly used in the Minimal Supersymmetric Standard Model (MSSM).
3. Lepton-Specific 2HDM: Here, one Higgs doublet exclusively interacts with leptons, while the other interacts with quarks. This can lead to interesting phenomena involving changes in lepton flavors. Occasionally, this is referred to as Type-X 2HDM [45].
4. Flipped 2HDM: In this variation, the roles of the two Higgs doublets are reversed compared to Type-II. The doublet that couples to up-type quarks in Type-II now couples to down-type quarks and leptons, and vice versa. This variation is sometimes referred to as Type-Y 2HDM [46].
5. Type-III 2HDM: In this model, both Φ_1 and Φ_2 couple to both up-type and down-type quarks as well as charged leptons. This type is known for its tendency to generate Flavor Changing Neutral Current (FCNC) interactions at the tree level [47]. To comply with strict experimental limits, specific assumptions on the Yukawa couplings must be made.

The choice of the 2HDM type depends on the specific physics phenomena under consideration and the experimental constraints. 2HDMs can have a much richer Higgs boson phenomenology compared to the SM, including the presence of additional Higgs bosons: a heavy neutral CP-even Higgs boson (H), a pseudo-scalar (A), and charged Higgs bosons ($H^{\pm}$). Moreover, these models allow for the potential occurrence of FCNCs and CP-violating effects.

It is important to emphasize that the 2HDM does not alter the successful predictions of the SM but rather enriches the scalar particle spectrum. This extension opens the door for the existence of new particles beyond those predicted by the SM. Additionally, 2HDMs are not limited to SM but can also be incorporated into larger frameworks such as Supersymmetry.

These models are actively studied both theoretically and experimentally to explore their predictions and assess whether they can explain observed phenomena that the SM cannot. On the experimental front, this includes searching for additional Higgs bosons and measuring their properties in

particle collider experiments such as those conducted at the Large Hadron Collider (LHC).

2.1 2HDM SCALAR POTENTIAL

The most general $SU(2)_L \times U(1)_Y$ -invariant scalar potential of the 2HDM involving two complex scalar doublets Φ_1 and Φ_2 is given by [48, 49]:

$$\begin{aligned} V(\Phi_1,\Phi_2) \quad &= m_{11}^2\Phi_1^\dagger\Phi_1 + m_{22}^2\Phi_2^\dagger\Phi_2 - \left[m_{12}^2\Phi_1^\dagger\Phi_2 + \text{h.c.}\right] + \frac{1}{2}\lambda_1(\Phi_1^\dagger\Phi_1)^2 \\ &\quad + \frac{1}{2}\lambda_2(\Phi_2^\dagger\Phi_2)^2 + \lambda_3(\Phi_1^\dagger\Phi_1)(\Phi_2^\dagger\Phi_2) + \lambda_4(\Phi_1^\dagger\Phi_2)(\Phi_2^\dagger\Phi_1) \\ &\quad + \left[\frac{1}{2}\lambda_5(\Phi_1^\dagger\Phi_2)^2 + \lambda_6(\Phi_1^\dagger\Phi_1)(\Phi_1^\dagger\Phi_2) + \lambda_7(\Phi_2^\dagger\Phi_2)(\Phi_1^\dagger\Phi_2) + \text{h.c.}\right]. \end{aligned} \tag{2.1}$$

Here, $m_{11}^2, m_{22}^2, \lambda_{1,2,3,4}$ are real, while $m_{12}^2, \lambda_{5,6,7}$ are generally complex, leading to 14 real independent parameters.

Discrete Symmetry and FCNC Suppression

To suppress FCNCs at tree level, a Z_2 symmetry is imposed:

$$\Phi_1 \to -\Phi_1, \quad \Phi_2 \to \Phi_2, \tag{2.2}$$

which eliminates terms with $m_{12}^2 = \lambda_6 = \lambda_7 = 0$. Soft breaking of Z_2 is allowed via a non-zero but real m_{12}^2 to retain CP conservation.

Theoretical Constraints

To ensure physical viability, the 2HDM parameters must satisfy several theoretical constraints [48, 49]:

1. Perturbativity: Couplings must remain perturbative: $|\lambda_i| \lesssim 4\pi$.
2. Tree-Level Unitarity: Scattering amplitudes must satisfy partial wave unitarity bounds, restricting combinations of λ_i.

3. Vacuum Stability: The potential must be bounded from below. This implies:

$$\lambda_1 > 0, \quad \lambda_2 > 0, \quad \lambda_3 > -\sqrt{\lambda_1 \lambda_2}, \quad \lambda_3 + \lambda_4 - |\lambda_5| > -\sqrt{\lambda_1 \lambda_2}. \tag{2.3}$$

4. Electroweak Precision Constraints: The model must comply with *S, T*, and *U* parameter bounds.
5. FCNC Constraints: FCNCs are avoided by the Z_2 symmetry; further suppression can be achieved by proper Yukawa alignment.
6. Naturalness: Large hierarchies between m_H and M_Z introduce fine-tuning. Define:

$$\Delta = \max_i \left| \frac{\partial \ln M_Z^2}{\partial \ln p_i} \right| \quad \text{where} \, p_i \in \{m_{ij}^2, \lambda_k\}. \tag{2.4}$$

Vacuum Expectation Values and CP Conservation

To preserve electric charge and CP symmetry, only the neutral CP-even components develop VEVs:

$$\langle \Phi_1 \rangle = \frac{1}{\sqrt{2}} \begin{pmatrix} 0 \\ v_1 \end{pmatrix}, \qquad \langle \Phi_2 \rangle = \frac{1}{\sqrt{2}} \begin{pmatrix} 0 \\ v_2 \end{pmatrix}, \tag{2.5}$$

with $v^2 = v_1^2 + v_2^2 = (246\,\text{GeV})^2$. The minimization conditions yield:

$$m_{11}^2 = m_{12}^2 \frac{v_2}{v_1} - \frac{1}{2} \lambda_1 v_1^2 - \lambda_{345} v_2^2, \tag{2.6}$$

$$m_{22}^2 = m_{12}^2 \frac{v_1}{v_2} - \frac{1}{2} \lambda_2 v_2^2 - \lambda_{345} v_1^2, \tag{2.7}$$

where $\lambda_{345} = \lambda_3 + \lambda_4 + \lambda_5$. In CP-conserving 2HDMs with softly broken Z_2, the model is characterized by eight parameters:

$$\lambda_1, \lambda_2, \lambda_3, \lambda_4, \lambda_5, m_{12}^2, \tan\beta = \frac{v_2}{v_1}, \text{ and } v. \tag{2.8}$$

2.2 THE HIGGS SPECTRUM OF THE 2HDM

The scalar sector of the 2HDM consists of two $SU(2)_L$ scalar doublets, Φ_1 and Φ_2, each with hypercharge $+1$. They can be parameterized in the unitary gauge as:

$$\Phi_1 = \begin{pmatrix} \phi_1^+ \\ \frac{1}{\sqrt{2}}(v_1 + \phi_1 + i\eta_1) \end{pmatrix}, \quad \Phi_2 = \begin{pmatrix} \phi_2^+ \\ \frac{1}{\sqrt{2}}(v_2 + \phi_2 + i\eta_2) \end{pmatrix}, \tag{2.9}$$

where v_1 and v_2 are the VEVs of the doublets with $v^2 = v_1^2 + v_2^2 \simeq (246\,\text{GeV})^2$. The 8 real degrees of freedom decompose into three Goldstone bosons, eaten by the $W^\pm$ and Z bosons, and five physical Higgs states: two CP-even scalars (h, H), one CP-odd pseudoscalar (A), and two charged scalars ($H^\pm$) [48, 49].

Charged Higgs Sector

The mass matrix for the charged scalars $\phi_1^\pm, \phi_2^\pm$ is given by:

$$M_{H^\pm}^2 = \left(m_{12}^2 - \frac{1}{2}(\lambda_4 + \lambda_5) v_1 v_2 \right) \begin{pmatrix} \frac{v_2}{v_1} & -1 \\ -1 & \frac{v_1}{v_2} \end{pmatrix}, \tag{2.10}$$

which yields one zero eigenvalue corresponding to the charged Goldstone boson $G^\pm$, and one massive eigenstate:

$$m_{H^\pm}^2 = \frac{m_{12}^2}{v_1 v_2} v^2 - \frac{1}{2}(\lambda_4 + \lambda_5) v^2. \tag{2.11}$$

The physical charged Higgs boson is:

$$H^{\pm} = -\sin\beta\,\phi_1^{\pm} + \cos\beta\,\phi_2^{\pm}, \quad \tan\beta = \frac{v_2}{v_1}.$$

(2.12)

CP-Odd Scalar Sector

The pseudoscalar mass matrix in the (η_1, η_2) basis reads:

$$M_A^2 = \left(\frac{m_{12}^2}{v_1 v_2} - \lambda_5\right)\begin{pmatrix} v_2^2 & -v_1 v_2 \\ -v_1 v_2 & v_1^2 \end{pmatrix},$$

(2.13)

yielding one massless Goldstone boson G^0 and one physical CP-odd scalar with mass:

$$m_A^2 = \frac{m_{12}^2}{v_1 v_2} v^2 - \lambda_5 v^2,$$

(2.14)

and eigenstate:

$$A = -\sin\beta\,\eta_1 + \cos\beta\,\eta_2.$$

(2.15)

CP-Even Scalar Sector

The CP-even scalar fields ϕ_1 and ϕ_2 mix to form the mass eigenstates h and H. Their mass matrix is:

$$M_H^2 = \begin{pmatrix} m_{12}^2 \frac{v_2}{v_1} + \lambda_1 v_1^2 & -m_{12}^2 + \lambda_{345} v_1 v_2 \\ -m_{12}^2 + \lambda_{345} v_1 v_2 & m_{12}^2 \frac{v_1}{v_2} + \lambda_2 v_2^2 \end{pmatrix},$$

(2.16)

where $\lambda_{345} = \lambda_3 + \lambda_4 + \lambda_5$. Diagonalizing this matrix via a mixing angle α yields the mass eigenstates:

$$h \quad = -\sin\alpha\,\phi_1 + \cos\alpha\,\phi_2,$$

(2.17)

$$H \quad = \cos\alpha\,\phi_1 + \sin\alpha\,\phi_2,$$

(2.18)

with $m_h^2 \leq m_H^2$ by convention. The lighter scalar h is typically identified with the observed Higgs boson at 125 GeV.

2.3 2HDM INTERACTIONS

2HDM leads to richer phenomenology, including the possibility of FCNCs and new interactions involving the Higgs and gauge bosons, as well as fermions. In this section, we explore the key interactions in the 2HDM, focusing on the gauge boson and Yukawa interactions.

Gauge Bosons in 2HDM

In the 2HDM, the gauge bosons interact with the Higgs bosons in a manner similar to the SM. The kinetic terms for the Higgs doublets are given by:

$$\mathscr{L}_\Phi = (D_\mu \Phi_1)^\dagger (D^\mu \Phi_1) + (D_\mu \Phi_2)^\dagger (D^\mu \Phi_2),$$

where D_μ represents the covariant derivative acting on the doublet fields. It accounts for the interaction of the Higgs fields with the gauge fields while maintaining gauge invariance. For a doublet field Φ_i, the covariant derivative is expressed as:

$$D_\mu \Phi_i = (\partial_\mu - ig\frac{\sigma^a}{2}W_\mu^a - ig'\frac{Y}{2}B_\mu)\Phi_i,$$

where g and $g^{'}$ are the gauge coupling constants for the $SU(2)_L$ and $U(1)_Y$ gauge groups, respectively, W_μ^a and B_μ are the gauge fields associated with the $SU(2)_L$ and $U(1)_Y$ groups, σ^a are the Pauli matrices, and Y represents the weak hypercharge.

After spontaneous symmetry breaking, the Higgs doublets acquire VEVs, denoted as v_1 and v_2. From the kinetic terms $\mathscr{L}_\Phi$, one derives mass terms for the gauge bosons, resulting in the following expressions for the gauge boson masses:

$$M_W = \frac{1}{4} g^2 v^2, \quad M_Z = \frac{1}{4}(g^2 + g'^2)v^2, \quad M_A^2 = 0,$$

where $v = \sqrt{v_1^2 + v_2^2}$ is the total vacuum expectation value. Additionally, the neutral Higgs bosons couple to the W and Z gauge bosons. These couplings are given by:

$$\begin{aligned} \mathscr{L}_\Phi \supset & \frac{g^2 + g'^2}{4} v \left[\sin(\beta - \alpha) ZZh + \cos(\beta - \alpha) ZZH \right] \\ & + \frac{g^2}{2} v \left[\sin(\beta - \alpha) WWh + \cos(\beta - \alpha) WWH \right], \end{aligned} \tag{2.19}$$

where h and H denote the light and heavy CP-even Higgs mass eigenstates, respectively, and α and β are the mixing angles in the Higgs sector.

Yukawa Interactions in 2HDM

In the 2HDM, the most general gauge-invariant Lagrangian for the Yukawa interactions between the Higgs doublets and SM fermions is given by:

$$\mathscr{L}_{\text{Yukawa}} = - \sum_{i=1,2} Y_i^d \overline{Q}_L \Phi_i d_R + Y_i^u \overline{Q}_L \tilde{\Phi}_i u_R + Y_i^\ell \overline{L}_L \Phi_i \ell_R + \text{h.c.},$$

where i indexes the two Higgs doublets (Φ_1 and Φ_2), and $\tilde{\Phi}_i = i\sigma_2 \Phi_i^*$ denotes the conjugate of the Higgs doublet Φ_i. The Yukawa coupling matrices for the up-type quarks, down-type quarks, and leptons are represented by Y_i^u, Y_i^d, and Y_i^ℓ, respectively.

After electroweak symmetry breaking, the Higgs fields acquire VEVs, resulting in fermion masses. The Yukawa couplings can be related to the mass matrices. For example, the up-type quark mass matrix M_u is given by:

$$M_u = \frac{v}{\sqrt{2}} (Y_1^u + \tan\beta Y_2^u),$$

where $\tan\beta = v_2/v_1$ is the ratio of the Higgs VEVs. This relation shows that diagonalizing the fermion mass matrix does not necessarily diagonalize the Yukawa coupling matrices, thus allowing for FCNCs at tree level. These FCNCs can have observable consequences, such as in $H \to ds$ decays, which contribute to $K - \bar{K}$ oscillations [48]. To suppress these effects, it is often required that the neutral flavor-changing mediator be heavy, with a

mass scale around 10 TeV. One common method to reduce FCNCs is to impose a Z_2 symmetry, which can lead to Type I or Type II 2HDMs.

As previously noted, in the Type I 2HDM, all quarks couple to a single Higgs doublet. In contrast, the Type II 2HDM assigns fermions to different doublets based on their electric charge: up-type quarks ($Q = +2/3$) couple to Φ_1, while down-type quarks ($Q = -1/3$) couple to Φ_2. This structure plays a crucial role in suppressing FCNCs. The corresponding Z_2 symmetry charge assignments for Type I and Type II models are summarized in Table 2.1.

TABLE 2.1 Z_2 charge assignments for the Higgs doublets, up-type quarks, down-type quarks, and leptons in both Type I and Type II 2HDMs.

Field	Type I Z_2 Charge	Type II Z_2 Charge
Φ_1	+1	+1
Φ_2	-1	-1
Up-type quarks	+1	+1
Down-type quarks	+1	-1
Leptons	+1	-1

In Type I and Type II 2HDMs, the Yukawa couplings to the neutral Higgs bosons *h, H*, and *A* Higgs bosons are given by:

$$\begin{aligned}\mathscr{L}_{\text{Yukawa}} = & -\sum_{f=u,d,\ell} \frac{m_f}{v}\left(\xi_h^f \bar{f} f h + \xi_H^f \bar{f} f H - i\xi_A^f \bar{f}\gamma_5 f A\right) \\ & -\left\{\frac{\sqrt{2}V_{ud}}{v}\,\bar{u}\left(m_u \xi_A^u P_L + m_d \xi_A^d P_R\right) d H^+ \right. \\ & \left. + \frac{\sqrt{2} m_\ell \xi_A^\ell}{v}\,\overline{\nu_L}\,\ell_R H^+ + h.c.\right\},\end{aligned} \tag{2.20}$$

where $P_{L/R}$ denotes the projection operators for left-/right-handed fermions, and the corresponding factors ξ are outlined in Table 2.2.

TABLE 2.2 Yukawa couplings of u, d, ℓ to the neutral Higgs bosons *h,H,A* in the four different

models. The couplings to the charged Higgs bosons follow Eq. 2.20. ⏎

	Type I	Type II
ξ_h^u	$\cos\alpha/\sin\beta$	$\cos\alpha/\sin\beta$
ξ_h^d	$\cos\alpha/\sin\beta$	$-\sin\alpha/\cos\beta$
ξ_h^ℓ	$\cos\alpha/\sin\beta$	$-\sin\alpha/\cos\beta$
ξ_H^u	$\sin\alpha/\sin\beta$	$\sin\alpha/\sin\beta$
ξ_H^d	$\sin\alpha/\sin\beta$	$\cos\alpha/\cos\beta$
ξ_H^ℓ	$\sin\alpha/\sin\beta$	$\cos\alpha/\cos\beta$
ξ_A^u	$\cot\beta$	$\cot\beta$
ξ_A^d	$-\cot\beta$	$\tan\beta$
ξ_A^ℓ	$-\cot\beta$	$\tan\beta$

2.4 PHENOMENOLOGICAL CONSEQUENCES

The 2HDM gives rise to distinctive signatures that can be tested through collider experiments and precision measurements. This section highlights key phenomenological implications, focusing on the decay modes of the Higgs bosons, their production channels at the LHC, and potential contributions to the anomalous magnetic moment of the muon.

2.4.1 Higgs Decays

We examine the dominant decay channels of the heavy neutral scalars H and A, as well as the charged Higgs boson $H^\pm$, in Type I and Type II 2HDMs. Our analysis is performed in the alignment limit, $\sin(\beta-\alpha)\simeq 1$, in which the light CP-even scalar h exhibits SM-like couplings and reproduces the observed Higgs boson properties [48]. In this limit, the tree-level couplings of H to WW and ZZ vanish, while A and $H^\pm$ do not couple to gauge boson pairs at tree level for any value of $\sin(\beta-\alpha)$.

The partial decay widths of the heavy scalars into fermion pairs are given by [50]:

$$\Gamma(\varphi \to f\bar{f}) \quad = N_C \frac{G_F m_\varphi m_f^2}{4\sqrt{2}\pi} (\xi_\varphi^f)^2 \times \begin{cases} \beta_f^3, & \varphi = h, H, \\ \beta_f, & \varphi = A, \end{cases} \tag{2.21}$$

$$\begin{aligned} \Gamma(H^+ \to f\bar{f}') \quad = N_C \frac{G_F m_{H^\pm}}{4\sqrt{2}\pi} |V_{ff'}|^2 \beta_{ff'} \Big[\Big(m_f^2 (\xi_A^f)^2 + m_{f'}^2 (\xi_A^{f'})^2 \Big) \\ \left(1 - \frac{m_f^2 + m_{f'}^2}{m_{H^\pm}^2} \right) - \frac{4 m_f^2 m_{f'}^2 \xi_A^f \xi_A^{f'}}{m_{H^\pm}^2} \Big], \end{aligned} \tag{2.22}$$

where:

- $N_C = 3$ for quarks and $N_C = 1$ for leptons,
- G_F is the Fermi constant,
- m_φ denotes the mass of the decaying scalar $\varphi = h, H, A$,
- $m_{H^\pm}$ is the mass of the charged Higgs,
- $m_f, m_{f'}$ are the masses of the final-state fermions,
- $V_{ff'}$ is the CKM matrix element (or 1 for leptonic decays),
- $\beta_f = \sqrt{1 - 4m_f^2/m_\varphi^2}$, and
- $\beta_{ff'} = \lambda^{1/2} \left(\frac{m_f^2}{m_{H^\pm}^2}, \frac{m_{f'}^2}{m_{H^\pm}^2} \right)$,
- ξ_φ^f are the model-dependent Yukawa coupling modifiers [48].

We also consider the loop-induced decays of the scalar particles, including the decay modes $\varphi \to \gamma\gamma$, $\varphi \to Z\gamma$, and $\varphi \to gg$, where φ represents any of the heavy scalars H, A, or $H^\pm$. The corresponding decay widths are given by [51]:

$$\Gamma(\varphi \to \gamma\gamma) \quad = \frac{G_F \alpha_{\mathrm{EM}}^2 m_\varphi^3}{128\sqrt{2}\pi^3} \left| \sum_f Q_f^2 I_f^\varphi(m_f, N_C) + I_W^\varphi + I_{H^\pm}^\varphi \right|^2, \tag{2.23}$$

$$\Gamma(\varphi \to Z\gamma) \quad = \frac{G_F \alpha_{\rm EM}^2 m_\varphi^3}{64\sqrt{2}\pi^3}\left(1-\frac{m_Z^2}{m_\varphi^2}\right)^3 \left|\sum_f Q_f J_f^\varphi(m_f, N_C) + J_W^\varphi + J_{H^\pm}^\varphi\right|^2, \tag{2.24}$$

$$\Gamma(\varphi \to gg) \quad = \frac{G_F \alpha_S^2 m_\varphi^3}{64\sqrt{2}\pi^3} \left|\sum_{f=q} I_f^\varphi(m_f, 1)\right|^2, \tag{2.25}$$

where the fermionic loop functions I_f^φ and J_f^φ depend on the particle masses and Yukawa couplings. The fermionic loop functions are as follows [51]:

$$I_f^\varphi(m_f, N_C) \quad = \xi_\varphi^f \times \begin{cases} -N_C \frac{4m_f^2}{m_\varphi^2}\left[2 - \beta_f^2 m_\varphi^2 C_0(0,0,m_\varphi^2, m_f^2, m_f^2, m_f^2)\right] \\ \text{for } \varphi = h, H, \\ +4N_C m_f^2 C_0(0,0,m_\varphi^2, m_f^2, m_f^2, m_f^2) \\ \text{for } \varphi = A, \end{cases} \tag{2.26}$$

$$J_f^\varphi(m_f, N_C) \quad = \xi_\varphi^f \times \begin{cases} -4N_C c_V^f \left[J_1(m_f) - J_2(m_f)\right] & \text{for } \varphi = h, H, \\ -4N_C c_V^f \left[-J_2(m_f)\right] & \text{for } \varphi = A, \end{cases} \tag{2.27}$$

where c_V^f is the vector coupling of the fermion f to the Z-boson, given by $c_V^f = \frac{1}{2 s_W c_W}\left(T_{3L}^f - 2Q_f s_W^2\right)$, with T_{3L}^f denoting the third component of the weak isospin for fermion f. The functions $J_1(m_f)$ and $J_2(m_f)$ are given by:

$$\begin{aligned} J_1(m_f) \quad &= \frac{2m_f^2}{m_\varphi^2 - m_Z^2}\Big\{1 + 2m_f^2 C_0(0, m_Z^2, m_\varphi^2, m_f^2, m_f^2, m_f^2) \\ &\quad + \frac{m_Z^2}{m_\varphi^2 - m_Z^2}\left[B_0(m_\varphi^2, m_f^2, m_f^2) - B_0(m_Z^2, m_f^2, m_f^2)\right]\Big\}, \end{aligned} \tag{2.28}$$

$$J_2(m_f) \quad = m_f^2 C_0(0, m_Z^2, m_\varphi^2, m_f^2, m_f^2, m_f^2),$$

(2.29)

where B_0 and C_0 are the Passarino-Veltman functions [52]. These functions are defined as:

$$B_0(m_\varphi^2, m^2, m^2) \quad = \Delta - 2g\left(\frac{4m^2}{m_\varphi^2}\right),$$

(2.30)

$$C_0(0, 0, m_\varphi^2, m^2, m^2, m^2) \quad = \frac{-2}{m_\varphi^2} f\left(\frac{4m^2}{m_\varphi^2}\right),$$

(2.31)

with Δ denoting the regularization constant and $g(x)$ and $f(x)$ defined as:

$$g(x) \quad = \begin{cases} (x-1)\arcsin\left(\sqrt{\frac{1}{x}}\right) & \text{for } x \geq 1, \\ \frac{1}{2}(1-x)\left[\ln\left(\frac{1+\sqrt{1-x}}{1-\sqrt{1-x}}\right) - i\pi\right] & \text{for } x < 1, \end{cases}$$

(2.32)

$$f(x) \quad = \begin{cases} \left[\arcsin\left(\sqrt{\frac{1}{x}}\right)\right]^2 & \text{for } x \geq 1, \\ -\frac{1}{4}\left[\ln\left(\frac{1+\sqrt{1-x}}{1-\sqrt{1-x}}\right) - i\pi\right]^2 & \text{for } x < 1. \end{cases}$$

(2.33)

Finally, the loop functions I_W^φ, $I_{H^\pm}^\varphi$, J_W^φ, and $J_{H^\pm}^\varphi$ are common to all types of Yukawa interactions and can be found in Ref. [51].

In the type-I 2HDM, the decay of the neutral Higgs boson H into a gauge boson pair, such as $\gamma\gamma$ or $Z\gamma$, can be enhanced for large values of $\tan\beta$. This enhancement occurs because, while the fermionic decays (including the gg mode) are suppressed at large $\tan\beta$, the charged scalar loop contribution to the $\gamma\gamma$ and $Z\gamma$ decay modes is not always suppressed. On the other hand, such an enhancement does not occur in the decay of A, as there is no AH^+H^- coupling.

For charged Higgs boson decays with $m_{H^\pm} = 150\,\text{GeV}$, the dominant decay mode in both the type-I and type-II 2HDM is into $\tau\nu$ for $\tan\beta \gtrsim 1$, while hadronic decay modes can also dominate in the type-Y 2HDM [53].

2.4.2 Higgs Production at the LHC

At the LHC, neutral and charged Higgs bosons can be produced through several key mechanisms, depending on the Higgs sector structure. In the type-II 2HDM, the production of the additional neutral Higgs bosons H and A occurs predominantly via:

- Gluon fusion: $gg \to H, A$, a loop-induced process mediated primarily by top and bottom quarks. The effective coupling is enhanced at low $\tan\beta$ by top loops and at high $\tan\beta$ by bottom loops.
- *Associated production with bottom quarks:* $pp \to b\bar{b}H, b\bar{b}A$, relevant at large $\tan\beta$ where the Yukawa couplings to down-type quarks are enhanced.
- Associated production with top quarks: $pp \to t\bar{t}H, t\bar{t}A$, most sensitive at $\tan\beta \sim 1$.

On the other hand, vector boson fusion $VV \to H$ and associated production with gauge bosons are suppressed in the alignment limit ($\sin(\beta-\alpha) \simeq 1$), and forbidden for the CP-odd Higgs A due to the absence of VVA couplings.

The dominant decay channels of H and A depend on mass and $\tan\beta$. At high $\tan\beta$, decays to down-type fermions dominate: $H/A \to b\bar{b}, \tau^+\tau^-$, though these suffer from significant QCD and Drell-Yan backgrounds. Decays to $\mu^+\mu^-$ offer better mass resolution despite lower branching ratios, and can be competitive at low Higgs masses [54]. Simulations show that the $b\bar{b}H/A \to b\bar{b}\tau^+\tau^-$ channel provides better sensitivity than gluon fusion in the high $\tan\beta$ regime [55, 56].

The charged Higgs bosons $H^\pm$ provide distinctive signatures that can be probed at colliders:

- For $m_{H^\pm} < m_t$, they can be produced through top quark decays, $t \to H^+ b$. In the type-II Two-Higgs-Doublet Model (2HDM), such decays offer discovery potential for $\tan\beta \lesssim 2$ and $\tan\beta \gtrsim 20$, given sufficient integrated luminosity [57].
- For $m_{H^\pm} > m_t$, direct production channels such as $gb \to tH^-$ and pair production via $q\bar{q}, gg \to H^+H^-$ become significant. These processes are governed by the Yukawa interaction:

$$\mathscr{L}_{H^{\pm}tb} = \frac{g}{\sqrt{2}M_W} H^+ \bar{t}\,(m_b \tan\beta\, P_R + m_t \cot\beta\, P_L) b + \text{h.c.}$$

(2.34)

The cross-sections are enhanced for both low and high values of $\tan\beta$, making these channels complementary in probing the parameter space of the model.

2.4.3 Muon Anomalous Magnetic Moment

The anomalous magnetic moment of the muon, defined as $a_\mu \equiv \frac{1}{2}(g_\mu - 2)$, is a precisely measured observable that provides a sensitive probe of physics beyond the SM. The latest combined measurement by the Fermilab Muon $g-2$ experiment and the earlier E821 experiment at Brookhaven reports a discrepancy with the SM prediction at the level of $4.2\,\sigma$ [15, 16]:

$$\Delta a_\mu \equiv a_\mu^{\text{exp}} - a_\mu^{\text{SM}} = (251 \pm 59) \times 10^{-11}.$$

(2.35)

This suggests that potential new physics contributions should lie in the range:

$$215 \times 10^{-11} \leq \Delta a_\mu^{\text{NP}} \leq 637 \times 10^{-11}.$$

(2.36)

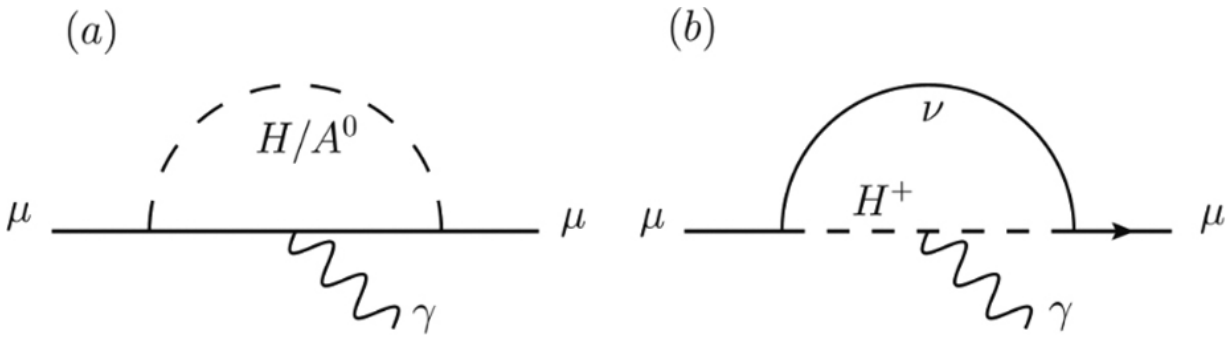

Figure 2.1 One-loop Feynman diagrams for the muon $g-2$.

In the 2HDM, additional contributions to a_μ arise from both one-loop and two-loop diagrams involving the extra scalar states $H, A, H^\pm$. At one loop, the electromagnetic vertex correction for a lepton ℓ has the general form:

$$\bar{\ell}(p')\Gamma^{\mu}\ell(p) = \bar{\ell}(p')\left[\gamma^{\mu}F_1(k^2) + \frac{i\sigma^{\mu\nu}k_{\nu}}{2m_{\ell}}F_2(k^2)\right]\ell(p),$$

(2.37)

where the anomalous magnetic moment is given by $a_{\ell} = F_2(0)$.

The 2HDM one-loop contribution is [58]:

$$\Delta a_{\mu}^{\text{1-loop}} = \frac{G_F}{4\pi^2}\frac{m_{\mu}^2}{\sqrt{2}}\sum_j (\xi_{\mu}^j)^2\, r_{\mu}^j\, f_j(r_{\mu}^j),$$

(2.38)

where $j = h, H, A, H^{\pm}$, $r_{\mu}^j = m_{\mu}^2/M_j^2$, and the loop functions $f_j(r)$ are:

$$f_{h,H}(r) = \int_0^1 dx \frac{x^2(2-x)}{1-x+rx^2},$$

(2.39)

$$f_A(r) = \int_0^1 dx \frac{-x^3}{1-x+rx^2},$$

(2.40)

$$f_{H^{\pm}}(r) = \int_0^1 dx \frac{-x(1-x)}{1-(1-x)r}.$$

(2.41)

However, one-loop effects are typically too small to explain the observed anomaly unless the scalar masses are of order a few tens of GeV. A more significant contribution arises from two-loop Barr-Zee type diagrams [59, 60], especially when involving heavy fermion loops.

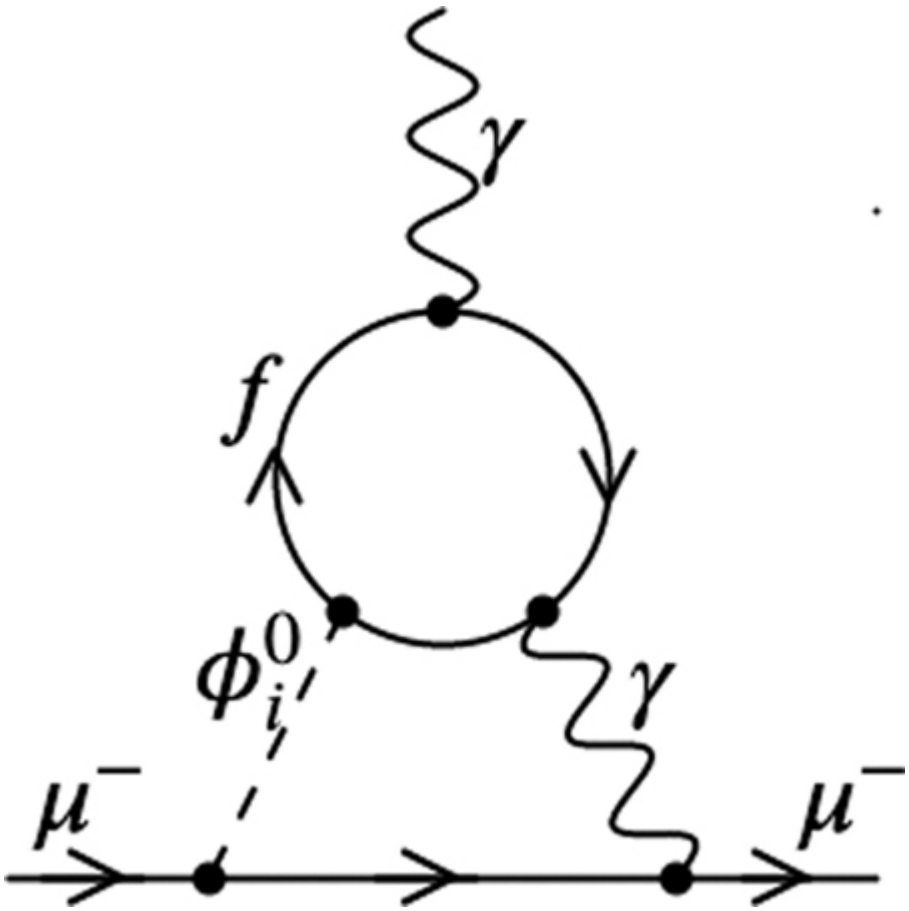

Figure 2.2 Barr-Zee two-loop Feynman diagrams for the muon $g-2$.

The dominant two-loop Barr-Zee contribution is:

$$\Delta a_\mu^{\rm BZ} = \frac{G_F\,\alpha_{\rm em}}{4\sqrt{2}\pi^3} m_\mu^2 \sum_{i,f} N_c^f Q_f^2\, \xi_\mu^i \xi_f^i\, \frac{m_f^2}{M_i^2}\, g_i\left(\frac{m_f^2}{M_i^2}\right),$$

(2.42)

where $i = h, H, A$, and Q_f, m_f, N_c^f are the electric charge, mass, and color factor of the loop fermion, respectively. The loop functions are:

$$g_{h,H}(x) \;= \int_0^1 dx \frac{2x(1-x)-1}{x(1-x)-x} \ln\left[\frac{x(1-x)}{x}\right],$$

(2.43)

$$g_A(x) \;= \int_0^1 dx \frac{1}{x(1-x)-x} \ln\left[\frac{x(1-x)}{x}\right].$$

(2.44)

The pseudoscalar A yields a positive contribution to Δa_μ, while the CP-even scalars h,H give negative ones. Thus, a light pseudoscalar with enhanced couplings to leptons, particularly in Type-II 2HDM with large $\tan\beta$, can provide a viable explanation for the observed anomaly.

2.5 INERT HIGGS DOUBLET

Within the framework of the 2HDM, the Inert Higgs Doublet Model (IHDM) arises when one of the Higgs doublets, typically denoted as Φ_1, does not acquire a VEV, while the second doublet Φ_2 does. This leads to the vacuum structure:

$$\langle \Phi_1 \rangle = \begin{pmatrix} 0 \\ 0 \end{pmatrix}, \quad \langle \Phi_2 \rangle = \begin{pmatrix} 0 \\ v \end{pmatrix}.$$

(2.45)

As a result, Φ_2 is responsible for electroweak symmetry breaking and generates masses for the SM particles, whereas Φ_1 remains inert: it does not participate in symmetry breaking nor couple to fermions at tree level.

The inert nature of Φ_1 is ensured by imposing a discrete $\mathbb{Z}_2$ symmetry under which $\Phi_1 \to -\Phi_1$, while all SM fields and Φ_2 remain even. This symmetry forbids Φ_1 from acquiring a VEV and ensures that its components interact only in pairs, preventing tree-level mixing with Φ_2 [61].

After electroweak symmetry breaking, the doublets are parameterized as:

$$\Phi_1 = \begin{pmatrix} H^+ \\ \frac{1}{\sqrt{2}}(S + iA) \end{pmatrix}, \quad \Phi_2 = \begin{pmatrix} G^+ \\ \frac{1}{\sqrt{2}}(v + h + iG^0) \end{pmatrix},$$

where G^+ and G^0 are the Goldstone bosons absorbed by the W^+ and Z bosons, respectively. The fields S, A, and $H^\pm$ originating from Φ_1 are physical scalars, which are stabilized by the unbroken $\mathbb{Z}_2$ symmetry and thus become potential DM candidates.

The scalar potential, constrained by the exact $\mathbb{Z}_2$ symmetry (which forbids the $m_{12}^2 \Phi_1^\dagger \Phi_2$ term), takes the form:

$$
\begin{aligned}
V \quad &= \mu_1^2|\Phi_1|^2 + \mu_2^2|\Phi_2|^2 + \lambda_1|\Phi_1|^4 + \lambda_2|\Phi_2|^4 + \lambda_3|\Phi_1|^2|\Phi_2|^2 \\
&\quad + \lambda_4|\Phi_1^\dagger \Phi_2|^2 + \frac{\lambda_5}{2}\left[(\Phi_1^\dagger \Phi_2)^2 + \text{h.c.}\right].
\end{aligned}
\tag{2.46}
$$

After minimizing the potential, the physical scalar masses are:

$$
m_h^2 \quad = 2\lambda_2 v^2,
\tag{2.47}
$$

$$
m_S^2 \quad = \mu_1^2 + \frac{1}{2}(\lambda_3 + \lambda_4 + \lambda_5)v^2 = \mu_1^2 + \lambda_L v^2,
\tag{2.48}
$$

$$
m_A^2 \quad = \mu_1^2 + \frac{1}{2}(\lambda_3 + \lambda_4 - \lambda_5)v^2 = \mu_1^2 + \lambda_A v^2,
\tag{2.49}
$$

$$
m_{H^\pm}^2 \quad = \mu_1^2 + \frac{1}{2}\lambda_3 v^2,
\tag{2.50}
$$

where $\lambda_{L,A} = \frac{1}{2}(\lambda_3 + \lambda_4 \pm \lambda_5)$. The model's independent parameters can be expressed as $\{m_h, m_S, m_A, m_{H^\pm}, \lambda_2, \lambda_L\}$, with the DM candidate identified as the lighter neutral scalar between S and A. Here, we assume the CP-odd scalar A is the lightest and thus serves as the DM candidate.

Assuming a standard thermal history of the Universe, the relic abundance of inert scalar DM is determined by its annihilation cross-sections into SM final states, including:

$$
\begin{aligned}
&AA \to f\bar{f} \quad (f = t, b, c, \tau, \mu), \\
&AA \to W^+W^-,\, ZZ,\, \gamma\gamma,\, \gamma Z, \\
&AA \to H^+H^-.
\end{aligned}
$$

For $m_A < m_{W,Z}$, three- and four-body final states from off-shell vector bosons (VV^* and V^*V^*, with $V = W, Z$) become relevant. The relic density Ωh^2 is obtained by solving the Boltzmann equation, which at freeze-out yields the approximate expression:

$$
\Omega h^2 \approx \frac{1.07 \times 10^9\,\text{GeV}^{-1}}{M_{\text{Pl}}\sqrt{g_*}\,\langle\sigma v\rangle},
$$

(2.51)

where $M_{\rm Pl}$ is the Planck mass, g_* is the effective number of relativistic degrees of freedom, and $\langle \sigma v \rangle$ is the thermally averaged annihilation cross-section. Detailed relic density computations often require numerical tools such as `MicrOMEGAs` [62], ensuring consistency with the latest observational data from Planck:

$$\Omega_{\rm CDM} h^2 = 0.120 \pm 0.001$$

(2.52)

The IHDM thus presents a minimal, well-motivated framework where a stable scalar, protected by an exact symmetry, can account for the observed DM in the Universe, while remaining consistent with current collider and cosmological constraints.

CHAPTER 3

Minimal $B - L$ extension of the Standard Mode

DOI: 10.1201/9781003457701-3

As discussed in Chapter 1, the SM of electroweak and strong interactions has been remarkably successful in accounting for a wide range of experimental observations. Nevertheless, he discovery of non-zero neutrino masses provides direct and compelling evidence for physics BSM. The phenomenon of neutrino oscillations, confirmed by solar and atmospheric neutrino experiments, implies that at least two neutrino species must possess non-zero mass [13, 14].

A particularly well-motivated and minimal extension of the SM that accommodates neutrino masses is based on the enlarged gauge group:

$$SU(3)_C \times SU(2)_L \times U(1)_Y \times U(1)_{B-L},$$

where $B-L$ denotes the difference between baryon (B) and lepton (L) numbers. This extension, commonly referred to as the $B-L$ extended SM (BLSM), is particularly attractive from a theoretical standpoint because it becomes anomaly-free upon the inclusion of three SM singlet fermions, one per generation. These additional fermions are naturally identified as RH neutrinos [63, 64].

In the minimal B-L model, the breaking of the extra $U(1)_{B-L}$ gauge symmetry is achieved via a complex scalar SM-singlet field that develops a VEV at the TeV scale [64]. This gives rise to of an additional neutral gauge boson Z', and a new scalar particle. These new states can lead to observable

signals at the LHC, such as resonant production of Z' bosons or extended Higgs-sector signatures [65, 66].

The minimal $B-L$ model is considered "minimal" in both its scalar and fermion sectors:

- A single additional complex scalar singlet is introduced to spontaneously break the $U(1)_{B-L}$ symmetry.
- Exactly three RH neutrinos, transforming as $\nu_R \sim (1, 1, 0, -1)$, are included to cancel all gauge and gravitational anomalies associated with the extended gauge symmetry.

As we will discuss, this model offers a simple, testable, and elegant framework to explain the origin of neutrino masses via the type-I seesaw mechanism, while predicting new particles accessible at current or near-future collider energies.

3.1 CONSTRUCTING THE BLSM

The particle content of the BLSM includes, in addition to the SM fields, the following new states:

(i) A scalar field χ, which is a SM singlet carrying a $B-L$ charge of $+2$. Its VEV spontaneously breaks the $U(1)_{B-L}$ gauge symmetry.

(ii) Three SM-singlet fermions ν_i $(i = 1, 2, 3)$, each with a $B-L$ charge of -1. These fermions serve a dual purpose: they cancel the $B-L$ gauge anomalies and enable the implementation of the type-I seesaw mechanism for generating light neutrino mass generation.

Table 3.1 summarizes the particle content of the BLSM, along with their charge assignments under the extended gauge group.

TABLE 3.1 The $SU(2)_L \times U(1)_Y$ and $U(1)_{B-L}$ quantum numbers of the particles in the model.

	l	ν_R	e_R	Q	u_R	d_R	ϕ
$SU(2)_L \times U(1)_Y$	$(\mathbf{2}, -1/2)$	$(\mathbf{1}, 0)$	$(\mathbf{1}, -1)$	$(\mathbf{2}, 1/6)$	$(\mathbf{1}, 2/3)$	$(\mathbf{1}, -1/3)$	$(\mathbf{2}, 1/$
$U(1)_{B-L}$	-1	-1	-1	$1/3$	$1/3$	$1/3$	0

The minimal gauge-invariant Lagrangian of the $B-L$ extension of the SM can be written as [64]:

$$\mathscr{L}_{B-L} = \mathscr{L}_{\mathrm{YM}} + \mathscr{L}_f + \mathscr{L}_s + \mathscr{L}_Y,$$

(3.1)

where the Yang-Mills (gauge kinetic) part includes the kinetic terms for all gauge bosons:

$$\begin{aligned}\mathscr{L}_{\mathrm{YM}} \;=\; & -\tfrac{1}{4} G^{\alpha}_{\mu\nu} G^{\mu\nu\alpha} - \tfrac{1}{4} W^{a}_{\mu\nu} W^{\mu\nu a} - \tfrac{1}{4} B_{\mu\nu} B^{\mu\nu} \\ & -\tfrac{1}{4} B'_{\mu\nu} B'^{\mu\nu} - \tfrac{k}{2} B_{\mu\nu} B'^{\mu\nu},\end{aligned}$$

(3.2)

where k is a real parameter representing kinetic mixing between the two Abelian gauge fields. The field strengths are defined as

$$B_{\mu\nu} = \partial_\mu B_\nu - \partial_\nu B_\mu, \quad B'_{\mu\nu} = \partial_\mu B'_\nu - \partial_\nu B'_\mu.$$

(3.3)

The kinetic mixing term can be removed via a suitable field redefinition, leading to canonically normalized field strengths [66]. After diagonalization of the kinetic terms, the most general covariant derivative takes the form:

$$D_\mu = \partial_\mu - i g_S T^\alpha G^\alpha_\mu - i g \tau^a W^a_\mu - i g' Y B_\mu - i(\tilde{g} Y + g'' Y_{B-L}) B'_\mu,$$

(3.4)

where $g^{'}$ and $g^{''}$ are the gauge couplings of $U(1)_Y$ and $U(1)_{B-L}$, respectively, $\tilde{g}$ is a mixing parameter arising from the diagonalization procedure, and Y, Y_{B-L} are the respective charges.

The fermionic part of the Lagrangian is

$$\mathscr{L}_f = \sum_\psi \bar{\psi} i \gamma^\mu D_\mu \psi,$$

(3.5)

where the sum runs over all SM fermions, including the RH neutrinos ν_R, which are necessary for anomaly cancellation and for implementing the seesaw mechanism. The $B-L$ charges are:

$$
\begin{aligned}
Y_{B-L}(q_L, u_R, d_R) &= \frac{1}{3}, \\
Y_{B-L}(\ell_L, e_R, \nu_R) &= -1.
\end{aligned}
$$

The scalar content consists of the usual SM Higgs doublet H and an additional SM-singlet scalar χ, which is charged under $U(1)_{B-L}$ and is responsible for spontaneously breaking the $B-L$ symmetry. The scalar Lagrangian is

$$
\mathscr{L}_s = |D_\mu \phi|^2 + |D_\mu \chi|^2 - V(\phi, \chi),
$$

(3.6)

with the scalar potential

$$
V(\phi, \chi) = m_1^2 \phi^\dagger \phi + m_2^2 \chi^\dagger \chi + \lambda_1 (\phi^\dagger \phi)^2 + \lambda_2 (\chi^\dagger \chi)^2 + \lambda_3 (\chi^\dagger \chi)(\phi^\dagger \phi).
$$

(3.7)

Recall that the scalar field ϕ is a Higgs doublet, and χ is a singlet, with $B-L$ charges of 0 and +2, respectively.

Finally, the Yukawa interactions for quarks and charged leptons are as in the SM:

$$
\mathscr{L}_Y \supset -y_u \bar{q}_L \tilde{H} u_R - y_d \bar{q}_L \phi d_R - y_e \bar{\ell}_L \phi e_R + \text{h.c.}
$$

(3.8)

And for neutrinos, the presence of ν_R allows both Dirac and Majorana mass terms:

$$
\mathscr{L}_Y \supset -y_\nu \bar{\ell}_L \tilde{H} \nu_R - \frac{1}{2} y_M \bar{\nu}_R^c \chi \nu_R + \text{h.c.}
$$

(3.9)

The first term generates a Dirac mass after EW symmetry breaking, while the second provides a Majorana mass for ν_R when χ acquires a VEV, realizing the type-I seesaw mechanism.

3.2 $B-L$ BREAKING, HIGGS AND GAUGE MASSES

The spontaneous breaking of the $B-L$ symmetry proceeds analogously to electroweak symmetry breaking. It is triggered by a non-vanishing VEV of a scalar field that is a singlet under the SM gauge group but charged under $U(1)_{B-L}$. In this setup, the Higgs sector consists of:

- A complex $SU(2)_L$ singlet scalar field, $\chi \sim (1,1,0,2)$, responsible for breaking the $U(1)_{B-L}$ symmetry, and
- The usual SM Higgs doublet, $\phi \sim (1,2,1,0)$, which breaks the $SU(2)_L \times U(1)_Y$ symmetry down to $U(1)_{\text{em}}$.

The most general renormalizable scalar potential involving both fields can be written as:

$$V(\phi,\chi) = m_1^2\,\phi^\dagger\phi + m_2^2\,\chi^\dagger\chi + \begin{pmatrix}\phi^\dagger\phi & \chi^\dagger\chi\end{pmatrix}\begin{pmatrix}\lambda_1 & \frac{\lambda_3}{2}\\ \frac{\lambda_3}{2} & \lambda_2\end{pmatrix}\begin{pmatrix}\phi^\dagger\phi\\ \chi^\dagger\chi\end{pmatrix}. \tag{3.10}$$

As in the SM, for the potential to be bounded from below, the quartic terms must satisfy positivity conditions. This requirement translates into the following stability conditions:

$$\lambda_1, \lambda_2 \quad > 0, \tag{3.11}$$

$$4\lambda_1\lambda_2 - \lambda_3^2 \quad > 0. \tag{3.12}$$

To achieve spontaneous symmetry breaking with non-zero VEVs v and v', the mass-squared parameters must satisfy $m_1^2 < 0$ and $m_2^2 < 0$. Minimizing the potential with respect to the fields yields:

$$\frac{\partial V}{\partial \phi} = 0 \quad \Rightarrow m_1^2 + 2\lambda_1\phi^\dagger\phi + \lambda_3\chi^\dagger\chi = 0, \tag{3.13}$$

$$\frac{\partial V}{\partial \chi} = 0 \quad \Rightarrow m_2^2 + 2\lambda_2\chi^\dagger\chi + \lambda_3\phi^\dagger\phi = 0. \tag{3.14}$$

Solving these equations leads to the VEVs [64]:

$$v^2 = \frac{-4\lambda_2 m_1^2 + 2\lambda_3 m_2^2}{4\lambda_1\lambda_2 - \lambda_3^2}, \tag{3.15}$$

$$v'^2 = \frac{-4\lambda_1 m_2^2 + 2\lambda_3 m_1^2}{4\lambda_1\lambda_2 - \lambda_3^2}. \tag{3.16}$$

The vacuum configuration is taken to be:

$$\langle\phi\rangle = \frac{1}{\sqrt{2}}\begin{pmatrix}0\\ v\end{pmatrix}, \quad \langle\chi\rangle = \frac{v'}{\sqrt{2}}. \tag{3.17}$$

Since the denominators in Eqs. (3.15) and (3.16) are positive by Eq. (3.12), the numerators must also be positive to ensure real VEVs:

$$-2\lambda_2 m_1^2 + \lambda_3 m_2^2 > 0, \qquad -2\lambda_1 m_2^2 + \lambda_3 m_1^2 > 0. \tag{3.18}$$

These inequalities imply that both $m_1^2, m_2^2 > 0$ are not allowed, regardless of the sign of λ_3. Scenarios with mixed signs, such as $m_1^2 > 0, m_2^2 < 0$, require $\lambda_3 < 0$. For $m_1^2, m_2^2 < 0$, both signs of λ_3 are permitted. In the decoupling limit $\lambda_3 \to 0$, the two sectors become independent, and v^2 reduces to the familiar SM expression. Combining Eqs. (3.15) and (3.16), one can express v'^2 in terms of v:

$$v'^2 = \frac{-2(m_1^2 + \lambda_1 v^2)}{\lambda_3}. \tag{3.19}$$

This relation shows that if $v' \gg v$, then a fine-tuned cancellation between $\lambda_3 v'^2$ and $2m_1^2$ is needed to obtain the correct electroweak scale $v \approx 246\,\text{GeV}$. To avoid such fine-tuning, the $B-L$ symmetry should be broken at a relatively low scale, typically $v' \sim \mathcal{O}(1)\,\text{TeV}$. We assume that the singlet VEV $v^{'}$ is larger than the doublet VEV v, i.e.,

$$|\langle\chi\rangle| = \frac{v'}{\sqrt{2}} \gg |\langle\phi^0\rangle| = \frac{v}{\sqrt{2}}.$$

It is important to note that the scale $v^{'}$ is not fixed a priori. However, the mass of the $U(1)_{B-L}$ gauge boson B'_{μ}, as well as the masses of the right-handed neutrinos, depend directly on $v^{'}$. Thus, experimental bounds on extra neutral gauge bosons can be used to set lower limits on the $B-L$ breaking scale.

3.2.1 Higgs Masses

To determine the scalar mass spectrum, we expand the potential (3.7) around the VEVs, given in (3.15) and (3.16). Working in the unitary gauge, the scalar fields can be written as:

$$\phi(x) = \begin{pmatrix} 0 \\ \frac{v+h_1(x)}{\sqrt{2}} \end{pmatrix}, \quad \chi(x) = \frac{v' + h_2(x)}{\sqrt{2}}.$$

(3.20)

The scalar potential then becomes:

$$\begin{aligned} V(h_1, h_2) \quad &= \lambda_1 v^2 h_1^2 + \lambda_2 v'^2 h_2' 2 + \lambda_3 v v' h_1 h_2' + \frac{\lambda_3}{2}(v' h_1^2 h_2 + v h_1 h_2^2) \\ &+ \lambda_1 v h_1^3 + \lambda_2 v' h_2^3 + \frac{\lambda_1}{4} h_1^4 + \frac{\lambda_2}{4} h_2^4. \end{aligned}$$

(3.21)

The mass terms are given by the quadratic part of the potential:

$$\frac{1}{2} M^2(h_1, h_2) = \begin{pmatrix} h_1 & h_2 \end{pmatrix} \begin{pmatrix} \lambda_1 v^2 & \frac{\lambda_3}{2} v v' \\ \frac{\lambda_3}{2} v v' & \lambda_2 v'^2 \end{pmatrix} \begin{pmatrix} h_1 \\ h_2 \end{pmatrix}.$$

(3.22)

This matrix is diagonalized by an orthogonal transformation:

$$\begin{pmatrix} h \\ H \end{pmatrix} = \begin{pmatrix} \cos\theta & -\sin\theta \\ \sin\theta & \cos\theta \end{pmatrix} \begin{pmatrix} h_1 \\ h_2 \end{pmatrix},$$

(3.23)

where the mixing angle θ is defined as:

$$\tan 2\theta = \frac{|\lambda_3| v v'}{\lambda_1 v^2 - \lambda_2 v'^2}.$$

(3.24)

The masses of the physical Higgs bosons h and H are:

$$m_{h,H}^2 = \lambda_1 v^2 + \lambda_2 v'^2 \mp \sqrt{(\lambda_1 v^2 - \lambda_2 v'^2)^2 + \lambda_3^2 v^2 v'^2}.$$

(3.25)

Here, h corresponds to the SM-like Higgs and H is the heavy Higgs associated with the $B-L$ breaking sector. The parameter λ_3 controls the mixing between the two Higgs states [65]. In the limit $\lambda_3 \to 0$ or $v' \gg v$, the mixing vanishes, and we recover the SM Higgs mass $m_h = \sqrt{2\lambda_1} v$ and the $B-L$ Higgs mass $m_H = \sqrt{2\lambda_2} v'$. However, for non-zero λ_3 and moderate v', the SM-like Higgs mass receives corrections and can be lighter than in the pure SM case, which has important implications for Higgs phenomenology [67].

3.2.2 Gauge Sector and Mass Mixing

The gauge boson masses arise from the scalar kinetic terms after spontaneous symmetry breaking. In this $U(1)_{B-L}$ extension, the charged gauge bosons $W^\pm = (W_\mu^1 \mp i W_\mu^2)/\sqrt{2}$ acquire their standard masses $M_{W^\pm} = g v/2$, unaffected by the Abelian extension.

The neutral gauge bosons, however, mix due to the extra $U(1)_{B-L}$ symmetry. In the unitary gauge, the scalar kinetic terms yield:

$$\begin{aligned}\mathscr{L}_{\text{scalar}}^{\text{kin}} &= \frac{1}{2}\partial^\mu h_1\, \partial_\mu h_1 + \frac{1}{8}(h_1 + v)^2 \Big[g^2 |W_1^\mu - i W_2^\mu|^2 + (g W_3^\mu - g' B^\mu \\ &\quad - \tilde{g} B'^\mu)^2 \Big] + \frac{1}{2}\partial^\mu h_2\, \partial_\mu h_2 + \frac{1}{2}(h_2 + v')^2 (2 g'' B'^\mu)^2,\end{aligned}$$

(3.26)

In the basis (B^μ, W_3^μ, B'^μ), the neutral gauge boson mass matrix is:

$$\mathscr{M}^2 = \frac{v^2}{2} \begin{pmatrix} g'^2 & -g g' & g' \tilde{g} \\ -g g' & g^2 & -g \tilde{g} \\ g' \tilde{g} & -g \tilde{g} & \tilde{g}^2 + \left(\frac{4 v' g''}{v}\right)^2 \end{pmatrix}.$$

(3.27)

Applying the electroweak rotation:

$$R_{\mathrm{EW}}(\theta_w) = \begin{pmatrix} \cos\theta_w & \sin\theta_w & 0 \\ -\sin\theta_w & \cos\theta_w & 0 \\ 0 & 0 & 1 \end{pmatrix},$$

(3.28)

we isolate the massless photon and obtain the 2×2 submatrix for Z and $Z^{'}$. The physical eigenstates are:

$$\begin{pmatrix} A^{\mu} \\ Z^{\mu} \\ Z^{\prime\mu} \end{pmatrix} = \begin{pmatrix} \cos\theta_w & \sin\theta_w & 0 \\ -\sin\theta_w\cos\theta^{\prime} & \cos\theta_w\cos\theta^{\prime} & \sin\theta^{\prime} \\ \sin\theta_w\sin\theta^{\prime} & -\cos\theta_w\sin\theta^{\prime} & \cos\theta^{\prime} \end{pmatrix} \begin{pmatrix} B^{\mu} \\ W_3^{\mu} \\ B^{\prime\mu} \end{pmatrix},$$

(3.29)

where the mixing angle $\theta^{'}$ satisfies:

$$\tan 2\theta^{\prime} = \frac{2\tilde{g}\sqrt{g^2+g^{\prime 2}}}{\tilde{g}^2 + \left(\frac{4v^{\prime}g^{\prime\prime}}{v}\right)^2 - (g^2+g^{\prime 2})}.$$

(3.30)

The physical masses are:

$$M_A \quad = 0,$$

(3.31)

$$M_Z \quad = \frac{v\sqrt{g^2+g^{\prime 2}}}{2}\left[\frac{1}{2}\left(1 + \frac{\tilde{g}^2 + \left(\frac{4v^{\prime}g^{\prime\prime}}{v}\right)^2}{g^2+g^{\prime 2}}\right) - \frac{\tilde{g}}{s_{2\theta^{\prime}}\sqrt{g^2+g^{\prime 2}}}\right],$$

(3.32)

$$M_{Z^{\prime}} \quad = \frac{v\sqrt{g^2+g^{\prime 2}}}{2}\left[\frac{1}{2}\left(1 + \frac{\tilde{g}^2 + \left(\frac{4v^{\prime}g^{\prime\prime}}{v}\right)^2}{g^2+g^{\prime 2}}\right) + \frac{\tilde{g}}{s_{2\theta^{\prime}}\sqrt{g^2+g^{\prime 2}}}\right],$$

(3.33)

where

$$s_{2\theta'} = \frac{2\tilde{g}\sqrt{g^2+g'^2}}{\left(\tilde{g}^2 + \left(\frac{4v'g''}{v}\right)^2 - g^2 - g'^2\right)^2 + (2\tilde{g})^2}.$$

(3.34)

In the limit $\tilde{g} \to 0$, corresponding to the pure $B-L$ model, the mixing vanishes ($\theta' = 0$), and one recovers the SM result $M_Z = 1/2v\sqrt{g^2+g'^2}2$. We adopt $\tilde{g} = 0$ in what follows, consistent with experimental limits on Z--Z' mixing, which require it to be less than 10^{-3} [68].

3.3 NEUTRINO MASSES IN THE BLSM

In this section, we analyze neutrino masses and mixing in the $B-L$ extension of the SM, where the neutrino masses arise through a TeV-scale seesaw mechanism [64]. After $U(1)_{B-L}$ symmetry breaking, the field χ can be shifted around its VEV:

$$\chi = \frac{1}{\sqrt{2}}(h_2 + v').$$

The term $\frac{1}{2}y_M\overline{(\nu_R)^c}\chi\nu_R$ leads to a right-handed neutrino mass:

$$M_R = \frac{1}{2\sqrt{2}}y_M v'.$$

Similarly, after electroweak symmetry breaking, the field ϕ can be shifted as:

$$\phi = \begin{pmatrix} 0 \\ \frac{h_1+v}{\sqrt{2}} \end{pmatrix},$$

giving rise to a Dirac neutrino mass term:

$$m_D = \frac{1}{\sqrt{2}}y_\nu v.$$

Thus, the mass matrix for the left- and right-handed neutrinos is:

$$\mathscr{M} = \begin{pmatrix} 0 & m_D \\ m_D^T & M_R \end{pmatrix}.$$

The masses of the light and heavy neutrinos are given by diagonalizing this mass matrix:

$$m_{\nu_\ell} \simeq m_D M_R^{-1} m_D^T, \quad m_{\nu_H} \simeq M_R.$$

This is the seesaw mechanism, where large M_R results in very light neutrino masses, m_{ν_ℓ}, of the order 10^{-2} eV.

In the usual seesaw mechanism, M_R is typically assumed to be of the order of the Planck scale, $\sim 10^{14}$ GeV, to accommodate a Dirac neutrino mass m_D of order 100 GeV. However, there is no direct evidence that such a large scale is required, and a "low scale seesaw" with $M_R \sim$ TeV is an acceptable alternative, especially when Dirac neutrino masses are small, of order 10^{-4} GeV.

A commonly used parametrization for the Dirac neutrino mass matrix is [69]:

$$m_D = U_{PMNS} \sqrt{m_{\nu_\ell}^{\text{diag}}} R \sqrt{M_R},$$

where $m_{\nu_\ell}^{\text{diag}}$ is the diagonal light neutrino mass matrix, U_{PMNS} is the lepton mixing matrix, and R is an orthogonal matrix parametrized by three complex angles. A possible parametrization for R is:

$$R = \begin{pmatrix} c_2 c_1 & s_1 c_2 & s_2 \\ -s_1 c_3 - c_1 s_2 s_3 & c_1 c_3 - s_1 s_2 s_3 & s_1 c_2 \\ s_1 s_3 - c_3 s_2 c_1 & -c_1 s_3 - s_1 s_2 c_3 & c_3 c_2 \end{pmatrix},$$

where $c_i = \cos(\theta_i)$ and $s_i = \sin(\theta_i)$, for $i = 1, 2, 3$.

3.4 $Z^{'}$ GAUGE BOSON IN THE BLSM

The Lagrangian describing the dynamics and interactions of the additional $U(1)_{B-L}$ gauge boson, denoted by $Z^{'}$, is given by:

$$\begin{aligned} \mathscr{L}_{Z'} &= -\frac{1}{4} Z'_{\mu\nu} Z'^{\mu\nu} + \frac{1}{2} M_{Z'}^2 Z'_\mu Z'^\mu + 2 g''^2 Z'_\mu Z'^\mu \chi^2 + 4 g''^2 v' \chi Z'_\mu Z'^\mu \\ &\quad - g'' J_\mu^{B-L} Z'^\mu, \end{aligned}$$

(3.35)

where the $B-L$ current is

$$J_\mu^{B-L} = \frac{1}{3}\bar{u}\gamma_\mu u + \frac{1}{3}\bar{d}\gamma_\mu d - \bar{e}\gamma_\mu e - \bar{\nu}\gamma_\mu \nu.$$

(3.36)

Experimental constraints from LEP II and LHC searches place a lower bound on the Z' mass in $B-L$ models [70]. These constraints typically yield

$$\frac{M_{Z'}}{g''} \gtrsim 6\,\text{TeV},$$

(3.37)

implying a scale for breaking symmetry $v' \sim \mathcal{O}(\text{TeV})$, since $M_{Z'} = 2g''v'$. Here, the electroweak scale remains $v \simeq 246\,\text{GeV}$.

The interactions of the Z' boson with SM fermions are governed by their $B-L$ charges:

$$\mathscr{L}_{\text{int}}^{Z'} = \sum_f g'' Y_{B-L}^f \, Z'_\mu \, \bar{f}\gamma^\mu f.$$

(3.38)

In this minimal $B-L$ model, tree-level Z–Z' mixing is absent, and Z' couples directly to SM fermions via their $B-L$ quantum numbers [64]. The partial decay widths of the Z' boson are approximately given by:

$$\Gamma(Z' \to \ell^+\ell^-) \simeq \frac{(g'' Y_{B-L}^\ell)^2}{24\pi} M_{Z'},$$

(3.39)

$$\Gamma(Z' \to q\bar{q}) \simeq \frac{(g'' Y_{B-L}^q)^2}{8\pi} M_{Z'} \left(1 + \frac{\alpha_s}{\pi}\right),$$

(3.40)

$$\Gamma(Z' \to t\bar{t}) \simeq \frac{(g'' Y_{B-L}^t)^2}{8\pi} M_{Z'} \left(1 - \frac{m_t^2}{M_{Z'}^2}\right)\sqrt{1 - \frac{4m_t^2}{M_{Z'}^2}} \left(1 + \frac{\alpha_s}{\pi}\right).$$

(3.41)

As shown in Fig. 3.1, the leptonic branching ratio of the Z' boson is improved relative to its hadronic decays. This is due to $|Y^{\ell}_{B-L}| = 3|Y^{q}_{B-L}|$, leading to:

$$\mathrm{BR}(Z' \to \ell^+\ell^-) \simeq 20\%, \quad \text{versus} \quad \mathrm{BR}(Z \to \ell^+\ell^-) \simeq 3\%.$$

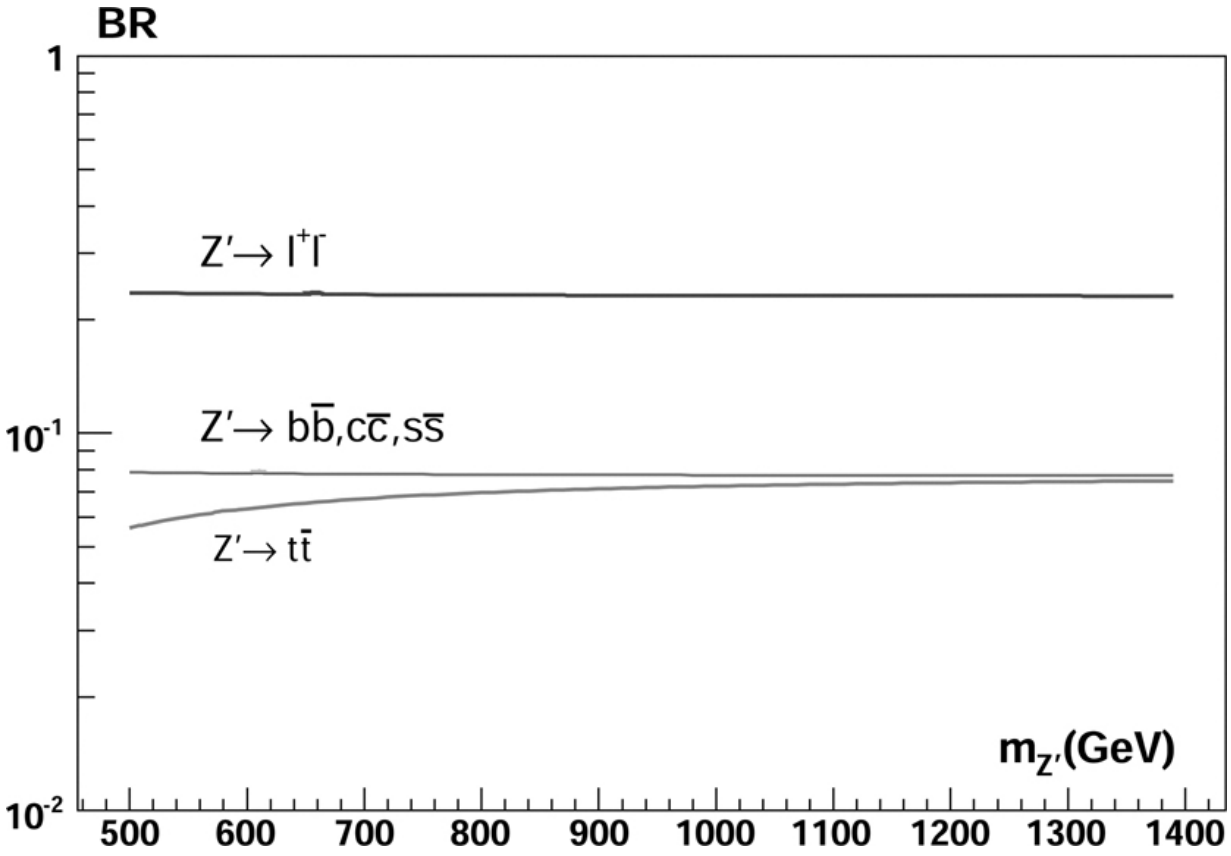

Figure 3.1 Branching ratios of the Z' boson as functions of $M_{Z'}$. Figure adapted from [65]. ⏎

Hence, the clean di-lepton signal makes Z' a promising early discovery channel at the LHC [64, 65, 71].

3.5 BLSM WITH INVERSE SEESAW MECHANISM

In this section, we review the TeV-scale $B-L$ extension of the SM incorporating the Inverse Seesaw (ISS) Mechanism, as proposed in Ref. [72]. The model is based on the extended gauge group

$SU(3)_C \times SU(2)_L \times U(1)_Y \times U(1)_{B-L}$, where the $U(1)_{B-L}$ symmetry is spontaneously broken by a SM singlet scalar field χ carrying a $B-L$ charge of -1. This breaking gives rise to a new neutral gauge boson Z'. To ensure anomaly cancellation, the model introduces three RH neutrinos ν_{R_i}, each with a $B-L$ charge of -1. In order to implement the ISS mechanism, the model also includes three additional SM-singlet fermions S_1 with $B-L$ charge -2, and three fermions S_2 with charge $+2$. The complete set of $B-L$ charge assignments for the fermions and scalar fields is summarized in Table 3.2.

TABLE 3.2 $B-L$ quantum numbers of fermions and Higgs partic

Particle	Q	u_R	d_R	L	e_R	ν_R	ϕ	χ	S_1	S
Y_{B-L}	$1/3$	$1/3$	$1/3$	-1	-1	-1	0	-1	-2	+

The relevant part of the Lagrangian is given by:

$$\begin{aligned}\mathscr{L}_{B-L} &= -\frac{1}{4}B'_{\mu\nu}B'^{\mu\nu} + i\overline{\ell_L}D_\mu\gamma^\mu\ell_L + i\overline{e_R}D_\mu\gamma^\mu e_R + i\overline{\nu_R}D_\mu\gamma^\mu\nu_R \\ &\quad + i\overline{S_1}D_\mu\gamma^\mu S_1 + i\overline{S_2}D_\mu\gamma^\mu S_2 + (D^\mu\phi)^\dagger D_\mu\phi + (D^\mu\chi)^\dagger D_\mu\chi \\ &\quad - V(\phi,\chi) - \left(y_e\overline{\ell_L}\phi e_R + y_\nu\overline{\ell_L}\tilde{\phi}\nu_R + y_S\overline{(\nu_R)^c}\chi S_2 + \text{h.c.}\right) \\ &\quad - \frac{1}{M^3}\overline{(S_1)^c}\chi^{\dagger 4}S_1 - \frac{1}{M^3}\overline{(S_2)^c}\chi^4 S_2,\end{aligned} \tag{3.42}$$

where $B'_{\mu\nu} = \partial_\mu B'_\nu - \partial_\nu B'_\mu$ is the field strength of $U(1)_{B-L}$, and D_μ is the covariant derivative. The last two terms in the Lagrangian are non-renormalizable and are required for generating small masses for S_1 and S_2 at the TeV scale, essential for the ISS.

After $B-L$ symmetry breaking, the Z' gauge boson acquires the mass:

$$M_{Z'} = g''v' \quad \text{with} \quad v' \sim \mathscr{O}(1\,\text{TeV}), \tag{3.43}$$

where $v' = \langle\chi\rangle/\sqrt{2}$ is the vacuum expectation value (VEV) of the χ field. The constraints from LEP II on $Z-Z'$ mixing lead to $M_{Z'}/g'' > 6$ TeV

[73].

The neutrino mass terms arising from the Yukawa interactions are:

$$\mathscr{L}_m^\nu = m_D \overline{\nu_L} \nu_R + M_R \overline{(\nu_R)^c} S_2 + \text{h.c.},$$

(3.44)

where $m_D = \frac{1}{\sqrt{2}} y_\nu v$ and $M_R = \frac{1}{\sqrt{2}} y_S v'$. These terms give rise to the neutrino mass matrix in the flavor basis:

$$\mathscr{M}_\nu = \begin{pmatrix} 0 & m_D & 0 \\ m_D^T & 0 & M_R \\ 0 & M_R^T & \mu_s \end{pmatrix},$$

(3.45)

where $\mu_s \sim 10^{-10}$ GeV is the Majorana mass term for S_2, and M_R is of order the TeV scale.

The diagonalization of the neutrino mass matrix leads to the light neutrino masses:

$$m_{\nu_\ell} = m_D M_R^{-1} \mu_s (M_R^T)^{-1} m_D^T.$$

(3.46)

Thus, the light neutrino masses can be of order eV, with a TeV-scale M_R if $\mu_s \ll M_R$. The heavy neutrino physics in this model can be probed at the LHC [64].

CHAPTER 4

Left-Right Symmetric Model

DOI: 10.1201/9781003457701-4

One of the most well-motivated extensions of the SM is the Left-Right Symmetric Model (LRSM). Originally introduced by Pati and Salam in 1974 [74], the LRSM was further developed and analyzed in detail by Mohapatra and Senjanović [22, 75]. These models provide a natural framework for addressing parity violation in weak interactions, as well as the origin of neutrino masses via the seesaw mechanism.

The LRSM is based on the extended gauge group:

$$SU(3)_C \times SU(2)_L \times SU(2)_R \times U(1)_{B-L}. \tag{4.1}$$

At low energies, this symmetry is spontaneously broken down to the SM gauge group, and eventually to electromagnetism. The symmetry breaking proceeds in two stages:

$$SU(2)_L \times SU(2)_R \times U(1)_{B-L} \longrightarrow SU(2)_L \times U(1)_Y \longrightarrow U(1)_{\mathrm{EM}},$$

where the electromagnetic charge operator is given by a generalized Gell-Mann–Nishijima relation:

$$Q = T_L^3 + T_R^3 + \frac{1}{2}(B - L). \tag{4.2}$$

This expression emerges naturally from the symmetry-breaking sequence in which the gauge group $SU(2)_R \times U(1)_{B-L}$ reduces to the SM hypercharge group $U(1)_Y$. The hypercharge itself is defined as a specific linear combination of the right-handed isospin and the $B - L$ quantum number. When substituted into the conventional expression for electric charge, this leads directly to the above generalized Gell-Mann–Nishijima relation. This formulation not only reproduces the correct electric charges for all SM fermions but also illustrates the consistent embedding of hypercharge within the extended gauge symmetry of the LRSM.

Like the SM, the LRSM includes strong interactions via the $SU(3)_C$ gauge group. However, its weak interaction sector is extended to $SU(2)_L \times SU(2)_R \times U(1)_{B-L}$, which implies the existence of additional heavy gauge bosons. In particular, the LRSM predicts two charged right-handed gauge bosons $W_R^{\pm}$ and a neutral gauge boson Z_R, in addition to the SM gauge bosons.

The phenomenology of the LRSM strongly depends on the scalar (Higgs) sector responsible for symmetry breaking. Various choices for the scalar content, such as bidoublets, triplets, or doublets under $SU(2)_{L,R}$, lead to different variants of the model with distinct features. These choices impact not only the mass spectrum of gauge and scalar bosons but also the nature of neutrino masses (type-I, type-II, or hybrid seesaw mechanisms), flavor structure, and potential collider signatures.

4.1 CONVENTIONAL LEFT-RIGHT MODEL

In the LRSM, RH fermions are grouped into doublets under $SU(2)_R$, and the $B - L$ quantum number plays a crucial role in anomaly cancellation and neutrino mass generation. The spontaneous symmetry breaking of $SU(2)_R \times U(1)_{B-L}$ to $U(1)_Y$ is achieved via a triplet scalar field Δ_R. The field content of this model and the associated quantum numbers are given in Table 4.1. Contrary to the SM, all RH components of fermion fields transform as doublets under $SU(2)_R$, reflecting the left-right symmetric nature of the model.

TABLE 4.1 Field content of the LRSM and respective quantum numbers.

Fields	**Components**	$SU(2)_L \times SU(2)_R \times U(1)_{B-L}$

Fields	Components	$SU(2)_L \times SU(2)_R \times U(1)_{B-L}$		
Fermions				
L_L	$\begin{pmatrix} \nu \\ e \end{pmatrix}_L$	2	1	$-\frac{1}{2}$
L_R	$\begin{pmatrix} \nu \\ e \end{pmatrix}_R$	1	2	$-\frac{1}{2}$
Q_L	$\begin{pmatrix} u \\ d \end{pmatrix}_L$	2	1	$+\frac{1}{6}$
Q_R	$\begin{pmatrix} u \\ d \end{pmatrix}_R$	1	2	$+\frac{1}{6}$
Gauge bosons				
W_L	$W_L^{\pm}, W_L^3$	triplet	singlet	singlet
W_R	$W_R^{\pm}, W_R^3$	singlet	triplet	singlet
B	B_μ	singlet	singlet	singlet
Scalars				
Φ	$\begin{pmatrix} \Phi_1^0 & \Phi_1^+ \\ \Phi_2^- & \Phi_2^0 \end{pmatrix}$	2	2	0
Δ_L	$\begin{pmatrix} \frac{\Delta^+}{\sqrt{2}} & \Delta^{++} \\ \Delta^0 & -\frac{\Delta^+}{\sqrt{2}} \end{pmatrix}_L$	3	1	$+1$
Δ_R	$\begin{pmatrix} \frac{\Delta^+}{\sqrt{2}} & \Delta^{++} \\ \Delta^0 & -\frac{\Delta^+}{\sqrt{2}} \end{pmatrix}_R$	1	3	$+1$

The full Lagrangian of the LRSM includes gauge, kinetic, scalar, and Yukawa parts:

$$\mathscr{L}_{\text{LRSM}} = \mathscr{L}_{\text{Gauge}} + \mathscr{L}_{\text{Kinetic}} + \mathscr{L}_{\text{Scalar}} + \mathscr{L}_{\text{Yukawa}}.$$

(4.3)

The gauge kinetic terms for the gauge bosons are

$$\mathscr{L}_{\text{Gauge}} = -\frac{1}{4} G^a_{\mu\nu} G^{a\mu\nu} - \frac{1}{4} W^i_{L\mu\nu} W_L^{i\mu\nu} - \frac{1}{4} W^i_{R\mu\nu} W_R^{i\mu\nu} - \frac{1}{4} V_{\mu\nu} V^{\mu\nu},$$

(4.4)

with field strength tensors:

$$G^a_{\mu\nu} = \partial_\mu G^a_\nu - \partial_\nu G^a_\mu - g_s f^{abc} G^b_\mu G^c_\nu, \tag{4.5}$$

$$W^i_{L\mu\nu} = \partial_\mu W^i_{L\nu} - \partial_\nu W^i_{L\mu} - g_L \epsilon^{ijk} W^j_{L\mu} W^k_{L\nu}, \tag{4.6}$$

$$W^i_{R\mu\nu} = \partial_\mu W^i_{R\nu} - \partial_\nu W^i_{R\mu} - g_R \epsilon^{ijk} W^j_{R\mu} W^k_{R\nu}, \tag{4.7}$$

$$V_{\mu\nu} = \partial_\mu V_\nu - \partial_\nu V_\mu. \tag{4.8}$$

The fermionic kinetic terms and their gauge interactions are encoded as:

$$\begin{aligned} \mathscr{L}_{\text{Kinetic}} = \sum_{j=1}^{3} \big[& \overline{L}_{Lj} i\gamma^\mu D_\mu L_{Lj} + \overline{L}_{Rj} i\gamma^\mu D_\mu L_{Rj} \\ & + \overline{Q}_{Lj} i\gamma^\mu D_\mu Q_{Lj} + \overline{Q}_{Rj} i\gamma^\mu D_\mu Q_{Rj} \big], \end{aligned} \tag{4.9}$$

where the covariant derivatives for the leptons and quarks take the form:

$$D_\mu L_L = \left(\partial_\mu - \frac{i g_L}{2} \sigma \cdot W_{L\mu} + \frac{i g_{BL}}{2} V_\mu \right) L_L, \tag{4.10}$$

$$D_\mu L_R = \left(\partial_\mu - \frac{i g_R}{2} \sigma \cdot W_{R\mu} + \frac{i g_{BL}}{2} V_\mu \right) L_R, \tag{4.11}$$

$$D_\mu Q_L = \left(\partial_\mu - \frac{i g_L}{2} \sigma \cdot W_{L\mu} - \frac{i g_{BL}}{6} V_\mu - i g_s \lambda \cdot G_\mu \right) Q_L, \tag{4.12}$$

$$D_\mu Q_R = \left(\partial_\mu - \frac{i g_R}{2} \sigma \cdot W_{R\mu} - \frac{i g_{BL}}{6} V_\mu - i g_s \lambda \cdot G_\mu \right) Q_R. \tag{4.13}$$

The scalar sector in the LRSM plays a crucial role in the sequential symmetry breaking:

$$SU(2)_L \times SU(2)_R \times U(1)_{B-L} \xrightarrow{\langle \Delta_R \rangle} SU(2)_L \times U(1)_Y \xrightarrow{\langle \Phi \rangle} U(1)_{\rm EM}\,.$$

In addition to breaking the gauge symmetry, the scalar VEVs are responsible for generating particle masses. The electroweak symmetry is broken by the VEV of the bidoublet scalar Φ, giving rise to the masses of SM fermions and gauge bosons, while the heavy masses of the RH gauge bosons W_R, Z_R and RH neutrinos are generated through the VEV of the RH triplet Δ_R.

The gauge-invariant Yukawa interaction $\overline{\psi}_L \Phi \psi_R$ requires that fermions transform as doublets under both $SU(2)_L$ and $SU(2)_R$, and the scalar field Φ transforms as a bidoublet under the extended gauge group. Specifically, Φ is a 2×2 complex matrix with $B - L = 0$, whose columns form doublets under $SU(2)_L$ and rows under $SU(2)_R$. As a result, the VEV of Φ does not break the $U(1)_{B-L}$ symmetry.

To spontaneously break $SU(2)_R \times U(1)_{B-L}$ and reduce the symmetry to that of the SM, an additional scalar field is introduced. This is typically chosen to be a right-handed triplet $\Delta_R \sim (1, 3, +2)$, which acquires a large VEV. For the restoration of discrete parity symmetry at high energies, a left-handed counterpart $\Delta_L \sim (3, 1, +2)$ is also included in the scalar sector [74].

The Lagrangian of scalar fields is given by

$$\mathscr{L}_{\rm Scalar} = \mathscr{L}^{\rm Kin}_{\rm Scalar} - V(\Phi, \Delta_{_L}, \Delta_{_R}),$$

(4.14)

where the kinetic Lagrangian is given by

$$\mathscr{L}^{\rm Kin}_{\rm Scalar} = {\rm Tr}[|D_\mu \Phi|^2] + {\rm Tr}[|D_\mu \Delta_{_L}|^2] + {\rm Tr}[|D_\mu \Delta_{_R}|^2].$$

(4.15)

The most general gauge invariant and renormalizable Higgs potential given as follows [76]:

$$
\begin{aligned}
V(\Phi,\Delta_{_L},\Delta_{_R}) &= -\mu_1^2\mathrm{Tr}(\Phi^\dagger\Phi) - \mu_2^2\mathrm{Tr}(\widetilde{\Phi}^\dagger\Phi + \Phi^\dagger\widetilde{\Phi}) - \mu_3^2\mathrm{Tr}(\Delta_{_L}^\dagger\Delta_{_L} + \Delta_{_R}^\dagger\Delta_{_R}) \\
&+ \lambda_1[\mathrm{Tr}(\Phi^\dagger\Phi)]^2 + \lambda_2\{[\mathrm{Tr}(\widetilde{\Phi}^\dagger\Phi)]^2 + [\mathrm{Tr}(\Phi^\dagger\widetilde{\Phi})]^2\} + \lambda_3\mathrm{Tr}(\widetilde{\Phi}^\dagger\Phi)\mathrm{Tr}(\Phi^\dagger\widetilde{\Phi}) \\
&+ \lambda_4\mathrm{Tr}(\Phi^\dagger\Phi)\mathrm{Tr}(\widetilde{\Phi}^\dagger\Phi + \Phi^\dagger\widetilde{\Phi}) + \rho_1\{[\mathrm{Tr}(\Delta_{_L}^\dagger\Delta_{_L})]^2 + [\mathrm{Tr}(\Delta_{_R}^\dagger\Delta_{_R})]^2\} \\
&+ \rho_2\{\mathrm{Tr}(\Delta_{_L}^\dagger\Delta_{_L}^\dagger)\mathrm{Tr}(\Delta_{_L}\Delta_{_L}) + \mathrm{Tr}(\Delta_{_R}^\dagger\Delta_{_R}^\dagger)\mathrm{Tr}(\Delta_{_R}\Delta_{_R})\} + \rho_3\{\mathrm{Tr}(\Delta_{_L}^\dagger\Delta_{_L}) \\
&\times \mathrm{Tr}(\Delta_{_R}^\dagger\Delta_{_R})\} + \rho_4\{\mathrm{Tr}(\Delta_{_L}\Delta_{_L})\mathrm{Tr}(\Delta_{_R}^\dagger\Delta_{_R}^\dagger) + \mathrm{Tr}(\Delta_{_R}\Delta_{_R})\mathrm{Tr}(\Delta_{_L}^\dagger\Delta_{_L}^\dagger)\} \\
&+ \alpha_1\mathrm{Tr}(\Phi\Phi^\dagger)[\mathrm{Tr}(\Delta_{_L}^\dagger\Delta_{_L} + \Delta_{_R}^\dagger\Delta_{_R})] + \alpha_2\{\mathrm{Tr}(\Phi^\dagger\widetilde{\Phi})\mathrm{Tr}(\Delta_{_L}^\dagger\Delta_{_L}) \\
&+ \mathrm{Tr}(\Phi\widetilde{\Phi}^\dagger)\mathrm{Tr}(\Delta_{_R}^\dagger\Delta_{_R})\} + \alpha_2^*\{\mathrm{Tr}(\Phi^\dagger\widetilde{\Phi})\mathrm{Tr}(\Delta_{_R}^\dagger\Delta_{_R}) + \mathrm{Tr}(\Phi\widetilde{\Phi}^\dagger)\mathrm{Tr}(\Delta_{_L}^\dagger\Delta_{_L})\} \\
&+ \alpha_3\mathrm{Tr}(\Phi\Phi^\dagger\Delta_{_L}\Delta_{_L}^\dagger + \Phi^\dagger\Phi\Delta_{_R}\Delta_{_R}^\dagger) + \beta_1\mathrm{Tr}(\Delta_{_L}^\dagger\Phi\Delta_{_R}\Phi^\dagger + \Delta_{_R}^\dagger\Phi^\dagger\Delta_{_L}\Phi) \\
&+ \beta_2\mathrm{Tr}(\Delta_{_L}^\dagger\widetilde{\Phi}\Delta_{_R}\Phi^\dagger + \Delta_{_R}^\dagger\widetilde{\Phi}^\dagger\Delta_{_L}\Phi)\} + \beta_3\mathrm{Tr}(\Delta_{_L}^\dagger\Phi\Delta_{_R}\widetilde{\Phi}^\dagger + \Delta_{_R}^\dagger\Phi^\dagger\Delta_{_L}\widetilde{\Phi})\},
\end{aligned}
\tag{4.16}
$$

where the conjugate Higgs bidoublet is defined as

$$
\widetilde{\Phi} = \sigma_2\Phi^*\sigma_2 = \begin{pmatrix} \Phi_2^{0*} & -\Phi_2^+ \\ -\Phi_1^- & \Phi_1^{0*} \end{pmatrix},
\tag{4.17}
$$

which transforms in the same way as Φ.

Finally, the Yukawa interactions responsible for fermion masses are given by:

$$
\begin{aligned}
\mathscr{L}_Y \quad &= \overline{Q}_L\left(Y_q\Phi + \tilde{Y}_q\tilde{\Phi}\right)Q_R + \overline{L}_L\left(Y_\ell\Phi + \tilde{Y}_\ell\tilde{\Phi}\right)L_R \\
&\quad + f_L L_L^T C i\sigma_2 \Delta_L L_L + f_R L_R^T C i\sigma_2 \Delta_R L_R + \text{h.c.}
\end{aligned}
\tag{4.18}
$$

Here, $Y_q, \tilde{Y}_q, Y_\ell, \tilde{Y}_\ell$ are Dirac-type Yukawa matrices for quarks and leptons, and f_L, f_R are symmetric Majorana-type couplings for neutrinos. After symmetry breaking, the Lagrangian generates:

- Dirac masses for charged fermions and neutrinos via $\langle\Phi\rangle$,
- Majorana masses for neutrinos via $\langle\Delta_{L,R}\rangle$,

naturally realizing both the type-I and type-II seesaw mechanisms [20]. The LRSM thus provides a compelling framework for addressing open questions in the SM, including the origin of neutrino masses, the nature of parity violation, and new physics at the TeV scale [77].

4.2 SPONTANEOUS SYMMETRY BREAKING IN THE LRSM

The gauge symmetries imply that all gauge bosons and fermions must be massless, thus the symmetry with massive gauge bosons (short-range forces like the weak interaction) must be spontaneously broken. The spontaneous symmetry breaking (SSB) in the LRSM occurs in two stages, and the mechanism is similar to that of the SM. Specifically, it is achieved by the VEV of scalar Higgs multiplets. The symmetry breaking scheme is as follows:

$$SU(2)_L \times SU(2)_R \times U(1)_{B-L} \xrightarrow{\langle \Delta_R \rangle} SU(2)_L \times U(1)_Y, \tag{4.19}$$

at this stage, only the RH scalar Higgs triplet gets a VEV and breaks the LR symmetry down to the electroweak (EW) symmetry. After this stage of symmetry breaking, the physical $W_R^{\pm}$ and Z_R gauge bosons acquire masses through interactions with the right-handed triplet Higgs. Additionally, the hypercharge operator Y appears as a linear combination of the difference between baryon and lepton numbers and the third component of the right-handed isospin:

$$Y = T_R^3 + Q_{B-L}, \tag{4.20}$$

where Q_{B-L} is the generator of the $U(1)_{B-L}$ group, as defined in Eq. (4.2). The values of the new gauge couplings g_R and g_{B-L} are related to the SM hypercharge coupling g_Y by:

$$g_Y = \frac{g_R g_{B-L}}{\sqrt{g_R^2 + g_{B-L}^2}}. \tag{4.21}$$

From the definition of the hypercharge, it follows that $Y(\Delta_R^0) = 0$, ensuring that hypercharge remains an exact symmetry. Note that Δ_R is a singlet under the $SU(2)_L$ gauge group, so it remains an exact symmetry at this stage as well.

The second stage of symmetry breaking further reduces the symmetry, breaking the electroweak group down to electromagnetism, just like in the SM but with an extended Higgs sector. The breaking is achieved by the neutral components of the bidoublet Higgs Φ and the left-handed triplet Higgs Δ_L, which acquire VEVs, as follows:

$$SU(2)_L \times U(1)_Y \xrightarrow{\langle\Phi\rangle,\langle\Delta_L\rangle} U(1)_{\rm EM}. \tag{4.22}$$

Here the neutral components of the bidoublet Higgs and LH triplet get VEVs and break the EW symmetry down to EM. After this stage of symmetry breaking, physical $W^{\pm}_{L\mu}$ and $Z_{L\mu}$ gauge bosons acquire masses. Without loss of generality, the VEVs of the neutral components of the Higgs fields can be written as

$$\langle\Phi\rangle = \frac{1}{\sqrt{2}}\begin{pmatrix} k_1 & 0 \\ 0 & k_2 \end{pmatrix}, \quad \langle\Delta_R\rangle = \frac{1}{\sqrt{2}}\begin{pmatrix} 0 & 0 \\ v_R & 0 \end{pmatrix}, \quad \langle\Delta_L\rangle = \frac{1}{\sqrt{2}}\begin{pmatrix} 0 & 0 \\ v_L & 0 \end{pmatrix}. \tag{4.23}$$

The minimization conditions of the scalar potential $V(k_1, k_2, v_L, v_R)$ with respect to the neutral VEVs yield four equations from the derivatives with respect to k_1, k_2, v_L, and v_R. Solving these, one obtains the following relations among the potential parameters and VEVs:

$$\beta_3 = -\frac{\beta_2 k_1^2 + \beta_1 k_1 k_2 - \rho_{13}^{-} v_L v_R}{k_2^2}, \tag{4.24}$$

$$\mu_3^2 = \frac{1}{2}\big(\alpha_1 k_1^2 + 4\alpha_2 k_1 k_2 + \alpha_{13} k_2^2 + 2\rho_1 (v_L^2 + v_R^2)\big), \tag{4.25}$$

$$v_L v_R = \frac{\beta_2 k_1^2 + \beta_1 k_1 k_2 + \beta_3 k_2^2}{\rho_{13}^{-}}, \tag{4.26}$$

$$v_L^2 + v_R^2 = \frac{1}{2\rho_1}\big(2\mu_3^2 - \alpha_1 k_1^2 - 4\alpha_2 k_1 k_2 - \alpha_{13} k_2^2\big),$$

(4.27)

where the shorthand notations are defined as:

$$\alpha_{13} = \alpha_1 + \alpha_3, \quad \rho_{13}^{-} = 2\rho_1 - \rho_3, \quad v_+^2 = v_L^2 + v_R^2, \quad v_\times^2 = v_L v_R.$$

The expressions for the mass parameters μ_1^2 and μ_2^2 are more involved and are omitted for brevity. In the phenomenologically relevant limit where $v_L \ll k_{1,2} \ll v_R$, the SM VEV is given by

$$\sqrt{k_1^2 + k_2^2} \equiv v \simeq 246\,\text{GeV}.$$

4.2.1 Gauge Boson Masses in the LRSM

After SSB, the gauge bosons masses are generated as follows, from Higgs kinetic term $\text{Tr}|D_\mu \langle \Delta_R \rangle|^2$ one obtains the mass terms:

$$\frac{g_R^2 v_R^2}{2} W_R^{\mu -} W_{R\mu}^{+} + \frac{v_R^2}{2}(g_R W_R^{\mu 3} - g_{BL} V^\mu)(g_R W_{R\mu}^{3} - g_{BL} V_\mu)$$

(4.28)

Defining the mass eigenstates via:

$$W_R^{\pm} = \frac{W_R^1 \mp i W_R^2}{\sqrt{2}}, \quad \begin{pmatrix} Z_R \\ B \end{pmatrix} = \begin{pmatrix} \cos\varphi & -\sin\varphi \\ \sin\varphi & \cos\varphi \end{pmatrix} \begin{pmatrix} W_R^3 \\ V \end{pmatrix},$$

(4.29)

where the mixing angle φ is defined as:

$$\sin\varphi = \frac{g_{BL}}{\sqrt{g_R^2 + g_{BL}^2}}, \quad \cos\varphi = \frac{g_R}{\sqrt{g_R^2 + g_{BL}^2}},$$

(4.30)

the massless field B is identified with the hypercharge gauge boson, while Z_R is a heavy neutral boson that decouples at low energies.

In the second stage, the electroweak symmetry is broken by the bidoublet Higgs Φ acquiring a VEV $\langle \Phi \rangle = \text{diag}(k_1, k_2)$ and the left-handed triplet Δ_L developing a small VEV $\langle \Delta_L \rangle = v_L$. The kinetic terms yield masses for the SM gauge bosons:

$$\begin{aligned}\mathrm{Tr}|D_\mu\langle\Phi\rangle|^2 \quad &\supset \frac{v^2}{4}(g_L^2 W_L^+ W_L^- + g_R^2 W_R^+ W_R^-) - \frac{g_L g_R k_1 k_2}{2}(W_L^+ W_R^- + \text{h.c.}) \\ &+ \frac{v^2}{8}(g_L W_L^3 - g_Y B)^2,\end{aligned} \tag{4.31}$$

$$\mathrm{Tr}|D_\mu\langle\Delta_L\rangle|^2 \quad \supset \frac{g_L^2 v_L^2}{2} W_L^+ W_L^- + \frac{v_L^2}{2}(g_L W_L^3 - g_Y B)^2, \tag{4.32}$$

where g_Y is the hypercharge coupling:

$$g_Y = \frac{g_R g_{BL}}{\sqrt{g_R^2 + g_{BL}^2}}. \tag{4.33}$$

Neutral gauge bosons in the LRSM

After diagonalization, the neutral gauge bosons mix via the Weinberg angle θ_W as in the Standard Model:

$$\begin{pmatrix} Z_L \\ A \end{pmatrix} = \begin{pmatrix} \cos\theta_W & -\sin\theta_W \\ \sin\theta_W & \cos\theta_W \end{pmatrix} \begin{pmatrix} W_L^3 \\ B \end{pmatrix}, \tag{4.34}$$

with

$$\sin\theta_W = \frac{g_Y}{\sqrt{g_L^2 + g_Y^2}}, \quad \cos\theta_W = \frac{g_L}{\sqrt{g_L^2 + g_Y^2}}. \tag{4.35}$$

The full neutral gauge boson mass matrix in the basis (W_L^3, W_R^3, V) is given by [20]:

$$M_{V^0}^2 = \frac{1}{4}\begin{pmatrix} g_L^2(4v_L^2 + v^2) & -g_L g_R v^2 & -4 g_L g_{BL} v_L^2 \\ -g_L g_R v^2 & g_R^2(4v_R^2 + v^2) & -4 g_R g_{BL} v_R^2 \\ -4 g_L g_{BL} v_L^2 & -4 g_R g_{BL} v_R^2 & g_{BL}^2(4v_L^2 + 4v_R^2) \end{pmatrix}. \tag{4.36}$$

This matrix can be diagonalized to extract the masses of the physical bosons (Z_L, A, Z_R) by

$$\begin{pmatrix} W^3_{L\mu} \\ W^3_{R\mu} \\ V_\mu \end{pmatrix} = \begin{pmatrix} \dfrac{e}{g_Y} & \dfrac{e}{g_L} & 0 \\ \dfrac{-e g_Y}{g_L\, g_R} & \dfrac{e}{g_R} & \dfrac{g_Y}{g_{BL}} \\ \dfrac{-e g_Y}{g_L\, g_{BL}} & \dfrac{e}{g_{BL}} & \dfrac{-g_Y}{g_R} \end{pmatrix} \begin{pmatrix} Z_{L\mu} \\ A_\mu \\ Z_{R\mu} \end{pmatrix}.$$

(4.37)

The bidoublet Φ induces mixing between the neutral gauge bosons Z_L and Z_R, resulting in the mass-squared matrix in the basis $\{Z_{L\mu}, Z_{R\mu}\}$:

$$M^2_{Z_L Z_R} = \begin{pmatrix} M^0_{LL} & M^0_{LR} \\ M^0_{LR} & M^0_{RR} \end{pmatrix},$$

(4.38)

where the matrix elements depend on the gauge couplings (g_L, g_R, g_{BL}) and the VEVs $(k_{1,2}, v_{L,R})$. The physical states Z and Z' are obtained via a mixing angle ϑ,

$$\tan 2\vartheta = \frac{2M^0_{LR}}{M^0_{LL} - M^0_{RR}}, \quad \begin{pmatrix} Z \\ Z' \end{pmatrix} = \begin{pmatrix} \cos\vartheta & \sin\vartheta \\ -\sin\vartheta & \cos\vartheta \end{pmatrix} \begin{pmatrix} Z_L \\ Z_R \end{pmatrix},$$

(4.39)

with corresponding eigenvalues:

$$M^2_{Z,Z'} = \frac{1}{2}\left(M^0_{LL} + M^0_{RR} \mp \sqrt{(M^0_{LL} - M^0_{RR})^2 + 4(M^0_{LR})^2} \right).$$

(4.40)

In the limit $v_R \gg v$, one finds $Z \simeq Z_L$ and $Z' \simeq Z_R$. Experimental constraints require $\vartheta \lesssim 10^{-3}$ and $M_{Z'} \gtrsim 2$ TeV [78].

Charged Gauge Bosons in the LRSM

The bidoublet Φ, transforming under both $SU(2)_L \times SU(2)_R$, induces mixing between $W_L^\pm$ and $W_R^\pm$ through the mass matrix:

$$M_{V^\pm} = \frac{1}{4}\begin{pmatrix} g_L^2(k_1^2+k_2^2+2v_L^2) & -2g_Lg_Rk_1k_2 \\ -2g_Lg_Rk_1k_2 & g_R^2(k_1^2+k_2^2+2v_R^2) \end{pmatrix}. \tag{4.41}$$

The physical states $W_1^\pm$ and $W_2^\pm$ arise via an orthogonal rotation:

$$\begin{pmatrix} W_1^\pm \\ W_2^\pm \end{pmatrix} = \begin{pmatrix} \cos\xi & e^{-i\omega}\sin\xi \\ -\sin\xi & e^{-i\omega}\cos\xi \end{pmatrix} \begin{pmatrix} W_L^\pm \\ W_R^\pm \end{pmatrix}, \tag{4.42}$$

where ξ is the mixing angle, constrained to $\xi < 10^{-3}$ [79].

Defining $k_1 = v\cos\beta$, $k_2 = v\sin\beta$ with $v = 246$ GeV, the trace and determinant of the matrix are:

$$T^{g^\pm} = \frac{1}{4}\left((g_L^2+g_R^2)v^2 + 2(g_L^2v_L^2+g_R^2v_R^2)\right), \tag{4.43}$$

$$D^{g^\pm} = \frac{1}{16}g_L^2g_R^2\left[(v^2+2v_L^2)(v^2+2v_R^2) - 4v^4\sin^2\beta\cos^2\beta\right]. \tag{4.44}$$

The masses are given by:

$$M^2_{W_1,W_2} = \frac{1}{2}\left(T^{g^\pm} \mp \sqrt{(T^{g^\pm})^2 - 4D^{g^\pm}}\right), \tag{4.45}$$

with

$$\tan 2\xi = \frac{2M_{LR}}{M_{LL}-M_{RR}} \approx \frac{4g_{RL}k_1k_2}{2g_{RL}^2v_R^2 + (g_{RL}^2-1)v^2}$$

and

$$g_{RL} \equiv g_R/g_L.$$

In the limit $\xi \to 0$, the mass eigenstates reduce to:

$$M_{W_L} = \frac{vg_L}{2}, \quad M_{W_R} = \frac{v_Rg_R}{\sqrt{2}}.$$

(4.46)

4.2.2 Fermion Masses in the LRSM

Fermion masses arise from Yukawa couplings to the bidoublets Φ, $\widetilde{\Phi}$, and the triplets $\Delta_{L,R}$:

$$\begin{aligned} -\mathscr{L}_{\text{Yukawa}} \supset \; & \overline{L}_L(y^L\langle\Phi\rangle + \tilde{y}^L\langle\widetilde{\Phi}\rangle)L_R + \overline{Q}_L(y^Q\langle\Phi\rangle + \tilde{y}^Q\langle\widetilde{\Phi}\rangle)Q_R \\ & + iy^M\left(L_L^T C\sigma^2\langle\Delta_L\rangle L_L + L_R^T C\sigma^2\langle\Delta_R\rangle L_R\right) + \text{h.c.} \end{aligned}$$

(4.47)

The Dirac mass matrices for quarks and leptons are given by:

$$M_u = \frac{1}{\sqrt{2}}(y^Q k_1 + \tilde{y}^Q k_2), \quad M_d = \frac{1}{\sqrt{2}}(y^Q k_2 + \tilde{y}^Q k_1),$$

(4.48)

$$M_\nu = \frac{1}{\sqrt{2}}(y^L k_1 + \tilde{y}^L k_2), \quad M_e = \frac{1}{\sqrt{2}}(y^L k_2 + \tilde{y}^L k_1),$$

(4.49)

while the Majorana mass matrices for the left- and right-handed neutrinos are:

$$M_{\nu_L} = \frac{1}{\sqrt{2}} y^M v_L, \quad M_{\nu_R} = \frac{1}{\sqrt{2}} y^M v_R.$$

(4.50)

The charged fermion mass matrices can be diagonalized using biunitary transformations:

$$V_L^{u\dagger} M_u V_R^u = M_u^{\text{diag}}, \quad V_L^{d\dagger} M_d V_R^d = M_d^{\text{diag}}, \quad V_L^{e\dagger} M_e V_R^e = M_e^{\text{diag}}.$$

(4.51)

Neutrino mass terms receive contributions from both Dirac (y^L, $\tilde{y}^L$) and Majorana (y^M) couplings. It is convenient to express them using self-conjugate Majorana spinors [20, 22, 76]:

$$\nu = \frac{\nu_L + \nu_L^c}{\sqrt{2}}, \quad N = \frac{\nu_R^c + \nu_R}{\sqrt{2}}.$$

(4.52)

We also define the Dirac Yukawa coupling as:

$$y_D \equiv \frac{1}{\sqrt{2}} \frac{y^L k_1 + \tilde{y}^L k_2}{v} = \frac{M_\nu}{v},$$

(4.53)

which governs the magnitude of the Dirac-type neutrino mass.

In terms of y_D and y^M, the full neutrino mass matrix in the (ν, N) basis becomes:

$$\begin{pmatrix} \overline{\nu} & \overline{N} \end{pmatrix} \begin{pmatrix} \sqrt{2} y^M v_L & y_D v \\ y_D v & \sqrt{2} y^M v_R \end{pmatrix} \begin{pmatrix} \nu \\ N \end{pmatrix}.$$

(4.54)

For natural values of Yukawa couplings $y^M \sim y_D \sim M_e/v$, and the hierarchy $v_R \gg v \gg v_L$ (required for $M_{W_R} \gg M_{W_L}$), the light and heavy neutrino states become approximate flavor eigenstates with masses given by the seesaw mechanism [76]:

$$m_N \simeq \sqrt{2} y^M v_R, \quad m_\nu \simeq \sqrt{2} \left(y^M v_L - \frac{v^2}{2 v_R} y_D (y^M)^{-1} y_D^T \right).$$

(4.55)

Finally, the light and heavy neutrino mass matrices m_ν and m_N are diagonalized by unitary matrices V_L^ν and V_R^N:

$$V_L^{\nu\dagger} m_\nu V_L^\nu = m_\nu^{\text{diag}}, \quad V_R^{N\dagger} m_N V_R^N = m_N^{\text{diag}}.$$

(4.56)

4.3 ELECTROWEAK INTERACTIONS IN THE LRSM

In the LRSM, the electroweak interactions arise from the covariant derivatives acting on fermion fields in the kinetic Lagrangian:

$$\begin{aligned}\mathscr{L}_{\text{kin}} &= i\sum_{j=1}^{3}\Big(\bar{L}_{Lj}\gamma^{\mu}D_{\mu}L_{Lj} + \bar{L}_{Rj}\gamma^{\mu}D_{\mu}L_{Rj} + \bar{Q}_{Lj}\gamma^{\mu}D_{\mu}Q_{Lj} \\ &\quad + \bar{Q}_{Rj}\gamma^{\mu}D_{\mu}Q_{Rj}\Big),\end{aligned} \tag{4.57}$$

where $L_{L,R}$ and $Q_{L,R}$ are the left- and right-handed lepton and quark doublets, respectively. The electric charge of any fermion in LRSM is given by:

$$Q = T_L^3 + T_R^3 + \frac{B-L}{2}, \tag{4.58}$$

with $T_{L,R}^3$ being the third generators of $SU(2)_{L,R}$ and $B-L$ the baryon-minus-lepton number. This leads to the correct embedding of electromagnetic and weak interactions [75].

After symmetry breaking, the gauge bosons mix to yield the photon, the SM-like Z, a heavier $Z^{'}$, and the charged bosons $W_L^{\pm}$ and $W_R^{\pm}$. The gauge interactions of fermions then include:

- Charged currents: mediated by $W_L^{\pm}$ and $W_R^{\pm}$, involving left- and right-handed fermions respectively, with mixing encoded in CKM and RH-CKM matrices.
- Neutral currents: mediated by Z, Z', and the photon A, coupling to combinations of T_L^3, T_R^3, and $B-L$.

Summarizing the weak interaction terms:

$$\begin{aligned}\mathscr{L}_{\text{weak}} \supset\ & \bar{\psi}\gamma^{\mu}\left[\frac{g_L}{\sqrt{2}}\left(W_L^{+}T_L^{+} + W_L^{-}T_L^{-}\right)P_L + \frac{g_R}{\sqrt{2}}\left(W_R^{+}T_R^{+} + W_R^{-}T_R^{-}\right)P_R\right]\psi \\ & + \bar{\psi}\gamma^{\mu}\left[g_L T_L^3 W_L^3 + g_R T_R^3 W_R^3 + g_{BL}\frac{B-L}{2}V_{\mu}\right]\psi,\end{aligned} \tag{4.59}$$

where ψ represents any SM fermion field. After diagonalization, these interactions yield the familiar electromagnetic coupling and the neutral/charged weak currents, now extended by right-handed counterparts [22].

4.4 HIGGS SECTOR IN THE LRSM

The scalar content of the LRSM consists of a complex bidoublet Φ and two triplets $\Delta_{L,R}$, all complex. As emphasized above, the neutral scalar components are expanded around their VEVs as:

$$\begin{aligned}\Phi_1^0 &= \frac{1}{\sqrt{2}}(k_1 + h_1^0 + i\varphi_1^0),\\ \Phi_2^0 &= \frac{1}{\sqrt{2}}(k_2 + h_2^0 + i\varphi_2^0),\\ \Delta_{L,R}^0 &= \frac{1}{\sqrt{2}}(v_{L,R} + h_{L,R}^0 + i\varphi_{L,R}^0).\end{aligned} \tag{4.60}$$

The mass spectrum of the physical Higgs scalar states is summarized as follows [76]:

Doubly-Charged Scalars

In the basis $(\Delta_L^{\pm\pm}, \Delta_R^{\pm\pm})$, the doubly-charged mass matrix is a 2×2 symmetric matrix $M^{\pm\pm}$, whose eigenvalues are:

$$m^2_{1,2\pm\pm} = \frac{1}{2}\left(\mathrm{Tr}(M^{\pm\pm}) \pm \sqrt{\left[\mathrm{Tr}(M^{\pm\pm})\right]^2 - 4\,\det\,(M^{\pm\pm})}\right). \tag{4.61}$$

The physical states are obtained via a unitary transformation Z^D:

$$Z^{D\dagger} M^{\pm\pm} Z^D = \mathrm{diag}(m^2_{1\pm\pm}, m^2_{2\pm\pm}). \tag{4.62}$$

Singly-Charged Scalars

In the basis $(\phi_1^\pm, \phi_2^\pm, \Delta_L^\pm, \Delta_R^\pm)$, the singly-charged mass matrix $M^\pm$ is 4×4 and has two physical eigenstates and two Goldstone modes. The non-zero eigenvalues are:

$$m^2_{1,2\pm} = \frac{1}{2}\left(T^\pm \pm \sqrt{(T^\pm)^2 - 4D_2^\pm}\right),$$

(4.63)

where $T^{\pm} = \mathrm{Tr}(M^{\pm})$ and $D_2^{\pm}$ is the second principal invariant: $D_2 = \frac{1}{2}\left[(\mathrm{Tr}(M^{\pm}))^2 - \mathrm{Tr}((M^{\pm})^2)\right]$. The matrix is diagonalized by $Z^{\pm}$:

$$Z^{\pm\dagger} M^{\pm} Z^{\pm} = \mathrm{diag}(m_{1\pm}^2, m_{2\pm}^2, 0, 0).$$

(4.64)

with two physical charged states and two Goldstone modes. The eigenvalues follow:

Neutral Pseudoscalars

The pseudoscalar sector consists of four fields $(\varphi_1^0, \varphi_2^0, \varphi_L^0, \varphi_R^0)$ forming a 4×4 symmetric mass matrix. Two eigenstates correspond to Goldstone bosons; the other two are physical pseudoscalars with masses determined analogously.

Neutral Scalars

The CP-even neutral scalars form a 4×4 real symmetric mass matrix in the basis

$$S_i^{0t} = (\phi_1^{\mathrm{re}}, \phi_2^{\mathrm{re}}, \Delta_L^{\mathrm{re}}, \Delta_R^{\mathrm{re}}),$$

with entries determined by the scalar potential parameters and VEVs $k_{1,2}, v_{L,R}$. The mass eigenstates are obtained by diagonalizing the matrix via a unitary transformation:

$$Z^{S\dagger} M^H Z^S = \mathrm{diag}(m_1^2, m_2^2, m_3^2, m_4^2),$$

where one eigenstate corresponds to the SM-like Higgs boson with $m_h \approx 125\,\mathrm{GeV}$. The characteristic equation is quartic and solvable analytically [80], allowing constraints on model parameters.

4.5 HIGGS INTERACTIONS IN THE LRSM

The kinetic terms of the Higgs fields in the LRSM encode their interactions with the gauge bosons via the covariant derivatives. For the bidoublet field Φ, the covariant derivative is given by

$$D_\mu \Phi = \partial_\mu \Phi - i g_{_L} (W_{L\mu} \cdot T_L) \Phi + i g_{_R} \Phi (W_{R\mu} \cdot T_R),$$

(4.65)

where $W^a_{L\mu}$ and $W^a_{R\mu}$ are the gauge fields of $SU(2)_L$ and $SU(2)_R$, respectively. In terms of the physical gauge bosons $W^\pm_{L,R}$, Z_L, Z_R, and A, the derivative becomes

$$\begin{aligned} D_\mu \Phi \quad &= \partial_\mu \Phi - i \frac{g_L}{\sqrt{2}} \left(W^+_{L\mu} T^+_L + W^-_{L\mu} T^-_L \right) \Phi \\ &\quad + i \frac{g_R}{\sqrt{2}} \Phi \left(W^+_{R\mu} T^+_R + W^-_{R\mu} T^-_R \right) - ie \left(T^3_L \Phi - \Phi T^3_R \right) A_\mu \\ &\quad - i Z_{L\mu} \left(\frac{g_L}{\cos\theta_W} T^3_L \Phi + \frac{g_Y}{\tan\varphi} \Phi T^3_R \right) + i \frac{g_Y}{\tan\varphi} \Phi T^3_R Z_{R\mu}. \end{aligned}$$

(4.66)

Expanding the Higgs fields in components allows extraction of the interaction terms between the physical gauge bosons and scalar fields, which are essential for phenomenological analyses.

In the LRSM, the bidoublet Φ couples to quarks through Yukawa interactions:

$$\mathscr{L}_Y \supset \overline{Q}_L (y^Q \Phi + \tilde{y}^Q \widetilde{\Phi}) Q_R + \text{h.c.}$$

(4.67)

After symmetry breaking, the Yukawa couplings are expressed in terms of the physical quark masses:

$$y^Q \quad = \frac{\sqrt{2}}{k_1^2 - k_2^2} (k_1 V^u_L M^{\text{diag}}_u V^{u\dagger}_R - k_2 V^d_L M^{\text{diag}}_d V^{d\dagger}_R),$$

(4.68)

$$\tilde{y}^Q \quad = \frac{\sqrt{2}}{k_1^2 - k_2^2} (-k_2 V^u_L M^{\text{diag}}_u V^{u\dagger}_R + k_1 V^d_L M^{\text{diag}}_d V^{d\dagger}_R).$$

(4.69)

This leads to flavor-changing couplings between the neutral components of Φ and the mass eigenstate quarks:

$$\mathscr{L}_Y \quad \supset \bar{u}_L (y^Q \Phi^0_1 + \tilde{y}^Q \Phi^{0*}_2) u_R + \bar{d}_L (y^Q \Phi^0_2 + \tilde{y}^Q \Phi^{0*}_1) d_R + \text{h.c.}$$

(4.70)

With the scalar and pseudoscalar fields rotated to their mass eigenstates, the quark couplings are given by:

$$\mathscr{L}_Y \supset \bar{u}_i \left(\lambda_{ijk}^{H\bar{U}U} H_k + i\lambda_{ijk}^{A\bar{U}U} A_k \gamma^5\right) u_j + \bar{d}_i \left(\lambda_{ijk}^{H\bar{D}D} H_k - i\lambda_{ijk}^{A\bar{D}D} A_k \gamma^5\right) d_j,$$

(4.71)

with couplings

$$\lambda_{ijk}^{H\bar{U}U} = \frac{k_1 Z_{S,1k} - k_2 Z_{S,2k}}{k_1^2 - k_2^2} M_{u_i} \delta_{ij} + \frac{-k_2 Z_{S,1k} + k_1 Z_{S,2k}}{k_1^2 - k_2^2} \sum_l V_{il}^L M_{d_l} V_{jl}^{R*},$$

(4.72)

$$\lambda_{ijk}^{H\bar{D}D} = \frac{k_1 Z_{S,1k} - k_2 Z_{S,2k}}{k_1^2 - k_2^2} M_{d_i} \delta_{ij} + \frac{-k_2 Z_{S,1k} + k_1 Z_{S,2k}}{k_1^2 - k_2^2} \sum_l V_{li}^{L*} M_{u_l} V_{lj}^R,$$

(4.73)

$$\lambda_{ijk}^{A\bar{U}U} = \frac{k_1 Z_{P,1k} + k_2 Z_{P,2k}}{k_1^2 - k_2^2} M_{u_i} \delta_{ij} - \frac{k_2 Z_{P,1k} + k_1 Z_{P,2k}}{k_1^2 - k_2^2} \sum_l V_{il}^L M_{d_l} V_{jl}^{R*},$$

(4.74)

$$\lambda_{ijk}^{A\bar{D}D} = \frac{k_1 Z_{P,1k} + k_2 Z_{P,2k}}{k_1^2 - k_2^2} M_{d_i} \delta_{ij} - \frac{k_2 Z_{P,1k} + k_1 Z_{P,2k}}{k_1^2 - k_2^2} \sum_l V_{li}^{L*} M_{u_l} V_{lj}^R.$$

(4.75)

The off-diagonal terms in these couplings are induced by the nontrivial structure of the mixing matrices V^L and V^R, leading to tree-level flavor-changing neutral currents (FCNC). These interactions are tightly constrained by experimental limits on FCNC processes [76]. A similar mechanism applies in the leptonic sector due to the non-diagonality of the PMNS matrix.

4.6 PROBLEMS IN THE LRSM

While the LRSM elegantly addresses several shortcomings of the SM, such as restoring parity symmetry at high energies and explaining non-zero

neutrino masses through a natural seesaw mechanism, it also faces significant theoretical and phenomenological challenges:

- Doubly Charged Higgs Bosons: The scalar triplet fields $\Delta_{L,R}$ introduced to break the LR symmetry and implement the seesaw mechanism predict the existence of doubly charged Higgs bosons, $H^{\pm\pm}$. These exotic states have yet to be observed at collider experiments, such as the LHC, and current bounds place stringent constraints on their masses and couplings. The absence of detection challenges the minimal LRSM or pushes the relevant scale beyond current experimental reach.
- Fine-Tuning of the Left-Handed Triplet VEV: To generate light neutrino masses via the type-I or type-II seesaw mechanism, the VEV of the LH triplet, v_L, must be highly suppressed ($v_L \lesssim \mathcal{O}(1\,\mathrm{eV})$). However, the scalar potential naturally induces a non-zero v_L through terms proportional to the RH triplet VEV, v_R. Achieving a sufficiently small v_L requires delicate fine-tuning of parameters in the scalar potential, raising concerns about naturalness and stability.
- Extended Higgs Sector: The minimal LRSM contains a large number of scalar fields: a bidoublet Φ and two triplets Δ_L and Δ_R. This rich scalar content leads to a complicated scalar potential with many parameters and mass eigenstates. Diagonalizing the full scalar mass matrices and analyzing the physical spectrum and couplings becomes a technically challenging task. Moreover, the mixing among scalars complicates the phenomenology and makes it harder to identify SM-like Higgs signatures.
- Tree-Level FCNC: In the minimal LRSM, both the up-type and down-type quark mass matrices receive contributions from two Yukawa couplings due to the bidoublet Φ, leading to a non-diagonal structure in the physical basis. As a result, the Higgs-mediated neutral current interactions are not flavor-diagonal at tree level. This gives rise to FCNC processes such as $K^0 - \bar{K}^0$ and $B^0 - \bar{B}^0$ mixing, which are tightly constrained by experiment. Suppressing these FCNCs either requires fine-tuning the Yukawa matrices or introducing additional symmetries or mechanisms.

Due to these challenges, various extensions and modifications of the LRSM have been proposed. In the following chapter, we explore one such alternative: the LRSM with an inverse seesaw mechanism, which alleviates some of the aforementioned problems while preserving the appealing features of LR symmetry.

CHAPTER 5

Doublet Left-Right Symmetric Model

DOI: 10.1201/9781003457701-5

In the previous chapter, it was emphasized that the conventional LRSM suffers from a non-minimal Higgs sector, typically involving a bidoublet and two triplet scalar fields. This setup complicates the model and often leads to tensions with low-scale phenomenology. An alternative approach is to consider a simplified Higgs sector consisting of a single bidoublet and one $SU(2)_R$ doublet Higgs field, with the possible inclusion of an $SU(2)_L$ doublet in certain extensions. This minimal configuration defines the *Doublet LRSM*, which offers a more economical structure and improved compatibility with experimental constraints [81, 82].

In this framework, neutrino masses are generated via the Inverse Seesaw (IS) or Linear Seesaw (LS) mechanisms, as discussed in Chapter 1.

5.1 MODEL STRUCTURE

The DLRSM is based on the extended gauge group:

$$SU(3)_C \times SU(2)_L \times SU(2)_R \times U(1)_{B-L}.$$

The fermion content mirrors that of the conventional LRSM, with left- and RH doublets for both quarks and leptons:

$$\begin{aligned} Q_L &= \begin{pmatrix} u_L \\ d_L \end{pmatrix} \sim (3,2,1,1/3), \qquad Q_R = \begin{pmatrix} u_R \\ d_R \end{pmatrix} \sim (3,1,2,1/3), \\ L_L &= \begin{pmatrix} \nu_L \\ e_L \end{pmatrix} \sim (1,2,1,-1), \qquad L_R = \begin{pmatrix} \nu_R \\ e_R \end{pmatrix} \sim (1,1,2,-1). \end{aligned} \tag{5.1}$$

Parity symmetry is manifest at high energies, implying invariance of the Lagrangian under the exchange $Q_L \leftrightarrow Q_R$, $L_L \leftrightarrow L_R$. Notably, the presence of the RH neutrino ν_R is required for the completeness of the lepton doublet.

To implement the IS mechanism, the model introduces three SM singlet fermions S_1 with $B-L=-2$ and three singlets S_2 with $B-L=+2$. This pairwise inclusion ensures cancellation of $U(1)_{B-L}$ anomalies [72]. To avoid a direct Majorana mass term $M\bar{S}_1^c S_2$, which would spoil the structure of the IS, a discrete Z_2 symmetry is imposed, under which all fields are even except S_1, which is odd. Here, we consider the following Higgs sector consists of:

- A scalar bidoublet ϕ, responsible for EW symmetry breaking,
- An $SU(2)_R$ scalar doublet χ_R, which breaks $SU(2)_R \times U(1)_{B-L}$ down to $U(1)_Y$.

The hypercharge is defined via the relation:

$$Y = 2T_R^3 + (B-L),$$

where T_R^3 is the third component of the $SU(2)_R$ isospin. The full field content and their quantum numbers under the gauge group are summarized in Table 5.1.

TABLE 5.1 Field content of the DLRSM and their gauge quantum numbers. ⏎

Fields	$SU(3)_C \times SU(2)_L \times SU(2)_R \times U(1)_{B-L}$
$Q_L = \begin{pmatrix} u_L \\ d_L \end{pmatrix}$	$(\mathbf{3},\mathbf{2},\mathbf{1},\frac{1}{3})$
$Q_R = \begin{pmatrix} u_R \\ d_R \end{pmatrix}$	$(\mathbf{3},\mathbf{1},\mathbf{2},\frac{1}{3})$
$L_L = \begin{pmatrix} \nu_L \\ e_L \end{pmatrix}$	$(\mathbf{1},\mathbf{2},\mathbf{1},-1)$
$L_R = \begin{pmatrix} \nu_R \\ e_R \end{pmatrix}$	$(\mathbf{1},\mathbf{1},\mathbf{2},-1)$
S_1	$(\mathbf{1},\mathbf{1},\mathbf{1},-2)$
S_2	$(\mathbf{1},\mathbf{1},\mathbf{1},2)$
$\phi = \begin{pmatrix} \phi_1^0 & \phi_1^+ \\ \phi_2^- & \phi_2^0 \end{pmatrix}$	$(\mathbf{1},\mathbf{2},\mathbf{2},0)$

Fields	$SU(3)_C \times SU(2)_L \times SU(2)_R \times U(1)_{B-L}$
$\chi_R = \begin{pmatrix} \chi_R^+ \\ \chi_R^0 \end{pmatrix}$	$(\mathbf{1}, \mathbf{1}, \mathbf{2}, 1)$

This LR extension with IS, henceforth referred to as LRIS, leads to rich phenomenological implications, including TeV-scale RH gauge bosons and observable lepton flavor violation, which have been studied in Refs. [72, 81–84]. The symmetry breaking in the LRIS model proceeds in two stages. The first stage reduces the gauge symmetry $SU(2)_L \times SU(2)_R \times U(1)_{B-L}$ to the SM gauge group via the VEV of a RH scalar doublet χ_R:

$$SU(2)_L \times SU(2)_R \times U(1)_{B-L} \xrightarrow{\langle \chi_R \rangle} SU(2)_L \times U(1)_Y. \tag{5.2}$$

This breaking occurs when χ_R develops a VEV in its neutral component:

$$\langle \chi_R \rangle = \frac{1}{\sqrt{2}} \begin{pmatrix} 0 \\ v_R \end{pmatrix}, \tag{5.3}$$

where $v_R \gg 1\,\text{TeV}$ ensures that the associated gauge bosons $W_R^\pm$ and Z_R acquire large masses [85, 86].

The SM hypercharge is identified as a combination of the $SU(2)_R$ and $U(1)_{B-L}$ generators:

$$Y = T_R^3 + Q_{B-L}, \tag{5.4}$$

which is unbroken by $\langle \chi_R \rangle$, since:

$$Y(\langle \chi_R \rangle) = T_R^3(\langle \chi_R \rangle) + Q_{B-L}(\langle \chi_R \rangle) = 0. \tag{5.5}$$

The corresponding gauge couplings obey:

$$\frac{1}{g_Y^2} = \frac{1}{g_R^2} + \frac{1}{g_{B-L}^2}. \tag{5.6}$$

The second stage of symmetry breaking, from the SM to electromagnetism, is driven by the VEVs of the neutral components of a Higgs bidoublet Φ:

$$SU(2)_L \times U(1)_Y \xrightarrow{\langle \Phi \rangle} U(1)_{\rm EM},$$

(5.7)

with

$$\langle \Phi \rangle = \frac{1}{\sqrt{2}} \begin{pmatrix} k_1 & 0 \\ 0 & k_2 \end{pmatrix},$$

(5.8)

where $\sqrt{k_1^2 + k_2^2} = v = 246\,\text{GeV}$ is the electroweak scale. At this stage, the gauge bosons $W_L^{\pm}$ and Z_L acquire masses, and the electromagnetic coupling constant satisfies:

$$\frac{1}{e^2} = \frac{1}{g_L^2} + \frac{1}{g_R^2} + \frac{1}{g_{B-L}^2} = \frac{1}{g_L^2} + \frac{1}{g_Y^2}.$$

(5.9)

5.2 NEUTRINO AND FERMION MASSES IN THE LRIS

The Yukawa Lagrangian gives Dirac masses for fermions and light neutrino masses via the IS mechanism for all three generations. The relevant terms are:

$$\begin{aligned} \mathscr{L}_{\rm Y} = \quad & \sum_{i,j=1}^{3} \Big[y_{ij}^{L} \bar{L}_{Li} \phi L_{Rj} + \tilde{y}_{ij}^{L} \bar{L}_{Li} \tilde{\phi} L_{Rj} + y_{ij}^{Q} \bar{Q}_{Li} \phi Q_{Rj} \\ & + \tilde{y}_{ij}^{Q} \bar{Q}_{Li} \tilde{\phi} Q_{Rj} + y_{ij}^{s} \bar{L}_{Ri} \tilde{\chi}_R S_{2j}^{c} \Big] + \text{h.c.} \end{aligned}$$

(5.10)

The bidoublet ϕ and its conjugate $\tilde{\phi}$ couple to both quarks and leptons, generating Dirac masses. The RH doublet χ_R couples only to leptons and sterile singlet fermions S_2, generating the IS mechanism for neutrino masses. After $B-L$ breaking, a small Majorana mass term $\mu_s \bar{S}_2^c S_2$ arises from a dimension-seven non-renormalizable operator, yielding:

$$\mu_s = \lambda_s \frac{v_R^4}{M^3} \lesssim \mathscr{O}(1)\,\text{keV},$$

(5.11)

where λ_s is a dimensionless coupling. For $v_R \sim \mathscr{O}(10^3)$ GeV, $\mu_s \sim 10^{-7}$ GeV for $M \sim 10^3$ TeV and $\lambda_s \sim \mathscr{O}(1)$ [87]. Tus the neutrino mass terms are:

$$\mathscr{L}_m^{\nu} = M_D \bar{\nu}_L \nu_R + M_R \bar{\nu}_R^c S_2 + \mu_s \bar{S}_2^c S_2 + \text{h.c.},$$

(5.12)

where $M_D = \frac{v}{\sqrt{2}}(y^L \boldsymbol{s}_\beta + \tilde{y}^L \boldsymbol{c}_\beta)$ is the Dirac mass matrix, and $M_R = \frac{v_R}{\sqrt{2}} y^s$. The complete 9×9 neutrino mass matrix in the basis $\psi = (\nu_L^c, \nu_R, S_2)$ is:

$$\mathscr{M}_\nu = \begin{pmatrix} 0 & M_D & 0 \\ M_D^T & 0 & M_R \\ 0 & M_R^T & \mu_s \end{pmatrix}.$$

(5.13)

This matrix yields three light neutrino masses:

$$m_{\nu_\ell} = M_D M_R^{-1} \mu_s (M_R^T)^{-1} M_D^T,$$

(5.14)

and six heavy states with masses:

$$m_{\nu_h}^2 = M_R^2 + M_D^2.$$

(5.15)

The matrix $\mathscr{M}_\nu$ is diagonalized by a unitary matrix V such that:

$$V^T \mathscr{M}_\nu V = \mathscr{M}_\nu^{\text{diag}}.$$

(5.16)

The light neutrino mass matrix in Eq. (5.14) is diagonalized by the physical lepton mixing matrix, known as the PMNS matrix U_{MNS} [88], according to the relation:

$$U_{MNS}^T \, m_{\nu_l} \, U_{MNS} = m_{\nu_l}^{\text{diag}} \equiv \text{diag}(m_{\nu_e}, m_{\nu_\mu}, m_{\nu_\tau}).$$

(5.17)

This allows us to express the Dirac neutrino mass matrix as:

$$m_D = U_{MNS} \sqrt{m_{\nu_l}^{\text{diag}}} \, R \sqrt{\mu_s^{-1}} \, M_N,$$

(5.18)

where R is a general orthogonal matrix. This expression extends the well-known Casas-Ibarra parameterization for type-I seesaw [69], which corresponds to

$$m_D = U_{MNS} \sqrt{m_{\nu_l}^{\text{diag}}} \, R \sqrt{M_N}.$$

The full 9×9 neutrino mass matrix $\mathscr{M}_\nu$ is diagonalized by a unitary matrix V such that

$$V^T \mathscr{M}_\nu V = \mathscr{M}_\nu^{\text{diag}},$$

(5.19)

where V has the block structure:

$$V = \begin{pmatrix} V_{3\times3} & V_{3\times6} \\ V_{6\times3} & V_{6\times6} \end{pmatrix}.$$

(5.20)

The submatrix $V_{3\times3}$, which governs the mixing among the light neutrinos, is approximately given by

$$V_{3\times3} \simeq \left(1 - \frac{1}{2} F F^T\right) U_{MNS},$$

(5.21)

where the correction term $\frac{1}{2} F F^T$ characterizes the deviation from unitarity due to mixing with the heavy neutrino states. Here, F is defined as

$$F = m_D M_N^{-1}.$$

(5.22)

Hence, in general, $V_{3\times3}$ is not exactly unitary, and the extent of non-unitarity is governed by the size of $F F^T$. The matrix $V_{3\times6}$, which encodes the mixing between light and heavy neutrinos, takes the form:

$$V_{3\times6} = (\mathbf{0}_{3\times3},\, F) V_{6\times6},$$

(5.23)

while $V_{6\times6}$ is the matrix that diagonalizes the mass matrix in the heavy neutrino sector involving v_R and S_2.

Furthermore, after electroweak symmetry breaking, quarks and charged leptons acquire masses via the Higgs mechanism:

$$\begin{aligned} M_u &= \frac{v}{\sqrt{2}} (y^Q s_\beta + \tilde{y}^Q c_\beta), \\ M_d &= \frac{v}{\sqrt{2}} (y^Q c_\beta + \tilde{y}^Q s_\beta), \end{aligned}$$

(5.24)

(5.25)

$$M_\ell \;= \frac{v}{\sqrt{2}}(y^L c_\beta + \tilde{y}^L s_\beta),$$

(5.26)

with $k_1 = v s_\beta$, $k_2 = v c_\beta$, and $v = 246$ GeV. Diagonalization of these matrices gives the physical masses:

$$M_f^{\text{diag}} = V_L^{f\dagger} M_f' V_R^f, \quad f = u, d, \ell.$$

(5.27)

The original Yukawa matrices are expressed as:

$$y^Q \;= -\frac{\sqrt{2}}{v c_{2\beta}}(s_\beta V_L^u M_u V_R^{u\dagger} - c_\beta V_L^d M_d V_R^{d\dagger}),$$

(5.28)

$$\tilde{y}^Q \;= -\frac{\sqrt{2}}{v c_{2\beta}}(c_\beta V_L^u M_u V_R^{u\dagger} - s_\beta V_L^d M_d V_R^{d\dagger}).$$

(5.29)

Unlike the SM, fermion masses arise from two distinct VEVs, leading to a non-trivial flavor structure and the potential for tree-level FCNCs via neutral Higgs exchange.

5.3 HIGGS SECTOR IN LRIS

The Higgs sector of the LRIS model consists of a bidoublet Φ and a RH doublet χ_R. The symmetry breaking occurs in two stages:

$$SU(2)_L \times SU(2)_R \times U(1)_{B-L} \;\to SU(2)_L \times U(1)_Y,$$

(5.30)

$$SU(2)_L \times U(1)_Y \;\to U(1)_{\text{EM}}.$$

(5.31)

The neutral components of these Higgs fields expand around their VEVs as:

$$\Phi_1^0 = \frac{k_1 + h_1^0 + i\varphi_1^0}{\sqrt{2}}, \quad \Phi_2^0 = \frac{k_2 + h_2^0 + i\varphi_2^0}{\sqrt{2}}, \quad \chi_R^0 = \frac{v_R + h_R^0 + i\varphi_R^0}{\sqrt{2}}.$$

Before symmetry breaking, the model contains 12 scalar degrees of freedom (8 from Φ and 4 from χ_R). After breaking, 6 scalars remain as physical Higgs bosons: two charged Higgs bosons, one pseudoscalar, and three neutral CP-even Higgs bosons.

Singly Charged Scalars

The mass matrix for the charged Higgs bosons in the basis $(\phi_1^\pm, \phi_2^\pm, \chi_R^\pm)$ is given by:

$$M_{H^\pm}^2 = \frac{\alpha_{32}}{2}\begin{pmatrix} \frac{v_R^2 s_\beta^2}{c_{2\beta}} & \frac{v_R^2 s_{2\beta}}{2c_{2\beta}} & -vv_R s_\beta \\ . & \frac{v_R^2 c_\beta^2}{c_{2\beta}} & -vv_R c_\beta \\ . & . & v^2 c_{2\beta} \end{pmatrix}.$$

Diagonalizing this matrix leads to a physical charged Higgs mass:

$$m_{H^\pm}^2 = \frac{\alpha_{32}}{2}\left(\frac{v_R^2}{c_{2\beta}} + v^2 c_{2\beta}\right),$$

where $\alpha_{32} = \alpha_3 - \alpha_2$. The mass is typically in the range of hundreds of GeV for $v_R \sim \mathscr{O}(\text{TeV})$.

The physical charged Higgs is a combination of $\phi_1^\pm$, $\phi_2^\pm$, and $\chi_R^\pm$, with the following mixing:

$$H^\pm = Z_{13}^{H^\pm}\phi_1^\pm + Z_{23}^{H^\pm}\phi_2^\pm + Z_{33}^{H^\pm}\chi_R^\pm.$$

Neutral Pseudoscalars

For the neutral *CP*-odd Higgs bosons, the mass matrix is:

$$M_A^2 = \frac{1}{2}\left(\frac{v_R^2\alpha_{32}}{c_{2\beta}} - 4v^2(2\lambda_2 - \lambda_3)\right)\begin{pmatrix} c_\beta^2 & s_\beta c_\beta & 0 \\ . & s_\beta^2 & 0 \\ . & . & 0 \end{pmatrix}.$$

The eigenvalue for the pseudoscalar mass is:

$$m_A^2 = \frac{1}{2}\left(\frac{v_R^2}{c_{2\beta}}\alpha_{32} - 4v^2(2\lambda_2 - \lambda_3)\right),$$

which is typically in the range of a few hundred GeV for $v_R \sim \mathscr{O}(\text{TeV})$.

The physical pseudoscalar is given by:

$$A = c_\beta\phi_1^{0I} + s_\beta\phi_2^{0I},$$

where $s_\beta \ll 1$, so $A \approx \phi_1^{0I}$.

Neutral Scalar

The mass matrix for the neutral *CP*-even Higgs bosons is:

$$M_H^2 = \frac{\partial^2 V(\phi, \chi_{L,R})}{\partial \phi_i^{0R} \partial \phi_j^{0R}}\Big|_{\langle \phi_{i,j}^{0R} \rangle = 0}.$$

This matrix can be diagonalized to yield the masses of the physical neutral Higgs bosons. In particular, one of the eigenvalues corresponds to the SM-like Higgs boson, while the other three eigenvalues correspond to the heavy Higgs bosons. However, there is the possibility that one of the new scalar states could be lighter than the SM Higgs, with a mass of order 95 GeV, potentially explaining some observed anomalies (such as deviations in Higgs-like particle searches at the LHC). The mass spectrum can therefore exhibit a light new Higgs state below the standard 125 GeV threshold, which could also affect phenomenology at colliders.

5.4 PHENOMENOLOGICAL IMPLICATIONS OF THE LRIS MODEL

The LRIS model offers a rich and testable phenomenology at both low-energy precision experiments and high-energy collider searches. Its extended gauge structure, additional Higgs fields, and the presence of quasi-Dirac heavy neutrinos lead to distinctive experimental BSM signatures. In this section, we explore three key phenomenological aspects of the LRIS framework. First, we examine its potential to address the long-standing discrepancy in the muon's anomalous magnetic moment, $(g-2)_\mu$, through loop contributions involving new gauge and scalar degrees of freedom. Second, we investigate the prospects for detecting heavy Higgs bosons predicted by the model at the LHC, focusing on their production channels and decay patterns. Finally, we analyze the lepton flavor violating process $\mu \to e\gamma$, which can receive significant enhancements in the LRIS scenario due to the interplay between the IS mechanism and new flavor-violating interactions. These complementary probes collectively constrain the parameter space of the LRIS model and offer promising avenues for its experimental verification.

5.4.1 Muon $g-2$ in the LRIS Framework

In this section, we investigate the contributions of the LRIS model to the muon anomalous magnetic moment, a_μ, arising from the exchange of both light and

heavy gauge bosons (W, W', Z, Z'), neutral scalars (h_i, A), and charged Higgs bosons ($H^\pm$), as illustrated in Fig. 5.1 [89].

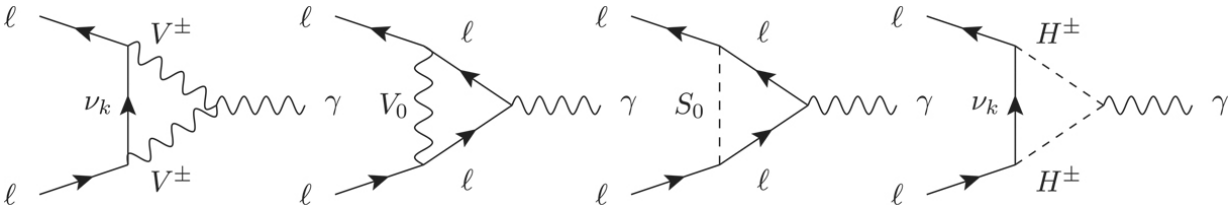

Figure 5.1 One-loop LRIS contributions to lepton $g_\ell - 2$ via massive neutrino loops. The exchanged particles include $V^\pm = W, W'$, $V^0 = Z, Z'$, $S^0 = h_i, A$, and the charged Higgs boson $H^\pm$.

The total new physics contribution to a_μ in this framework is given by

$$\delta a_\mu \equiv a_\mu^{\text{LRIS}} = a_\mu^W + a_\mu^{W'} + a_\mu^Z + a_\mu^{Z'} + a_\mu^h + a_\mu^A + a_\mu^{H^\pm},$$

(5.32)

where the individual terms, neglecting $W - W'$ and $Z - Z'$ mixing, are given by

$$a_\ell^W = G_{\text{F}}^\ell \sum_{k=1}^{9} |U_{k,|\ell|}|^2 \left(\frac{10}{3} + \mathscr{F}_2(x_W^{\nu_k}) \right),$$

(5.33)

$$a_\ell^{W'} = G_{\text{F}}^\ell \sum_{k=1}^{9} |U_{k,3+|\ell|}|^2 \left(\frac{10}{3} + \mathscr{F}_2(x_{W'}^{\nu_k}) \right) \left[\frac{1}{c_w} x_{W'}^W \right],$$

(5.34)

$$a_\ell^Z = G_{\text{F}}^\ell \, (c_{4w} - 5) \left(\frac{1}{3} \right),$$

(5.35)

$$a_\ell^{Z'} = G_{\text{F}}^\ell \, (c_{4w'} - 12 c_{2w'} - 5) \left[\frac{t_w^2}{48 s_{2w'}^2} x_{Z'}^W \right],$$

(5.36)

$$a_\ell^h = G_{\text{F}}^\ell \sum_{i=1}^{3} x_{h_i}^\ell (\Gamma_{\ell\ell}^{h_i})^2 \left(\frac{7}{6} + \log x_{h_i}^\ell \right),$$

(5.37)

$$a_\ell^A = -\frac{1}{2} G_{\text{F}}^\ell x_A^\ell (\Gamma_{\ell\ell}^A)^2 \left(\frac{7}{6} + \log x_A^\ell \right),$$

(5.38)

with $|\ell| = 1, 2$ for $\ell = e, \mu$, and $G_{\rm F}^{\ell} = \frac{G_{\rm F} m_{\ell}^2}{8\sqrt{2}\pi^2}$. The mass ratios are defined as $x_b^a = m_a^2/m_b^2$. The mixing angles are $s_{w'} = g_Y/g_R$ and $s_w = e/g_L$, with $\tan\theta_{w'} \lesssim 10^{-4}$ [90], and the charged gauge boson mass satisfies $m_{W'} \gtrsim \mathcal{O}(4\,\text{TeV})$.

Among these, the Z', W', h_i, and A contributions are highly suppressed due to small mass ratios and can be neglected. Additionally, the second term in Eq. (5.33), which involves heavy RH neutrino loops, contributes only $\mathcal{O}(10^{-2})$, less than 0.4% of the dominant term, and is further suppressed by the GIM mechanism [91] due to the unitarity of the full 9×9 neutrino mixing matrix [87, 92, 93].
The charged Higgs contribution $a_{\ell}^{H^{\pm}}$ takes the form

$$a_{\ell}^{H^{\pm}} = G_{\rm F}^{\ell}\,\Gamma_{\gamma}^{H^{\pm}} \sum_{k=1}^{9} \left(|\zeta'_{k\ell}|^2\, \mathscr{F}_2(x_{H^{\pm}}^{\nu_k}) + 2\,\zeta'_{k\ell}\xi'_{k\ell}\, \mathscr{F}_1(x_{H^{\pm}}^{\nu_k}) \right),$$

(5.39)

where $\zeta'_{k\ell} = \frac{v}{m_{\nu_k}}\zeta_{k\ell}$, $\xi'_{k\ell} = \frac{v}{m_{\ell}}\xi_{k\ell}$, and the loop functions are

$$\mathscr{F}_k(x) = \frac{x\,\mathscr{P}_k(x)}{(x-1)^{k+1}} - \frac{6x^{k+1}\log x}{(x-1)^{k+2}},$$

(5.40)

$$\mathscr{P}_1(x) = 3x + 3, \quad \mathscr{P}_2(x) = 2x^2 + 5x - 1.$$

(5.41)

In the limit $x \to 1$, $\mathscr{F}_1(1) = 1$ and $\mathscr{F}_2(1) = \frac{1}{2}$. Over all x, the ratio $\mathscr{F}_2/\mathscr{F}_1$ remains $\mathcal{O}(1)$, ranging between $1/3$ and $2/3$.

The effective photon coupling is approximated by

$$\Gamma_{\gamma}^{H^{\pm}} \simeq \frac{1}{6e}(g_L U_{21}^0 + g_R U_{31}^0),$$

(5.42)

valid in the limit $v_R \gg v$, with a typical value $\Gamma_{\gamma}^{H^{\pm}} \sim 0.076$. The first term in the sum contributes only about 0.02% of the second term, which dominates. Thus, the leading contribution is

$$a_{\ell}^{H^{\pm}} \simeq 2G_{\rm F}^{\ell}\,\Gamma_{\gamma}^{H^{\pm}} \sum_{k=4}^{9} \zeta'_{k\ell}\xi'_{k\ell}\, \mathscr{F}_1(x_{H^{\pm}}^{\nu_k}) \lesssim \frac{3\Gamma_{\gamma}^{H^{\pm}}}{8\pi^2}\, m_{\ell} \sum_{k=4}^{9} \frac{\zeta_{k\ell}\xi_{k\ell}}{m_{\nu_k}}.$$

(5.43)

This contribution is enhanced by the inverse dependence on the charged lepton mass in $\xi'_{k\ell}$, making it potentially significant in explaining the a_μ anomaly, as shown in Fig. 5.2.

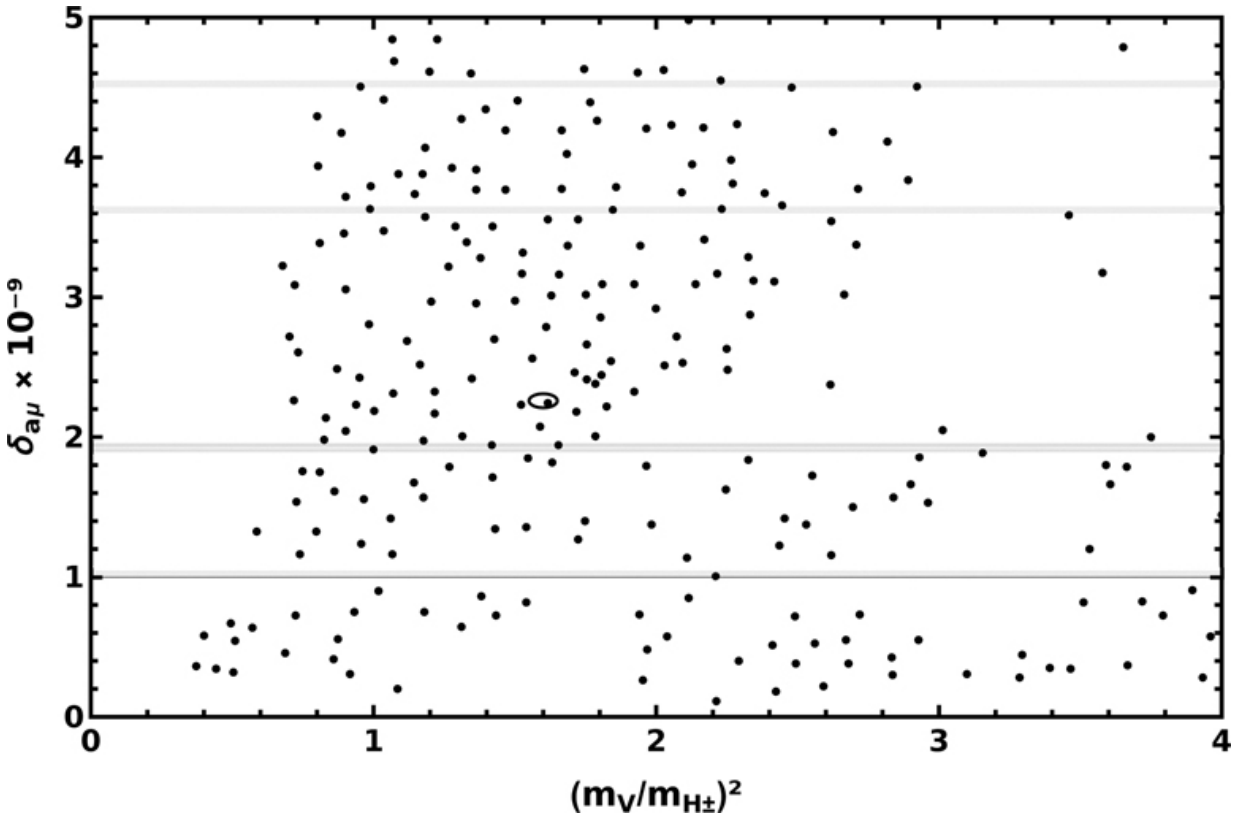

Figure 5.2 Muon magnetic moment anomaly δa_μ as a function of the mass ratio parameter $x_{H^\pm}^{\nu_5} = m_{\nu_5}^2/m_{H^\pm}^2$, where m_{ν_5} and $m_{H^\pm}$ denote the second-heaviest neutrino and charged Higgs masses, respectively. The 1σ and 2σ confidence regions from experimental measurements are shown with bands between horizontal lines. The benchmark point, circulated in *dark–shaded region*, was considered in Ref. [89]. ⏎

5.4.2 Heavy Higgs Search in the LRIS Model at the LHC

As discussed above, following Left-Right and electroweak symmetry breaking, the CP-even neutral Higgs mass matrix M_H^2 is diagonalized by the unitary matrix Z^H. The lightest eigenstate, $H_1 \equiv h$, is identified with the SM-like Higgs boson. The remaining two eigenvalues are given by

$$m_{H_{2,3}}^2 = \frac{1}{2}\left(T^h - m_h^2 \mp \sqrt{(T^h - m_h^2)^2 - \frac{4D^h}{m_h^2}}\right),$$

(5.44)

where $T^h = \mathrm{Tr}(M_H^2)$ and $D^h =$det (M_H^2) denote the trace and determinant of the mass matrix, respectively.

From Eq. (5.44), the next-to-lightest *CP*-even neutral Higgs boson, $H_2 \equiv h'$, can acquire a mass in the few hundred GeV range. In our analysis, we scan the scalar potential parameters within the ranges:

$$\begin{aligned} &\lambda_1 \in [0.18, 0.30], \quad \lambda_4 \in [0.70, 0.99], \quad \alpha_1 \in [0.06, 0.16], \\ &\alpha_4 \in [0.60, 0.99], \quad \rho_1 \in [0.08, 0.14], \quad \lambda_{23} \in [-0.1, 3]. \end{aligned}$$

(5.45)

The physical eigenstate $h^{'}$ is composed of real parts of neutral scalar fields:

$$h' = Z_{21}^H \, \phi_1^{0R} + Z_{22}^H \, \phi_2^{0R} + Z_{23}^H \, \chi_R^{0R},$$

(5.46)

where Z^H is the CP-even Higgs mixing matrix. Benchmark points with $m_{h'} = 250$, 400, and 600 GeV are adopted as in Ref. [94]. The $h^{'}$ state is dominantly composed of the ϕ_1 component, with subdominant contributions from ϕ_2 and χ_R.

The trilinear coupling of $h^{'}$ with two SM-like Higgs bosons is given by:

$$g_{h'hh} \approx -2i Z_{21}^H Z_{12}^H \left\{ v \left[(\lambda_1 - \lambda_{23}) \cos\beta + 3\lambda_4 \sin\beta \right] Z_{12}^H + \alpha_4 v_R Z_{13}^H \right\},$$

(5.47)

where we fix $g_L = g_R = g_2 = 0.663$, $g_{BL} = 0.422$, and $v_R = 6400$ GeV, while the scalar potential parameters are varied as in Eq. (5.45). At the LHC, the heavy Higgs boson $h^{'}$ is predominantly produced via gluon-gluon fusion (ggF), which accounts for approximately 90% of its total production. For $m_{h'} \leq 600\,\mathrm{GeV}$, the decay branching ratio $\mathrm{BR}(h' \to hh)$ remains sizable, typically exceeding 10%, making this channel promising for discovery.

Among the possible final states, the decay chain $h' \to hh \to b\bar{b}\gamma\gamma$ offers a clean experimental signature and manageable background. The corresponding Feynman diagram is shown in Fig. 5.3. We perform a dedicated analysis for the three benchmark masses of $h^{'}$: 250, 400, and 600 GeV.

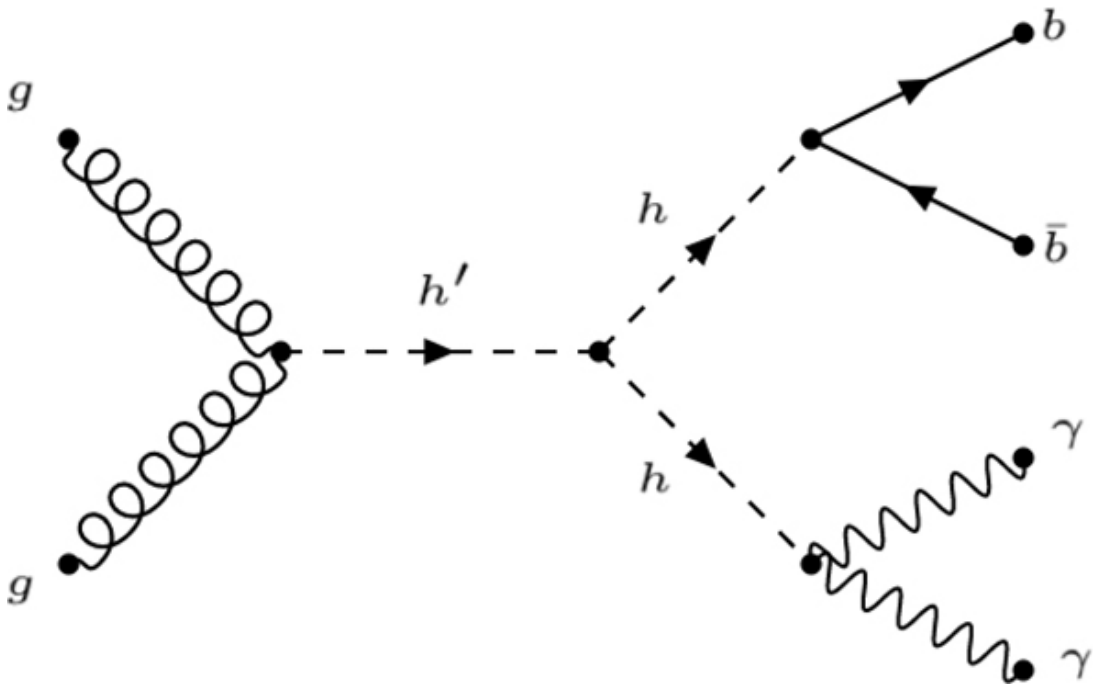

Figure 5.3 Feynman diagram for h' production via ggF and decay into $hh \to b\bar{b}\gamma\gamma$.

Using the narrow width approximation, the total cross-section for the process is:

$$\begin{aligned}\sigma(pp \to h' \to hh \to b\bar{b}\gamma\gamma) \quad &\approx \sigma(pp \to h') \times \mathrm{BR}(h' \to hh) \\ &\times \mathrm{BR}(h \to b\bar{b}) \times \mathrm{BR}(h \to \gamma\gamma).\end{aligned}$$

Table 5.2 summarizes the production cross-section, branching ratio, and total signal rate for the three considered h' masses. To assess the discovery potential, we analyze the signal and background distributions at $\sqrt{s} = 14$ TeV with an integrated luminosity of $300\,\mathrm{fb}^{-1}$. Figure 5.4 shows the number of signal events for $m_{h'} = 250$ and 400 GeV before and after applying selection cuts, following the procedure of Ref. [94].

TABLE 5.2 Production cross-section and decay branching ratios for different values of $m_{h'}$.

$m_{h'}$ (GeV)	$\sigma(pp \to h')$ (pb)	$\mathrm{BR}(h' \to hh)$	$\sigma(pp \to h' \to hh \to b\bar{b}\gamma\gamma)$ (fb)
250	12.140	0.30	6.30
400	5.050	0.20	1.01
600	0.504	0.18	0.05

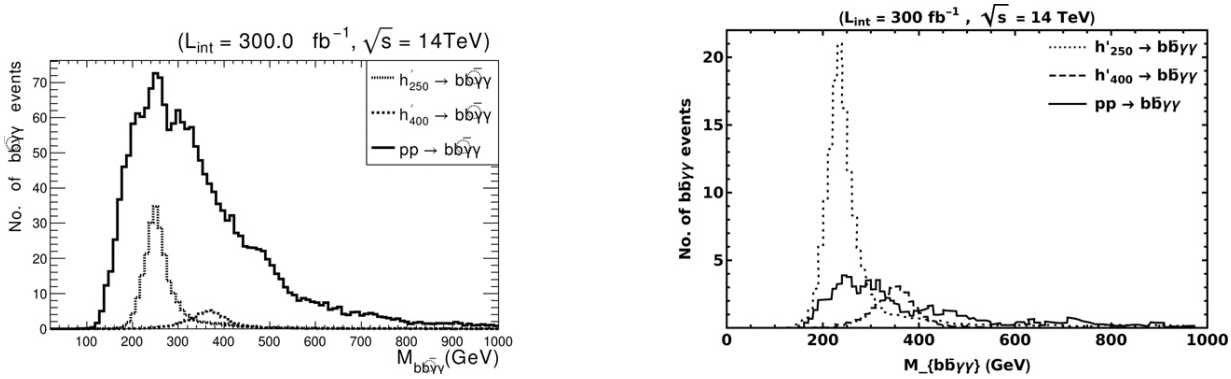

Figure 5.4 Signal event distributions for $h' \to b\bar{b}\gamma\gamma$ at $m_{h'} = 250$ GeV (dotted line) and 400 GeV (dashed line), compared to the SM background (solid line), before (left) and after (right) applying selection cuts at $\sqrt{s} = 14\,\text{TeV}$ and $L_{\text{int}} = 300\,\text{fb}^{-1}$ [94]. ⏎

5.4.3 $\mu \to e\gamma$ in the TeV-Scale $B - L$ Model with IS

We now examine the charged lepton flavor violating (LFV) process $\mu \to e\gamma$ within the framework of LRIS. A number of experimental efforts have been dedicated to probing such LFV decays, with the $\mu \to e\gamma$ channel receiving particular attention. The most stringent upper limit to date, reported by the MEG collaboration [95], is:

$$\text{BR}(\mu \to e\gamma) < 4.2 \times 10^{-13}. \tag{5.48}$$

Future experiments aim to enhance this sensitivity by up to three orders of magnitude.

It is worth noting that, within the SM augmented by tiny neutrino masses, the branching ratio for this decay is extremely suppressed:

$$\text{BR}(\mu \to e\gamma)^{\text{SM}} \simeq 10^{-55}, \tag{5.49}$$

rendering any experimental signal of this process a definitive indicator of new physics.

The decay amplitude receives contributions from both light and heavy neutrinos in the loop, along with the W boson, as depicted in Fig. 5.5. In the limit $m_e \to 0$, the amplitude can be expressed as:

$$A(\mu \to e\gamma) \simeq \frac{m_\mu G_F}{32\sqrt{2}\pi^2} \sum_{i=1}^{9} V_{\mu i}^* V_{ei} f(r_i) \times \bar{u}(p)[2e(p' \cdot \epsilon)]u(p'), \tag{5.50}$$

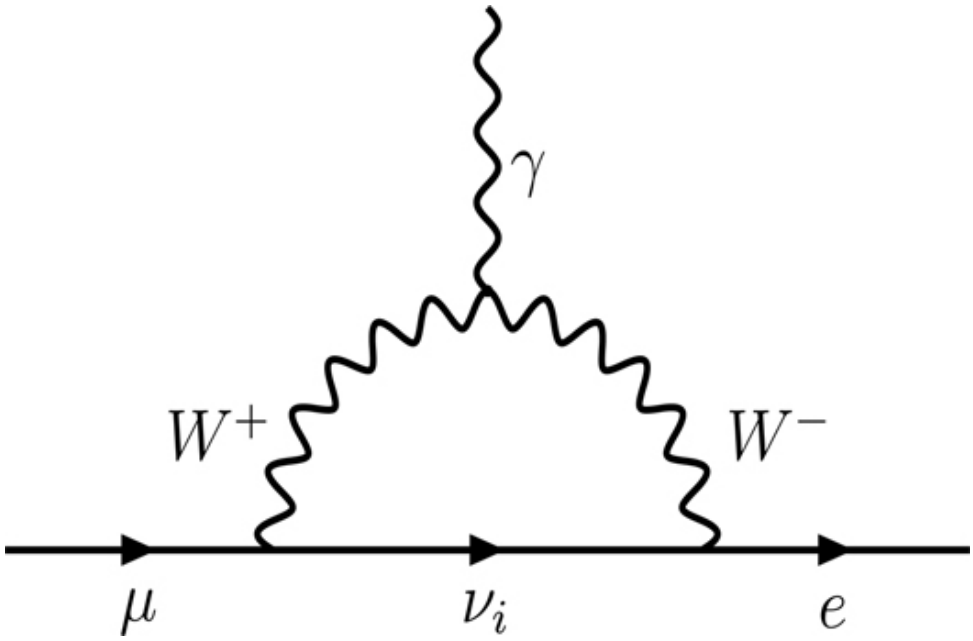

Figure 5.5 Feynman diagram for the dominant contribution to $\mu \to e\gamma$ in the LRIS. ⏎

where $f(r_i)$ is the loop function and $r_i = m_{\nu_i}^2/M_W^2$.

Defining the overall amplitude coefficient as:

$$a = \frac{e m_\mu G_F}{32\sqrt{2}\pi^2} \sum_{i=1}^{9} V_{\mu i}^* V_{ei} f(r_i),$$

(5.51)

the decay width becomes:

$$\Gamma(\mu \to e\gamma) = \frac{m_\mu^3}{8\pi} |a|^2.$$

(5.52)

Normalizing to the standard muon decay width $\Gamma(\mu \to e\nu\bar{\nu}) \simeq m_\mu^5 G_F^2/(192\pi^3)$, the branching ratio is given by:

$$\mathrm{BR}(\mu \to e\gamma) = \frac{\Gamma(\mu \to e\gamma)}{\Gamma(\mu \to e\nu\bar{\nu})} = \frac{3\alpha}{64\pi} \left| \sum_{i=1}^{9} V_{\mu i}^* V_{ei} f(r_i) \right|^2,$$

(5.53)

with $\alpha = e^2/(4\pi) \simeq 1/137$.

From the MEG upper limit in Eq. (5.48), one obtains the constraint:

$$\left|\sum_{i=1}^{9} V_{\mu i}^{*} V_{ei} f(r_i)\right| < 1.95 \times 10^{-5}. \tag{5.54}$$

In the limit where LH neutrinos are extremely heavy, the mixing matrix $V_{3\times3}$ becomes nearly unitary, and the light neutrino contributions ($i = 1, 2, 3$) to the amplitude are negligible. Additionally, in this regime, the heavy neutrino contributions are highly suppressed due to the smallness of the mixing terms ($V_{\mu i}, V_{ei} \sim m_D/M_N \sim \mathcal{O}(10^{-9})$), ensuring that the bound in Eq. (5.54) is easily satisfied and $\mathrm{BR}(\mu \to e\gamma) \ll 10^{-12}$.

Conversely, in the TeV-scale IS scenario, the lepton mixing matrix is significantly non-unitary, and the mixing between light and heavy neutrinos is no longer suppressed ($m_D/M_N \sim \mathcal{O}(0.1)$). In this context, the constraint can be rewritten as:

$$\left|\frac{10}{3}\sum_{i=1}^{3} V_{\mu i}^{*} V_{ei} + \sum_{j=4}^{9} V_{\mu j}^{*} V_{ej} f(r_j)\right| < 1.95 \times 10^{-5}, \tag{5.55}$$

where $r_j = (m_{\nu_{H_j}}/M_W)^2$ and the mixing elements $V_{e(\mu)j}$ are given by:

$$\begin{aligned} V_{e(\mu)j} &= \left[\left(0, m_D M_N^{-1}\right) V_{6\times6}\right]_{1(2),j-3} \\ &= \left[\left(0, U_{MNS}\sqrt{m_{\nu_l}^{\mathrm{diag}}}\, R \sqrt{\mu_s^{-1}}\right) V_{6\times6}\right]_{1(2),j-3}. \end{aligned} \tag{5.56}$$

Assuming $r_j \gg 1$ so that $f(r_j) \simeq 4/3$, the constraint simplifies to:

$$\left|\sum_{i=1}^{3} V_{\mu i}^{*} V_{ei}\right| < 0.8 \times 10^{-5}, \tag{5.57}$$

which imposes the condition $(FF^T)_{21,12} \lesssim 10^{-4}$. This limit is typically satisfied in the IS framework, given the restrictions on the off-diagonal components of the non-unitary U_{MNS} matrix.

CHAPTER 6

$SU(5)$ Grand Unified Theory

DOI: 10.1201/9781003457701-6

The $SU(5)$ theory stands as a widely studied example of a simple Grand Unified Theory (GUT), first proposed by Georgi and Glashow in 1974 [96]. Unlike SM, $SU(5)$ is a rank-four group[1]. Since the SM gauge group, $SU_C(3) \times SU_L(2) \times U_Y(1)$, also has rank four, any viable GUT must have at least this rank. Possible candidate groups with rank four include:

$$[SU(3)]^2, \quad [SU(2)]^4, \quad O(9), \quad O(8), \quad Sp(8), \quad SU(5),$$
$$F_4 \text{ (exceptional group)}.$$

After careful examination, only $[SU(3)]^2$ and $SU(5)$ remain viable candidates, as complex representations are required to accommodate chiral fermions. In the SM, left- and RH fermions transform differently, *e.g.*, $e_L^\dagger \neq e_R$. However, $[SU(3)]^2$ is ultimately excluded because it implies that leptons carry color quantum numbers and leads to unphysical flavor assignments, both of which are incompatible with experimental observations. Consequently, $SU(5)$ stands out as the unique minimal candidate for unification.

[1] *The rank of a group is the number of mutually commuting generators that can be simultaneously diagonalized.*

6.1 SU (5) FERMION CONTENT

A defining feature of GUTs, particularly $SU(5)$, is the unification of the SM matter content into irreducible representations of higher dimensions of the unified group. This must be achieved while preserving the correct transformation properties under the SM subgroup.

Each generation of SM fermions consists of 15 left-handed Weyl spinors. We organize them using the fundamental representations of $SU(5)$, that is, 5 and its conjugate 5^*. These decompose under $SU(3)_C \times SU(2)_L \times U(1)_Y$ as [97]:

$$5 = (3,1)_{-1/3} \oplus (1,2)_{1/2}, \quad 5^* = (3^*,1)_{1/3} \oplus (1,2)_{-1/2}. \tag{6.1}$$

Here, we adopt the convention that the first three components correspond to $SU(3)_C$ and the last two to $SU(2)_L$. The hypercharge is embedded to satisfy the tracelessness condition of $SU(5)$ generators. In particular, a decomposition such as $(3,1)_{2/3} \oplus (1,2)_{1/2}$ would violate tracelessness and is therefore not allowed.

The 5 representation can be populated as:

$$5 \equiv (\psi_i)_R = \begin{pmatrix} d_r \\ d_g \\ d_b \\ e^+ \\ -\nu_e^c \end{pmatrix}_R , \tag{6.2}$$

where $d_{r,g,b}$ are RH down-type quarks, and e^+ and ν_e^c denote the RH charged lepton and neutrino, respectively.

Applying charge conjugation, $(\psi_R)^c = C\gamma_0 \psi_R^* \equiv (\psi^c)_L$, we obtain the 5^* representation:

$$5^* \equiv (\psi^i)_L \equiv \psi_L^c = \begin{pmatrix} d_r^c \\ d_g^c \\ d_b^c \\ e^- \\ -\nu_e \end{pmatrix}_L . \tag{6.3}$$

This assignment matches precisely the quantum numbers of SM particles.

To incorporate the remaining left-handed SM fermions, we consider higher-dimensional representations built from tensor products:

$$5 \otimes 5 = 15_S \oplus 10_A, \quad 5 \otimes 5^* = 24 \oplus 1,$$

(6.4)

where the subscripts denote symmetric (S) and antisymmetric (A) parts. Their decompositions are:

$$15 = (6,1)_{-4/3} \oplus (3,2)_{1/3} \oplus (1,3)_2,$$

(6.5)

$$10 = (3^*,1)_{-4/3} \oplus (3,2)_{1/3} \oplus (1,1)_2.$$

(6.6)

The 15 representation contains exotic color sextets not observed experimentally, while the 10 representation beautifully matches the SM content.

Explicitly, the antisymmetric 10 representation, accommodating u_L^c, Q_L, and e_L^+, is given by:

$$10 \equiv (\chi_{ij})_L = \frac{1}{\sqrt{2}} \begin{pmatrix} 0 & u_3^c & -u_2^c & u_1 & d_1 \\ -u_3^c & 0 & u_1^c & u_2 & d_2 \\ u_2^c & -u_1^c & 0 & u_3 & d_3 \\ -u_1 & -u_2 & -u_3 & 0 & e^+ \\ -d_1 & -d_2 & -d_3 & -e^+ & 0 \end{pmatrix}_L .$$

(6.7)

Thus, the SM fermions of a single generation neatly fit into the $5^* \oplus 10$ of $SU(5)$.

6.2 CHARGE QUANTIZATION IN $SU(5)$

One of the profound successes of $SU(5)$ GUTs is the natural explanation of electric charge quantization [98]. In this framework, charge quantization arises from two key principles:

- The SM gauge groups $SU(3)_C$, $SU(2)_L$, and $U(1)_Y$ commute, implying that particles differing only by color or weak isospin have identical hypercharges.
- The $SU(5)$ generators are traceless, constraining the embedding of $U(1)_Y$.

Remarkably, the sum of electric charges within a given $SU(5)$ multiplet vanishes. For instance, in the 5^* representation:

$$3q(d^c) + q(e^-) + q(\nu_e) = 0,$$

(6.8)

leading to the relation $3(-\frac{1}{3}) + (-1) + 0 = 0$, which fixes the down quark charge as $q(d) = -1/3$. This elegant result is a direct consequence of group theory and provides deep insight into one of the most mysterious features of the SM.

6.3 SU (5) GENERATORS

The group $SU(n)$ is defined as the set of $n \times n$ unitary matrices with determinant one. A general $SU(n)$ transformation is expressed as

$$U = \exp\left(i \sum_{a=1}^{n^2-1} B^a \, T_a\right) = \exp\left(-i \, \mathbf{B} \cdot \, \mathbf{T}\right),$$

(6.9)

where the T_a are the generators of the Lie algebra, satisfying the properties of being Hermitian, traceless, and normalized according to

$$\mathrm{Tr}(\lambda_a \lambda_b) = 2\delta_{ab},$$

(6.10)

with λ_a the analogs of Gell-Mann matrices. For $SU(5)$, there are 24 generators ($a = 1, \ldots, 24$), corresponding to the dimension of the group.

To identify the 24 associated vector bosons, denoted by $\mathbf{A}_\mu = A^a_\mu \, T_a = A^a_\mu \lambda_a/2$, we embed the SM gauge group

$SU(3)_C \times SU(2)_L \times U(1)_Y$ into $SU(5)$ as follows:

- Eight generators $(T_1, \ldots, T_8)$ are associated with the $SU(3)_C$ subgroup,
- Three generators (T_9, T_{10}, T_{11}) correspond to $SU(2)_L$,
- One generator (T_{12}) is assigned to $U(1)_Y$.

The $SU(3)$ generators act on the first three indices, while the $SU(2)$ generators act on the last two, ensuring their commutativity. Explicitly:

$$T_{1\ldots8} = \frac{1}{2} \begin{pmatrix} & & & 0 & 0 \\ & \lambda_{1\ldots8} & & 0 & 0 \\ & & & 0 & 0 \\ 0 & 0 & 0 & 0 & 0 \\ 0 & 0 & 0 & 0 & 0 \end{pmatrix},$$

(6.11)

where $\lambda_{1\ldots8}$ are the usual $SU(3)_C$ Gell-Mann matrices. Similarly, the $SU(2)_L$ generators are embedded as

$$T_{9,10,11} = \frac{1}{2} \begin{pmatrix} 0 & 0 & 0 & 0 & 0 \\ 0 & 0 & 0 & 0 & 0 \\ 0 & 0 & 0 & 0 & 0 \\ 0 & 0 & 0 & \sigma_{1,2,3} & \\ 0 & 0 & 0 & & \end{pmatrix},$$

(6.12)

where $\sigma_{1,2,3}$ are the Pauli matrices.

The $SU(2)_L$ weak isospin third generator, corresponding to T_{11}, is given explicitly by

$$T_{11} = \begin{pmatrix} 0 & 0 & 0 & 0 & 0 \\ 0 & 0 & 0 & 0 & 0 \\ 0 & 0 & 0 & 0 & 0 \\ 0 & 0 & 0 & 1/2 & 0 \\ 0 & 0 & 0 & 0 & -1/2 \end{pmatrix}.$$

(6.13)

The generator associated with $U(1)_Y$ is chosen to respect commutation with $SU(3)_C$ and $SU(2)_L$ generators, tracelessness, and correct hypercharge normalization:

$$T_{12} = \sqrt{\frac{3}{5}} \begin{pmatrix} -\frac{1}{3} & 0 & 0 & 0 & 0 \\ 0 & -\frac{1}{3} & 0 & 0 & 0 \\ 0 & 0 & -\frac{1}{3} & 0 & 0 \\ 0 & 0 & 0 & \frac{1}{2} & 0 \\ 0 & 0 & 0 & 0 & \frac{1}{2} \end{pmatrix}.$$

(6.14)

Thus, the SM gauge group is embedded naturally inside $SU(5)$, and the twelve corresponding gauge bosons are associated with the above generators.

The remaining twelve generators correspond to massive vector bosons X and Y, responsible for transitions between quarks and leptons and mediating proton decay. They are represented as off-diagonal matrices connecting the $SU(3)_C$ triplet and $SU(2)_L$ doublet indices. Schematically, they are of the form:

$$T \sim \frac{1}{\sqrt{2}} \begin{pmatrix} 0_{3\times 3} & \mathbf{M}_{3\times 2} \\ \mathbf{M}^{\dagger}_{2\times 3} & 0_{2\times 2} \end{pmatrix},$$

(6.15)

where $\mathbf{M}$ contains elements corresponding to raising and lowering operators between color and weak indices.

Finally, we note that $SU(5)$ is a rank 4 group, having four diagonal generators. These can be identified as T_3 and T_8 from $SU(3)_C$, T_{11} from $SU(2)_L$, and T_{12} from $U(1)_Y$, consistent with the SM structure.

Charge Operator

In the SM, the Gell-Mann-Nishijima relation expresses the electric charge Q as

$$Q = T_3 + \frac{Y}{2},$$

(6.16)

where I_3 is the third component of weak isospin and Y is the weak hypercharge.

In $SU(5)$, the electromagnetic charge operator Q is expected to be a linear combination of the four diagonal generators. Since Q must commute with all $SU(3)_C$ generators (implying that quarks of the same flavor have the same electric charge irrespective of color), we can express Q as

$$Q = T_{11} + T_{12} \equiv T_{11} + \frac{3}{5} Y,$$

(6.17)

where T_{11} is the third generator of $SU(2)_L$ and Y is the properly normalized hypercharge generator defined earlier.

Substituting the explicit matrix forms of T_{11} and T_{12}, the action of the charge operator Q on the fundamental representation 5 yields

$$Q(\psi_i) = \begin{pmatrix} -\frac{1}{3} & 0 & 0 & 0 & 0 \\ 0 & -\frac{1}{3} & 0 & 0 & 0 \\ 0 & 0 & -\frac{1}{3} & 0 & 0 \\ 0 & 0 & 0 & 1 & 0 \\ 0 & 0 & 0 & 0 & 0 \end{pmatrix} \equiv Q_i \, \delta_{ij}.$$

(6.18)

Accordingly, the fundamental conjugate representation $\bar{5}$ (i.e., 5^*) transforms with opposite charges:

$$Q(\psi^i) = -Q_i \, \delta_{ij} = \begin{pmatrix} \frac{1}{3} & 0 & 0 & 0 & 0 \\ 0 & \frac{1}{3} & 0 & 0 & 0 \\ 0 & 0 & \frac{1}{3} & 0 & 0 \\ 0 & 0 & 0 & -1 & 0 \\ 0 & 0 & 0 & 0 & 0 \end{pmatrix}.$$

(6.19)

To determine the charge assignment for the 10 representation, we recall that it transforms as an antisymmetric tensor:

$$\psi_{ij} \to U_{ik} \, U_{jl} \, \psi_{kl},$$

(6.20)

where $U = e^{i\alpha^a T_a}$ is an element of $SU(5)$. Infinitesimally, the variation under a generator T_a reads

$$\delta\psi_{ij} = i\left((T_a)_{ik}\psi_{kj} + (T_a)_{jl}\psi_{il}\right),$$

(6.21)

which implies that the charge operator acts as

$$Q(\chi_{ij}) = \left(Q_i + Q_j\right)\chi_{ij}.$$

(6.22)

Thus, the charge of a component χ_{ij} is simply the sum of the charges Q_i and Q_j corresponding to the fundamental indices i and j.

For example, taking $i = 1, j = 2$ yields

$$Q(\chi_{12}) = Q_1 + Q_2 = -\frac{1}{3} - \frac{1}{3} = -\frac{2}{3},$$

(6.23)

which matches the charge of an up-type quark.

Explicitly, the full charge matrix for the 10 is

$$\begin{pmatrix} 0 & -\frac{2}{3} & -\frac{2}{3} & -\frac{2}{3} & -\frac{1}{3} \\ -\frac{2}{3} & 0 & -\frac{2}{3} & \frac{2}{3} & -\frac{1}{3} \\ -\frac{2}{3} & -\frac{2}{3} & 0 & \frac{2}{3} & -\frac{1}{3} \\ -\frac{2}{3} & \frac{2}{3} & \frac{2}{3} & 0 & 1 \\ -\frac{1}{3} & -\frac{1}{3} & -\frac{1}{3} & 1 & 0 \end{pmatrix}.$$

(6.24)

An important consequence of charge quantization in $SU(5)$ arises from the tracelessness condition imposed on the generators. Specifically, for the quarks and leptons, the condition

$$3Q_d + Q_{e^+} = 0$$

(6.25)

must hold, where Q_d denotes the down-type quark charge and Q_{e^+} the positron charge. This naturally explains why quarks carry electric charge

$1/3$ of that of leptons in grand unified theories [96–98].

6.4 GAUGE BOSONS

The $SU(5)$ group possesses $5^2 - 1 = 24$ gauge bosons. Twelve of these correspond to the well-known gauge bosons of the SM, including the photon, $W^{\pm}$, Z^0, and the eight gluons. The remaining twelve are exotic gauge bosons capable of transforming quarks into leptons and vice versa, a distinctive feature of grand unification [96].

This distinction becomes apparent when decomposing the $SU(5)$ adjoint representation under the SM subgroup:

$$24 = (8,1)_0 \oplus (3,2)_{-5/3} \oplus (\bar{3},2)_{5/3} \oplus (1,3)_0 \oplus (1,1)_0. \tag{6.26}$$

Here, the $(8,1)_0$ corresponds to the eight gluons of $SU(3)_C$, the $(1,3)_0$ corresponds to the three weak gauge bosons $W^{\pm}$ and W^3, and the $(1,1)_0$ is the $U(1)_Y$ hypercharge boson B. The $(3,2)_{-5/3}$ and $(\bar{3},2)_{5/3}$ components represent the twelve new heavy gauge bosons, often called X and Y bosons, which mediate baryon and lepton number-violating interactions.

Following the construction of the $SU(5)$ generators, these 24 gauge fields can be organized in matrix form as:

$$\begin{aligned}\mathbf{A}_\mu = A_\mu^a T_a \quad &= \frac{1}{\sqrt{2}} \begin{pmatrix} & & & \bar{X}_\mu^r & \bar{Y}_\mu^r \\ & G_\mu^8 & & \bar{X}_\mu^g & \bar{Y}_\mu^g \\ & & & \bar{X}_\mu^b & \bar{Y}_\mu^b \\ X_\mu^r & X_\mu^g & X_\mu^b & W_\mu^3 & W_\mu^+ \\ Y_\mu^r & Y_\mu^g & Y_\mu^b & W_\mu^- & -\frac{1}{\sqrt{2}} W_\mu^3 \end{pmatrix} \\ &+ \sqrt{\frac{3}{5}} \begin{pmatrix} -\frac{1}{3} & 0 & 0 & 0 & 0 \\ 0 & -\frac{1}{3} & 0 & 0 & 0 \\ 0 & 0 & -\frac{1}{3} & 0 & 0 \\ 0 & 0 & 0 & \frac{1}{2} & 0 \\ 0 & 0 & 0 & 0 & \frac{1}{2} \end{pmatrix} B_\mu,\end{aligned} \tag{6.27}$$

where $G_\mu^8 = A_\mu^{1\cdots8} T_{1\ldots8}$ are the gluons, $W_\mu^\pm = \frac{1}{\sqrt{2}}(A_\mu^9 \mp i A_\mu^{10})$ are the charged weak bosons, $W_\mu^3 = A_\mu^{11} T_{11}$, and $B_\mu = A_\mu^{12} T_{12}$ corresponds to hypercharge.

The twelve new gauge bosons are defined via linear combinations, for example:

$$\bar{X}_\mu^r = \frac{1}{\sqrt{2}}(A_\mu^{13} - i A_\mu^{14}), \qquad X_\mu^r = \frac{1}{\sqrt{2}}(A_\mu^{13} + i A_\mu^{14}),$$

(6.28)

and similarly for the other color indices *g* and *b*.

The charges of these gauge bosons, obtained analogously using Eq. (6.17), are:

$$\begin{pmatrix} 0 & 0 & 0 & -\frac{4}{3} & -\frac{1}{3} \\ 0 & 0 & 0 & -\frac{4}{3} & -\frac{1}{3} \\ 0 & 0 & 0 & -\frac{4}{3} & -\frac{1}{3} \\ \frac{4}{3} & \frac{4}{3} & \frac{4}{3} & 0 & 1 \\ \frac{1}{3} & \frac{1}{3} & \frac{1}{3} & -1 & 0 \end{pmatrix}.$$

(6.29)

Eqs. (6.27) and (6.29) reveal that the X and Y gauge bosons transform under the SM gauge group as $(\bar{3}, 2)_{-5/3}$, and not as their conjugate representations.

These new bosons can be organized as doublets in color space:

$$\begin{pmatrix} X \\ Y \end{pmatrix} : \quad (\bar{3}, 2)_{-5/3}, \qquad \begin{pmatrix} \bar{X} \\ \bar{Y} \end{pmatrix} : \quad (3, 2)_{5/3}.$$

(6.30)

The existence of these twelve heavy gauge bosons leads to distinct new interactions. As previously noted, in $SU(5)$, quarks and leptons are unified into common multiplets [98]. Thus, the X and Y bosons can mediate transitions between quarks and leptons, or between two quarks, thereby enabling baryon and lepton number-violating processes. In particular, the combination of two such vertices can induce proton decay, a key prediction

of $SU(5)$ grand unified theories [99], which will be discussed in detail in the next section.

6.5 INTERACTIONS

The Lagrangian for the $SU(5)$ gauge field theory incorporates the dynamics of fundamental particles and their interactions. It includes terms governing gauge fields, matter fields, and their mutual couplings. A simplified expression for the $SU(5)$ interaction Lagrangian reads [96, 98]:

$$\mathscr{L} = \mathscr{L}_{\text{gb}} + \mathscr{L}_f + \mathscr{L}_\Phi + \mathscr{L}_Y,$$

(6.31)

where each term corresponds to a distinct sector of the theory. We now describe these contributions in more detail.

Gauge Boson Sector

The kinetic term for the $SU(5)$ gauge bosons is governed by the field strength tensor $F^a_{\mu\nu}$. The gauge boson Lagrangian is given by

$$\mathscr{L}_{\text{gb}} = -\frac{1}{4} F^a_{\mu\nu} F^{a\mu\nu},$$

(6.32)

where the field strength tensor is defined as

$$F^a_{\mu\nu} = \partial_\mu A^a_\nu - \partial_\nu A^a_\mu + g f^{abc} A^b_\mu A^c_\nu,$$

(6.33)

with f^{abc} denoting the structure constants of $SU(5)$. The structure constants are given by

$$f_{abc} = \frac{1}{4i} \text{Tr}\left(\lambda_a \left[\lambda_b, \lambda_c\right]\right),$$

(6.34)

where λ_a are the generators of $SU(5)$ in the fundamental representation.

The covariant derivative acting on a field in the fundamental representation is

$$D_\mu = \partial_\mu - ig_G \sum_{a=1}^{24} A_\mu^a \frac{\lambda_a}{2} \equiv \partial_\mu - ig_G \, \mathbf{A}_\mu,$$

(6.35)

where g_G is the unified gauge coupling constant, and $\mathbf{A}_\mu$ collectively denotes the gauge fields.

Explicitly, the action of the covariant derivative on a fundamental field ψ_p reads

$$D_\mu \psi_p = \partial_\mu \psi_p - ig_G (A_\mu)_{pq} \psi_q,$$

(6.36)

whereas for a two-index tensor field χ_{pq} (such as the antisymmetric $\mathbf{10}$ representation), the covariant derivative is

$$D_\mu \chi_{pq} = \partial_\mu \chi_{pq} - ig_G (A_\mu)^{pr} \chi_{rq} - ig_G (A_\mu)^{qs} \chi_{ps}.$$

(6.37)

These structures form the basis for understanding the dynamics and interactions of matter and gauge fields within the $SU(5)$ grand unified theory framework.

Fermion Sector

The kinetic term for the matter fields, denoted by $\mathscr{L}_f$, describes the propagation and gauge interactions of the fermions ψ_i. It incorporates the covariant derivative D_μ to ensure local $SU(5)$ gauge invariance. The fermion Lagrangian reads

$$\mathscr{L}_f = i(\bar{\psi}^p)_L \gamma^\mu D_\mu (\psi_p)_L + i(\bar{\chi}^{pq})_L \gamma^\mu D_\mu (\chi_{pq})_L,$$

(6.38)

where ψ_p and χ_{pq} represent the left-handed Weyl fermions in the $\mathbf{5}^*$ and $\mathbf{10}$ representations, respectively.

Substituting the explicit forms of the covariant derivatives from Eqs. (6.36) and (6.37), the Lagrangian becomes

$$\begin{aligned}\mathscr{L}_f \quad &= i\,\overline{\psi}^{p}\gamma^{\mu}\partial_{\mu}\psi_{p} + g_G\,\overline{\psi}^{p}\gamma^{\mu}(A_{\mu})_{pq}\psi_{q} + i\,\overline{\chi}^{pq}\gamma^{\mu}\partial_{\mu}\chi_{pq} \\ &\quad - ig_G(A_{\mu})^{pr}\overline{\chi}^{pq}\gamma^{\mu}\chi_{rq} - ig_G(A_{\mu})^{qs}\overline{\chi}^{pq}\gamma^{\mu}\chi_{ps},\end{aligned} \tag{6.39}$$

clearly exhibiting both the kinetic terms (independent of g_G) and the interaction terms between gauge bosons and fermions.

In particular, the interactions involving the heavy X and Y gauge bosons with the SM fermions are given by

$$\begin{aligned}\mathscr{L}_{(X,Y)} = \frac{g_G}{\sqrt{2}}\Big[&\overline{X}^{\alpha}_{\mu}\left(\bar{d}_{\alpha R}\gamma^{\mu}e_R^{+} + \bar{d}_{\alpha L}\gamma^{\mu}e_L^{+} + \epsilon_{\alpha\beta\gamma}\overline{u}_L^{c\gamma}\gamma^{\mu}u_{\beta L}\right) \\ &+\overline{Y}^{\alpha}_{\mu}\left(-\bar{d}_{\alpha R}\gamma^{\mu}\nu_R^{c} + \overline{u}_{\alpha L}\gamma^{\mu}e_L^{+} + \epsilon_{\alpha\beta\gamma}\overline{u}_L^{c\gamma}\gamma^{\mu}d_{\beta L}\right)\Big] + \text{h.c},\end{aligned} \tag{6.40}$$

where α, β, γ are color indices, and $\epsilon_{\alpha\beta\gamma}$ is the totally antisymmetric tensor. These interactions lead to baryon and lepton number violation, providing a framework for proton decay predictions in $SU(5)$ GUTs [98, 99].

Scalar Sector

The scalar sector of $SU(5)$ plays a crucial role in achieving spontaneous symmetry breaking. In particular, scalar fields belonging to the adjoint $\mathbf{24}$ representation and the fundamental $\mathbf{5}$ representation are responsible for breaking $SU(5)$ down to the SM gauge group and further to $U(1)_{\text{EM}}$.

The adjoint scalar field Φ acquires a VEV that triggers the breaking $SU(5) \to SU(3)_C \times SU(2)_L \times U(1)_Y$, while the 5-plet scalar field H_5 is responsible for electroweak symmetry breaking and giving masses to fermions via Yukawa interactions.

The scalar Lagrangian $\mathscr{L}_{\Phi}$ is given by

$$\mathscr{L}_{\Phi} = \text{Tr}\left[(D_{\mu}\Phi)^{\dagger}(D^{\mu}\Phi)\right] + (D_{\mu}H_5)^{\dagger}(D^{\mu}H_5) - V(\Phi, H_5), \tag{6.41}$$

where the trace is taken over the group indices and the covariant derivatives are defined as

$$D_\mu \Phi = \partial_\mu \Phi + i g_G [A_\mu, \Phi],$$

(6.42)

$$D_\mu H_5 = (\partial_\mu - i g_G \, \mathbf{A}_\mu) H_5.$$

(6.43)

The scalar potential $V(\Phi, H_5)$ governs the self-interactions and the mixing between Φ and H_5. A simple form of the potential can be written as [96, 97]

$$\begin{aligned} V(\Phi, H_5) \quad &= \mu_{\mathbf{24}}^2 \, \mathrm{Tr}(\Phi^\dagger \Phi) + \mu_{H_5}^2 \, (H_5^\dagger H_5) + \lambda_{\mathbf{24}} \, [\mathrm{Tr}(\Phi^\dagger \Phi)]^2 \\ &\quad + \lambda_{H_5} \, (H_5^\dagger H_5)^2 + \lambda_{\mathbf{24}H_5} \, \mathrm{Tr}(\Phi^\dagger \Phi) \, (H_5^\dagger H_5), \end{aligned}$$

(6.44)

where $\mu_{\mathbf{24}}^2$, $\mu_{H_5}^2$ are mass parameters and $\lambda_{\mathbf{24}}$, λ_{H_5}, $\lambda_{\mathbf{24}H_5}$ are dimensionless couplings controlling the strengths of the interactions.

These terms dictate the vacuum structure of the theory and the mass spectra of the resulting scalar and gauge bosons after spontaneous symmetry breaking.

Yukawa sector

In the construction of the SU(5) invariant Yukawa Lagrangian, the tensor product decompositions are given by:

$$\begin{aligned} 5^* \times 10 \quad &= 5 + 45^*, \\ 10 \times 10 \quad &= 5^* + 45 + 50, \\ 5^* \times 5^* \quad &= 10^* + 15^*. \end{aligned}$$

The above decompositions reveal that, in adhering to the scalar representations of the minimal $SU(5)$ theory, namely $H_5 \equiv 5_H$ and $\Phi \equiv 24_H$, only two invariant Yukawa mass terms exist:

$$5^* \otimes 10 \otimes 5_H^*,$$

(6.45)

$$10 \otimes 10 \otimes 5_H.$$

(6.46)

Consequently, the Yukawa Lagrangian at the GUT scale becomes:

$$\mathscr{L}_Y^G = \Gamma_1 \, (5_L^{C\alpha})^T \, C \, 10_L^{\alpha\beta} \, 5_H^{*\beta} + \Gamma_2 \, \epsilon_{\alpha\beta\gamma\delta r} \, (10_L^{\alpha\beta})^T \, C \, 10_L^{\gamma\delta} \, 5^r + \text{h.c.},$$

(6.47)

where Γ_1 and Γ_2 denote the Yukawa couplings.

6.6 SPONTANEOUS SYMMETRY BREAKING

As discussed previously, the scalar potential for the adjoint Higgs multiplet Φ in $SU(5)$ is given by [96]:

$$V(\Phi) = m_1^2 \, \mathrm{Tr}(\Phi^2) + \lambda_1 \big[\mathrm{Tr}(\Phi^2)\big]^2 + \lambda_2 \, \mathrm{Tr}(\Phi^4),$$

(6.48)

where Φ is expanded over the generators T^a of the adjoint representation:

$$\Phi = \sum_{a=1}^{24} \phi^a T^a.$$

(6.49)

To achieve symmetry breaking $SU(5) \to SU(3)_c \times SU(2)_L \times U(1)_Y$, we align the VEV of Φ along the T^{24} generator:

$$\langle \Phi \rangle = \phi_{24} T^{24} = \frac{1}{\sqrt{15}} \phi_{24} \, \mathrm{Diag}(-2,-2,-2,3,3).$$

(6.50)

This choice leaves the SM subgroup unbroken while breaking the rest of $SU(5)$. Symmetry is preserved for generators T satisfying $[\Phi, T] = 0$, with the transformation $\Phi \to U \Phi U^\dagger$, $U = \exp(-i \underline{\alpha} \cdot \underline{T})$. The VEV $\langle \Phi \rangle$ commutes with the SM generators but not with the X and Y leptoquark generators, indicating partial symmetry breaking [98]. We find:

$$\mathrm{Tr}(\Phi^2) = 2\phi_{24}^2, \quad \big[\mathrm{Tr}(\Phi^2)\big]^2 = 4\phi_{24}^4,$$

(6.51)

and

$$\mathrm{Tr}(\Phi^4) = \frac{14}{15}\phi_{24}^4.$$

(6.52)

Minimizing the potential yields:

$$\frac{\delta V}{\delta \Phi} = \phi_{24}\left[-4m_1^2 + \left(16\lambda_1 + \frac{56}{15}\lambda_2\right)\phi_{24}^2\right] = 0,$$

(6.53)

leading to the VEV:

$$\phi_{24}^2 = v_\Phi^2 = \frac{m_1^2}{4\lambda_1 + \frac{14}{15}\lambda_2},$$

(6.54)

with stability conditions:

$$\lambda_2 > 0, \quad \lambda_1 > -\frac{7}{30}\lambda_2.$$

(6.55)

Thus, the explicit form of the VEV is:

$$\langle \Phi \rangle = \frac{v_\Phi}{\sqrt{15}} \begin{pmatrix} -2 & & & & \\ & -2 & & & \\ & & -2 & & \\ & & & 3 & \\ & & & & 3 \end{pmatrix}.$$

(6.56)

The VEV generates masses for the X and Y gauge bosons via the kinetic term:

$$\mathscr{L}_{\text{mass}} = -g_G^2\,\mathrm{Tr}([A_\mu, \Phi]^2),$$

(6.57)

leading to:

$$\mathscr{L}_{\text{mass}} = \frac{20}{3} g_G^2 v_\Phi^2 \sum_{i=1}^{3} \left(\overline{X}_i^\mu X_{i\mu} + \overline{Y}_i^\mu Y_{i\mu} \right),$$

(6.58)

with gauge boson masses:

$$m_X^2 = m_Y^2 = \frac{20}{3} g_G^2 v_\Phi^2.$$

(6.59)

Thus, X and Y bosons acquire superheavy masses of order M_{GUT} and decouple from low-energy physics [97, 98].

In the second stage, the scalar field H_5 acquires a VEV, breaking $SU(3)_c \times SU(2)_L \times U(1)_Y$ down to $SU(3)_c \times U(1)_{\text{em}}$. The scalar potential reads:

$$V(H_5) = \frac{m_2^2}{2} H_5^\dagger H_5 + \frac{\lambda_3}{4} (H_5^\dagger H_5)^2.$$

(6.60)

Choosing the VEV in the neutral component:

$$\langle H_5 \rangle = \begin{pmatrix} 0 \\ 0 \\ 0 \\ 0 \\ v_H \end{pmatrix},$$

(6.61)

and minimizing the potential gives:

$$v_H^2 = -\frac{m_2^2}{\lambda_3}.$$

(6.62)

This mechanism is analogous to electroweak symmetry breaking in the SM, generating $W^\pm$ and Z^0 masses.

The fermion mass terms arise from Yukawa couplings:

$$\begin{aligned}\mathscr{L}_m &= Y_1(\bar{d}_L^C C d_L + \bar{e}_L^T C e_L^C)\frac{v_H^*}{\sqrt{2}} + 4Y_2(\bar{u}_L^T C u_L + \bar{u}_L^{CT} C u_L)\frac{v_H}{\sqrt{2}} + \text{h.c.} \\ &= (Y_1 \bar{d}_R d_L - Y_1^T \bar{e}_R e_L)\frac{v_H^*}{\sqrt{2}} + 4(Y_2 \bar{u}_R u_L - Y_2^T \bar{u}_R u_L)\frac{v_H}{\sqrt{2}}.\end{aligned} \tag{6.63}$$

At tree level, the minimal $SU(5)$ model predicts:

$$m_d = m_e, \tag{6.64}$$

$$m_s = m_\mu, \tag{6.65}$$

$$m_b = m_\tau, \tag{6.66}$$

at the unification scale [96]. However, renormalization effects modify these relations. Notably, at low energies:

$$m_b \approx 3 m_\tau, \tag{6.67}$$

consistent with observations [100]. Yet, discrepancies arise for lighter generations:

$$m_s \approx 3 m_\mu, \tag{6.68}$$

$$\frac{m_\mu}{m_e} \approx \frac{m_s}{m_d}. \tag{6.69}$$

The ratios $m_d/m_s \simeq 1/24$ and $m_e/m_\mu \simeq 1/207$ are starkly different, posing a major flaw in minimal $SU(5)$ [101].

Possible remedies include: (i) extending the Higgs sector by adding a 45 representation [102]; (ii) introducing higher-dimensional operators suppressed by the Planck scale [100].

6.7 DOUBLET-TRIPLET SPLITTING PROBLEM

The coupling terms between the 24-Higgs scalar representation and the 5-Higgs scalar representation, denoted as $V(\Phi, H)$, are given by:

$$\begin{aligned} V(\Phi, H) =& m_1^2 \mathrm{Tr}\Phi^2 + \lambda_1[\mathrm{Tr}(\Phi^2)]^2 + \lambda_2 \mathrm{Tr}\Phi^4 + \frac{m_2^2}{2} H_5^\dagger H_5 \\ &+ \frac{\lambda_3}{4}(H_5^\dagger H_5)^2 + \underline{\alpha H^\dagger H \mathrm{Tr}\Phi^2 + \beta H^\dagger \Phi^2 H}, \end{aligned} \tag{6.70}$$

where the underlined terms yield coupling between h_3 (triplet colored Higgs scalars) and h_2 (SM Higgs doublet) with 24-Higgs. Consequently, the 5-Higgs scalars acquire mass as follows:

$$(2\alpha + \frac{4}{15}\beta) v_\Phi^2 h_3^\dagger h_3 + (2\alpha + \frac{9}{15}\beta) v_\Phi^2 h_2^\dagger h_2. \tag{6.71}$$

However, this leads to a problem: the mass of both h_3 (Higgs triplet) and h_2 (Higgs doublet) would be of the order of $v_\Phi^2 \approx 10^{15}$ GeV. While this may be acceptable for h_3, as it can contribute to proton decay, the doublet Higgs h_2 should ideally have a mass of around 100 GeV to facilitate electroweak symmetry breaking. This discrepancy is known as the doublet-triplet splitting problem [96, 103].

Nevertheless, it is possible to fine-tune the parameters in the equation to make the second term zero, which yields:

$$\alpha = -\frac{9}{30}\beta \qquad \text{and} \qquad \beta < 0. \tag{6.72}$$

The doublet-triplet splitting problem has motivated the development of various mechanisms to naturally generate the splitting without extreme fine-tuning. One of the most notable proposals is the so-called “missing VEV mechanism” [104], originally introduced in the context of supersymmetric GUTs. More sophisticated solutions often involve introducing extended symmetries, additional Higgs fields, or extra dimensions [105]. Resolving

this issue remains essential for ensuring the consistency and viability of realistic GUT models.

6.8 GAUGE COUPLING UNIFICATION IN $SU(5)$

The possibility of unifying the gauge couplings within a GUT was first proposed in the seminal work of Georgi and Glashow [96]. In the SM, there are three gauge couplings corresponding to the SM gauge groups. The renormalization group equations (RGEs) describe how the coupling constants of a quantum field theory evolve with the energy scale at which the theory is probed. The RGEs for the gauge couplings in the SM, $\alpha_i = g_i^2/4\pi$ with $i = 1, 2, 3$ referring to $U(1)_Y$, $SU(2)_L$, and $SU(3)_C$, respectively, can be written as:

$$\frac{d\alpha_i}{dt} = \frac{\alpha_i^2}{2\pi} b_i,$$

(6.73)

where $t = \ln \mu$ and μ is the renormalization scale. The solution to these equations is given by

$$\alpha_i^{-1}(\mu) = \alpha_i^{-1}(M_X) + \frac{b_i}{2\pi} \ln\left(\frac{M_X}{\mu}\right).$$

(6.74)

Here, the running is from the low scale μ (e.g., M_Z) up to a high energy scale M_X. The beta function coefficients, b_i, in the SM with n_f families are given by:

$$b_1 = \frac{1}{10} + \frac{4}{3} n_f,$$

(6.75)

$$b_2 = -\frac{43}{6} + \frac{4}{3} n_f,$$

(6.76)

$$b_3 = -11 + \frac{4}{3} n_f.$$

(6.77)

For $n_f = 3$, one obtains $b_1 = \frac{41}{10}$, $b_2 = -\frac{19}{6}$, and $b_3 = -7$. Since b_1 is positive, α_1 increases with energy, while α_2 and α_3 decrease. However, α_3 decreases more rapidly than α_2. Thus, at some scale higher than the Fermi scale, the strength of the strong interactions may become comparable to the strength of the electroweak interactions.

The evolution of the SM gauge couplings is illustrated in Fig. 6.1, emphasizing that there is no high-energy scale M_X where the gauge couplings meet at a single point. Consequently, their unification within the framework of the SM is not achieved [98].

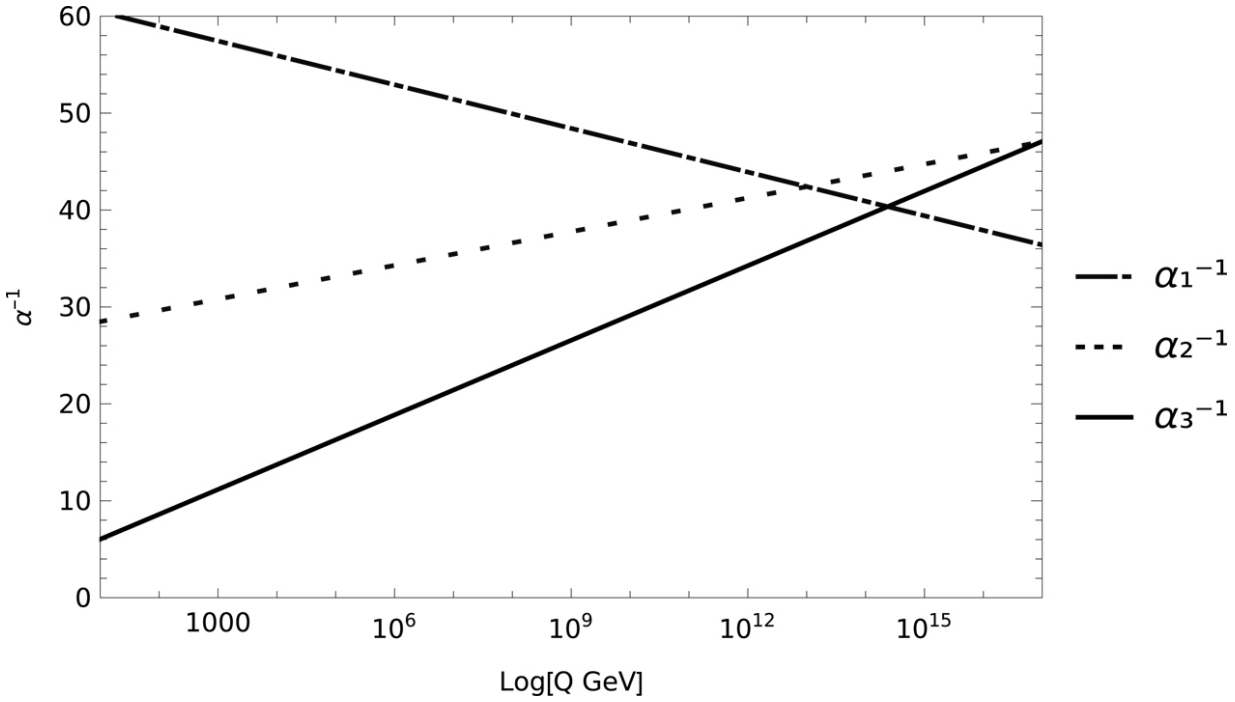

Figure 6.1 Evolution of the inverse of the SM three coupling constants.

In the context of the SU(5) GUT, the primary goal is to consolidate all fundamental forces under a single gauge coupling at a high energy scale conventionally denoted as M_X. At energy scales $Q > M_X$, the theory predicts a unique coupling constant g_G associated with the unified gauge group. Thus, at these energies, the strong, weak, and electromagnetic interactions are governed by identical couplings:

$$g_G = g_3 = g_2 = g_1.$$

(6.78)

This unification provides an elegant framework for understanding the fundamental forces within a single theoretical structure.

Given the normalization condition imposed on λ_{12}, one has $Y = \sqrt{\frac{5}{3}}\lambda_{12}$, leading to $g' = \sqrt{\frac{3}{5}}g_1$. Consequently, one finds that the Weinberg mixing angle at the unification scale satisfies:

$$\sin^2\theta_W = \frac{g'^2}{g'^2 + g^2} = \frac{3}{8},$$

(6.79)

which holds at M_X. For scales $Q < M_X$, the running of the couplings follows

$$\alpha_i^{-1}(Q) = \alpha_5^{-1} + \frac{b_i}{2\pi}\ln\left(\frac{M_X}{Q}\right),$$

(6.80)

where α_5 denotes the unified coupling at the scale M_X. This running is depicted in Fig. 6.2.

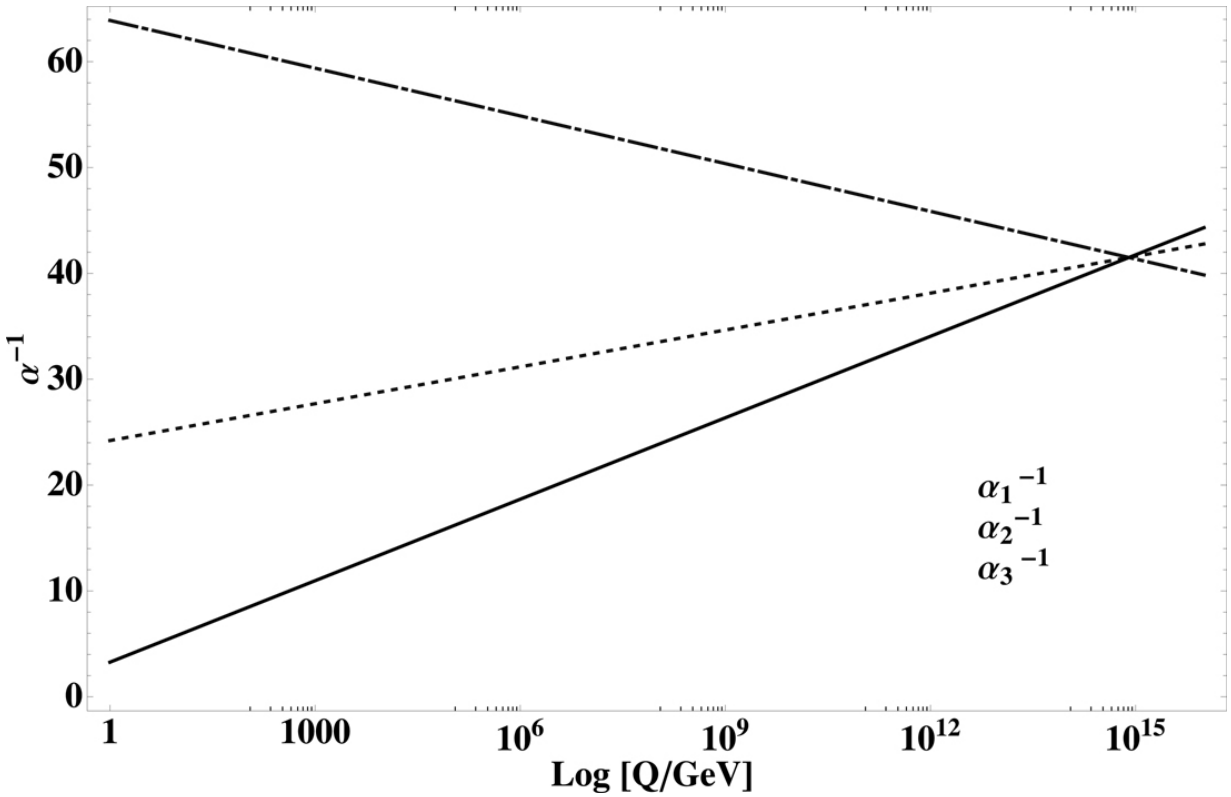

Figure 6.2 The predicted unification scale by the minimal-SU(5) theory for the SM gauge coupling constants. ⏎

The inputs to the problem are the measurable values of the $U(1)_{\rm em}$ and $SU(3)_C$ couplings at low energies, given by [106]:

$$\alpha_{em} = \frac{3}{5}\alpha_1 \cos^2\theta_W = \alpha_2 \sin^2\theta_W,$$

(6.81)

which implies

$$\alpha_{em}^{-1} = \frac{5}{3}\alpha_1^{-1} + \alpha_2^{-1}.$$

(6.82)

From Eq. (6.80), it follows that

$$\alpha_1^{-1} - \alpha_2^{-1} \quad = \frac{b_1 - b_2}{2\pi}\ln\left(\frac{M_X}{Q}\right),$$

(6.83)

$$\alpha_2^{-1} - \alpha_3^{-1} = \frac{b_2 - b_3}{2\pi} \ln\left(\frac{M_X}{Q}\right). \tag{6.84}$$

For $Q = M_Z$, one finds

$$\alpha_{em}^{-1} = \frac{8}{3}\alpha_3^{-1} + \frac{22}{2\pi} \ln\left(\frac{M_X}{M_Z}\right), \tag{6.85}$$

which leads to $M_X \simeq 8 \times 10^{14}\,\text{GeV}$. Furthermore, the unified coupling is given by $\alpha_5^{-1} \simeq 41.5$.

Additionally, one can estimate $\sin^2\theta_W(M_Z)$ as follows:

$$\begin{aligned} \sin^2\theta_W(M_Z) &= \frac{\alpha_{em}(M_Z)}{\alpha_2(M_Z)} \\ &= \alpha_{em}(M_Z)\left[\frac{1}{\alpha_3(M_Z)} + \frac{22}{12\pi}\ln\left(\frac{M_X}{M_Z}\right)\right] \\ &= \frac{5}{9}\frac{\alpha_{em}(M_Z)}{\alpha_3(M_Z)} + \frac{1}{6} \simeq 0.201, \end{aligned} \tag{6.86}$$

which deviates significantly from the experimental value

$$[\sin^2\theta_W(M_Z)]_{\text{exp}} = 0.23120 \pm 0.00015$$

reported in [106]. Thus, minimal SU(5) with the SM particle content does not successfully achieve gauge coupling unification [98].

6.9 PROTON DECAY

In $SU(5)$ GUTs, the unification of quarks and leptons into common multiplets naturally predicts baryon number violation, leading to proton decay [96, 98]. Proton decay processes are primarily mediated by the heavy X and Y leptoquark gauge bosons, whose interactions with fermions are described by the Lagrangian in Eq. (6.40). These interactions give rise to various proton decay channels, the most notable being $p \to e^+\pi^0$, as illustrated in Fig. 6.3.

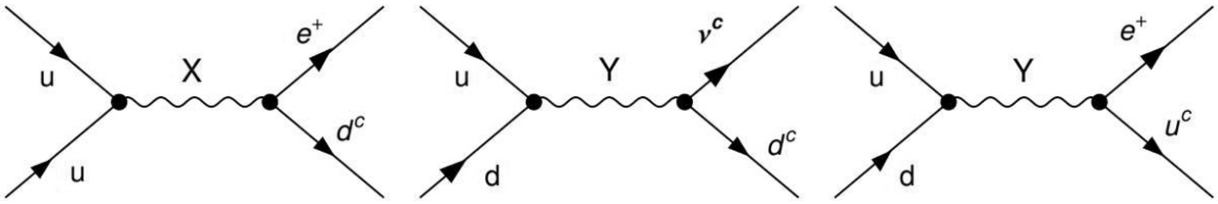

Figure 6.3 Baryon number violating processes at the lowest order via X and Y boson exchange. ⏎

Experimentally, the Super-Kamiokande collaboration has set a lower bound on the proton lifetime [107]:

$$\tau_p(p \to e^+\pi^0) \gtrsim 5 \times 10^{33}\,\text{years}. \tag{6.87}$$

On the theoretical side, the model-independent estimate for the proton decay width due to dimension-6 operators is given by

$$\Gamma_p \approx \alpha_{GUT}^2 \frac{m_p^5}{M_X^4}, \tag{6.88}$$

where α_{GUT} is the unified coupling constant, m_p is the proton mass, and M_X is the mass scale of the heavy leptoquark gauge bosons.

This leads to a lower bound on the M_X scale, assuming $\alpha_{GUT} \sim 1/40 - 1/25$:

$$M_X \gtrsim 3.2 \times 10^{15}\,\text{GeV}. \tag{6.89}$$

However, in minimal $SU(5)$ models, gauge coupling unification predicts $M_X \sim 10^{14}\,\text{GeV}$ [108], which is in tension with the experimental lower limits on proton lifetime. This discrepancy highlights a major challenge for minimal $SU(5)$ GUTs, motivating extensions such as supersymmetric unification, missing partner mechanisms, or higher-dimensional constructions [109].

6.10 *SU*(5) ASSESSMENT

6.10.1 Advantages

1. $SU(5)$ is the only GUT with rank 4. While other GUTs, such as $SO(10)$, have higher ranks, which provide greater flexibility in their breaking patterns, they may sacrifice predictability.
2. A distinctive feature of $SU(5)$ is the quantization of electric charge (Q), where $\mathrm{Tr}Q|_5 = 0$ implies $Q(d) = \frac{1}{3}Q(e^-)$.
3. The prediction for the weak mixing angle, $\sin^2\theta_W$, is in excellent agreement with current experimental data.
4. $SU(5)$ predicts a ratio $m_b/m_\tau \simeq 3$ at low energy, which is consistent with experimental observations.
5. The simplest version of $SU(5)$, with a single Higgs 5-plet, avoids tree-level FCNCs.
6. The model is free of gauge anomalies, making it a consistent quantum field theory.
7. $SU(5)$ explains the baryon asymmetry by enabling baryon number violating processes required for baryogenesis; proton decay is a low-energy manifestation of such processes.
8. The minimal $SU(5)$ model makes unique, testable predictions regarding the weak mixing angle $\sin^2\theta_W$ and nucleon lifetime, both of which can be probed experimentally.

6.10.2 Disadvantages

1. The $SU(5)$ model faces significant challenges from new experimental constraints on proton decay, especially the $P \to e^+\pi^0$ channel. If the proton lifetime bound of 10^{32} years is confirmed, the minimal $SU(5)$ model may be ruled out, requiring extensions that reduce predictability.
2. In the minimal version of the model, which only includes Higgs 5-plets, the ratio m_e/m_μ is predicted to be equal to m_d/m_s, which does not match the experimentally observed mass hierarchy of leptons and quarks.

3. Fermions in the $SU(5)$ model are assigned to reducible representations ($5^* + 10$), which complicates the understanding of their properties.
4. $SU(5)$ does not provide a clear explanation for the masses of fermions. The Yukawa couplings and the structure of the Higgs potential must be fine-tuned to fit experimental data.
5. There exists a significant gap (the "great desert") between the W boson mass (M_W) and the X boson mass (M_X), with no natural explanation for the intermediate mass scale.
6. The Higgs scalar potential introduces considerable arbitrariness due to undetermined parameters in the Higgs potential and the Yukawa Lagrangian.
7. Despite the proximity of the GUT scale M_X to the Planck scale M_P, gravity remains excluded from the unified gauge group picture in $SU(5)$.
8. The gauge hierarchy problem remains unsolved within the $SU(5)$ framework, requiring additional mechanisms such as supersymmetry or extra dimensions.

CHAPTER 7

Non-Minimal *SU*(5) Model

DOI: 10.1201/9781003457701-7

In this chapter, we discuss the non-minimal $SU(5)$ GUT in which the Higgs sector is extended by the inclusion of a scalar field in the 45 representation [102]. The 45 arises from the tensor product of the antisymmetric 10 representation and the conjugate fundamental 5^* representation, as follows:

$$5 \times 5 = 10_A \oplus 15_S, \tag{7.1}$$

$$10_A \times 5^* = 45 \oplus 5. \tag{7.2}$$

The 45 representation consists of two upper indices from the 10 and a lower index corresponding to the 5^*. To isolate the 45 component from a general tensor $T_\gamma^{\alpha\beta}$, we need to construct a combination that is antisymmetric in α and β, traceless, and satisfies the condition of vanishing total antisymmetrization over all three indices. This leads to the projected form

$$45_\gamma^{\alpha;\beta} = 45_\gamma^{\alpha\beta} + 45_\alpha^{\gamma\beta} - 45_\alpha^{\beta\gamma} - 45_\beta^{\alpha\gamma}, \tag{7.3}$$

which ensures the proper mixed symmetry required for the irreducible 45 representation. Therefore, the 45 Higgs scalars field satisfy the following conditions:

$$45_\gamma^{\alpha\beta} = -45_\gamma^{\beta\alpha}, \quad \sum_\alpha^5 (45)_\alpha^{\alpha\beta} = 0, \tag{7.4}$$

with

$$\sum_{i=1}^{3} < 45 >_i^{i5} = - < 45 >_4^{45}$$

and

$$v_{45} = < 45 >_1^{15} = < 45 >_2^{25} = < 45 >_3^{35},$$

where the VEVs are defined as v_{45}.

The SU(5)-invariant Higgs potential for the 45_H representation is given by [110]:

$$\begin{aligned} V(45_H) \quad &= -\frac{1}{2}\mu_{45}^2(45_\gamma^{\alpha\beta}45_{\alpha\beta}^\gamma) + \lambda_1(45_\gamma^{\alpha\beta}45_{\alpha\beta}^\gamma)^2 \\ &+\lambda_2 45_\gamma^{\alpha\beta}45_{\alpha\beta}^\delta 45_\delta^{k\lambda}45_{k\lambda}^\gamma \\ &+\lambda_3 45_\gamma^{\alpha\beta}45_{\alpha\beta}^\delta 45_\lambda^{k\gamma}45_{k\delta}^\lambda + \lambda_4 45_\beta^{\alpha\delta}45_{\alpha\gamma}^\beta 45_\lambda^{k\gamma}45_{k\delta}^\lambda \\ &+\lambda_5 45_\delta^{\alpha\gamma}45_{\gamma e}^\beta 45_\alpha^{k\delta}45_{k\beta}^e + \lambda_6 45_\delta^{\alpha\gamma}45_{\gamma e}^\beta 45_\alpha^{ke}45_{k\beta}^\delta \\ &+\lambda_7 45_\delta^{\alpha\gamma}45_{\gamma e}^\beta 45_\beta^{k\delta}45_{k\alpha}^e + \lambda_8 45_\delta^{\alpha\gamma}45_{\gamma e}^\beta 45_\beta^{ke}45_{k\alpha}^\gamma. \end{aligned} \tag{7.5}$$

The SM decomposition of the 45 Higgs representation is given by [97]:

$$\begin{aligned} 45_H \quad =& (8,2)_{1/2} \oplus (6^*,1)_{-1/3} \oplus (3,3)_{-1/3} \oplus (3^*,2)_{-7/6} \oplus (3,1)_{-1/3} \\ &\oplus (3^*,1)_{4/3} \oplus (1,2)_{1/2}. \end{aligned} \tag{7.6}$$

This decomposition follows directly from the tensor product relations in Eq. (7.1) and Eq. (7.2). These components correspond to the fields defined in the spectrum table (Table 7.1).

TABLE 7.1 45-Higgs scalars spectrum.

$(6^*,1,-1/3)_k^{ij}$	$\equiv$	ϕ_k^{ij}	$= \frac{1}{6}\,\epsilon^{ijl}\phi_{lk}$
$(3^*,2,-7/6)_c^{ij}$	$\equiv$	ϕ_c^{ij}	$= \frac{1}{6}\,\epsilon^{ijl}\phi_{lc} = \frac{1}{6}\,\epsilon^{ijl}45_{lc}$
$(3^*,1,4/3)_k^{ab}$	$\equiv$	ϕ_k^{ab}	$= \frac{1}{2}\,\delta^{ab}45_k$
$(3,1,1/3)_c^{ib}$ $(3,1,1/3)_k^{ij}$	$\equiv$	T_1^i	$= \frac{1}{2}\,\delta_c^b 45^i = -\frac{1}{2}\,\delta_k^j 45^i$
$(3,3,-1/3)_c^{ib}$	$\equiv$	T_3^i	$= 45_c^{ib} - \frac{1}{2}\delta_c^b 45_d^{id}$
$(1,2,1/2)_c^{ab}$ $(1,2,1/2)_k^{ib}$	$\equiv$	D^b	$= \frac{1}{2}\,\delta_c^a 45^b = -\frac{1}{2}\,\delta_k^i 45^b$

The color octet scalars are defined as:

$$(8,2,1/2)_j^{ia} \equiv S_j^{ia} = (45_H)_j^{ia} - \frac{1}{3}\delta_j^i(45_H)_m^{ma}. \tag{7.7}$$

7.1 LOW ENERGY IMPLICATIONS OF 45-HIGGS

7.1.1 Fermion Masses

From the above mentioned decompositions, the SU(5) invariant Yukawa Lagrangian can be extended to include the 45-Higgs representation as follows [102, 111, 112]:

$$\begin{aligned} L_Y^G = \; & \Gamma_1 \, (5_L^{C\alpha})^T C \, 10_L^{\alpha\beta} \, 5_H^{*\beta} + \Gamma_2 \, (5_L^{C\gamma})^T C \, 10_L^{\alpha\beta} \, 45_\gamma^{*\alpha\beta} \\ & + \epsilon_{\alpha\beta\gamma\delta r} \left[\Gamma_3 \, (10_L^{\alpha\beta})^T C \, 10_L^{\gamma\delta} \, 5^r + \Gamma_4 \, (10_L^{\alpha\beta})^T C \, 10_L^{m\gamma} \, 45_m^{\delta r} \right]. \end{aligned} \tag{7.8}$$

After electroweak symmetry breaking, the fermion masses are given by:

$$\begin{aligned} L_m = \; & (Y_1 \, \bar{d}_{Ri} \, d_{Li} + Y_1^T \, \bar{e}_R \, e_L) \frac{\upsilon_5^*}{\sqrt{2}} + (2Y_2 \, \bar{d}_{Ri} \, d_{Li} - 6Y_2^T \, \bar{e}_R \, e_L) \frac{\upsilon_{45}^*}{\sqrt{2}} \\ & + [4(Y_3 + Y_3^T) \frac{\upsilon_5}{\sqrt{2}} - 8(Y_4 - Y_4^T) \frac{\upsilon_{45}}{\sqrt{2}}] \bar{u}_{Ri} u_{Li}. \end{aligned} \tag{7.9}$$

The fermion masses are then:

$$\begin{aligned} M_E &= Y_1^T \frac{\upsilon_5^*}{\sqrt{2}} - 6Y_2^T \frac{\upsilon_{45}^*}{\sqrt{2}}, \\ M_D &= Y_1 \frac{\upsilon_5^*}{\sqrt{2}} + 2Y_2 \frac{\upsilon_{45}^*}{\sqrt{2}}, \\ M_U &= 4(Y_3 + Y_3^T) \frac{\upsilon_5}{\sqrt{2}} - 8(Y_4 - Y_4^T) \frac{\upsilon_{45}}{\sqrt{2}}, \end{aligned} \tag{7.10}$$

where $\upsilon^2 = \upsilon_5^2 + \upsilon_{45}^2$. This formulation corrects the fermion mass relations from the previous chapter.

7.1.2 Nucleon Decay Constraints on 45-Higgs Masses

Nucleon decay can be induced by dimension-five operators involving color-triplet Higgs multiplets, where the decay rate is proportional to the square of the Higgs masses ($\tau_{n.p}^{-1} \propto M_\Phi^{-2}$). Therefore, matter stability provides a strong experimental constraint on the masses of new scalars in GUT theories, particularly those carrying color quantum numbers.

The 45-Higgs fields contributing to nucleon decay are derived from the GUT Yukawa Lagrangian:

$$L_Y^{45_H} = \Gamma_2 \, (5_L^{C\gamma})^T C \, 10_L^{\alpha\beta} \, 45_\gamma^{\alpha\beta \, *} + \epsilon_{\alpha\beta\gamma\delta r} \, \Gamma_4 \, (10_L^{\alpha\beta})^T C \, 10_L^{m\gamma} \, 45_m^{\delta r}. \tag{7.11}$$

Starting with the colored octet scalars, S_j^{ia}, we have:

$$S_j^{ia} = \begin{pmatrix} S_j^{i4} \\ S_j^{i5} \end{pmatrix} = \begin{pmatrix} S_j^{i+} \\ S_j^{i0} \end{pmatrix} \equiv S^A T^A,$$

where $A = 1, \ldots, 8$ and T^A are the $SU(3)$ generators. The relevant Yukawa interactions are:

$$\begin{aligned} L_Y^S &= 2Y_2\,(5_L^{Cj})^T C\,10_L^{ia}\,S^* + 4Y_4\left[\epsilon_{klbia}\,(10_L^{kl})^T C\,10_L^{jb}\right. \\ &\quad \left. +\epsilon_{kblia}\,(10_L^{kb})^T C\,10_L^{jl}\right] S + \text{h.c.} \\ &= 2Y_2\,\bar{d}_{Ri}\,S^\dagger\,Q_{Lj} - 4\epsilon_{\alpha\beta}(Y_4 - Y_4^T)\,\bar{u}_{Ri}\,Q_{Lj}^\alpha\,S^\beta + \text{h.c.}. \end{aligned} \tag{7.12}$$

For the 45-Higgs doublet, D^a:

$$D^a = \begin{pmatrix} D^+ \\ D^0 \end{pmatrix}, \tag{7.13}$$

the Yukawa interactions are:

$$L_Y^D = Y_2^{eT}\,\bar{e}_R\,D^\dagger\,l_L + Y_2^d\,\bar{d}_R\,D^\dagger\,Q_L + 2\epsilon_{\alpha\beta}Y_4\,\bar{u}_R\,Q_L^\alpha\,D^\beta + \text{h.c.}. \tag{7.14}$$

Table 7.2 summarizes the interactions of the 45-Higgs scalar multiplets with matter, showing which fields contribute to nucleon decay [111]. Experimental lower bounds on the proton decay rate, such as $\tau(p \to k^+\bar{\nu}) > 2.3 \times 10^{33}$ years [113], require the scalars responsible for nucleon decay to be superheavy.

TABLE 7.2 The interactions of 45-Higgs scalars with matter and their contributions to proton decay.

45_H Scalar	$Y^2_{AB}5^*_A10_B45^*$	$Y^4_{AB}10_A10_B45$	Interactions	Proton Decay
$(6^*,1,-1/3)$	$2Y^2_{AB}d^{cT}_{Ak}Cu^c_{Bl}\phi^{lk*}$	$4Y^4_{AB}(u^{lT}_A Cd^k_B - d^{lT}_A Cu^k_B)\phi_{lk}$	$\bar{U}\bar{D}$, UD	No
$(3^*,2,-7/6)$	$2Y^2_{AB}e^T_A Cu^c_{Bi}\phi^{i1*}$ $-2Y^2_{AB}\nu^T_A Cu^c_{Bi}\phi^{i2*}$	$4(Y^4_{AB} - Y^4_{BA})u^{iT}_A Ce^c_B\phi_{i1}$ $4(Y^4_{AB} - Y^4_{BA})d^{iT}_A Ce^c_B\phi_{i2}$	$L\bar{U}, Q\bar{E}$	No
$(3^*,1,4/3)$	$2Y^2_{AB}d^{cT}_{Ak}Ce^c_B\phi^{k*}$	$4(Y^4_{AB} - Y^4_{BA})\epsilon^{mnk}u^{cT}_{Am}Cu^c_{Bn}\phi_k$	$\bar{E}\bar{D}, \bar{U}\bar{U}$	Yes
$(3,1,-1/3)$	$2Y^2_{AB}e^T_A Cu^i_B T^*_i$ $-2Y^2_{AB}\nu^T_A Cd^i_B T^*_i$ $2Y^2_{AB}\epsilon_{lkj}d^{cT}_{Al}Cu^c_{Bk}T^*_j$	$4(Y^4_{AB} - Y^4_{BA})u^{cT}_{Ai}Ce^c_B T^i$	$LQ, \bar{U}\bar{D}\,\bar{U}\bar{E}$	Yes
$(3,3,-1/3)$	$-2Y^2_{AB}\nu^T_A Cu^i_B T^*_{i1}$	$4(Y^4_{AB} - Y^4_{BA})\epsilon_{jki}d^T_{Aj}Cd_{Bk}T^{i1}$	LQ, QQ	Yes

45_H Scalar	$Y^2_{AB}5^*_A10_B45^*$	$Y^4_{AB}10_A10_B45$	Interactions	Proton Decay
	$Y^2_{AB}e^T_A C u^i_B T^*_{i2}$ $-Y^2_{AB}\nu^T_A C d^i_B T^*_{i2}$	$2(Y^4_{AB}-Y^4_{BA})\epsilon_{jki}u^T_{Aj}Cu_{Bk}T^{i2}$		
	$2Y^2_{AB}e^T_A C d^i_B T^*_{i3}$	$4(Y^4_{AB}-Y^4_{BA})\epsilon_{jki}d^T_{Aj}Cu_{Bk}T^{i3}$		

7.1.3 Gauge Coupling Unification

The minimal SU(5) model fails to achieve gauge coupling unification at a consistent scale and is incompatible with current experimental limits on nucleon decay. To address these issues, we propose an effective SU(5) framework featuring two Higgs doublets, H_5 and D_{45}, at the electroweak scale [114]. In addition, we introduce color-octet scalars with masses in the 1–2 TeV range, and color-triplet scalars T^i_3 with masses around 10^8 GeV. The remaining components of the 45-dimensional Higgs multiplet acquire GUT-scale masses via their couplings with the adjoint 24_H scalar.

The one-loop b_i-coefficients in these effective models are:

$$b_i^{EW}=\left(\frac{21}{5},-3,-7\right), b_i^S=\left(5,-\frac{5}{3},-5\right), b_i^T=\left(\frac{26}{5},\frac{1}{3},-\frac{9}{5}\right).$$

(7.15)

Thus, the renormalization group equations (RGEs) become:

$$\alpha^{-1}(M_X)= \alpha_1^{-1}(100)-\frac{1}{2\pi}\left[b_1^{(SM+2HD)}\,ln\frac{O_S}{Q_{EW}}+b_1^{(SM+2HD+S)}\,ln\frac{O_T}{Q_S} + b_1^{(SM+2HD+S+\Phi)}\,ln\frac{M_X}{Q_T}\right],$$

(7.16)

$$\alpha^{-1}(M_X)= \alpha_2^{-1}(100)-\frac{1}{2\pi}\left[b_2^{(SM+2HD)}\,ln\frac{O_S}{Q_{EW}}+b_2^{(SM+2HD+S)}\,ln\frac{O_T}{Q_S} + b_2^{(SM+2HD+S+\Phi)}\,ln\frac{M_X}{Q_T}\right],$$

(7.17)

$$\alpha^{-1}(M_X)= \alpha_3^{-1}(100)-\frac{1}{2\pi}\left[b_3^{(SM+2HD)}\,ln\frac{O_S}{Q_{EW}}+b_3^{(SM+2HD+S)}\,ln\frac{O_T}{Q_S} + b_3^{(SM+2HD+S+\Phi)}\,ln\frac{M_X}{Q_T}\right].$$

(7.18)

Solving these equations at $Q_S\sim 1-2$ TeV and $Q_T\sim 10^8$ GeV results in a unification at $M_X\sim 10^{16}$ GeV, as shown in Fig. 7.1 [115], consistent with grand unification scale predictions.

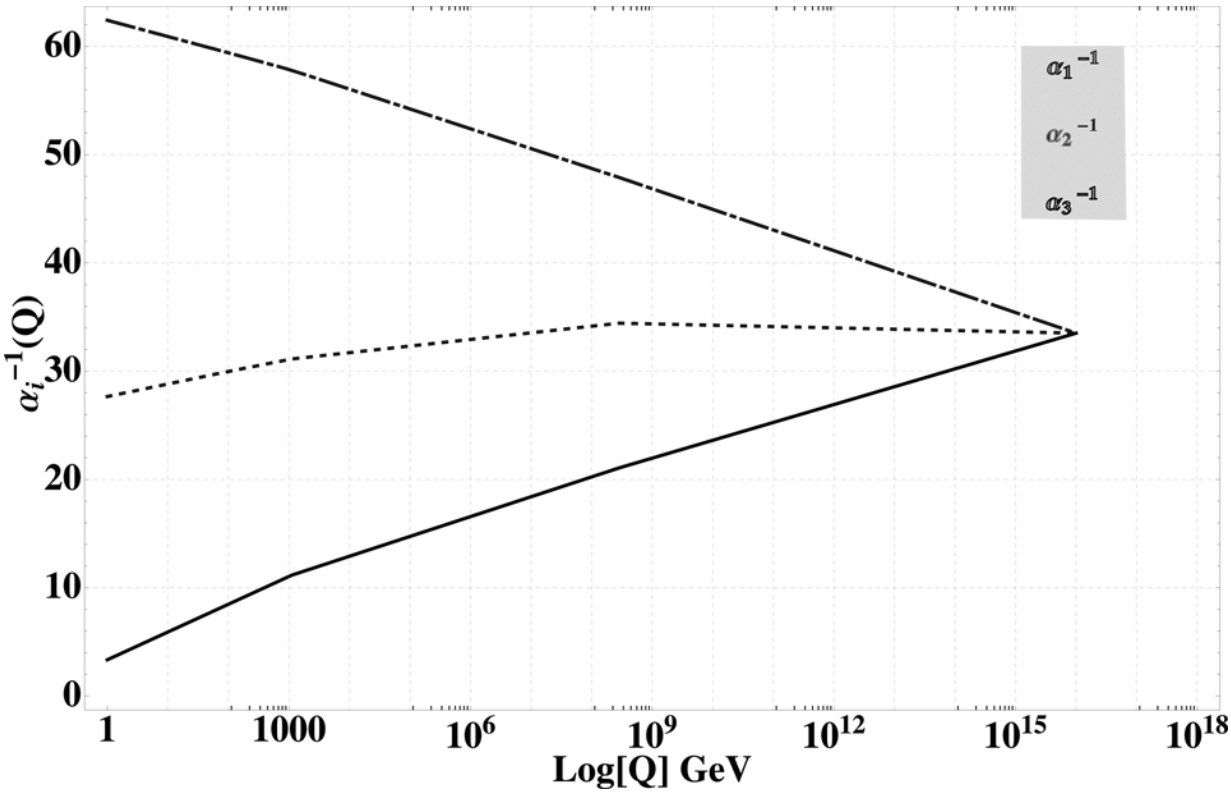

Figure 7.1 Gauge coupling running in the effective $SU(5)$ model with 2HD, TeV-scale octet, and intermediate-scale triplet scalars. ⏎

7.2 EFFECTIVE *SU*(5)TWO-HIGGS-DOUBLET MODEL

After the breaking of the $SU(5)$ GUT to the SM, the scalar sector contains two electroweak doublets: one from the $\mathbf{5}_H$ and one from the $\mathbf{45}_H$ representations. These doublets are defined as

$$H \equiv (1,2)_{1/2} = \begin{pmatrix} H^+ \\ H^0 \end{pmatrix}, \quad D \equiv (1,2)_{1/2} = \begin{pmatrix} D^+ \\ D^0 \end{pmatrix}. \tag{7.19}$$

Electroweak symmetry breaking induces vacuum expectation values (vevs),

$$\langle H \rangle = \begin{pmatrix} 0 \\ v_5 \end{pmatrix}, \quad \langle D \rangle = \begin{pmatrix} 0 \\ -3v_{45} \end{pmatrix}, \tag{7.20}$$

where we define $v_1 \equiv v_5$, $v_2 \equiv -3v_{45}$, and $v = \sqrt{v_1^2 + v_2^2}$. The angle $\tan\beta = v_2/v_1$ parameterizes the ratio of vevs. The effective scalar potential at low energies takes the form [114, 116]:

$$
\begin{aligned}
V(H,D) = \quad & -\mu_H^2 H^\dagger H + \lambda_1 (H^\dagger H)^2 - \mu_D^2 D^\dagger D + \lambda_2 (D^\dagger D)^2 \\
& + \lambda_3 (H^\dagger H)(D^\dagger D) + \lambda_4 |H^\dagger D|^2 + \left[\frac{\lambda_5}{2} (H^\dagger D)^2 + \text{h.c.} \right],
\end{aligned}
\tag{7.21}
$$

where λ_4 and λ_5 encode the mixing between the doublets. The minimization conditions yield:

$$
\mu_H^2 = \lambda_1 v_1^2 + \tfrac{1}{2}(\lambda_3 + \lambda_4 + \lambda_5) v_2^2,
\tag{7.22}
$$

$$
\mu_D^2 = \lambda_2 v_2^2 + \tfrac{1}{2}(\lambda_3 + \lambda_4 + \lambda_5) v_1^2.
\tag{7.23}
$$

Expanding around the vevs,

$$
H = \begin{pmatrix} H^+ \\ v_1 + h_1 + i a_1 \end{pmatrix}, \quad D = \begin{pmatrix} D^+ \\ v_2 + h_2 + i a_2 \end{pmatrix},
\tag{7.24}
$$

the CP-even Higgs mass matrix is

$$
\mathscr{M}_R^2 = \begin{pmatrix} 2\lambda_1 v_1^2 & (\lambda_3 + \lambda_4 + \lambda_5) v_1 v_2 \\ (\lambda_3 + \lambda_4 + \lambda_5) v_1 v_2 & 2\lambda_2 v_2^2 \end{pmatrix}.
\tag{7.25}
$$

This matrix is diagonalized by the mixing angle α, defined by

$$
\tan 2\alpha = \frac{(\lambda_3 + \lambda_4 + \lambda_5) v_1 v_2}{\lambda_1 v_1^2 - \lambda_2 v_2^2}.
\tag{7.26}
$$

The mass eigenstates h and H are given by:

$$
\begin{pmatrix} H \\ h \end{pmatrix} = \begin{pmatrix} \cos\alpha & \sin\alpha \\ -\sin\alpha & \cos\alpha \end{pmatrix} \begin{pmatrix} h_1 \\ h_2 \end{pmatrix},
\tag{7.27}
$$

with masses

$$
M_{H,h}^2 = \lambda_1 v_1^2 + \lambda_2 v_2^2 \pm \sqrt{(\lambda_1 v_1^2 - \lambda_2 v_2^2)^2 + ((\lambda_3 + \lambda_4 + \lambda_5) v_1 v_2)^2}.
\tag{7.28}
$$

This effective 2HDM structure emerges naturally in non-minimal SU(5) extension and plays a key role in scalar sector phenomenology, including potential implications for

flavor, CP violation, and collider signatures.

The effective Yukawa couplings of the SM-like Higgs doublet arise from interactions involving the 5_H and 45_H Higgs representations. After symmetry breaking, the relevant Yukawa Lagrangian takes the form:

$$\begin{aligned}\mathscr{L}_Y \quad &= \bar{e}_R \left(Y_1^{eT} H^\dagger + Y_2^{eT} D^\dagger\right) l_L + \bar{d}_R \left(Y_1^d H^\dagger + Y_2^d D^\dagger\right) Q_L \\ &+ \epsilon_{\alpha\beta} \bar{u}_R \left(Y_3' H^\beta + Y_4' D^\beta\right) Q_L^\alpha + \text{h.c.},\end{aligned}$$

(7.29)

where $Y_3' = 4(Y_3 + Y_3^T)$ and $Y_4' = 2Y_4$. The couplings Y_1 and Y_2 can be related to fermion mass matrices as:

$$Y_1 = \frac{3M_D + M_E}{4v_5}, \quad Y_2 = \frac{M_D - M_E}{8v_{45}}.$$

(7.30)

In the physical basis, assuming flavor diagonal charged leptons and up-quarks, and that the down-quark mass matrix is diagonalized by left-handed rotations only ($V_L^d = V_{CKM}, V_R^d = I$), the couplings of the SM-like Higgs to fermions are:

$$Y_{huu} \quad = -Y_3' \sin\alpha + Y_4' \cos\alpha = -\frac{m_U}{v} \frac{\sin\alpha}{\cos\beta} + Y_4' \cos\alpha,$$

(7.31)

$$Y_{hdd} \quad = -\left(\frac{3m_D + m_E V_{CKM}}{4v_5}\right) \sin\alpha + \left(\frac{m_D - m_E V_{CKM}}{4v_{45}}\right) \cos\alpha,$$

(7.32)

$$Y_{hee} \quad = -\left(\frac{3m_D V_{CKM} + m_E}{4v_5}\right) \sin\alpha + \left(\frac{m_D V_{CKM} - m_E}{4v_{45}}\right) \cos\alpha.$$

(7.33)

The up-quark mass relation $m_U = Y_3' v_5 - 8(Y_4^T - Y_4)v_{45}$ implies that Y_4' vanishes if Y_4 is symmetric.

The couplings of the SM-like Higgs to electroweak gauge bosons arise from the kinetic terms of H and D:

$$\mathscr{L}_{\text{kin}} = (D^\mu H)^\dagger (D_\mu H) + (D^\mu D)^\dagger (D_\mu D).$$

(7.34)

After electroweak symmetry breaking and field redefinitions, the couplings to massive vector bosons are:

$$g_{hW^+W^-} \quad = g M_W \sin(\beta - \alpha),$$

(7.35)

$$g_{hZZ} = \frac{gM_Z}{\cos\theta_W}\sin(\beta-\alpha).$$

(7.36)

The effective Yukawa couplings of the SM-like Higgs doublet arise from interactions involving the 5_H and 45_H Higgs representations. After symmetry breaking, the relevant Yukawa Lagrangian takes the form:

$$\begin{aligned}\mathscr{L}_Y &= \bar{e}_R\left(Y_1^{eT}H^\dagger + Y_2^{eT}D^\dagger\right)l_L + \bar{d}_R\left(Y_1^{d}H^\dagger + Y_2^{d}D^\dagger\right)Q_L \\ &\quad + \epsilon_{\alpha\beta}\bar{u}_R\left(Y_3'H^\beta + Y_4'D^\beta\right)Q_L^\alpha + \text{h.c.},\end{aligned}$$

(7.37)

where $Y_3' = Y_3 + Y_3^T$ and $Y_4' = Y_4 - Y_4^T$. In the up-quark sector, the contraction $\epsilon_{\alpha\beta}\bar{u}_R D^\beta Q_L^\alpha$ is antisymmetric in SU(2) indices. Therefore, only the antisymmetric part of Y_4 contributes to this interaction, and if Y_4 is symmetric, the contribution vanishes.

The couplings Y_1 and Y_2 are related to fermion mass matrices as:

$$Y_1 = \frac{3M_D + M_E}{4v_5}, \quad Y_2 = \frac{M_D - M_E}{8v_{45}}.$$

(7.38)

In the physical basis, assuming flavor-diagonal up-type quarks and charged leptons, and that the down-type quark mass matrix is diagonalized by a left-handed CKM rotation only (i.e., $V_L^d = V_{\text{CKM}}$, $V_R^d = \mathbb{1}$), the couplings of the SM-like Higgs to fermions become:

$$Y_{huu} = -Y_3'\sin\alpha + Y_4'\cos\alpha = -\frac{m_U}{v}\frac{\sin\alpha}{\cos\beta} + Y_4'\cos\alpha,$$

(7.39)

$$Y_{hdd} = -\left(\frac{3m_D + m_E V_{\text{CKM}}}{4v_5}\right)\sin\alpha + \left(\frac{m_D - m_E V_{\text{CKM}}}{8v_{45}}\right)\cos\alpha,$$

(7.40)

$$Y_{hee} = -\left(\frac{3m_D V_{\text{CKM}} + m_E}{4v_5}\right)\sin\alpha + \left(\frac{m_D V_{\text{CKM}} - m_E}{8v_{45}}\right)\cos\alpha.$$

(7.41)

Here, m_U, m_D, m_E are the diagonal mass matrices for up-type quarks, down-type quarks, and charged leptons, respectively.

Note that the up-quark mass relation

$$m_U = Y_3'v_5 + Y_4'v_{45}$$

(7.42)

implies that $Y_4' = 0$ if the original Y_4 is symmetric, since $Y_4' = 2Y_4$ and antisymmetric parts cancel out due to fermion symmetries.

The couplings of the SM-like Higgs to the electroweak gauge bosons originate from the kinetic terms of the scalar fields:

$$\mathscr{L}_{\text{kin}} = (D^\mu H)^\dagger (D_\mu H) + (D^\mu D)^\dagger (D_\mu D).$$

(7.43)

After electroweak symmetry breaking and rotation to the Higgs mass eigenstates, the trilinear couplings to massive vector bosons are given by:

$$g_{hW^+W^-} = g M_W \sin(\beta - \alpha),$$

(7.44)

$$g_{hZZ} = \frac{g M_Z}{\cos\theta_W} \sin(\beta - \alpha),$$

(7.45)

where α is the mixing angle between the CP-even Higgs bosons, and $\tan\beta = v_5/v_{45}$ is the ratio of vacuum expectation values.

7.3 CHARGED HIGGS IN NON-MINIMAL $SU(5)$

In the non-minimal $SU(5)$, the physical charged Higgs field emerges as the orthogonal combination to the Goldstone boson eaten by the $W^\pm$ bosons:

$$H^\pm = -\sin\beta\, H_5^\pm + \cos\beta\, D^\pm, \quad \tan\beta = \frac{v_{45}}{v_5}.$$

(7.46)

From the $SU(5)$ -invariant scalar potential, one obtains the following charged Higgs mass matrix in the $(H^\pm, D^\pm)$ basis is then given by

$$\mathscr{M}^2_{\text{charged}} = \begin{pmatrix} \mu_5^2 + \lambda_5 v_5^2 & \mu_{54} v \\ \mu_{54} v & \mu_{45}^2 + \lambda_{45} v_{45}^2 \end{pmatrix},$$

(7.47)

where λ_5, λ_{45} are effective quartic couplings. Diagonalizing this matrix yields one Goldstone boson and a physical charged Higgs boson $H^\pm$ with mass:

$$m^2_{H^\pm} \simeq \mu_{45}^2 + \lambda_{45} v^2 + \Delta m^2,$$

(7.48)

where Δm^2 encodes contributions from the mixing parameter μ_{54} and possible loop corrections.

The charged Higgs couplings to fermions depend on both Y_2 and Y_3 and can introduce non-trivial flavor structures:

$$\mathscr{L}_{H^\pm} \supset H^+ \, \bar{u}_i \left[V_{ij} \left(A_{dj} P_R + A_{uj} P_L \right) \right] d_j + H^+ \, \bar{\nu}_i \, A_{eij} \, P_R \, e_j + \text{h.c.},$$

(7.49)

with A_{fij} determined by the underlying Yukawa structure and $\tan\beta$. These interactions can lead to flavor-violating processes not present in standard 2HDMs, such as $H^\pm \to \mu\nu$, $H^\pm \to c\bar{s}$, or $t\bar{b}$ with non-standard rates.

7.4 COLORED OCTET SCALARS

In our SU(5) effective model, the color octet scalars arise from the 45_H representation as defined above, with

$$S^{ia}_j = (45^{ia}_j)_H - \frac{1}{3}\delta^i_j (45^{ma}_m)_H, \qquad S^{ia}_j \equiv (8,2)_{1/2} = S^A T^A,$$

(7.50)

where $i,j = 1,2,3$, $A = 1,\ldots,8$, and T^A are the SU(3) generators. These scalars preserve $SU(3)_C$ due to their vanishing VEVs.

The scalar potential involving the octets can be derived from the SU(5)-invariant potential terms [114, 116]. After electroweak symmetry breaking, the mass terms become:

$$m^2_{S^\pm} = -m_S^2 + \lambda' v_{45}^2, \quad m^2_{S^0_{R,I}} = -m_S^2 + \lambda' v_{45}^2,$$

(7.51)

$$m^2_{S^\pm,5} = -m_S^2 + \lambda_3 v_5^2, \quad m^2_{S^0_{R,I},5} = -m_S^2 + (\lambda_3 + \lambda_4 \pm \lambda_5) v_5^2,$$

(7.52)

where $\lambda' = \lambda'_2 + \lambda'_3 + \lambda'_4 - \lambda'_6$. The VEV v_5 induces a mass splitting between the charged and neutral components.

The octet scalars couple to fermions via SU(5) Yukawa interactions:

$$\mathscr{L}^S_Y = 2Y_2 \, \bar{d}_{Ri} Q_{Lj} S^\dagger - 4\epsilon_{\alpha\beta}(Y_4 - Y_4^T) \bar{u}_{Ri} Q^\alpha_{Lj} S^\beta + \text{h.c.}$$

(7.53)

Assuming that Y_4 is symmetric, then the couplings to up-quarks vanish. Using Eq. (7.38), the interaction simplifies to:

$$\mathscr{L}_Y^S = \frac{1}{4v_{45}} \bar{d}_{Ri}(M_D - M_E^T) S^\dagger Q_{Lj} + \text{h.c.}$$

(7.54)

In the physical basis and assuming $V_R^d = \mathbf{I}$, $V_L^d = V_{\text{CKM}}$, we find:

$$\begin{aligned}\mathscr{L}_Y^S = &\frac{1}{4v_{45}} \Big[\bar{d}_{Ri}(M_D^{\text{diag}} V_{\text{CKM}}^\dagger - M_E^{\text{diag}}) u_{Lj} S^- \\ &+ \bar{d}_{Ri}(M_D^{\text{diag}} - M_E^{\text{diag}} V_{\text{CKM}}) d_{Lj} S^0 \Big] + \text{h.c.}\end{aligned}$$

(7.55)

This leads to flavor-violating couplings of the neutral octet scalar due to the misalignment of M_D and M_E [114, 116]. While the minimal flavor violation hypothesis suppresses these effects, we consider Y_2 as a generic matrix without assuming MFV.

The kinetic term $\text{Tr}[(D_\mu 45_H)^\dagger D^\mu 45_H]$ induces interactions between octet scalars and gluons. The covariant derivative acting on the octet scalar S_j^{ia} is:

$$D_\mu S_j^{ia} = \partial_\mu S_j^{ia} - i\frac{g_s}{2}(G_\mu^\alpha T^\alpha)^{ik} S_j^{ka} - i\frac{g_s}{2}(G_\mu^\alpha T^\alpha)_j^n S_n^{ia} + \cdots,$$

(7.56)

resulting in gluon interactions:

$$\begin{aligned}\mathscr{L}_{Sgg} = &\, i g_s \mathscr{F}^{ABD} \left(S^{A-} G^{\mu B} \partial_\mu S^{D+} + S_{R,I}^{A0} G^{\mu B} \partial_\mu S_{R,I}^{D0} \right) \\ &+ g_s^2 \mathscr{F}^{ABCD} \left(S^{A-} G^{\mu B} G_\mu^C S^{D+} + S_{R,I}^{A0} G^{\mu B} G_\mu^C S_{R,I}^{D0} \right) + \text{h.c.},\end{aligned}$$

(7.57)

with structure constants $\mathscr{F}^{ABD} = \text{Tr}(T^A T^B T^D)$ and $\mathscr{F}^{ABCD} = \text{Tr}(T^A T^B T^D t^E)$. The SU(3) generators satisfy:

$$\{t^A, t^B\} = \frac{1}{N}\delta^{AB} + d^{ABC} t^C, \qquad [t^A, t^B] = i f^{ABC} t^C,$$

(7.58)

where d^{ABC} and f^{ABC} are the symmetric and antisymmetric structure constants, respectively.

7.5 SCALAR LEPTOQUARK IN NON-MINIMAL *SU*(5)

As emphasized in Table 7.2 that while the scalar triplets ϕ_k^{ab} and ϕ_c^{ib} contribute to the proton decay and they must be superheavy, the scalar triplet ϕ_c^{ij} does not. It has no interaction terms that would cause proton decay. By writing ϕ_c^{ij} as $(\phi_1^i, \phi_2^i)^T$, one can demonstrate that the scalar triplet has the following peculiar interactions:

$$\begin{aligned}\mathscr{L} =& 2Y^2_{AB} e^T_A C u^c_{Bi} \phi^{i1*} + 4(Y^4_{AB} - Y^4_{BA}) u^{iT}_A C e^c_B \phi_{i1} \\ & - 2Y^2_{AB} \nu^T_A C u^c_{Bi} \phi^{i2*} + 4(Y^4_{AB} - Y^4_{BA}) d^{iT}_A C e^c_B \phi_{i2}.\end{aligned} \tag{7.59}$$

The first two interaction terms would imply the decay of $b \to s\ell^+\ell^-$ through scalar triplet leptoquark ϕ^{i1} mediation, while the last two interaction terms clearly account for the decay $b \to c\tau\nu$ via scalar triplet leptoquark ϕ^{i2} mediation. These terms can be written as

$$\mathscr{L} = 2Y^2_{AB} \bar{u}_{Bi} P_L \nu_A \phi^{i2*} - 4Y^{4'}_{AB} \bar{e}_B P_L d^i_A \phi_{i2} + h.c.\,, \tag{7.60}$$

where we used $C^T = -C$ and $\bar{\Psi} = \Psi^{cT}_L$, and define $Y^{4'}_{AB} \equiv (Y^4_{AB} - Y^4_{BA})$. In the mass eigenstate basis, where

$$d_A \to V^{CKM}_{AB} d_B,\ \nu_A \to V^{\rm PMNS}_{AB} \nu_B,\ u_A \to u_A,\ e_A \to e_A,$$

the above Lagrangian takes the form:

$$\begin{aligned}\mathscr{L} =& 2Y^2_{AB} \bar{u'}_{Bi} P_L V^{\rm PMNS}_{AK} \nu'_k \phi^{i2*} - 4Y^{4'}_{AB} \bar{e'}_B P_L V^{\rm CKM}_{AK} d'_K \phi_{i2} \\ & + h.c.\end{aligned} \tag{7.61}$$

In this regards, the amplitude of $b \to c\tau\nu$ transition is given by

$$\begin{aligned}\mathscr{M} =& -\frac{8Y^{4'}_{13} V^{\rm CKM}_{13}}{M^2_\phi} \Big[\frac{1}{2} (\bar{u}_\tau P_L v_{\nu_\tau})(\bar{u}_C P_L u_b) \\ & + \frac{1}{8} (\bar{u}_\tau \sigma^{\mu\nu} P_L v_{\nu_\tau})(\bar{u}_C P_L \sigma^{\mu\nu} u_b) \times \Big(Y^2_{12} V^{\rm PMNS}_{13} \\ & + Y^2_{22} V^{\rm PMNS}_{23} + Y^2_{32} V^{\rm PMNS}_{33} \Big) \Big] + \Big(Y^{4'}_{13} V^{\rm CKM}_{13} \to Y^{4'}_{23} V^{\rm CKM}_{23} \Big).\end{aligned} \tag{7.62}$$

Because V^{CKM}_{13} and V^{CKM}_{23} are so small (10^{-3} and 10^{-2}, respectively), the amplitude of $b \to c\tau\nu$ is essentially determined by the leptoquark masses $M_\phi, Y^2_{22}, Y^2_{32}$, and $Y^{4'}_{13}$.

CHAPTER 8

Supersymmetry: Central Candidate for BSM

DOI: 10.1201/9781003457701-8

Supersymmetry (SUSY) is a theoretical framework that extends the symmetries of space-time. At its core is the Super Poincaré algebra [117, 118], which includes:

- P_μ (Translation): This represents the symmetry of translations in space and time.
- $M_{\mu\nu}$ (Rotation and Lorentz Transformation): These are the symmetries of rotations and Lorentz transformations, crucial for maintaining the consistency of relativistic theories.
- Q_α (SUSY Transformation): The SUSY transformation introduces a symmetry between fermions and bosons, extending the standard symmetries of space-time.

SUSY plays a critical role in addressing some of the fundamental challenges in modern theoretical physics:

1. Stability of the Hierarchy: SUSY provides a mechanism that ensures the stability of the hierarchy between the weak scale and the Planck scale. Without SUSY, the vast difference between these scales could be destabilized by quantum corrections, leading to a severe fine-tuning problem in the SM.
2. Unified Theory BSM: Supersymmetric theories are promising candidates for a unified theory that extends beyond the SM. They offer a framework that could potentially integrate all fundamental forces under a single theoretical umbrella.
3. Natural Electroweak Symmetry Breaking: SUSY makes the mechanism of electroweak symmetry breaking more natural. In the SM, the Higgs boson mass is sensitive to quantum corrections, leading to a fine-tuning problem. SUSY alleviates this issue by introducing superpartners that cancel out the problematic corrections, thereby stabilizing the Higgs boson mass.

Overall, Supersymmetry offers a compelling extension to our understanding of the universe, providing solutions to some of the most profound challenges in high-energy physics [118].

8.1 HIERARCHY PROBLEM AND SUPERSYMMETRY

One of the significant challenges in modern physics is the hierarchy problem, which arises when attempting to unify gravity with the other fundamental forces. Theories like string theory and GUTs suggest that the fundamental forces should unify at a very high energy scale, close to the Planck scale (10^{19} GeV). However, this presents a dilemma when considering the vastly lower energy scale associated with the electroweak interactions, particularly the mass of the Higgs boson.

The main issue is that quantum corrections to the Higgs boson mass are extremely sensitive to the highest energy scales, leading to potential divergences that require severe fine-tuning. Specifically, without any additional mechanisms, the Higgs boson mass would need to be fine-tuned to an accuracy of $\mathcal{O}(10^{34})$, which is an extraordinarily unnatural requirement.

SUSY offers a compelling solution to this problem by introducing a symmetry between fermions and bosons. In SUSY, the quantum corrections to the Higgs mass from standard particles are exactly canceled by the corresponding contributions from their superpartners. This cancellation occurs because the loop diagrams that are quadratically divergent in the SM cancel out, term by term, against equivalent diagrams involving the superpartners. This mechanism avoids the problematic fine-tuning and stabilizes the Higgs boson mass at a natural scale.

For SUSY to effectively address the hierarchy problem, the superpartner masses should lie around $\mathcal{O}(1)\,\text{TeV}$, especially given the observed Higgs boson mass of $m_H \approx 125\,\text{GeV}$. This prediction implies that some of these superpartners should be detectable at the LHC, providing a testable aspect of the theory. Through this mechanism, SUSY provides a natural framework for solving the hierarchy problem, making it a central candidate for BSM [118].

8.2 GAUGE COUPLING UNIFICATION

A compelling motivation for low-scale SUSY, particularly around the TeV scale, stems from the idea of gauge coupling unification. In the SM, the gauge couplings, α_1 (U(1)_Y), α_2 (SU(2)_L), and α_3 (SU(3)_C), evolve differently with energy due to quantum corrections, as governed by the renormalization group equations (RGEs).

The one-loop RGE for the gauge coupling α_i is:

$$\frac{d\alpha_i(t)}{dt} = \frac{b_i}{2\pi}\alpha_i^2(t), \quad t = \ln(\mu),$$

(8.1)

where b_i are beta function coefficients that depend on the field content of the theory. In the SM, the beta function coefficients for $n_g = 3$ generations and $n_H = 1$ Higgs doublet are:

$$b_1^{\mathrm{SM}} = \frac{41}{10}, \tag{8.2}$$

$$b_2^{\mathrm{SM}} = -\frac{19}{6}, \tag{8.3}$$

$$b_3^{\mathrm{SM}} = -7. \tag{8.4}$$

These couplings do not unify at a single scale, suggesting that the SM alone does not naturally lead to unification.

However, in the Minimal Supersymmetric Standard Model (MSSM), the particle content is extended to include superpartners and typically $n_H = 2$ Higgs doublets. The beta function coefficients become:

$$b_1^{\mathrm{MSSM}} = \frac{33}{5}, \tag{8.5}$$

$$b_2^{\mathrm{MSSM}} = 1, \tag{8.6}$$

$$b_3^{\mathrm{MSSM}} = -3. \tag{8.7}$$

With these values, the RG evolution of the gauge couplings leads to convergence at a common unification scale, around $M_{\mathrm{GUT}} \sim 10^{16}\,\mathrm{GeV}$ [119–121]. This elegant unification strongly supports the MSSM and motivates the presence of superpartners near the TeV scale, potentially within reach of collider experiments such as the LHC.

8.3 WHAT IS SUPERSYMMETRY?

SUSY is a theoretical framework that postulates a fundamental symmetry between two distinct classes of particles: bosons (integer spin) and fermions (half-integer spin). In SUSY, each bosonic state has a corresponding fermionic partner and vice versa. This symmetry is encapsulated by the action of fermionic operators Q_α and their Hermitian conjugates $\bar{Q}_{\dot{\alpha}}$, which satisfy:

$$Q_\alpha|\text{Boson}\rangle = |\text{Fermion}\rangle, \quad Q_\alpha|\,\text{Fermion}\rangle = |\text{Boson}\rangle.$$

(8.8)

Since Q_α carries spin-$\frac{1}{2}$, SUSY extends the symmetries of space-time, making it a space-time symmetry rather than a purely internal one.

Supersymmetry was first formulated as an extension of the Poincaré group, which underlies special relativity, by Golfand and Likhtman in 1971 [122], and later developed into a full quantum field theoretic framework in 1973 [123]. In quantum field theory, symmetries are generally classified as:

1. External (Space-Time) Symmetries: These include translations $x^\mu \to x^\mu + a^\mu$ and Lorentz transformations $x^\mu \to \Lambda^\mu_\nu x^\nu$.
2. Internal Symmetries: These act on the fields themselves, e.g., $\phi^a(x) \to M^a_b \phi^b(x)$, and include gauge symmetries like $U(1)$, $SU(2)$, and $SU(3)$.

According to Noether's theorem, every continuous symmetry corresponds to a conserved quantity. In particle physics, conserved quantities such as energy, momentum, electric charge, and color charge are associated with these fundamental symmetries.

Efforts to unify internal and space-time symmetries into a larger algebraic structure encountered a major obstacle: the Coleman-Mandula theorem [124]. It states that under certain reasonable assumptions, the most general symmetry group of the S-matrix is a direct product of the Poincaré group and an internal symmetry group, implying no non-trivial unification is possible.

SUSY evades this restriction by introducing fermionic symmetry generators that transform as spinors, rather than scalars. These additional generators extend the Poincaré algebra to the so-called Super-Poincaré algebra, enabling a consistent and non-trivial unification of space-time and internal symmetries.

SUSY Algebra and Mass Degeneracy

The complete set of SUSY generators includes not only those of the Poincaré group but also two additional spinor generators, Q and $\bar{Q}$, which act on the fields. These spinor generators introduce a symmetry between bosons and fermions and satisfy specific algebraic relations:

$$\{Q_\alpha, Q_\beta\} = 0, \quad \{\bar{Q}_{\dot{\alpha}}, \bar{Q}_{\dot{\beta}}\} = 0, \quad \{Q_\alpha, \bar{Q}_{\dot{\beta}}\} = 2\sigma^\mu_{\alpha\dot{\beta}} P_\mu,$$

(8.9)

where $\sigma^\mu \equiv (1, \sigma^i)$ and $\bar{\sigma}^\mu \equiv (1, -\sigma^i)$. Here, $\alpha, \beta, \dot{\alpha}, \dot{\beta} = 1, 2$ are spinor indices, and P_μ represents the momentum operator [123, 125].

These generators also obey specific commutation relations with the generators of the Poincaré group:

$$
\begin{aligned}
&[P^\mu, Q_\alpha] = \left[P^\mu, \bar{Q}_{\dot{\alpha}}\right] = 0, \quad [M^{\mu\nu}, Q_\alpha] = -i(\sigma^{\mu\nu})_\alpha^\beta Q_\beta, \\
&\left[M^{\mu\nu}, \bar{Q}^{\dot{\alpha}}\right] = -i(\bar{\sigma}^{\mu\nu})_{\dot{\beta}}^{\dot{\alpha}} \bar{Q}^{\dot{\beta}}.
\end{aligned}
\tag{8.10}
$$

The commutators of Q_α and $\bar{Q}_{\dot{\alpha}}$ with internal symmetry generators T_i generally vanish, indicating that SUSY transformations do not mix with internal symmetries.

The momentum squared operator $P^2 = P_\mu P^\mu$ serves as a Casimir operator in the SUSY algebra, meaning it is invariant under SUSY transformations:

$$
\left[Q_\alpha, P^2\right] = 0.
\tag{8.11}
$$

This invariance implies that particles related by SUSY transformations, such as a fermion $|F\rangle$ and a boson $|B\rangle$, must have the same mass. Specifically, if a fermion state $|F\rangle$ is obtained from a bosonic state $|B\rangle$ through the action of the SUSY generator Q_α, then:

$$
\begin{aligned}
m_F|F\rangle = \quad & P^2|F\rangle = P^2 Q_\alpha |B\rangle = Q_\alpha P^2 |B\rangle = m_B Q_\alpha |B\rangle = m_B |F\rangle \\
\implies \quad & m_F = m_B.
\end{aligned}
\tag{8.12}
$$

This relation confirms that particles within the same irreducible representation of the SUSY algebra, such as a boson and its corresponding fermion partner, share the same mass, a defining prediction of supersymmetric theories [122, 125].

8.4 SUPERSPACE AND SUSY TRANSFORMATIONS

Supersymmetric theories are naturally formulated in *superspace*, an extension of spacetime incorporating both bosonic coordinates x^μ and anticommuting fermionic coordinates θ^α, $\bar{\theta}^{\dot{\alpha}}$. Fields in this space are represented by superfields $\Phi(x, \theta, \bar{\theta})$, which encapsulate entire SUSY multiplets.

Supersymmetry extends spacetime translations by introducing fermionic generators Q_α and $\bar{Q}_{\dot{\alpha}}$. A finite SUSY transformation induces specific shifts in superspace coordinates:

$$
\begin{aligned}
x^\mu &\to x^\mu + y^\mu + i\eta\sigma^\mu\bar{\theta} - i\theta\sigma^\mu\bar{\eta}, \\
\theta^\alpha &\to \theta^\alpha + \eta^\alpha, \\
\bar{\theta}^{\dot{\alpha}} &\to \bar{\theta}^{\dot{\alpha}} + \bar{\eta}^{\dot{\alpha}},
\end{aligned}
\tag{8.13}
$$

where η^α, $\overline{\eta}^{\dot{\alpha}}$ are Grassmann-valued parameters. These transformations unify bosonic and fermionic degrees of freedom through geometry.

Expanding an infinitesimal transformation allows identification of the SUSY generators:

$$\begin{aligned} P_\mu &= i\partial_\mu, \\ Q_\alpha &= i\left(\partial_{\theta^\alpha} + i\sigma^\mu_{\alpha\dot{\alpha}}\overline{\theta}^{\dot{\alpha}}\partial_\mu\right), \\ \overline{Q}_{\dot{\alpha}} &= i\left(\partial_{\overline{\theta}^{\dot{\alpha}}} - i\theta^\alpha\sigma^\mu_{\alpha\dot{\alpha}}\partial_\mu\right). \end{aligned} \tag{8.14}$$

To construct SUSY-invariant actions, one introduces covariant derivatives that anticommute with the supercharges:

$$\begin{aligned} D_\alpha &= \partial_{\theta^\alpha} + i\sigma^\mu_{\alpha\dot{\alpha}}\overline{\theta}^{\dot{\alpha}}\partial_\mu, \\ \overline{D}_{\dot{\alpha}} &= -\partial_{\overline{\theta}^{\dot{\alpha}}} - i\theta^\alpha\sigma^\mu_{\alpha\dot{\alpha}}\partial_\mu, \end{aligned} \tag{8.15}$$

with the algebra:

$$\{D_\alpha, \overline{D}_{\dot{\beta}}\} = 2i\sigma^\mu_{\alpha\dot{\beta}}\partial_\mu, \quad \{D_\alpha, D_\beta\} = \{\overline{D}_{\dot{\alpha}}, \overline{D}_{\dot{\beta}}\} = 0. \tag{8.16}$$

This framework forms the basis for constructing supersymmetric field theories and ensures manifest SUSY invariance in superspace [117, 118, 125].

8.5 SUSY LAGRANGIANS

Supersymmetric theories unify bosons and fermions through superfields. Two essential types are the chiral and vector superfields. A chiral superfield Φ satisfies $\overline{D}_{\dot{\alpha}}\Phi = 0$, depending only on the shifted coordinate $y^\mu = x^\mu + i\theta\sigma^\mu\bar{\theta}$. Its component expansion includes a complex scalar ϕ, a Weyl fermion ψ, and an auxiliary field F [117, 126]. Chiral superfields are closed under multiplication, enabling the construction of supersymmetric superpotentials.

Vector superfields V, satisfying $V = V^\dagger$, describe gauge bosons. Gauge redundancies are removed via SUSY gauge transformations $V \to V + \Lambda + \Lambda^\dagger$, with Λ chiral. In the Wess-Zumino (WZ) gauge, V contains only the physical components: gauge field v_μ, gauginos λ, $\bar{\lambda}$, and auxiliary field D [117].

A general renormalizable SUSY Lagrangian in superspace reads:

$$\mathscr{L} = \Phi_i^\dagger\Phi^i\big|_{\theta^2\bar{\theta}^2} + W(\Phi_i)\big|_{\theta^2} + \bar{W}(\Phi_i^\dagger)\big|_{\bar{\theta}^2},$$

(8.17)

where the superpotential W is:

$$W(\Phi_i) = \frac{1}{2} M_{ij} \Phi^i \Phi^j + \frac{1}{3} Y_{ijk} \Phi^i \Phi^j \Phi^k.$$

(8.18)

Expanding Φ in components gives:

$$\Phi(x, \theta, \bar{\theta}) \quad = \phi + \sqrt{2}\theta\psi + \theta\theta F + i\theta\sigma^\mu\bar{\theta}\partial_\mu\phi$$

(8.19)

$$-\frac{i}{\sqrt{2}}\theta\theta\sigma^\mu\bar{\theta}\partial_\mu\psi + \frac{1}{4}\theta\theta\bar{\theta}\bar{\theta}\Box\phi.$$

(8.20)

The kinetic term is:

$$\Phi_i^\dagger \Phi^i \big|_{\theta^2\bar{\theta}^2} = \partial_\mu \phi_i^\dagger \partial^\mu \phi_i + i\bar{\psi}_i \bar{\sigma}^\mu \partial_\mu \psi_i + F_i^* F_i.$$

(8.21)

The full component Lagrangian becomes:

$$\mathscr{L} \quad = \partial_\mu \phi_i^\dagger \partial^\mu \phi_i + i\bar{\psi}_i \bar{\sigma}^\mu \partial_\mu \psi_i + F_i^* F_i$$

(8.22)

$$+ \left[M_{ij}(\phi_i F_j - \frac{1}{2}\psi_i \psi_j) + Y_{ijk}(\phi_i \phi_j F_k - \psi_i \psi_j \phi_k) + \text{h.c.} \right].$$

(8.23)

Eliminating the auxiliary field via its equation of motion:

$$F_i^* = -\frac{\partial W}{\partial \phi_i},$$

(8.24)

yields the on-shell Lagrangian:

$$\mathscr{L} \quad = \partial_\mu \phi_i^\dagger \partial^\mu \phi_i + i\bar{\psi}_i \bar{\sigma}^\mu \partial_\mu \psi_i - \left| \frac{\partial W}{\partial \phi_i} \right|^2$$

(8.25)

$$- \left(\frac{1}{2} M_{ij} \psi_i \psi_j + Y_{ijk} \psi_i \psi_j \phi_k + \text{h.c.} \right).$$

(8.26)

The scalar potential is:

$$V = \sum_i \left| \frac{\partial W}{\partial \phi_i} \right|^2.$$

(8.27)

For Abelian gauge fields, define the field strength superfields:

$$W_\alpha = -\frac{1}{4}\bar{D}\bar{D}D_\alpha V, \quad \bar{W}_{\dot{\alpha}} = -\frac{1}{4}DD\bar{D}_{\dot{\alpha}}V.$$

(8.28)

In the WZ gauge:

$$V_{\text{WZ}} = \theta\sigma^\mu\bar{\theta}v_\mu + i\theta\theta\bar{\theta}\bar{\lambda} - i\bar{\theta}\bar{\theta}\theta\lambda + \frac{1}{2}\theta\theta\bar{\theta}\bar{\theta}D,$$

(8.29)

and the vector Lagrangian becomes:

$$\int d^2\theta\, W^\alpha W_\alpha = \frac{1}{2}D^2 - \frac{1}{4}v^{\mu\nu}v_{\mu\nu} - i\lambda\sigma^\mu\partial_\mu\bar{\lambda}.$$

(8.30)

The potential is:

$$V = \frac{1}{2}D^2.$$

(8.31)

In non-Abelian SUSY gauge theories, the chiral superfields transform as $\Phi \to e^{i\Lambda}\Phi$, with $\Lambda = \Lambda^a T^a$, where T^a are Lie algebra generators obeying:

$$[T^a, T^b] = if^{abc}T^c, \quad \text{Tr}(T^aT^b) = \frac{1}{2}\delta^{ab}.$$

(8.32)

The vector superfield transforms as:

$$e^V \to e^{i\Lambda^\dagger}e^V e^{-i\Lambda}.$$

(8.33)

Define:

$$W_\alpha = -\frac{1}{4}\bar{D}\bar{D}\left(e^{-V}D_\alpha e^V\right), \quad W_\alpha \to e^{i\Lambda}W_\alpha e^{-i\Lambda}.$$

(8.34)

The complete non-Abelian SUSY Lagrangian is:

$$\mathscr{L} = \Phi_i^\dagger (e^V)^i_j \Phi^j \big|_{\theta^2\bar{\theta}^2} + \frac{1}{4g^2}\mathrm{Tr}[W^\alpha W_\alpha]\big|_{\theta^2} + W(\Phi^i)\big|_{\theta^2} + \text{h.c.}$$

(8.35)

After eliminating auxiliary fields:

$$V_{\text{SUSY}} = \frac{1}{2} D^a D^a + F_i^* F^i, \quad F^i = \frac{\partial W}{\partial \phi_i}, \quad D^a = g^a \phi_i^* T^a \phi_i.$$

(8.36)

8.6 SUPERSYMMETRY BREAKING

SUSY, while theoretically well-motivated, cannot be an exact symmetry of nature. If it were unbroken, superpartners of the SM particles, such as electrons and squarks, would have the same masses as their SM counterparts, which is clearly not the case experimentally. The absence of such degenerate states implies that SUSY must be broken. To stabilize the electroweak scale and resolve the hierarchy problem, SUSY breaking should occur at or moderately above the electroweak scale.

As with other symmetries, SUSY can be broken spontaneously, dynamically, or explicitly. The SUSY algebra is given by

$$\{Q_\alpha, \bar{Q}_{\dot{\alpha}}\} = 2\sigma^\mu_{\alpha\dot{\alpha}} P_\mu,$$

(8.37)

which, upon contraction with $(\bar{\sigma}^\nu)^{\dot{\beta}\alpha}$, leads to

$$H = \frac{1}{4}\left(\bar{Q}_1 Q_1 + Q_1 \bar{Q}_1 + \bar{Q}_2 Q_2 + Q_2 \bar{Q}_2\right) \geq 0.$$

(8.38)

This implies a semi-positive definite Hamiltonian. For a supersymmetric vacuum where $Q_\alpha|0\rangle = \bar{Q}_{\dot{\alpha}}|0\rangle = 0$, the vacuum energy vanishes:

$$E_{\text{vac}} = \langle 0|H|0\rangle = 0.$$

(8.39)

Conversely, if the vacuum is not annihilated by some SUSY generators, then $E_{\text{vac}} > 0$, signaling spontaneous SUSY breaking.

Spontaneous SUSY breaking implies that the variation of some field under SUSY transformations acquires a non-zero vacuum expectation value (VEV). For a chiral superfield,

$$\langle 0|\delta_\xi \psi(x)|0\rangle \propto \langle 0|F|0\rangle \neq 0,$$

(8.40)

and for a vector superfield,

$$\langle 0|\delta_\xi \lambda(x)|0\rangle \propto \langle 0|D|0\rangle \neq 0.$$

(8.41)

While spontaneous SUSY breaking is conceptually attractive, constructing realistic models remains challenging. Alternatively, SUSY can be broken explicitly by introducing terms in the Lagrangian that violate SUSY but do not reintroduce quadratic divergences. These are the so-called soft SUSY breaking terms, classified in [127]:

- Scalar mass terms: $\tilde{m}_{ij}^2 \phi_i^* \phi_j$,
- Gaugino mass terms: $\frac{1}{2} M_a \lambda^a \lambda^a + \text{h.c.}$,
- Bilinear scalar terms: $B_{ij} \phi_i \phi_j + \text{h.c.}$,
- Trilinear scalar terms: $A_{ijk} \phi_i \phi_j \phi_k + \text{h.c.}$.

These soft terms are essential for phenomenology: they shape the SUSY mass spectrum and contribute to radiative electroweak symmetry breaking [118]. Ultimately, a full understanding of SUSY breaking would allow all soft terms to be derived from a fundamental theory, such as gravity mediation, gauge mediation, or anomaly mediation [118].

8.7 MINIMAL SUPERSYMMETRIC STANDARD MODEL

The Minimal Supersymmetric Standard Model (MSSM) is the simplest supersymmetric extension of the SM that retains its gauge group $SU(3)_C \times SU(2)_L \times U(1)_Y$ while introducing a superpartner for each SM particle [118, 126]. The MSSM arranges fields into supermultiplets, pairing SM particles with superpartners differing in spin by $1/2$:

Supermultiplet	**SM Particle**	**SUSY Partner**	$SU(3)_C \times SU(2)_L \times U(1)_Y$
Q_L	$(u_L, d_L)^T$	$(\tilde{u}_L, \tilde{d}_L)^T$	$(3, 2, 1/6)$
U_L^c	u_L^c	$\tilde{u}_L^c$	$(\bar{3}, 1, -2/3)$
D_L^c	d_L^c	$\tilde{d}_L^c$	$(\bar{3}, 1, 1/3)$
L_L	$(\nu_L, e_L)^T$	$(\tilde{\nu}_L, \tilde{e}_L)^T$	$(1, 2, -1/2)$
E_L^c	e_L^c	$\tilde{e}_L^c$	$(1, 1, 1)$
H_u	(H_u^+, H_u^0)	$(\tilde{H}_u^+, \tilde{H}_u^0)$	$(1, 2, 1/2)$
H_d	(H_d^0, H_d^-)	$(\tilde{H}_d^0, \tilde{H}_d^-)$	$(1, 2, -1/2)$

Unlike the SM, the MSSM requires two Higgs doublets. This stems from the requirement that the superpotential be analytic in chiral superfields, thus excluding conjugate fields like H^* [117]. Furthermore, anomaly cancellation demands both H_u and H_d, since their fermionic superpartners (Higgsinos) contribute oppositely to the gauge anomalies [118]. The MSSM includes gauge superfields for each SM interaction:

- $(B_\mu, \tilde{B})$ for $U(1)_Y$,
- $(W_\mu^a, \tilde{W}^a)$ for $SU(2)_L$,
- $(G_\mu^a, \tilde{g}^a)$ for $SU(3)_C$.

The full MSSM Lagrangian is

$$\mathscr{L}_{\text{MSSM}} = \mathscr{L}_{\text{gauge}} + \mathscr{L}_{\text{matter}} + \mathscr{L}_{\text{superpotential}} + \mathscr{L}_{\text{soft}}.$$

(8.42)

The gauge and matter sectors follow from supersymmetric field theory [117]. The superpotential encodes Yukawa interactions and Higgs mixing:

$$W = Y_u Q U^c H_u + Y_d Q D^c H_d + Y_e L E^c H_d + \mu H_u H_d.$$

(8.43)

An explicit example involving the top quark superfield illustrates the structure of SUSY interactions:

$$\begin{aligned}\mathscr{L}_{\text{int}} =& -\frac{Y_t}{2}\left(t_L H_u t_L^c + \tilde{t}_L \tilde{H}_u t_L^c + t_L \tilde{H}_u \tilde{t}_L^c + \text{h.c.}\right) \\ & - Y_t^2 \left(|H_u \tilde{t}_L^c|^2 + |H_u \tilde{t}_L|^2 + |\tilde{t}_L \tilde{t}_L^c|^2\right).\end{aligned}$$

(8.44)

In addition to the standard top Yukawa interaction, SUSY introduces new interactions involving the scalar superpartners (stops) and the Higgsino. These additional terms are a distinctive feature of SUSY and play a crucial role in its phenomenology.

The Higgs and lepton doublets share gauge quantum numbers, allowing for lepton and baryon number-violating terms:

$$W' = \lambda_{ijk} L_i L_j E_k^c + \lambda'_{ijk} L_i Q_j D_k^c + \lambda''_{ijk} D_i^c D_j^c U_k^c + \mu'_i L_i H_u,$$

(8.45)

which can mediate rapid proton decay [118, 128]. For instance:

$$\frac{\lambda''_{211}\lambda'_{112}}{m_{\tilde{s}}^2}(u^c d^c)(u e),$$

(8.46)

contributes to $p \to e^+\pi^0$, with decay rate:

$$\Gamma \sim \lambda'_{112}\lambda''_{211}\frac{m_p^5}{m_{\tilde{s}}^4}, \quad \tau_p \sim 6\times 10^{-13}\,\mathrm{s}\Big(\frac{m_{\tilde{s}}}{1\,\mathrm{TeV}}\Big)^4 (\lambda'_{112}\lambda''_{211})^{-2}.$$

(8.47)

To satisfy experimental limits $\tau_p > 1.6\times 10^{33}\,\mathrm{yr}$, these couplings must be extremely suppressed:

$$\lambda'_{112}\lambda''_{211} < 3\times 10^{-26}.$$

(8.48)

To forbid these terms, *R*-parity is introduced, defined by:

$$R_P = (-1)^{3B+L+2S}.$$

(8.49)

Its consequences are:

1. SUSY particles must be pair-produced.
2. The lightest supersymmetric particle (LSP) is stable and a dark matter candidate.

Soft SUSY-breaking terms introduce masses and trilinear couplings:

$$\mathscr{L}_{\mathrm{soft}} = -\frac{1}{2}M_a\lambda^a\lambda^a - m_{\phi_i}^2\phi_i^*\phi_i - \Big(A_f Y_f \tilde{f}_L \tilde{f}_R H + B\mu H_u H_d + \mathrm{h.c.}\Big).$$

(8.50)

These terms, if unconstrained, introduce ~ 100 new parameters. The constrained MSSM (cMSSM) assumes GUT-scale universality:

$$m_{\tilde{f}}^2 = m_0^2, \quad m_{H_u}^2 = m_{H_d}^2 = m_0^2,$$

(8.51)

$$A_f = A_0, \quad M_1 = M_2 = M_3 = m_{1/2},$$

(8.52)

reducing the parameter space to $\{m_0, m_{1/2}, A_0, \tan\beta, \mathrm{sign}(\mu)\}$. This setup is often motivated by minimal supergravity (mSUGRA) models.

8.8 SUPERSYMMETRIC SPECTRUM IN THE MSSM

In the MSSM, each SM particle has a corresponding superpartner differing by half a unit of spin. These superpartners, collectively known sparticles, play a crucial role in stabilizing the electroweak scale and providing viable dark matter candidates. The MSSM particle spectrum includes gauginos, Higgsinos, squarks, and sleptons. This section discusses the mass generation, mixing, and phenomenological roles of the key supersymmetric particles: gluinos, charginos, neutralinos, squarks, and sleptons [118].

Gluinos

The gluino ($\tilde{g}$), the fermionic partner of the gluon, acquires mass from the soft SUSY-breaking term:

$$\mathscr{L}_{\text{soft}} \supset -\frac{1}{2} M_3 \tilde{g}^a \tilde{g}^a.$$

(8.53)

At tree level, the gluino mass is $m_{\tilde{g}} = |M_3(Q)|$. At one-loop, the gaugino mass parameters run as:

$$M_i(Q) = \frac{\alpha_i(Q)}{\alpha_i(M_X)} M_i(M_X), \quad i = 1, 2, 3,$$

(8.54)

with universal boundary condition $M_1 = M_2 = M_3 = m_{1/2}$ at the GUT scale. At the electroweak scale:

$$M_3 : M_2 : M_1 \approx 7 : 2 : 1.$$

(8.55)

Charginos

Charginos are mass eigenstates formed from charged winos ($\tilde{W}^\pm$) and Higgsinos ($\tilde{H}_u^+$, $\tilde{H}_d^-$). The mass terms arise from:

$$\mathscr{L} \supset -\begin{pmatrix} \tilde{W}^- & \tilde{H}_d^- \end{pmatrix} \mathscr{M}_C \begin{pmatrix} \tilde{W}^+ \\ \tilde{H}_u^+ \end{pmatrix} + \text{h.c.},$$

(8.56)

with

$$\mathscr{M}_C = \begin{pmatrix} M_2 & \sqrt{2} M_W \sin\beta \\ \sqrt{2} M_W \cos\beta & \mu \end{pmatrix}.$$

(8.57)

This matrix is diagonalized by unitary matrices U and V to yield the physical chargino masses $m_{\tilde{\chi}_1^\pm}$, $m_{\tilde{\chi}_2^\pm}$, where the lighter mass is often near the electroweak scale.

Neutralinos

Neutralinos are mixtures of bino ($\tilde{B}$), wino ($\tilde{W}^3$), and neutral Higgsinos ($\tilde{H}_u^0$, $\tilde{H}_d^0$). The mass matrix is:

$$\mathscr{M}_N = \begin{pmatrix} M_1 & 0 & -M_Z s_W c_\beta & M_Z s_W s_\beta \\ 0 & M_2 & M_Z c_W c_\beta & -M_Z c_W s_\beta \\ -M_Z s_W c_\beta & M_Z c_W c_\beta & 0 & -\mu \\ M_Z s_W s_\beta & -M_Z c_W s_\beta & -\mu & 0 \end{pmatrix}.$$

(8.58)

Diagonalization yields four neutralino mass eigenstates. The lightest, χ_1^0, is a dark matter candidate. Its composition is:

$$\chi = N_{11}\tilde{B} + N_{12}\tilde{W}^3 + N_{13}\tilde{H}_d^0 + N_{14}\tilde{H}_u^0.$$

(8.59)

The gaugino fraction $f_g = |N_{11}|^2 + |N_{12}|^2$ indicates the neutralino's character: gaugino-like ($f_g > 0.5$) or Higgsino-like ($f_g < 0.5$).

Squarks

Squarks are scalar partners of quarks. Their mass matrices include soft terms, Yukawa interactions, and D-term contributions. For third-generation squarks, mixing is significant due to large Yukawa couplings. The stop mass matrix is:

$$\mathscr{M}_{\tilde{t}}^2 = \begin{pmatrix} m_{\tilde{q}_L}^2 + m_t^2 - \frac{\cos 2\beta}{6}(M_Z^2 - 4M_W^2) & m_t(A_t - \mu \cot\beta) \\ m_t(A_t - \mu\cot\beta) & m_{\tilde{t}_L^c}^2 + m_t^2 + \frac{2}{3}M_Z^2 \sin^2\theta_W \cos 2\beta \end{pmatrix}.$$

(8.60)

The lighter stop mass $m_{\tilde{t}_1}$ can be significantly below the TeV scale.

Sleptons

Sleptons are scalar partners of leptons. The stau ($\tilde{\tau}$) mass matrix in mSUGRA takes the form:

$$\mathscr{M}_{\tilde{\tau}}^2 = \begin{pmatrix} m_{\tilde{\ell}_L}^2 + m_\tau^2 + \frac{\cos 2\beta}{2}(M_Z^2 - 2M_W^2) & m_\tau(A_\tau - \mu\tan\beta) \\ m_\tau(A_\tau - \mu\tan\beta) & m_{\tilde{\ell}_L^c}^2 + m_\tau^2 - M_Z^2\cos 2\beta \sin^2\theta_W \end{pmatrix}.$$

(8.61)

For large $\tan\beta$, significant left-right mixing occurs, which can impact LSP coannihilation and collider signals.

8.9 THE HIGGS SECTOR IN THE MSSM

The MSSM requires two Higgs doublets, H_u and H_d, to give mass to both up- and down-type fermions and ensure anomaly cancellation. These doublets acquire vacuum expectation values (VEVs) $v_u = v\sin\beta$ and $v_d = v\cos\beta$, with $v \simeq 246\,\text{GeV}$ and $\tan\beta = v_u/v_d$. The Higgs potential receives contributions from the superpotential, soft SUSY-breaking terms, and D-terms:

$$\begin{aligned} V =& (m_{H_u}^2 + |\mu|^2) H_u^\dagger H_u + (m_{H_d}^2 + |\mu|^2) H_d^\dagger H_d + (B\mu H_u \cdot H_d + \text{h.c.}) \\ &+ \frac{g^2 + g'^2}{8}(H_u^\dagger H_u - H_d^\dagger H_d)^2 + \frac{g^2}{2}|H_u^\dagger H_d|^2. \end{aligned}$$

(8.62)

Charged Higgs Bosons

The charged Higgs mass matrix, expressed in the basis $(H_d^\pm, H_u^\pm)$, yields a physical charged Higgs with mass:

$$m_{H^\pm}^2 = m_A^2 + m_W^2,$$

(8.63)

where m_A is the mass of the CP-odd Higgs. The light charged Higgs decays predominantly into $\tau^\pm\nu$ and $c\bar{s}$, while heavier states decay into $t\bar{b}$ or $\tau\nu$, depending on phase space.

CP-odd Higgs Boson

The CP-odd Higgs mass matrix in the (a_d, a_u) basis has one zero eigenvalue (Goldstone boson) and a massive pseudoscalar:

$$m_A^2 = \frac{2B\mu}{\sin 2\beta}.$$

(8.64)

This state decays primarily into heavy fermions such as $\tau^+\tau^-$ and $b\bar{b}$, with rates sensitive to $\tan\beta$.

CP-even Higgs Bosons

The CP-even Higgs mass matrix in the (h_d, h_u) basis is:

$$\mathscr{M}_H^2 = \begin{pmatrix} m_Z^2 \cos^2\beta + m_A^2 \sin^2\beta & -(m_Z^2 + m_A^2)\sin\beta\cos\beta \\ -(m_Z^2 + m_A^2)\sin\beta\cos\beta & m_Z^2 \sin^2\beta + m_A^2 \cos^2\beta \end{pmatrix}.$$

(8.65)

The lighter eigenstate satisfies $m_h \leq m_Z |\cos 2\beta|$ at tree level, necessitating radiative corrections to reach the observed value of $125\ \text{GeV}$ [129–131]. These loop corrections primarily involve top-stop loops:

$$V^{(1)} = \frac{1}{64\pi^2} \text{Str}\left[M^4(\varphi_i) \left(\ln \frac{M^2(\varphi_i)}{Q^2} - C_s \right) \right],$$

(8.66)

where C_s is a spin-dependent constant in the $\overline{\text{DR}}$ scheme.

8.10 SUSY SEARCHES AT THE LHC

The search for SUSY particles at the LHC is a central aspect of the experimental effort to discover new physics beyond the SM. At the LHC, SUSY particle production is predominantly driven by strongly interacting particles, such as squarks and gluinos. These particles have substantial production cross-sections due to their strong interactions, making them the primary focus of SUSY searches [132, 133].

In typical high-mass SUSY scenarios, the production of SUSY particles initiates with squarks and gluinos. These particles then undergo a series of decay steps, eventually leading to lighter SUSY particles and SM particles. The decay chains typically involve:

- Squarks and Gluinos: Decay into quarks, gluons, and lighter SUSY particles such as charginos and neutralinos.
- Charginos and Neutralinos: Further decay into electroweak gauge bosons (W and Z bosons), Higgs bosons, and eventually to the lightest SUSY particle, which is often the neutralino ($\tilde{\chi}_1^0$).

The decay processes result in final states characterized by energetic jets and significant missing transverse energy (E_T^{miss}), as the lightest SUSY particle escapes detection. The general search strategy involves identifying these distinctive signatures in the data collected by the LHC detectors [134, 135].

LHC Constraints on the MSSM Spectrum

The LHC has significantly constrained the parameter space of the MSSM spectrum, particularly in the context of SUSY particle masses, cross-sections, and decay modes

[135, 136]. Key constraints include:

- Gluino Mass: Lower bounds of $\sim 2.5\,\mathrm{TeV}$ in simplified models, reaching $\sim 2.7{-}3.0\,\mathrm{TeV}$ in complex scenarios [132].
- Squark Mass: $\sim 2.0\,\mathrm{TeV}$ for first/second-generation, and up to $\sim 2.5\,\mathrm{TeV}$ for stops/bottoms [135].
- Neutralino and Chargino Masses: Neutralino $\gtrsim 100{-}200\,\mathrm{GeV}$, chargino $\gtrsim 500{-}600\,\mathrm{GeV}$ [133].
- Higgs Sector: Light Higgs mass fixed at $\sim 125\,\mathrm{GeV}$, heavy Higgs and charged Higgs constrained above $\sim 100\,\mathrm{GeV}$ [136].
- Stop Mass: Approx. $\sim 1.0{-}1.5\,\mathrm{TeV}$, depending on decay channels [134].

Despite no direct SUSY signals yet, the exclusion of parameter space is substantial and continues to shape theoretical developments. Future LHC runs with higher luminosity will improve sensitivity [134].

CHAPTER 9

BSM and Extra Dimensions

DOI: 10.1201/9781003457701-9

9.1 INTRODUCTION

The concept of extra dimensions is a central theme in theories that extend beyond the SM of particle physics. By postulating the existence of additional spatial dimensions beyond the familiar three, these frameworks aim to resolve longstanding theoretical and phenomenological puzzles, such as the hierarchy problem, the unification of forces, and the formulation of a consistent theory of quantum gravity.

One of the earliest and most influential attempts to incorporate extra dimensions was the Kaluza-Klein theory [137, 138], which unified gravity and electromagnetism by introducing a compact fifth spatial dimension. This pioneering idea laid the foundation for modern approaches involving higher dimensions.

A major revival of interest came with the proposal of Large Extra Dimensions in Arkani-Hamed, Dimopoulos, and Dvali (ADD) model [139], which suggested that extra dimensions could be large compared to the Planck scale. This framework offers an elegant resolution to the hierarchy problem by lowering the fundamental scale of gravity. Subsequently, the Randall-Sundrum (RS) models [140, 141] introduced the idea of warped extra dimensions, providing an alternative geometric mechanism to address the same problem.

Beyond addressing the hierarchy problem, extra dimensions are integral to string theory, where consistency requires spacetime to be ten-dimensional [142], or eleven-dimensional in the context of M-theory [143]. These extra dimensions also appear in cosmological models, offering insights into early-universe inflation [144] and the nature of dark matter and dark energy [145].

9.2 GENERAL RELATIVITY IN 5D SPACETIME

One of the earliest attempts to formulate a unified field theory was introduced by Theodor Kaluza in 1921 [137]. Kaluza extended Einstein's theory of general relativity by proposing a five-dimensional spacetime, integrating both gravitational and electromagnetic forces within the same framework. This innovative approach set the foundation for many modern theories involving extra dimensions. In this five-dimensional model, the spacetime is described by a generalized line element:

$$d\hat{s}^2 = g_{MN} dx^M dx^N, \tag{9.1}$$

where g_{MN} is the metric tensor that encompasses all five dimensions, and M,N represent the spacetime indices ranging from 0 to 4. The five-dimensional metric tensor is structured as follows:

$$g_{MN} = \begin{pmatrix} g_{\mu\nu} - \kappa^2 \phi^2 A_\mu A_\nu & -\kappa \phi^2 A_\mu \\ -\kappa \phi^2 A_\nu & -\phi^2. \end{pmatrix} \tag{9.2}$$

Here, $g_{\mu\nu}$ represents the familiar four-dimensional gravitational field, A_μ is the electromagnetic four-potential, and ϕ is a scalar field. Together, they form the five-dimensional gravitational potential, where the electromagnetic and gravitational components are unified.

A key assumption in this model is that the five-dimensional metric is independent of the extra-dimensional coordinate, denoted by y. This assumption is known as the “cylindrical condition”:

$$\frac{\partial g_{MN}}{\partial x_4} = 0.$$

(9.3)

By adopting this condition, Kaluza was able to reduce the theory to a four-dimensional spacetime with an embedded electromagnetic field. After identifying $g_{44} = -\phi^2 = -1$ and $\kappa = \sqrt{\frac{16\pi G}{c^4}}$, the resulting field equations, $G_{MN} = 0$, naturally split into two familiar sets of equations:

$$\tilde{G}_{\mu\nu} = \frac{8\pi G}{c^4} T_{\mu\nu},$$

(9.4)

$$\nabla^{\mu} F_{\mu\nu} = 0$$

(9.5)

In these equations, $T_{\mu\nu}$ is the energy-momentum tensor for the electromagnetic field, defined as:

$$T_{\mu\nu} \equiv \frac{1}{2}\left(g_{\mu\nu} F_{\alpha\beta} F^{\alpha\beta} - F_{\mu}{}^{\alpha} F_{\nu\alpha}\right).$$

(9.6)

This remarkable result, where the field equations of general relativity yield both Einstein's gravitational equations and Maxwell's equations of electromagnetism, is often referred to as the “Kaluza miracle” [137]. It demonstrated, for the first time, how extra dimensions could provide a path toward unifying the fundamental forces of nature, laying the groundwork for more advanced theories like String Theory [142].

9.3 COMPACTIFIED EXTRA DIMENSION

To justify the cylindrical condition in Kaluza's five-dimensional theory, Oskar Klein proposed a groundbreaking idea in 1926: the extra dimension is not infinite and extended, but rather compactified, curled up into a microscopic, unobservable scale [138]. This compactification of the extra dimension is assumed to be toroidal, meaning that the extra spatial dimension is rolled into a circle with a small radius, R. The periodic nature of the compactified dimension is described as:

$$X(x^{\mu}, x^4) = X(x^{\mu}, x^4 + 2\pi R).$$

(9.7)

In this scenario and as shown in Fig. 9.1, the extra dimension $y = x_4$ is periodic, with each point in the dimension returning to itself after traveling a distance of $2\pi R$. This compactification allows the theory to remain consistent with the observation that we experience only four large dimensions while the fifth dimension remains hidden due to its extremely small size.

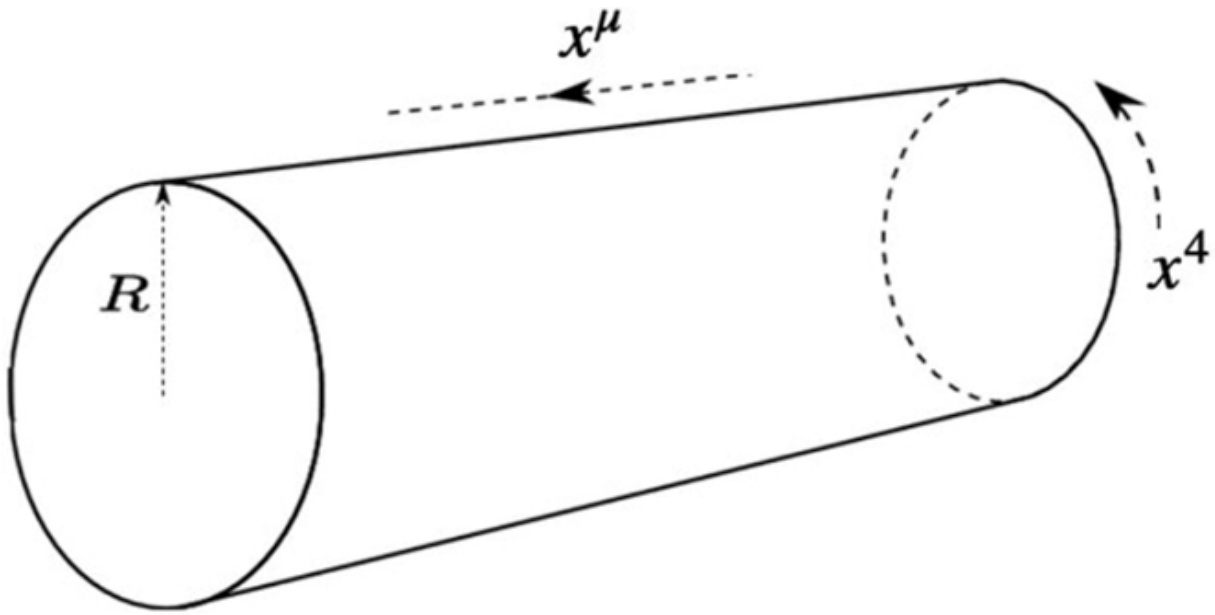

Figure 9.1 Fifth dimension compactification on a circle

Klein's assumption that all fields are periodic in the extra dimension led to the expansion of these fields into Fourier series. This approach allows each field to be decomposed into a series of harmonics, indexed by an integer n, corresponding to different modes of the compactified dimension. The expansions for the metric, electromagnetic potential, and scalar field are given by:

$$g_{\mu\nu}(x, y) = \sum_{n=-\infty}^{+\infty} g_{\mu\nu n}(x) e^{in \cdot y/R},$$

(9.8)

$$A_{\mu}(x, y) = \sum_{n=-\infty}^{+\infty} A_{\mu n}(x) e^{in \cdot y/R},$$

(9.9)

$$\phi(x,y) \quad = \sum_{n=-\infty}^{+\infty} \phi_n(x) e^{in\cdot y/R}.$$

(9.10)

Here, $g_{\mu\nu n}(x)$, $A_{\mu n}(x)$, and $\phi_n(x)$ represent the Fourier coefficients, corresponding to different Kaluza-Klein modes. These modes reflect the quantized nature of the extra dimension. The harmonics *n* introduce an entire tower of particles with increasing mass, known as Kaluza-Klein excitations. For consistency, the following relations hold between the Fourier components:

$$g^*_{\mu\nu n}(x) = g_{\mu\nu -n}(x), \quad A^*_{\mu n}(x) = A_{\mu -n}(x), \quad \phi^*_n(x) = \phi_{-n}(x).$$

(9.11)

These conditions ensure that the physical fields are real, with their complex conjugates satisfying the necessary symmetries.

The compactification of the extra dimension explains why we do not directly observe the fifth dimension. Since the dimension is microscopic, the higher Kaluza-Klein modes, corresponding to larger values of *n*, acquire masses that are too large to be detected at low energies, leaving only the zero modes to manifest as observable particles in four-dimensional spacetime. Thus, the compactified extra dimension provides a consistent framework to incorporate higher-dimensional theories while maintaining agreement with experimental observations. This compactification mechanism is crucial not only for Kaluza-Klein theory [137, 138] but also for modern approaches such as string theory [142], where additional dimensions are similarly compactified on complex geometrical shapes, like Calabi-Yau manifolds. The notion of compactified extra dimensions has deep implications, providing insight into the structure of spacetime and offering a pathway to unification of the fundamental forces.

The Kaluza-Klein theory describes an infinite number of four-dimensional fields, each corresponding to different modes of a compactified extra dimension. These fields obey the equations of motion derived from the five-dimensional action. The equations of motion for the metric, electromagnetic field, and scalar field in this framework are:

$$(\partial^\mu \partial_\mu - \partial^y \partial_y) g_{\mu\nu}(x,y) \quad = (\partial^\mu \partial_\mu + \frac{n^2}{R^2}) g_{\mu\nu n}(x) = 0,$$

(9.12)

$$(\partial^\mu \partial_\mu - \partial^y \partial_y) A_\mu(x,y) \quad = (\partial^\mu \partial_\mu + \frac{n^2}{R^2}) A_{\mu n}(x) = 0,$$

(9.13)

$$(\partial^\mu \partial_\mu - \partial^y \partial_y) \phi(x,y) \quad = (\partial^\mu \partial_\mu + \frac{n^2}{R^2}) \phi_n(x) = 0.$$

(9.14)

These resemble the Klein-Gordon equation, with an added term that gives rise to a “mass” for each field mode. The Kaluza-Klein modes introduce a mass scale for these fields, given by:

$$m_n \sim \frac{n}{R}.$$

(9.15)

Here, n denotes the mode of excitation, and R is the radius of compactification. The higher the mode n, the larger the associated mass of the field. In four-dimensional spacetime, these excited states appear with masses proportional to $O(n/R)$, and since the goal is to unify the electromagnetic interactions with gravity, the natural radius of compactification is of the order of the Planck length, $R = \frac{1}{M_p}$, where the Planck mass: $M_p \sim 10^{18}\,\mathrm{GeV}$.

The resulting action for the scalar field (often referred to as the “dilaton”) is expressed as:

$$S = \int d^4x \left\{ \frac{1}{2} \partial_\mu \phi^{(0)} \partial^\mu \phi^{(0)} + \sum_{n=1}^{\infty} \left[\partial_\mu \phi^{(n)\dagger} \partial^\mu \phi^{(n)} - \frac{n^2}{R^2} \phi^{(n)\dagger} \phi^{(n)} \right] \right\}.$$

(9.16)

This action describes both the zero mode and the infinite tower of massive Kaluza-Klein states, where each higher mode contributes a scalar field with a mass proportional to n/R.

From the four-dimensional perspective, the action describes an infinite series of particles, known as the Kaluza-Klein tower, with masses given by:

$$m_{(n)} = \frac{n}{R}.$$

(9.17)

If the original field $\Phi(x^\mu, y)$ in five dimensions has a mass m_0, the corresponding four-dimensional Kaluza-Klein particles will have masses:

$$m_{(n)}^2 = m_0^2 + \frac{n^2}{R^2}.$$

(9.18)

This relation introduces a mass spectrum for the Kaluza-Klein modes, where the lowest mode $n = 0$ represents the massless or lightest state, while the higher modes $n > 0$ are increasingly massive. The diagram in Fig. 9.2 illustrates the Kaluza-Klein mass spectrum for a field compactified on a circular dimension:

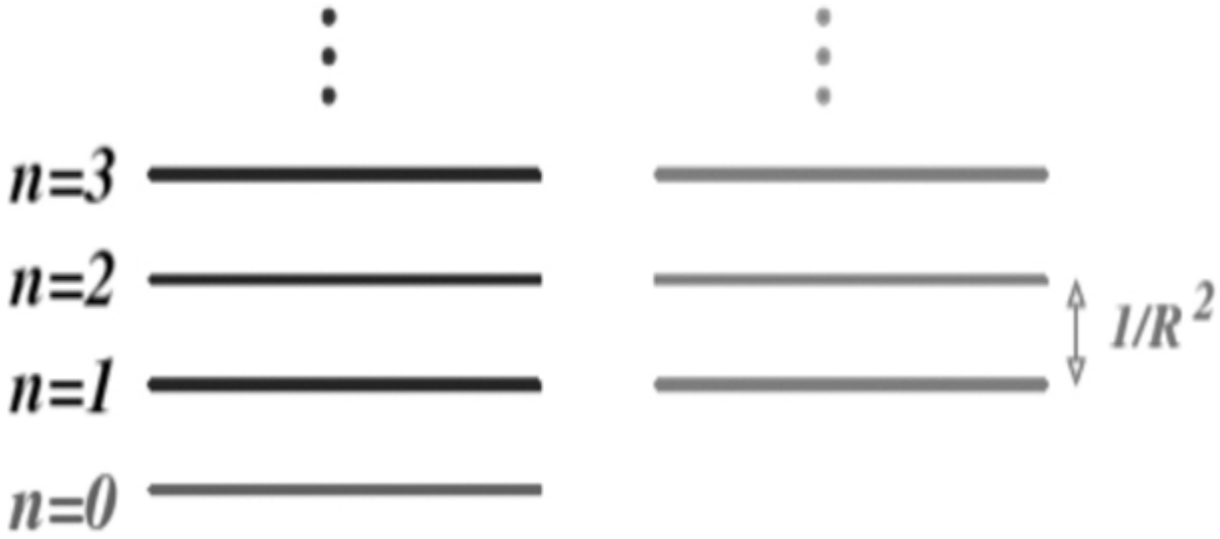

Figure 9.2 KK mass spectrum for a field on the circle

In this framework, the five-dimensional gauge field $A_M(x^\mu, y)$ has a Fourier decomposition along the compact dimension:

$$A_M(x^\mu, y) = \frac{1}{\sqrt{2\pi R}} \sum_n A_M^{(n)}(x^\mu) e^{i\frac{n}{R}y}.$$

(9.19)

The action for the five-dimensional gauge field can be written as:

$$S = \int d^4x\, dy \left[-\frac{1}{4} F_{MN} F^{MN} \right].$$

(9.20)

Upon compactification, the action becomes:

$$S = \int d^4x \Big\{ \Big(-\frac{1}{4} F^{(0)}_{\mu\nu} F^{(0)\mu\nu} + \frac{1}{2} \partial_\mu A^{(0)}_5 \partial^\mu A^{(0)}_5 \Big) + \sum_{n\geq 1} 2 \Big(-\frac{1}{4} F^{(-n)}_{\mu\nu} F^{(n)\mu\nu} + \frac{1}{2} \frac{n^2}{R^2} A^{(-n)}_\mu A^{(n)}_\mu \Big) \Big\}. \tag{9.21}$$

This shows that the zero modes consist of a four-dimensional gauge field and a real scalar field, while the higher modes include massive vector and scalar fields. These Kaluza-Klein excitations introduce a rich structure of particles that could be relevant in models of unification or physics beyond the SM [137, 138, 142].

Graviton Spectrum in Kaluza-Klein Theory

In the framework of Kaluza-Klein theory, the metric in higher-dimensional spacetime, specifically a five-dimensional (5D) spacetime, has 15 independent components due to the additional dimension. However, not all of these components represent physical degrees of freedom. To reduce this number, gauge fixing is required. The harmonic gauge condition is imposed to simplify the metric components by applying the following constraint:

$$\partial_M g^M_N - \frac{1}{2} \partial_N g^M_M = 0 \tag{9.22}$$

This condition eliminates 5 components, reducing the independent degrees of freedom to 10. Additionally, the residual gauge symmetry

$$g_{MN} \to g_{MN} + \partial_M \epsilon_N + \partial_N \epsilon_M \tag{9.23}$$

with the condition $\Box \epsilon_N = 0$, allows the imposition of 5 more constraints. Ultimately, the 5D graviton has 5 physical degrees of freedom.

In contrast, a massless graviton in four-dimensional (4D) spacetime possesses only 2 polarization states. This discrepancy indicates that upon compactification, the extra degrees of freedom manifest as additional fields from the 4D perspective, specifically, a vector field and a scalar field. This

decomposition of the higher-dimensional graviton forms the essence of the Kaluza-Klein spectrum [146].

These additional fields reflect the influence of the compactified extra dimension and provide the theoretical basis for the Kaluza-Klein spectrum, where the higher-dimensional graviton yields not only the usual graviton but also additional particles in four-dimensional spacetime.

To understand this more concretely, consider the five-dimensional Einstein-Hilbert action:

$$\hat{S} = \frac{1}{2\hat{k}^2} \int d^5\hat{x} \sqrt{-\hat{g}} \hat{R}.$$

(9.24)

Upon compactification of the fifth dimension on a circle of radius R, and focusing on the zero modes ($n = 0$), the effective four-dimensional action becomes:

$$S = \frac{1}{2k^2} \int d^4x \sqrt{-g} \left[R - \frac{1}{4} e^{-\sqrt{3}\phi} F^{(0)}_{\mu\nu} F^{\mu\nu(0)} - \frac{1}{2} \partial_\mu \phi^{(0)} \partial^\mu \phi^{(0)} \right].$$

(9.25)

Here, R is the Ricci scalar of the 4D spacetime, $F^{(0)}_{\mu\nu}$ corresponds to the field strength of a $U(1)$ gauge field arising from $g_{\mu 5}$, and $\phi^{(0)}$ is a scalar field (commonly called the dilaton) associated with g_{55}. These fields reflect the zero-mode decomposition of the 5D graviton and are the physical remnants of the higher-dimensional geometry in the compactified theory.

The higher Fourier modes ($n \neq 0$) correspond to massive spin-2 Kaluza-Klein excitations, which appear as a tower of massive gravitons in four-dimensional spacetime with masses quantized as $m_n = n/R$. These modes are generically suppressed at low energies if the compactification radius R is sufficiently small, typically near the Planck scale [147].

9.4 THEORIES WITH LARGE EXTRA DIMENSIONS

A key consideration in formulating theories with higher dimensions is ensuring that the low-energy limit, often referred to as the four-dimensional (4D) effective theory, matches experimental observations in our familiar 4D spacetime. This serves as a critical test of the viability of such theories. A

generalization of the Einstein-Hilbert action in $4+n$ dimensions is given by:

$$S_{4+n} = -M_*^{n+2} \int d^{4+n}x \sqrt{-g^{(4+n)}} R^{(4+n)},$$

(9.26)

where M_* is the fundamental mass scale of the higher-dimensional theory. The power $n+2$ ensures that the action remains dimensionless in natural units. In this framework, the extra dimensions are compactified on an n-sphere or torus with a characteristic radius R. The full spacetime metric is then:

$$ds^2 = \eta_{\mu\nu} dx^\mu dx^\nu - R^2 d\Omega_n^2,$$

(9.27)

where $\eta_{\mu\nu}$ denotes the flat Minkowski metric in four dimensions, and $d\Omega_n^2$ is the line element on the n-dimensional compact space.

To connect this higher-dimensional theory with 4D gravity, one must match the low-energy limit of the higher-dimensional Einstein-Hilbert action to the standard 4D action. This comparison yields:

$$-M_*^{n+2} \int d^n y \sqrt{g^{(n)}} \int d^4x \sqrt{-g^{(4)}} R^{(4)} = -M_{\rm Pl}^2 \int d^4x \sqrt{-g^{(4)}} R^{(4)},$$

(9.28)

where $M_{\rm Pl} \sim 10^{18}\,\text{GeV}$ is the four-dimensional Planck mass. The integral over the compact space gives its volume:

$$V_n(R) = \int d^n y \sqrt{g^{(n)}} = \frac{\pi^{n/2}}{\Gamma\left(\frac{n}{2}+1\right)} R^n,$$

(9.29)

which corresponds to the volume of an n-dimensional ball or torus, depending on the geometry.

Equating both sides, we find the relationship between the Planck scale and the fundamental scale of gravity:

$$M_{\rm Pl}^2 = M_*^{n+2} V_n(R).$$

(9.30)

Solving for the compactification radius gives:

$$R \sim \frac{M_{\mathrm{Pl}}^{2/n}}{M_*^{1+2/n}}.$$

(9.31)

This expression reveals how the size of the extra dimensions depends on the number of dimensions n and the fundamental scale M_*. For instance, if $M_* \sim 1\,\mathrm{TeV}$, a scale motivated by attempts to solve the hierarchy problem, then for $n = 2$, the radius R could be as large as a fraction of a millimeter, potentially within the reach of submillimeter gravitational experiments [139, 148].

Gauge Field in Higher Dimensions

The action for a gauge field in $4 + n$ dimensions generalizes the standard Yang-Mills action as:

$$S^{(4+n)} = -\int d^{4+n}x \, \frac{1}{4g_*^2} F_{MN} F^{MN} \sqrt{-g^{(4+n)}},$$

(9.32)

where F_{MN} is the field strength tensor in the higher-dimensional space, and g_* is the higher-dimensional gauge coupling. Assuming that $g_* \sim \mathcal{O}(1)$, we can match the higher-dimensional gauge action to its four-dimensional effective counterpart. This procedure yields the relation:

$$1 \approx R^n M_*^n,$$

(9.33)

where R is the radius of the compact extra dimensions and M_* is the fundamental scale of gravity. Combining this with the previous relation between M_{Pl}, M_*, and R,

$$M_{\mathrm{Pl}}^2 = M_*^{n+2} R^n,$$

(9.34)

we find that:

$$R \sim \frac{1}{M_{\rm Pl}},$$

(9.35)

if $M_* \sim M_{\rm Pl}$, implying extremely small compactification scales consistent with the absence of observed deviations from four-dimensional physics.

Historically, it was widely assumed that any extra dimensions must be compactified at the Planck scale, $R \sim 10^{-33}\,\text{cm}$, rendering their physical effects unobservable. However, this paradigm was revolutionized in the late 1990s by developments in string theory and brane-world scenarios. In particular, the idea that Standard Model fields may be localized on a four-dimensional submanifold (brane) embedded in a higher-dimensional bulk allowed for a radical rethinking of extra-dimensional geometry.

In the ADD model, only gravity propagates in the higher-dimensional bulk, while SM particles are confined to a 3-brane. This framework permits large compactification radii up to $R \lesssim 0.1\,\text{mm}$, without violating known experimental constraints from tests of Newtonian gravity at short distances.

In this scenario, the fundamental scale of gravity M_* can be as low as the electroweak scale, $M_* \sim 1\,\text{TeV}$, providing a compelling solution to the hierarchy problem. The apparent weakness of gravity at large distances is then explained as a consequence of its dilution into the extra dimensions.

Gravitational Field in Higher Dimensions

We consider a flat five-dimensional metric:

$$ds^2 = \eta_{MN} dx^M dx^N, \quad M,N = 0,1,2,3,4,$$

(9.36)

where η_{MN} is the Minkowski metric in 5D spacetime. In the weak-field limit and for static perturbations, the gravitational field equation generalizes Gauss's law to higher dimensions [139]:

$$\partial_i \partial^i \phi = 4\pi G_D \rho,$$

(9.37)

where G_D is the gravitational constant in D-dimensions and ρ is the mass density. Applying the divergence theorem, and defining the gravitational field as $\mathbf{g} \equiv -\nabla\phi$, we obtain:

$$\oint_S (\mathbf{g} \cdot \mathbf{n})\, dS = -4\pi G_D m,$$

(9.38)

where S is the surface enclosing a D-dimensional volume, and m is the enclosed mass.

In a space with n extra spatial dimensions (i.e., $D = 4 + n$), this surface becomes a sphere in $n + 3$ spatial dimensions:

$$\oint_{S^{n+2}} (\mathbf{g} \cdot \mathbf{n})\, dA = -4\pi G_D m.$$

(9.39)

The surface area of a $(n + 2)$ -dimensional sphere is related to the volume of the corresponding ball:

$$V_{n+2}(r) = \frac{\pi^{\frac{n}{2}+1}}{\Gamma\left(\frac{n}{2}+2\right)} r^{n+2}.$$

(9.40)

From this, the magnitude of the gravitational field is:

$$g = \frac{-4\Gamma\left(\frac{n}{2}+2\right) G_D m}{\pi^{n/2} r^{n+2}},$$

(9.41)

and integrating this expression yields the gravitational potential:

$$\phi(r) = \frac{4\Gamma\left(\frac{n}{2}+2\right) G_D m}{\pi^{n/2}} \int_{\infty}^{r} \frac{1}{r'^{n+2}}\, dr' = \frac{4\Gamma\left(\frac{n}{2}+2\right) G_D m}{\pi^{n/2} r^{n+1}}.$$

(9.42)

This result illustrates that gravity becomes stronger at short distances in the presence of extra dimensions due to the modified scaling of the potential, a central feature of models with large extra dimensions [148].

The higher-dimensional Newton constant G_D is related to the fundamental Planck scale $M_D \equiv M_{\mathrm{pl}(4+n)}$ by dimensional analysis. In natural units ($\hbar = c = 1$), its mass dimension is:

$$[G_D] = \frac{1}{{M_D}^{n+2}}.$$

(9.43)

This scaling is crucial for understanding how gravity can appear weak in 4D while being fundamentally strong in higher-dimensional theories [139, 148].

Matching to Newtonian Gravity

To recover an effective four-dimensional theory in the limit $R \ll r$, we compare the potential derived from the higher-dimensional theory to the familiar Newtonian potential:

$$\phi^{(4)} \sim \frac{m}{R^n r {M_{\mathrm{pl}(4+n)}}^{2+n}} \approx \frac{m}{M_{\mathrm{pl}}^2 r}.$$

(9.44)

This matching condition leads to the relation [139, 148]:

$$R^n = \frac{M_{\mathrm{pl}}^2}{{M_{\mathrm{pl}(4+n)}}^{2+n}}.$$

(9.45)

If we assume that the electroweak scale $m_{\mathrm{EW}} \sim 1\,\mathrm{TeV}$ is the fundamental Planck scale, we can choose the radius R of the extra dimensions to reproduce the observed four-dimensional Planck mass. This yields:

$$R \sim 10^{\frac{30}{n} - 17}\,\mathrm{cm} \times \left(\frac{1\,\mathrm{TeV}}{m_{\mathrm{EW}}}\right)^{1+\frac{2}{n}}.$$

(9.46)

Constraints from Experimental Bounds

For $n = 1$, the radius R of the extra dimension would be approximately $10^{13}\,\text{cm}$, comparable to the size of the solar system, and thus clearly excluded by observations. To remain consistent with current experimental constraints, at least two extra dimensions are required. For $n = 2$, the radius drops to about $100\,\mu\text{m}$, which lies within the current experimental bounds on deviations from Newtonian gravity at submillimeter scales [149].

9.5 RANDALL-SUNDRUM MODEL

Motivated by the large extra dimensions framework proposed by Arkani-Hamed, Dimopoulos, and Dvali (ADD) [139], a variety of models incorporating extra spatial dimensions have emerged. A particularly influential example is the Randall-Sundrum (RS) model, proposed in 1999 by Lisa Randall and Raman Sundrum [140, 141]. The RS model introduces a non-factorizable, warped geometry between our four-dimensional (4D) spacetime and an additional fifth dimension.

Specifically, the five-dimensional (5D) metric is a warped product between the 4D Minkowski space with coordinates x^μ and the extra-dimensional coordinate y, with the 4D geometry multiplied by a scalar warp factor $f(y)$. The general form of a warped product metric is:

$$ds^2 = f(y)\, g_{\mu\nu}(x)\, dx^\mu dx^\nu + g_{ab}(y)\, dy^a dy^b, \tag{9.47}$$

where $g_{\mu\nu}(x)$ is the metric of the 4D spacetime, and $g_{ab}(y)$ represents the geometry of the internal extra-dimensional space.

In the RS scenario, there is only a single extra dimension compactified on a circle S^1 of radius R, subject to a $\mathbb{Z}_2$ symmetry under reflection $y \to -y$, resulting in the orbifold $S^1/\mathbb{Z}_2$. This orbifold structure has strong roots in string-theoretic constructions, particularly in the Horava-Witten scenario [150], where eleven-dimensional M-theory is compactified on $R^{10} \times S^1/\mathbb{Z}_2$, with six dimensions curled up into a Calabi-Yau manifold. Such constructions motivate the effective appearance of five-dimensional physics at low energies.

Warped Metric and Einstein Field Equations

The RS model assumes that the induced 4D metric on the brane is flat, $g_{\mu\nu}(x) = \eta_{\mu\nu}$, while the warp factor depends solely on the extra dimension. The resulting metric becomes:

$$ds^2 = f(y)\,\eta_{\mu\nu}\,dx^\mu dx^\nu - dy^2,$$

(9.48)

where $\eta_{\mu\nu}$ is the Minkowski metric and $f(y)$ is to be determined.

To determine the functional form of $f(y)$, we consider the 5D Einstein-Hilbert action with a bulk cosmological constant Λ:

$$S = -\int d^5x\,\sqrt{-g}\,\big(R + \Lambda\kappa^2\big),$$

(9.49)

where $\kappa^2 = 1/M^3$, and M is the 5D Planck mass. The vacuum Einstein field equations take the form:

$$G_{MN} = -\frac{\Lambda}{2M^3}\,g_{MN},$$

(9.50)

where G_{MN} is the 5D Einstein tensor.

Solving for the Warp Factor

Using the metric in Eq. (9.48), the non-zero components of the Einstein tensor are:

$$\begin{aligned} G_{00} &= -\frac{3}{2}\,\frac{d^2 f(y)}{dy^2}, \quad G_{11} = G_{22} = G_{33} = \frac{3}{2}\,\frac{d^2 f(y)}{dy^2}, \\ G_{44} &= \frac{3}{2 f(y)^2}\left(\frac{df(y)}{dy}\right)^2. \end{aligned}$$

(9.51)

Substituting these into Eq. (9.50), we obtain:

$$\frac{d^2 f(y)}{dy^2} = -\frac{\Lambda\kappa^2}{3}\,f(y),$$

(9.52)

$$\frac{df(y)}{dy} = \pm\sqrt{\frac{-\Lambda\kappa^2}{3}}\, f(y).$$

(9.53)

These equations require $\Lambda < 0$, implying an anti-de Sitter (AdS_5) geometry. Solving Eqs. (9.52) and (9.53) for negative Λ gives:

$$f(y) = e^{\pm 2ky},$$

(9.54)

where $k = \sqrt{-\Lambda\kappa^2/6}$. Imposing the $\mathbb{Z}_2$ symmetry $y \to -y$ selects:

$$f(y) = e^{-2k|y|}.$$

(9.55)

The full RS metric is therefore:

$$ds^2 = e^{-2k|y|}\,\eta_{\mu\nu}dx^\mu dx^\nu - dy^2.$$

(9.56)

The exponential suppression factor $e^{-2k|y|}$ generates a large hierarchy of scales from modest input parameters, thus providing a geometric solution to the hierarchy problem.

Conformally Flat Form of the RS Metric

For certain applications, it is useful to express the RS metric in a conformally flat form. Defining a new coordinate z via:

$$dy = e^{-k|y|}dz,$$

(9.57)

and solving for z, the metric becomes:

$$ds^2 = f(z)\left(\eta_{\mu\nu}dx^\mu dx^\nu - dz^2\right),$$

(9.58)

where

$$f(z) = \frac{1}{(k|z|+1)^2}.$$

(9.59)

Thus, the RS metric in conformally flat coordinates takes the form:

$$ds^2 = \frac{1}{(k|z|+1)^2}\left(\eta_{\mu\nu}dx^\mu dx^\nu - dz^2\right),$$

(9.60)

which is particularly advantageous for calculations involving field propagation in the bulk.

Brane Tension

It is important to note that the metric (9.56) is not fully determined by the bulk field equations alone; rather, it arises from the specific physical setup of the S^1/Z_2 orbifold. To ensure consistency, we must verify that this metric satisfies the Einstein field equations, potentially requiring an additional interpretation of its source terms.

By transforming the RS metric into its conformally flat form (9.60), the Einstein tensor components can be computed straightforwardly. The relevant component for the four-dimensional spacetime is:

$$G_{\mu\nu} = \eta_{\mu\nu}\left(\frac{6k^2}{(k|z|+1)^2} + \frac{3k\,\mathrm{sgn}'(z)}{k|z|+1}\right).$$

(9.61)

The first term corresponds to the contribution of the negative bulk cosmological constant, as expected. The second term, however, is singular and proportional to the derivative of the sign function, indicating the presence of localized sources at the orbifold fixed points. Specifically, since $\mathrm{sgn}'(z) = 2\delta(z) - 2\delta(z-b)$, these contributions are delta functions centered at $z = 0$ and $z = b$, the locations of the two 3-branes.

To account for these singularities, one must introduce brane-localized energy-momentum sources, interpreted as the brane tensions. These are incorporated into the total action as:

$$S = S_{\text{gravity}} + S_{\text{vis}} + S_{\text{hid}},$$

(9.62)

where S_{vis} and S_{hid} are the contributions from the visible and hidden branes, respectively. These terms have the form:

$$S_{\text{brane}} = -\int d^4x \, \sqrt{-g_{\text{ind}}} \, \lambda,$$

(9.63)

where λ is the brane tension and g_{ind} is the induced 4D metric on the brane.

Matching the coefficients in the Einstein equations yields the fine-tuning condition:

$$\lambda_{\text{vis}} = -\lambda_{\text{hid}} = 24M^3k,$$

(9.64)

where M is the 5D Planck mass. This setup is characteristic of the original RS model (RS1) [140], which features a compact extra dimension bounded by two branes, one of which necessarily has negative tension.

The presence of a negative-tension brane in RS1 is often considered a theoretical drawback, as it may lead to instabilities and violates certain energy conditions. This issue is addressed in the second RS model (RS2) [141], where the extra dimension is extended to infinity, and only a single positive-tension brane remains at $z = 0$. In this configuration, the warp factor still localizes gravity near the brane, effectively reproducing four-dimensional Newtonian gravity despite the infinite extra dimension.

9.6 HIERARCHY PROBLEM

To understand the physical implications of the RS model, we now examine how it addresses its original motivation: the hierarchy problem. Specifically, we compute the effective four-dimensional Planck scale and mass parameters in terms of the five-dimensional fundamental scales.

Starting from the metric (9.56), we perform the coordinate transformation $y = r_c\phi$, where r_c is the compactification radius, and $\phi \in [-\pi, \pi]$. In the low-energy limit, we introduce weak-field perturbations $h_{\mu\nu}(x^\mu) \ll 1$, so the metric takes the form:

$$ds^2 = e^{-2kT(x^\mu)|\phi|}\,[\eta_{\mu\nu} + h_{\mu\nu}(x^\mu)]dx^\mu dx^\nu + T^2(x^\mu)d\phi^2,$$

(9.65)

where the modulus field $T(x)$ parametrizes the size of the extra dimension and is assumed to be stabilized at its vacuum expectation value $\langle T(x)\rangle = r_c$. The stabilization mechanism, such as the Goldberger–Wise (GW) mechanism [151], is essential to dynamically fix this scale without fine-tuning. For simplicity, we now treat the modulus as a constant, $T = r_c$, yielding the background metric:

$$ds^2 = e^{-2kr_c|\phi|}\,[\eta_{\mu\nu} + h_{\mu\nu}(x^\mu)]dx^\mu dx^\nu + r_c^2 d\phi^2.$$

(9.66)

The Ricci scalar in five dimensions includes the four-dimensional curvature term, scaled by the warp factor:

$$R^{(5)} \supset e^{2k|y|}R^{(4)}, \quad \sqrt{-g^{(5)}} \supset e^{-4k|y|}\sqrt{-g^{(4)}}.$$

(9.67)

Using this, the gravitational part of the action becomes:

$$\begin{aligned} S &= -M^3 \int d^5x \sqrt{-g^{(5)}}\left(R^{(5)} + \kappa^2\right) \\ &\supset -M^3 \int dy\, e^{-2k|y|} \int d^4x \sqrt{-g^{(4)}}\left(R^{(4)} + \kappa^2\right), \end{aligned}$$

(9.68)

where M is the 5D Planck scale and κ^2 is the bulk cosmological constant (here treated generically). Since the graviton zero mode is independent of y, the effective four-dimensional Planck scale is:

$$M_{\rm Pl}^2 = M^3 \int_{-b}^{b} dy\, e^{-2k|y|} = \frac{M^3}{k}\left(1 - e^{-2kb}\right).$$

(9.69)

This result shows that $M \sim M_{\rm Pl}$ even for moderately large values of b, unlike in the ADD model, where a large compactification volume is required. However, this alone does not fully resolve the hierarchy problem, we must still explain the smallness of the weak scale.

Let us now consider a matter field, such as the Higgs field, localized on the brane at $y = b$. The action for the Higgs scalar is:

$$S_H = \int d^4x \sqrt{-g^{\text{ind}}} \left[g^{\mu\nu}_{\text{ind}} D_\mu H D_\nu H - \lambda \left(H^\dagger H - v^2 \right)^2 \right],$$

(9.70)

where $g^{\text{ind}}_{\mu\nu} = e^{-2kb} \eta_{\mu\nu}$ is the induced metric on the brane. Substituting this yields:

$$S_H = \int d^4x \, e^{-4kb} \left[e^{2kb} \eta^{\mu\nu} D_\mu H D_\nu H - \lambda \left(H^\dagger H - v^2 \right)^2 \right].$$

(9.71)

We rescale the field to obtain a canonically normalized kinetic term: $\tilde{H} = e^{-kb} H$. The action becomes:

$$S_H = \int d^4x \left[\eta^{\mu\nu} \partial_\mu \tilde{H} \partial_\nu \tilde{H} - \lambda \left(\tilde{H}^\dagger \tilde{H} - (e^{-kb} v)^2 \right)^2 \right].$$

(9.72)

This is the standard 4D Higgs action, but with an effective vacuum expectation value:

$$\tilde{v} = e^{-kb} v.$$

(9.73)

Taking $v \sim M_{\text{Pl}}$ as the fundamental input scale, we find that choosing $kb \approx 37$ generates $\tilde{v} \sim \text{TeV}$, providing a natural explanation for the smallness of the electroweak scale relative to the Planck scale. Therefore, the brane at $y = b$ is referred to as the “TeV brane,” while the brane at $y = 0$ is the “Planck brane,” where physical masses remain at the fundamental scale.

This exponential suppression of energy scales via the warped geometry elegantly resolves the hierarchy problem without requiring a large extra dimension or fine-tuning of fundamental parameters.

Linearized field equations

We now proceed to explore the implications of gravity in the context of the RS model by studying graviton fluctuations around the metric in the conformal gauge. As discussed earlier, the presence of a negative-tension object at the TeV brane introduces nonphysical outcomes. A closer look at Eq. (9.69) suggests a potential alternative approach. Notably, even if the size of the extra dimension approaches the limit $b \to \infty$, the TeV brane can be excluded from the physical setup. This concept forms the basis of the RS2. Although this approach abandons the original solution for the hierarchy problem discussed in the previous section, RS2 focuses on studying the more intriguing aspects of gravity [141, 152].

In this modified model, where only one brane exists, Einstein's equations derived from the action take the form:

$$R_{MN} - \frac{1}{2} g_{MN} R = \Lambda g_{MN} + \sigma g_{\mu\nu} \delta(z) \delta^{\mu}_{M} \delta^{\nu}_{N},$$

(9.74)

where σ is the brane tension. The linearized field equations for a perturbed metric $ds^2 = e^{-A(z)} dx^M dx^N (\eta_{MN} + h_{\mu\nu})$ can be obtained using the relation that connects the Einstein tensor for a manifold with another conformally related manifold, i.e., $g_{MN} = e^{-A(z)} \tilde{g}_{MN}$, where $e^{-A(z)} = \frac{1}{(k|z|+1)^2}$ in our case:

$$\begin{aligned} G_{MN} =& \tilde{G}_{MN} + \frac{d-2}{d} \Big[\frac{1}{2} \tilde{\nabla}_M A \tilde{\nabla}_N A \\ &+ \tilde{\nabla}_M \tilde{\nabla}_N A - \tilde{g}_{MN} \left(\tilde{\nabla}_k \tilde{\nabla}^k A - \frac{d-3}{4} \tilde{\nabla}_k A \tilde{\nabla}^k A \right) \Big] . \end{aligned}$$

(9.75)

Here, $\tilde{\nabla}$ refers to the covariant derivative with respect to the perturbed metric $\tilde{g}_{MN} = (\eta_{MN} + h_{MN})$.

With the knowledge of $\tilde{G}_{MN}$ and the covariant derivatives of $A(z)$, the linearized Einstein equation takes the form:

$$-\frac{1}{2} \partial^M \partial_M h_{\mu\nu} + \frac{d-2}{4} \partial^M A \partial_M h_{\mu\nu} = 0.$$

(9.76)

The linear expansion of the perturbed metric is performed using Eq. (9.76) under the gauge condition $\partial^\mu h_{\mu\nu} = h^\mu_\mu = 0$, known as the RS gauge choice. A detailed discussion of this specific gauge choice can be found in [152]. After performing a separation of variables $h(x,y) = \psi(y)e^{ip\cdot x}$, the resulting equation of motion is:

$$\left[-\frac{m^2}{2}e^{2k|y|} - \frac{1}{2}\partial_y^2 - 2k\delta(y) + 2k^2\right]\psi(y) = 0,$$

(9.77)

where m represents the four-dimensional mass eigenvalue, $\Box h_{\mu\nu} = m^2 h_{\mu\nu}$. To cast this equation in a Schrödinger-like form, we perform a change of variables $z \equiv \text{sgn}(y)\frac{e^{k|y|}-1}{k}$, yielding:

$$\left[-\frac{1}{2}\partial_z^2 + V(z)\right]\psi(z) = m^2\psi(z),$$

(9.78)

with the potential

$$V(z) = \frac{15k^2}{8(k|z|+1)^2} - \frac{3k}{2}\delta(z).$$

(9.79)

This potential forms a "volcano" with a minimum at $z = 0$ due to the delta function. This equation predicts a Yukawa-like correction to the gravitational potential on the brane, similar to the screened Poisson equation:

$$U(r) \sim \frac{G_N M_1 M_2}{r} + \int_0^\infty dm \frac{G_N M_1 M_2}{r} e^{-mr}\psi_m^2(z),$$

(9.80)

where the integral is over the massive Kaluza-Klein modes. Equation (9.78) has a solution in terms of Bessel functions:

$$\psi_m = a_m z^{\frac{1}{2}} Y_{\alpha+\frac{1}{2}}(m(z+\frac{1}{k})) + b_m z^{\frac{1}{2}} J_{\alpha+\frac{1}{2}}(m(z+\frac{1}{k})),$$

(9.81)

For our purposes, we are primarily interested in the effective four-dimensional theory at the brane, where $\psi_m(0) \sim \sqrt{\frac{m}{k}}$. Thus, the corrected gravitational potential takes the form:

$$U(r) \sim \frac{G_N M_1 M_2}{r} + c \int_0^\infty dm \frac{G_N M_1 M_2}{kr} m e^{-mr} \tag{9.82}$$

$$= G_N \frac{M_1 M_2}{r} \left(1 + \frac{C}{r^2 k^2}\right), \tag{9.83}$$

where C is a constant related to the integration over m. With k of the order of the fundamental Planck scale, the correction to the Newtonian potential is highly suppressed. To detect these higher Kaluza-Klein modes, extraordinarily high energies beyond current experimental reach would be required. Thus, this RS2 model with a semi-infinite extra dimension successfully reproduces the ordinary four-dimensional Newtonian potential [141, 151, 152].

CHAPTER 10

BSM Collider Phenomenology

DOI: 10.1201/9781003457701-10

10.1 INTRODUCTION

Physicists are driven by the goal of understanding the fundamental nature of the universe, which has led them to explore ideas BSM of particle physics. Collider experiments have played a key role in this search, as they allow scientists to probe extremely high energies where new particles or forces might appear. The main goal of BSM collider studies is to search for signs of new particles predicted by theoretical models. These models aim to answer open questions in particle physics and improve our understanding of matter at the smallest scales. High-energy collisions at the Large Hadron Collider (LHC) and future colliders provide a unique opportunity to discover such new physics [153]. The main areas of focus include:

- Supersymmetric Particles: SUSY predicts a partner particle for each SM particle. These superpartners could help resolve major open questions, such as the hierarchy problem, and may provide a framework for unifying the fundamental forces [118].
- Extra Gauge Bosons: Particles like Z' and W' are predicted by extensions of the SM and may indicate new interactions that could help explain observed anomalies in current experimental data [78].
- Extended Higgs Sector: The discovery of additional Higgs bosons could reshape our understanding of electroweak symmetry breaking and the dynamics of the Higgs mechanism [48, 51].
- Dark Matter Candidates: Exploring particles such as Weakly Interacting Massive Particles (WIMPs) and axions may lead to significant breakthroughs in understanding dark matter's elusive nature [32, 33].

In addition to the search for new particles, collider experiments seek to identify signatures of new physics. These signatures offer crucial insights into the existence of BSM phenomena, including:

- Missing Energy: A hallmark of stable or weakly interacting particles that may indicate the production of new physics [154].
- Jet and Lepton Production: Observable events that suggest the involvement of new particles [155].
- Resonance Searches: The detection of specific decay products that could confirm the presence of new particles or interactions [156].

This chapter will explore the experimental strategies employed in probing BSM collider phenomenology. Due to the limited space available in this chapter, we will focus on a select few examples of new particle discoveries at the LHC and will not consider other future colliders.

10.2 SUPERSYMMETRY COLLIDER PHENOMENOLOGY

This section focuses on identifying signatures of SUSY particles, understanding their production mechanisms, and measuring their properties to test SUSY theories. SUSY particles can be produced at colliders through strong interactions, which primarily generate squarks and gluinos due to the strong coupling, as well as electroweak interactions, leading to the production of sleptons, neutralinos, and charginos. Additionally, associated production processes, such as gluino-neutralino or squark-neutralino pairs, contribute to the variety of production mechanisms.

Additionally, SUSY particles decay through cascades involving intermediate states, ultimately producing the lightest supersymmetric particle (LSP). Key observables include missing transverse energy (E_T^{miss}) from the undetectable LSP [157], multiple energetic jets and leptons from squark, gluino, or slepton decays, and potential signatures of long-lived particles, such as displaced vertices or charged tracks, arising from particles like staus or neutralinos [158, 159].

Here, we focus on three fundamental SUSY particles: the Lightest Supersymmetric Particle (LSP), typically the lightest neutralino and a prime candidate for dark matter; the gluino, a key participant in strong interactions and a potential gateway to new physics; and squarks, the superpartners of quarks, which provide insights into flavor physics and the hierarchy problem.

Search for gluinos, first and second generation squarks

As discussed in Chapter 8, within the MSSM, the gluino mass is approximately given by $m_{\tilde{g}} \approx 2.5\, m_{1/2}$, typically resulting in a value of at least a few TeV. The five light-flavored squark species $(\tilde{d}, \tilde{u}, \tilde{s}, \tilde{c}, \tilde{b})$, including both left- and right-chiral

components, are generally assumed to be mass-degenerate. In contrast, the third-generation squarks $\tilde{t}_L$ and $\tilde{t}_R$ experience significant left-right mixing, giving rise to two distinct mass eigenstates, $\tilde{t}_1$ and $\tilde{t}_2$. Notably, $\tilde{t}_1$ is considerably lighter than the other squark states, necessitating a dedicated discussion of its production mechanisms and decay channels [118].

At the LHC, squarks and gluinos can be produced in pairs $\{\tilde{g}\tilde{g}, \tilde{q}\tilde{q}, \tilde{q}\tilde{g}\}$ and decay through processes such as $\tilde{q} \to q\tilde{\chi}_1^0$ and $\tilde{g} \to q\bar{q}\tilde{\chi}_1^0$, where $\tilde{\chi}_1^0$ is the lightest neutralino, as depicted in Fig. 10.1. Searches for squarks and gluinos in final states with high transverse momentum jets and missing transverse momentum have been conducted by both the ATLAS and CMS experiments, using center-of-mass energies of $\sqrt{s} = 7, 8, 13$ TeV and a total integrated luminosity of approximately 20 fb^{-1} [160, 161]. No significant excess above the SM predictions was observed. In Fig. 10.2, we show the ATLAS exclusion limits at 95% confidence level for the MSSM model with $\tan\beta = 30$, $A_0 = -2m_0$, and $\mu > 0$, presented (left) in the $(m_{\tilde{g}} - m_{\tilde{q}})$ plane [160]. The CMS limits are quite similar [161]. It is noteworthy that values of $m_{1/2} < 340$ GeV are excluded for $m_0 < 6$ TeV in this scenario, consistent with constraints derived from the measured lightest Higgs mass of $m_h \approx 125$ GeV [162].

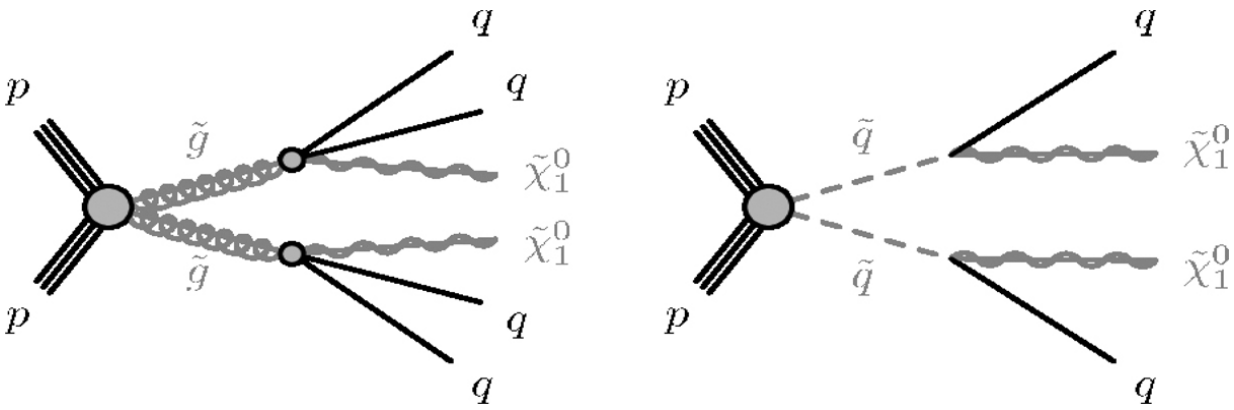

Figure 10.1 Representative diagrams for (left) gluino- and (right) squark-pair production and their direct decays: $\tilde{g} \to q\bar{q}\tilde{\chi}^0$ and $\tilde{q} \to q\tilde{\chi}^0$. ⏎

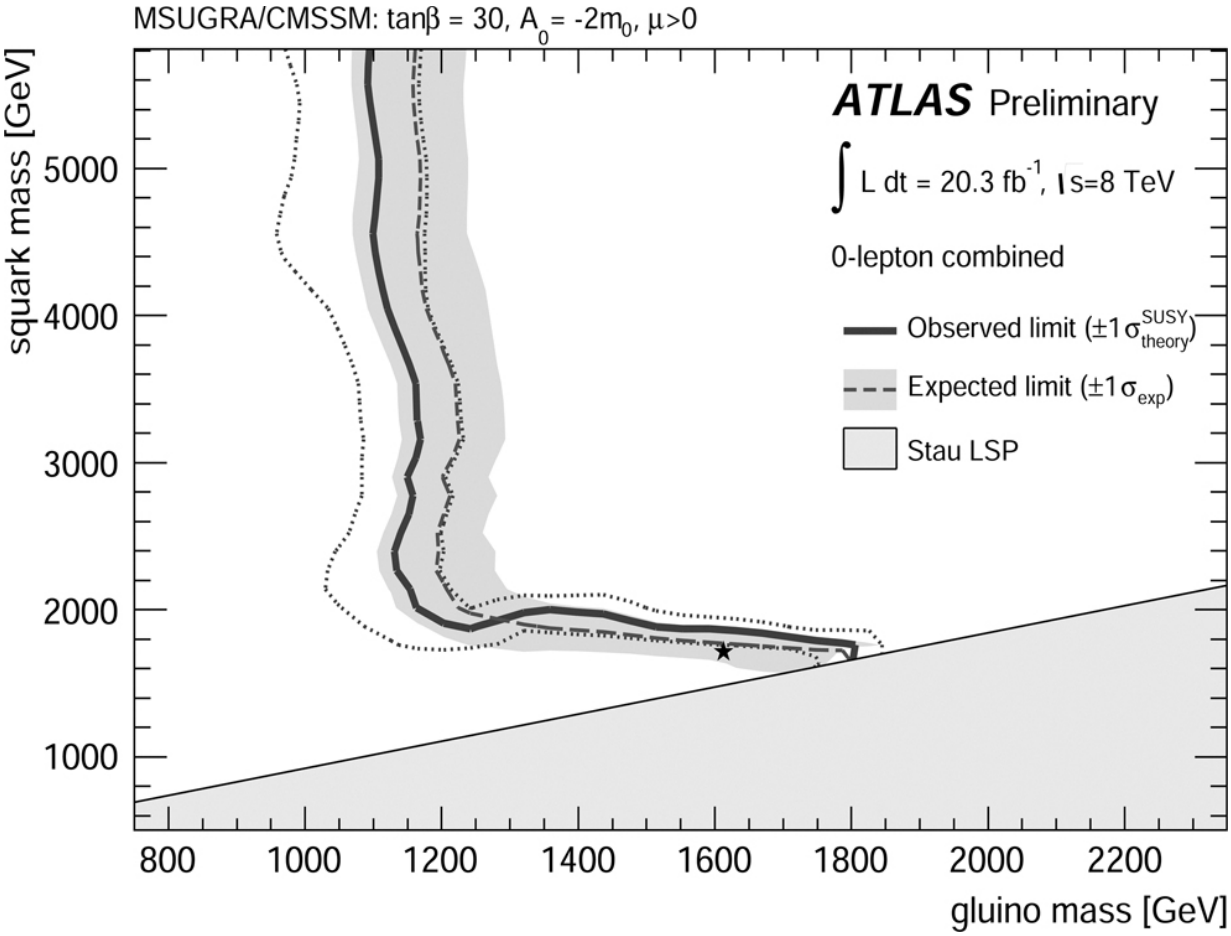

Figure 10.2 ATLAS exclusion limits, at 95% CL, for the MSSM model with $\tan\beta = 30$, $A_0 = -2m_0$ and $\mu > 0$, projected on the $(m_{\tilde{g}} - m_{\tilde{q}})$ plane [160]. CMS limits are quite similar [161]. ⏎

Search for stops

The stop plays an essential role in solving the hierarchy problem in the MSSM, through the cancellations of the quadratic divergences of top-quark loops. As mentioned, in most SUSY models, a light stop quark mass arises naturally. A search for the pair production of stop quarks has been performed by both the ATLAS and CMS experiments, using the full data set collected at $\sqrt{s} = 7, 8$ TeV and integrated luminosity of order $20\,\text{fb}^{-1}$. LHC searches focus on the semileptonic decay mode, where $\tilde{t} \to t\tilde{\chi}_1^0 \to bW^{\pm}\tilde{\chi}_1^0$ and $\tilde{t} \to b\tilde{\chi}_1^{\pm} \to bW^{\pm}\tilde{\chi}_1^0$, as shown in Fig. 10.3. Then one $W^{\pm}$ decays hadronically and the other leptonically. Thus, the final state searched for is $4j + \ell +$ missing energy ($\ell = e, \mu$) [163, 164].

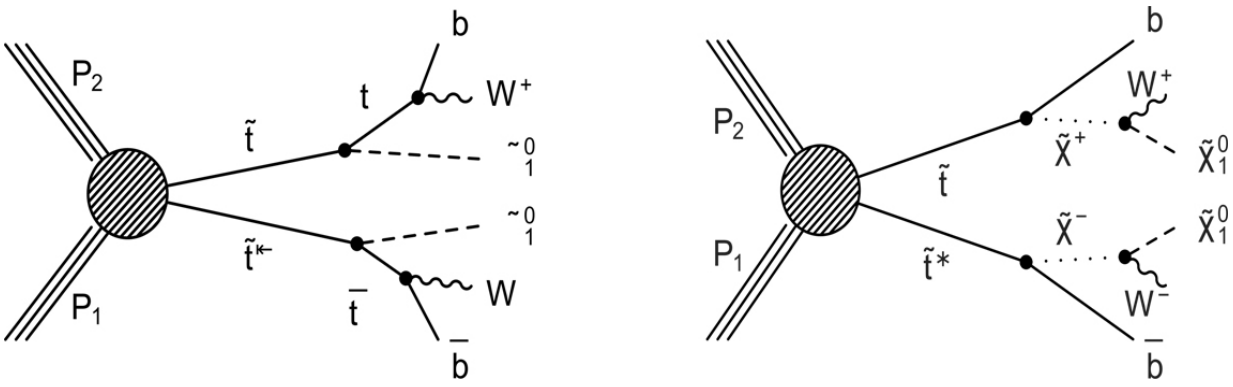

Figure 10.3 Representative diagrams for stop pair production and decay into $b\bar{b}$ W^+W^- $\tilde{\chi}_1^0\tilde{\chi}_1^0$.

An analysis of $\sim 13\,\text{fb}^{-1}$ and $\sqrt{s} = 13$ TeV at ATLAS [165] and CMS [166] detectors indicated no significant excess over the SM background. Exclusion limits at 95% CL, shown in Fig. 10.4, are reported. These limits are presented in terms of stop and lightest neutralino masses. In the considered simplified model, where $BR(\tilde{t} \to t\tilde{\chi}^0) = 1$, the stop masses between ~ 310 and ~ 820 GeV are excluded for $m_{\tilde{\chi}^0} < 160$ GeV.

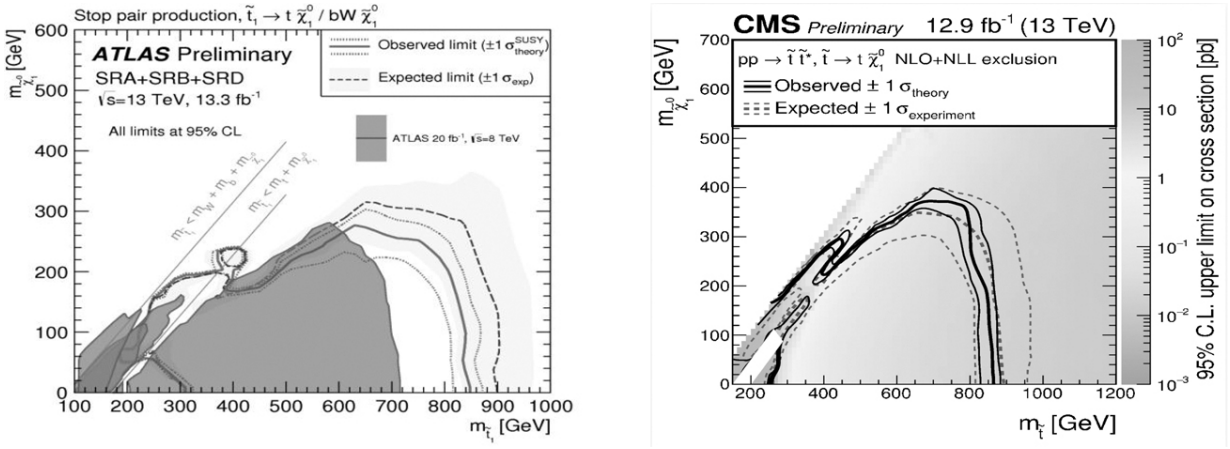

Figure 10.4 ATLAS (left) and CMS (right) exclusion limits at 95% CL for direct stop production, followed by the $\tilde{t} \to t\tilde{\chi}^0$ decay [165, 166].

Charginos and neutralinos

The lightest chargino ($\tilde{\chi}_1^{\pm}$) has several leptonic decay modes, producing an isolated lepton and missing energy, due to the undetectable neutrino and the LSP [167, 168]:

$$\tilde{\chi}_1^{\pm} \quad \to \tilde{\chi}_1^0 \ell^{\pm} \nu, \tag{10.1}$$

$$\tilde{\chi}_1^{\pm} \to \tilde{\ell}_L^{\pm}\,\nu \to \tilde{\chi}_1^0\,\ell^{\pm}, \tag{10.2}$$

$$\tilde{\chi}_1^{\pm} \to \tilde{\nu}_L\,\ell^{\pm} \to \tilde{\chi}_1^0\,\nu, \tag{10.3}$$

$$\tilde{\chi}_1^{\pm} \to \tilde{\chi}_1^0\,W^{\pm} \to \ell^{\pm}\,\nu. \tag{10.4}$$

In hadronic collisions, the charginos and neutralinos can be produced directly via 21 different reactions or through the cascade decays of strongly interacting sparticles.

The first searches for the direct electroweak production of supersymmetric charginos and neutralinos at $\sqrt{s} = 13$ TeV were conducted using *pp* collisions with a luminosity of approximately 13 fb^{-1} in the CMS detector [169]. These searches focus on signatures involving two same-flavor light leptons or three or more leptons, as illustrated in Fig. 10.5. The results are categorized based on the number, sign, and flavor of the leptons, as shown in Fig. 10.6. No significant deviation from Standard Model expectations was observed, and these results were used to set limits on simplified models with large chargino-neutralino pair production cross-sections. Specifically, they probe chargino and neutralino masses up to $400 - 1000$ GeV, depending on the assumed model parameters.

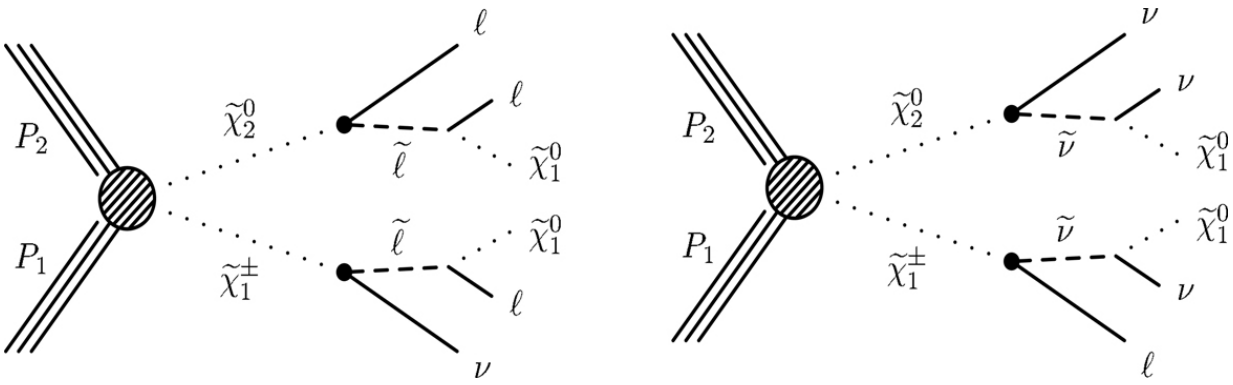

Figure 10.5 Representative diagrams for direct charginos/neutralinos production and decay mediated by sleptons (left) and sneutrinos (right), leading to leptonic final states. ⏎

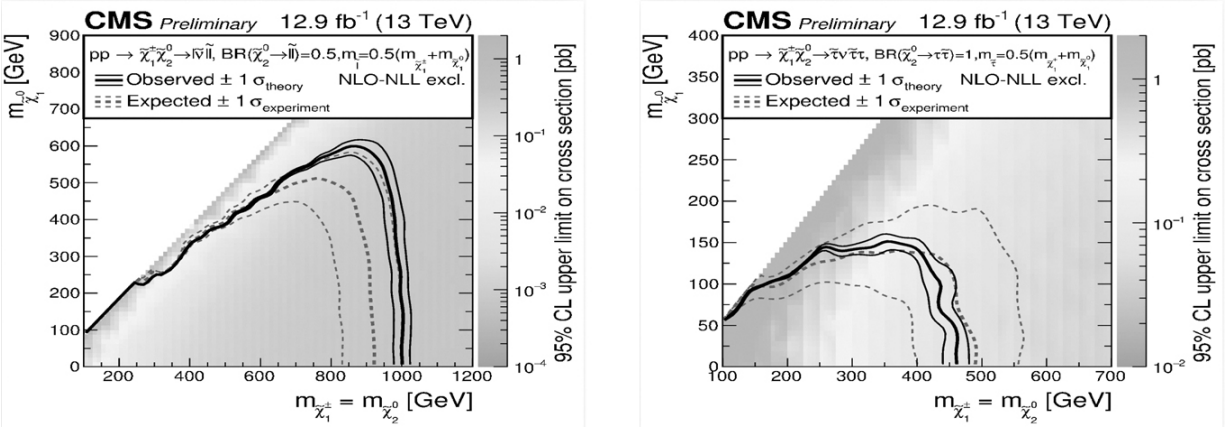

Figure 10.6 CMS results of the three-lepton search in the flavor-democratic signal model with the slepton/sneutrino mass given by $m_{\tilde{\ell}} = m_{\tilde{\nu}} = \frac{1}{2}(m_{\tilde{\chi}^+} + m_{\tilde{\chi}^0})$ [169]. ⏎

10.3 SEARCH FOR EXTRA GAUGE BOSONS AT THE LHC

The ATLAS and CMS experiments at the Large Hadron Collider (LHC) have conducted extensive searches for extra gauge bosons, such as Z' and W', predicted by various extensions of the SM. These searches are particularly compelling in the leptonic Drell-Yan (DY) channel, where heavy gauge bosons could manifest as resonant peaks in the invariant mass spectrum of lepton pairs (e^+e^- or $\mu^+\mu^-$). DY processes, characterized by the production of lepton pairs through quark-antiquark annihilation ($q\bar{q} \to Z'/W' \to \ell^+\ell^-$), offer a clean experimental signature and serve as powerful tools for discovering or constraining new physics involving heavy spin-1 gauge bosons [170, 171].

Searches for Z'-bosons focus on identifying resonances in the invariant mass spectrum, which could indicate the presence of new physics. These heavy gauge bosons arise in theoretical frameworks such as GUTs, Left-Right Symmetric Models, and models with additional $U(1)$ symmetries. Experimentally, a Z'-boson would appear as a narrow peak above SM backgrounds, with angular distributions and forward-backward asymmetry providing further discriminating power. Recent results from ATLAS and CMS have placed stringent lower bounds on Z'-boson masses, excluding them up to 4.5 TeV depending on the model [170, 171]. Future upgrades at the High-Luminosity LHC are expected to extend the reach of these searches, enabling sensitivity to even heavier Z'-bosons. Enhanced detector resolution and increased luminosity will allow the exploration of rarer events and further tighten constraints, maintaining Z'-searches as a cornerstone of BSM physics exploration at the energy frontier.

Search for Z' at the LHC

The existence of new neutral gauge bosons is a possible signature of GUT models, such as left-right-symmetric (LRS) models and $U(1)'$ extensions of the SM.

Searches for Z' bosons have been extensively conducted by the ATLAS and CMS Collaborations, resulting in stringent bounds on Z' boson production as a function of its mass, $m_{Z'}$, particularly in the $Z' \to \mu^+\mu^-$ and $Z' \to e^+e^-$ decay channels. By combining these two final states and adopting the sequential Standard Model (SSM) framework, the production of an SSM Z' boson has been excluded at the 95% confidence level (CL) for masses below 5.15 TeV (CMS) [172] and 5.10 TeV (ATLAS) [173]. The SSM assumes that the Z' boson has the same couplings to SM particles as the Z boson, specifically with generation-independent couplings to SM fermions.

In Fig. 10.7, the left panel shows the CMS upper limits [172] at the 95% confidence level (CL) on the product of the production cross-section and the branching fraction for a spin-1 resonance with a width equal to 0.6% of the resonance mass. These limits are normalized to the corresponding product for the SM Z boson. Results are provided for the (top left) dielectron channel, (top right) dimuon channel, and (bottom) the combined dilepton channels. The shaded bands represent the 68% and 95% quantiles of the expected limits. Simulated predictions for spin-1 Z'_{SSM} and Z'_{ψ} resonances are also included for comparison. The right panel presents the ATLAS upper limits [173] at 95% CL on the fiducial cross-section times branching ratio as a function of the pole mass for the combined dilepton channel. The limits are shown for signals with relative widths of zero, 3%, and 10%. Observed limits are depicted as solid lines, while expected limits are indicated by dotted or dashed lines. Theoretical cross-sections for the Z'_{SSM} resonance, with a width-to-mass ratio of $\Gamma/m = 3.0\%$, are overlaid for comparison. These results highlight the combined sensitivity of the CMS and ATLAS searches to Z' boson models with varying resonance widths.

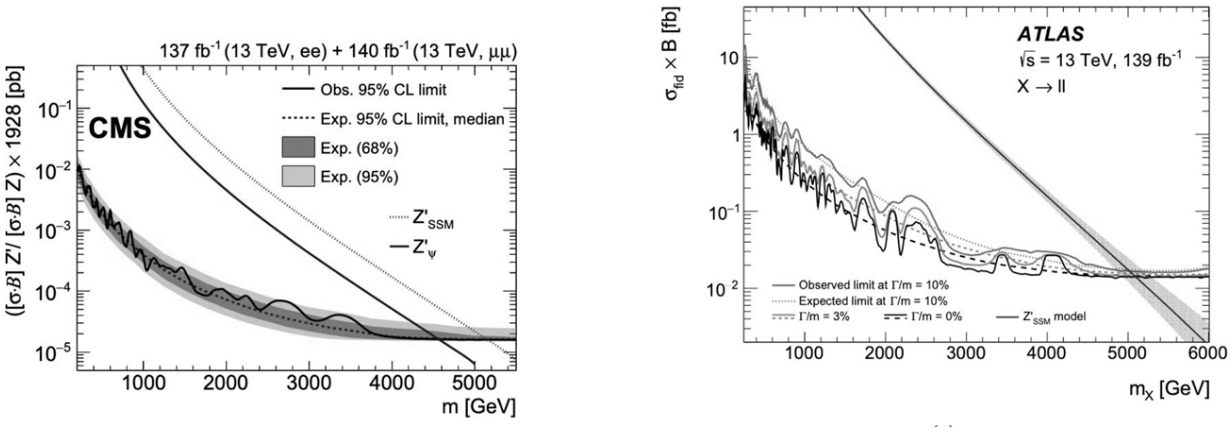

Figure 10.7 CMS and ATLAS Upper Limits on Z' Boson Production: Left: CMS 95% CL upper limits on the normalized cross-section times branching fraction for a spin-1

resonance [172]. Right: ATLAS 95% CL upper limits on the fiducial cross-section times branching ratio for combined dilepton channels with varying resonance widths [173]. ⏎

Search for W' at the LHC

Many extensions of the SM of particle physics predict the existence of new, heavy charged gauge bosons, often referred to as W' bosons. These additional particles arise in various theoretical frameworks, such as grand unified theories (GUTs), composite models, and certain models of extra dimensions. The search for these new W' bosons provides an essential tool for probing a wide range of new physics scenarios. By investigating the production and decay of W' bosons, experiments at particle colliders like the LHC can offer insights into the nature of new interactions, the possible structure of underlying physics beyond the SM, and the mass scale of new particles that could explain phenomena unexplained by the SM.

Searches for W' bosons, hypothetical heavier counterparts to the SM W boson, have been extensively conducted by the CMS and ATLAS collaborations. The production of a W' boson in proton-proton collisions at the LHC occurs primarily through quark-antiquark annihilation ($q\bar{q}' \to W'$). The production cross-section is influenced by the parton distribution functions (PDFs) of the quarks and antiquarks in the proton and the coupling strength of the W' boson to quarks. In models like the SSM, the W' boson has couplings similar to the SM W, while other models may propose different coupling patterns. The cross-section is sensitive to the mass of the W' boson, which decreases rapidly with increasing mass due to the behavior of PDFs at high momentum transfer. Experimental searches at the LHC focus on various decay channels, such as leptonic ($W' \to \ell\nu$) and hadronic ($W' \to q\bar{q}'$) decays, with additional sensitivity to the $W' \to tb$ decay mode, especially in models with enhanced couplings to third-generation fermions.

The decay modes of the W' boson provide distinctive signatures for experimental searches. In leptonic decays, the W' boson decays to a charged lepton and a neutrino, yielding a signature of high transverse momentum (p_T) leptons and missing transverse energy (E_T^{miss}), which are prominent in the final states. Hadronic decays lead to high-mass dijet systems, and the $W' \to tb$ decay produces top-bottom quark pairs, which require advanced reconstruction techniques due to the boosted top quarks. Searches by the CMS and ATLAS collaborations have set stringent upper limits on the mass of the W' boson. For example, CMS results exclude W' boson masses up to approximately 6.1 TeV in the leptonic decay channels [174], while ATLAS constraints in the same channels exclude masses up to about 5.9 TeV [170]. Limits for hadronic and heavy-flavor decays extend to approximately 4.5 TeV and 3.8 TeV, respectively.

Both the ATLAS and CMS collaborations have conducted searches for the decay $W' \to \ell\nu$ (where $\ell = e, \mu, \tau$). The ATLAS search sets an SSM mass limit of

$m_{W'} > 5.9\,\text{TeV}$, while the CMS search places a slightly stronger limit of $m_{W'} > 6.1\,\text{TeV}$. Fig. 10.8 illustrates the corresponding cross-section limits as a function of W' mass. As typically observed in these analyses, there is good agreement between the observed and expected limits, providing strong constraints on the mass of the W' boson in this decay channel.

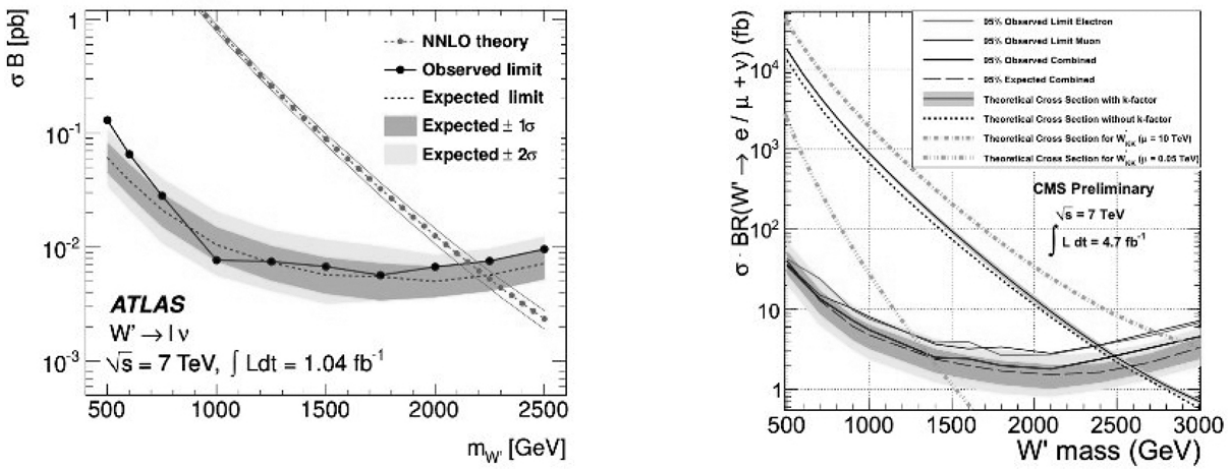

Figure 10.8 ATLAS [170] (left) and CMS [174] (right) cross-section limits on $W' \to \ell\nu$.

10.4 SEARCH FOR HEAVY HIGGS BOSONS AT THE LHC

As discussed in previous chapters, the heavy Higgs boson is a central feature of many BSM theories, including the 2HDM [48], the LRSM) [75], and the MSSM [118]. These models extend the Higgs sector to address unresolved challenges such as the hierarchy problem and the nature of dark matter. Typically possessing a mass in the multi-hundred GeV to TeV range, the heavy Higgs exhibits distinct couplings to fermions and gauge bosons and can decay into exotic particles. Its discovery would mark a breakthrough in the search for new physics, offering crucial insights into extended mechanisms of electroweak symmetry breaking and helping to differentiate between competing BSM frameworks.

The heavy Higgs boson, h', is predominantly produced at the LHC through the gluon-gluon fusion (ggF) process, which accounts for approximately 90% of its total production cross-section [175]. Other production mechanisms, such as vector boson fusion (VBF), Higgs strahlung, and top-associated Higgs production, contribute to the remaining 10%. Figure 10.9 illustrates the h' ggF production cross-section, $\sigma(pp \to h')$, as a function of its mass, $m_{h'}$, for a range of coupling values. Notably, $\sigma(pp \to h')$ can reach values $\gtrsim 2\,\text{pb}$ for $m_{h'} \lesssim 400\,\text{GeV}$. In this scenario, an integrated luminosity of $L_{\text{int}} = 300\,\text{fb}^{-1}$ is sufficient to probe a relatively light h',

while higher luminosities of $L_{\text{int}} = 3000\,\text{fb}^{-1}$ are required for heavier h' masses, at a center-of-mass energy of $\sqrt{s} = 14\,\text{TeV}$.

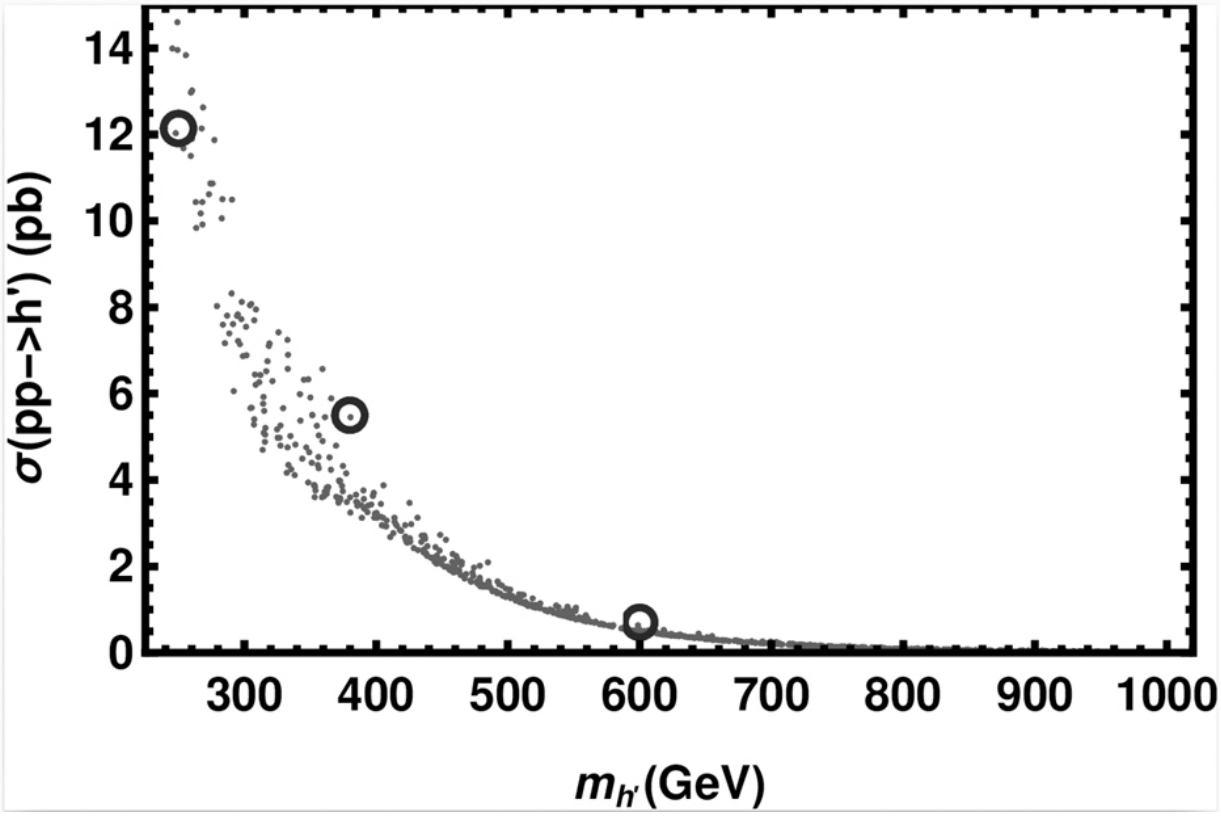

Figure 10.9 Left: The h' production cross-section from ggF as a function of its mass $m_{h'}$. Three benchmark points, under consideration, are surrounded by *dark-shaded region* circles [94]. ⏎

In Fig. 10.9 (right), we show the relevant h' decay branching ratios as functions of $m_{h'}$. It is remarkable to notice that for $m_{h'} \leq 600\,\text{GeV}$, the h' decay branching ratio to two SM Higgs bosons is not small, mainly $\text{BR}(h' \to hh) \geq 10\%$, which gives hope for probing this heavy Higgs boson through this channel.

One may begin with the decay $h' \to hh \to b\bar{b}b\bar{b}$ for probing h' at the LHC, as the branching ratio $\text{BR}(h \to b\bar{b})$ is the largest of h decays. However, this process has a huge background and the signal is much lower than the relevant background, even for a quite heavy Higgs boson. Therefore, the decay process $h' \to hh \to b\bar{b}\gamma\gamma$, given by the Feynman diagram in Fig. 10.10, is considered as the most relevant signal for probing h' [94]. We analyzed this process for $m_{h'} = 250\,\text{GeV}$, $400\,\text{GeV}$, and $600\,\text{GeV}$.

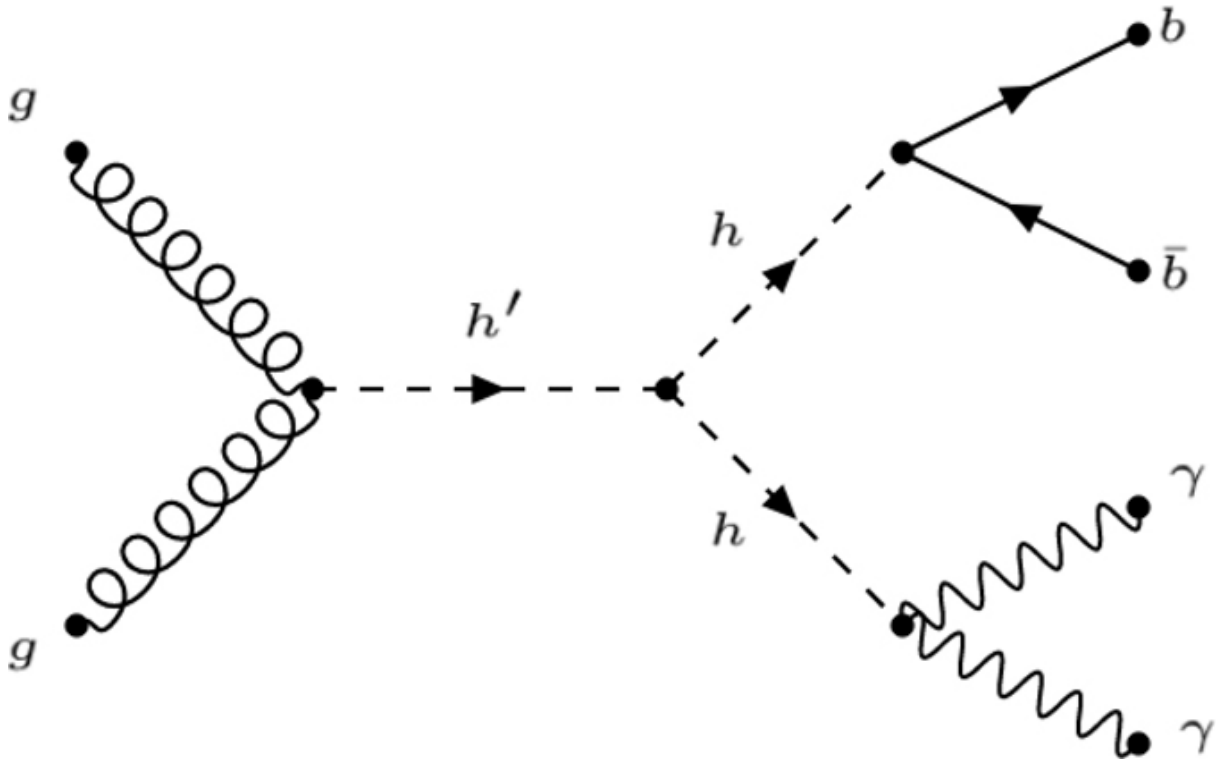

Figure 10.10 Feynman diagram for the h' ggF production and decay process $gg \to h' \to hh \to b\bar{b}\gamma\gamma$.

As the h' decay width $\Gamma_{h'}$ is much smaller than its mass, $\Gamma_{h'}/m_{h'} \ll 1$, the narrow width approximation can be used and the total cross-section $\sigma(pp \to h' \to hh \to b\bar{b}\gamma\gamma)$ can be approximated as

$$\begin{aligned}\sigma(pp \to h' \to hh \to b\bar{b}\gamma\gamma) \quad &\approx \sigma(pp \to h') \times \mathrm{BR}(h' \to hh) \\ &\times \mathrm{BR}(h \to b\bar{b}) \times \mathrm{BR}(h \to \gamma\gamma).\end{aligned} \tag{10.5}$$

The branching ratio of the $h' \to hh$ decay, $\mathrm{BR}(h' \to hh)$, is expressed in terms of the coupling $g_{h'hh}$. Table 10.1 presents the calculated cross-sections and decay branching ratios for the three considered $m_{h'}$ values, following the results from [94].

TABLE 10.1 $pp \to h'$ production cross-section and its $h' \to hh$ decay branching ratio and the total cross-section for its production and decay process $pp \to h' \to hh \to b\bar{b}\gamma\gamma$ for three different values of $m_{h'} = 250\,\mathrm{GeV}$, 400 GeV, and 600 GeV.

$m_{h'}(\mathrm{GeV})$	$\sigma(pp \to h')(\mathrm{pb})$	$\mathrm{BR}(h' \to hh)$	$\sigma(pp \to h' \to hh \to b\bar{b}\gamma\gamma)(\mathrm{fb})$
250	12.140	0.30	6.30
400	5.050	0.20	1.01
600	0.504	0.18	0.05

For potential discovery of $h^{'}$ at the LHC, we analyze both its signal and the corresponding relevant background from the SM processes. These backgrounds can be reduced by appropriate kinematical cuts [94]. Fig. 10.11 shows the number of signal events distributions for $m_{h'} = 250\,\text{GeV}$ and $400\,\text{GeV}$ with the relevant irreducible background before (left) and after (right) applying cuts, respectively. The benchmark point with $m_{h'} = 600\,\text{GeV}$ is not included here as its cross-section is quite tiny with the considered ($L_{\text{int}} = 300\,\text{fb}^{-1}$).

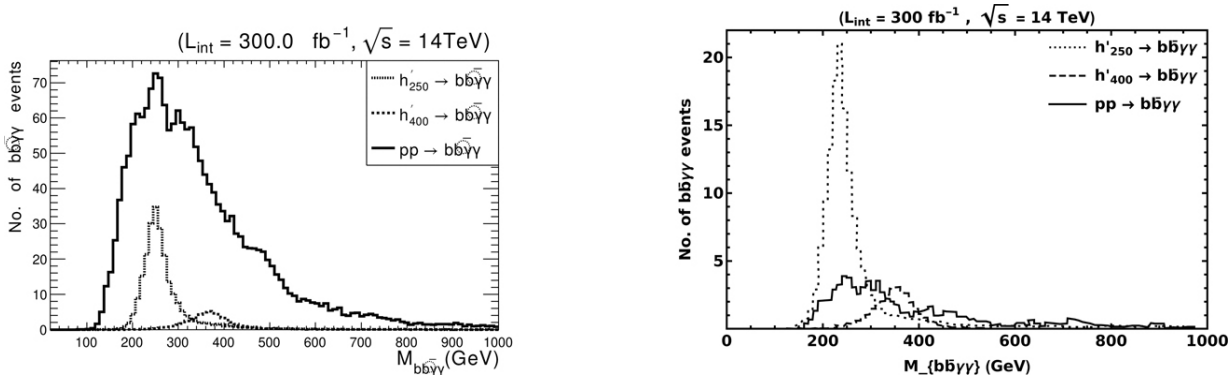

Figure 10.11 Number of signal events for $h' \to b\bar{b}\gamma\gamma$ decays at mass $m_{h'} = 250\,\text{GeV}$ (dotted line) and $400\,\text{GeV}$ (dashed line) induced by ggF versus the invariant mass of the final states $b\bar{b}\gamma\gamma$, at $\sqrt{s} = 14\,\text{TeV}$ and $L_{\text{int}} = 300\,\text{fb}^{-1}$ alongside the relevant background events (solid line) before (left) and after (right) applying the cut flow [94].. ⏎

As can be seen, the application of kinematic cuts effectively suppresses the majority of background events. These backgrounds exhibit broad distributions, as they originate primarily from non-resonant elastic scattering processes rather than resonant production in the signal region. The results clearly establish the $2\gamma + 2b$ -jet final state in SM Higgs boson pair production as a distinctive signature for probing the heavy *CP*-even Higgs ($h^{'}$) in models with enhanced $h'hh$ couplings.

10.5 COLLIDER SEARCHES FOR DARK MATTER

Collider searches for dark matter (DM) focus on the exciting prospect of identifying its particle content, which remains one of the most significant open questions in modern physics. While the existence of dark matter is well established through its gravitational effects on galaxies and galaxy clusters, as well as its impact on the cosmic microwave background, the exact nature of its constituent particles remains elusive. Various theories beyond the Standard Model (SM) suggest potential candidates for dark matter, including weakly interacting massive particles (WIMPs), axions, and dark photons, but none have been conclusively detected.

Colliders such as the LHC provide an ideal environment for probing DM by searching for missing transverse energy (E_T^{miss}) and other signatures indicative of DM production. These searches focus on events where DM is produced in high-energy collisions but does not interact directly with the detector, leaving a detectable imbalance in momentum. Through the analysis of such events, physicists aim to constrain the properties of DM, such as its mass and interactions. Despite the challenges, collider experiments remain one of the most promising avenues for shedding light on this mysterious component of the universe.

Initial state radiation (ISR), which can involve photons, jets, or vector bosons, or associated production as shown in Fig. 10.12, provides valuable signatures for tagging dark matter (DM) pair production in collider experiments. In these searches, the production of a Standard Model (SM) particle(s) X in conjunction with large missing transverse energy (E_T^{miss}) serves as a key indicator of DM interactions. The large E_T^{miss} arises from the undetected dark matter particles, which carry away momentum, resulting in an imbalance that can be measured [176, 177].

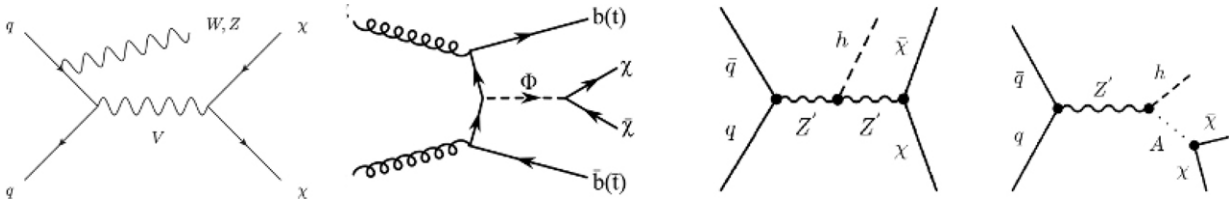

Figure 10.12 Initial state radiation vector boson, Associated production: scalar/pseudo-scalar, and mono-Higgs signatures.

The Monojet search is a very general DM search focusing on events with jets and large missing transverse energy (E_T^{miss}). The selection criteria for this search include:

(i) An energetic jet with transverse momentum $p_T > 150\,\text{GeV}$,

(ii) Missing transverse energy $E_T^{\text{miss}} > 200\,\text{GeV}$.

The primary SM backgrounds considered in this analysis include $Z+$ jets, $W+$ jets, diboson, and $t\bar{t}$ events. These backgrounds are estimated using control regions defined by final states with one or two leptons. The background contributions from $Z+$ jets and $W+$ jets processes are predicted with high precision, carrying uncertainties of approximately $\mathcal{O}(1\text{--}2\%)$ [176].

Both ATLAS and CMS employ semi-data-driven techniques in their analyses, utilizing statistically independent signal regions to enhance the robustness of their results. Backgrounds are estimated using control regions defined by events with one or two leptons, enabling precise validation of Standard Model predictions. Despite the sensitivity of these methods, no significant excess over the expected background has been observed so far.

Figure 10.13 displays the measured distributions of recoil transverse momentum p_T^{recoil} for events with $p_T^{\text{recoil}} > 200\,\text{GeV}$, compared against SM predictions in the signal region. These distributions are a crucial diagnostic tool for identifying potential deviations from SM expectations, which could indicate DM production or other new physics phenomena. The SM predictions shown include contributions from the dominant backgrounds: $Z+\text{jets}$, $W+\text{jets}$, diboson, and $t\bar{t}$, which are estimated and validated through control regions and precise theoretical calculations [177]. Comparing these distributions enables the identification of excesses or discrepancies in p_T^{recoil}, offering valuable insights into potential new physics.

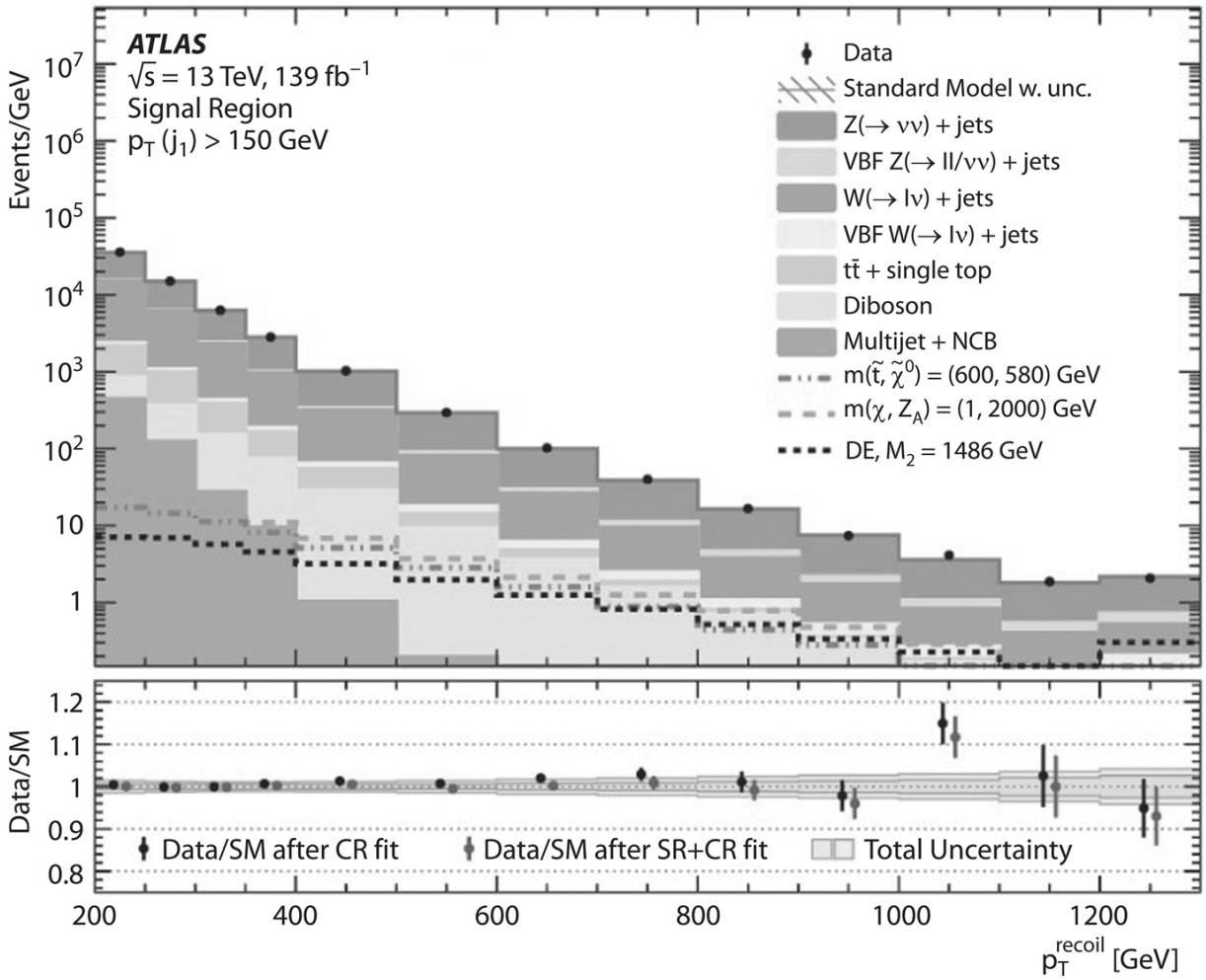

Figure 10.13 ATLAS results for the data and background predictions in the signal region [177]

CHAPTER 11

BSM Flavor Implications

DOI: 10.1201/9781003457701-11

11.1 INTRODUCTION

Flavor physics provides a powerful probe of BSM physics. The patterns of quark and lepton masses, mixing angles, and CP violation observed in nature remain unexplained within the SM, pointing to the need for a deeper theoretical framework. While the SM successfully describes these phenomena at the level of effective interactions, it provides no fundamental explanation for the origin of the flavor hierarchy, the smallness of neutrino masses, or the matter-antimatter asymmetry in the universe. These open questions strongly suggest the presence of new physics at higher energy scales.

BSM theories often address these questions by introducing new particles, symmetries, or dynamics that modify the SM's flavor structure. For example, mechanisms such as the seesaw mechanism for neutrino masses [20], flavor symmetries, or additional Higgs sectors can provide a more fundamental understanding of the observed flavor patterns. However, these modifications must carefully align with the stringent experimental constraints imposed by precision measurements of flavor-changing processes, such as neutral meson oscillations, rare decays, and lepton flavor violations [178, 179]. The absence of significant deviations from SM predictions in these processes places tight restrictions on the parameter

space of many BSM models, making flavor physics a key testing ground for new theories.

This chapter focuses on the theoretical implications of BSM physics for flavor phenomena. We explore how various BSM scenarios reshape our understanding of flavor. Particular attention is given to the mechanisms through which these theories generate flavor structures, including the role of spontaneous symmetry breaking, alignment mechanisms, and the dynamics of flavor-changing interactions. Additionally, we discuss the potential for new sources of CP violation beyond the SM, which could have profound implications for cosmology and the matter-antimatter asymmetry. Finally, we examine the interplay between flavor physics and other BSM phenomena, such as neutrino masses, dark matter, and the hierarchy problem, highlighting how flavor observables can provide indirect probes of these interconnected aspects of new physics.

11.2 THE FLAVOR PUZZLE AND BSM MOTIVATIONS

The SM of particle physics provides a remarkably successful description of fundamental particles and their interactions. However, when it comes to flavor: the patterns of quark and lepton masses, mixing angles, and CP violation, the SM falls short in providing a fundamental explanation. Key limitations include:

- Unexplained Mass Hierarchies: The masses of the fundamental fermions span many orders of magnitude, from the electron ($m_e \sim 0.5\,\mathrm{MeV}$) to the top quark ($m_t \sim 173\,\mathrm{GeV}$). The SM does not explain why these hierarchies exist or why the Yukawa couplings vary so dramatically.
- Neutrino Masses: The SM predicts neutrinos to be massless, yet neutrino oscillation experiments have conclusively shown that neutrinos have small but non-zero masses [180]. This requires an extension of the SM.
- Flavor Mixing and CP Violation: The observed patterns in the CKM (quark) and PMNS (lepton) mixing matrices are not predicted by the SM. The origin of CP violation in the quark sector (via the CKM phase) and the potential for CP violation in the lepton sector remain unexplained.

- No Fundamental Theory of Flavor: The SM treats Yukawa couplings as free parameters, with no underlying principle to determine their values. This lack of a predictive framework for flavor is a major theoretical gap.

These unresolved issues collectively form the "flavor puzzle," highlighting the need for a deeper theoretical framework beyond the SM [181].

11.3 FLAVOR SYMMETRIES AND MODEL BUILDING

Flavor symmetries are a cornerstone of BSM physics, providing a theoretical framework to explain the observed patterns in fermion masses and mixing angles [182, 183]. By imposing symmetry constraints on the Lagrangian, model builders can reduce the number of free parameters and predict specific structures in the fermion mass matrices. This section explores the role of discrete and continuous flavor symmetries in generating fermion masses and mixing patterns, highlighting their potential to address the flavor puzzle.

11.3.1 Discrete Flavor Symmetries

Discrete flavor symmetries are finite groups that act on the flavor space of quarks and leptons. They are particularly attractive because they can naturally explain the observed hierarchies and mixing patterns without introducing excessive complexity [184, 185]. As a widely studied example, we consider the A_4 **symmetry**, which is a discrete symmetry group with 12 elements. It is the group of even permutations of four objects and is isomorphic to the symmetry group of a regular tetrahedron. It has four irreducible representations:

- Three singlets: $\mathbf{1}$, $\mathbf{1}'$, and $\mathbf{1}''$.
- One triplet: $\mathbf{3}$.

The multiplication rules for these representations are as follows:

- $\mathbf{1}' \otimes \mathbf{1}' = \mathbf{1}''$
- $\mathbf{1}' \otimes \mathbf{1}'' = \mathbf{1}$

- $\mathbf{1}'' \otimes \mathbf{1}'' = \mathbf{1}'$
- $\mathbf{3} \otimes \mathbf{3} = \mathbf{1} \oplus \mathbf{1}' \oplus \mathbf{1}'' \oplus \mathbf{3}_1 \oplus \mathbf{3}_2$

These rules are essential for constructing invariant terms in the Lagrangian. In A_4 models, the three generations of leptons are typically assigned to the triplet representation $\mathbf{3}$, while the Higgs fields and right-handed neutrinos are assigned to either singlet or triplet representations [186].

We consider the following representations of fields under the discrete flavor symmetry group A_4:

- Left-handed lepton doublets: $L = (L_1, L_2, L_3) \sim \mathbf{3}$
- Right-handed neutrinos: $\nu_R = (\nu_{R1}, \nu_{R2}, \nu_{R3}) \sim \mathbf{3}$
- Standard Model Higgs: $H \sim \mathbf{1}$
- Flavons: $\phi, \chi \sim \mathbf{3}$, $\xi \sim \mathbf{1}$

Therefore, the Lagrangian for the lepton sector includes Yukawa terms and mass terms that are invariant under A_4. These terms are constructed as follows:

Charged Lepton Sector:

The Yukawa terms for charged leptons are constructed using the Higgs field H and the flavon field ϕ, as follows:

$$\mathscr{L}_Y = \frac{y_e}{\Lambda} \bar{L}\phi H e_R + \frac{y_\mu}{\Lambda} \bar{L}\phi H \mu_R + \frac{y_\tau}{\Lambda} \bar{L}\phi H \tau_R + \text{h.c.} \tag{11.1}$$

Here, Λ represents the non-renormalizable suppression scale, and the Yukawa interactions involve both the Higgs field H (for $SU(2)_L$ invariance) and the flavon field ϕ (for A_4 invariance). When the flavon field ϕ and Higgs field H acquire vacuum expectation values, the A_4 and $SU(2)_L$ symmetries are spontaneously broken, generating the charged lepton mass matrix.

After electroweak and flavor symmetry breaking:

$$
\begin{aligned}
\langle H \rangle &= v, \\
\langle \phi \rangle &= (v_\phi, v_\phi, v_\phi), \\
\langle \chi \rangle &= (v_\chi, v_\chi, v_\chi), \\
\langle \xi \rangle &= v_\xi.
\end{aligned}
$$

The charged lepton mass matrix is generated and given by:

$$
M_\ell = \frac{v_\phi v}{\Lambda} \begin{pmatrix} y_e & 0 & 0 \\ 0 & y_\mu & 0 \\ 0 & 0 & y_\tau \end{pmatrix}.
$$

(11.2)

In this context, the A_4 symmetry leads to a diagonal structure for the charged lepton mass matrix M_ℓ. Consequently, the observed hierarchy $m_e \ll m_\mu \ll m_\tau$ can be naturally accommodated by a corresponding hierarchy among the Yukawa couplings y_e, y_μ, y_τ. While the symmetry does not predict the specific values of these couplings, it provides a natural framework where the mass eigenstates coincide with the flavor eigenstates, simplifying the analysis of lepton mixing.

Neutrino Sector:

The neutrino mass terms arise from a combination of Dirac and Majorana terms, constructed to be invariant under A_4 symmetry. The relevant effective Lagrangian is:

$$
\mathscr{L}_\nu = \frac{y_D}{\Lambda} (\bar{L}\phi)_{\mathbf{1}} \tilde{H} \nu_R - \frac{1}{2} \nu_R^T C^{-1} (y_1 \xi + y_2 (\chi)_{\mathbf{3}}) \nu_R + \text{h.c.}
$$

(11.3)

The singlet flavon ξ is not strictly essential, but it is particularly useful. It allows for a simple invariant contraction $(\nu_R \nu_R)_{\mathbf{1}} \xi$ and provides flexibility in generating the structure and scale of the Majorana mass matrix M_R. The presence of both ξ and χ allows for the construction of more realistic models that can reproduce observed neutrino mass hierarchies and mixing angles.

The Dirac mass matrix m_D and Majorana mass matrix M_R are generated as follows:

$$
\begin{aligned}
m_D &= y_D \frac{v v_\phi}{\Lambda} \begin{pmatrix} 1 & 0 & 0 \\ 0 & 1 & 0 \\ 0 & 0 & 1 \end{pmatrix}, \\
M_R &= y_1 v_\xi \begin{pmatrix} 1 & 0 & 0 \\ 0 & 1 & 0 \\ 0 & 0 & 1 \end{pmatrix} + y_2 v_\chi \begin{pmatrix} 0 & 1 & 1 \\ 1 & 0 & 1 \\ 1 & 1 & 0 \end{pmatrix}
\end{aligned}
$$

The light neutrino mass matrix then follows from the type-I seesaw mechanism:

$$
m_\nu = -m_D M_R^{-1} m_D^T
\tag{11.4}
$$

With appropriate flavon VEV alignments, this framework can accommodate the observed neutrino mixing patterns, such as tri-bimaximal mixing pattern for the PMNS matrix, given by:

$$
U_{\text{PMNS}} = \begin{pmatrix} \frac{2}{\sqrt{6}} & \frac{1}{\sqrt{3}} & 0 \\ -\frac{1}{\sqrt{6}} & \frac{1}{\sqrt{3}} & -\frac{1}{\sqrt{2}} \\ -\frac{1}{\sqrt{6}} & \frac{1}{\sqrt{3}} & \frac{1}{\sqrt{2}} \end{pmatrix}.
\tag{11.5}
$$

This pattern predicts the following mixing angles: $\theta_{13} = 0$, $\theta_{23} = \pi/4$, and $\theta_{12} = \arcsin(1/\sqrt{3})$, which are consistent with early neutrino oscillation data but require modifications to account for the non-zero θ_{13} observed in later experiments. This discrepancy has motivated further refinements of A_4 models, such as the inclusion of additional flavons or small symmetry-breaking effects.

11.3.2 Continuous Flavor Symmetries

The simplest example of continuous symmetries is the $U(1)$ flavor symmetry that assigns different charges to the fermion generations. It is widely used in BSM physics to explain the observed hierarchies in fermion masses and mixing angles [187, 188]. The $U(1)$ symmetry is often spontaneously broken by the vacuum expectation value (VEV) of a scalar field (flavon), leading to hierarchical Yukawa couplings through the Froggatt-Nielsen mechanism.

The $U(1)$ flavor symmetry group consists of all complex numbers of unit modulus under multiplication. In the context of flavor physics, the $U(1)$ symmetry acts on the fermion and scalar fields, assigning them specific charges. Each fermion generation f_i (where $i = 1, 2, 3$) and the flavon field ϕ are assigned $U(1)$ charges:

$$f_i \to e^{iq_i\alpha} f_i, \quad \phi \to e^{iq_\phi\alpha}\phi,$$

(11.6)

where q_i and q_ϕ are the $U(1)$ charges of the fermions and flavon, respectively, and α is the transformation parameter.

The Yukawa couplings are constrained by the $U(1)$ symmetry. For example, the Yukawa term for the charged leptons takes the form:

$$\mathscr{L}_Y \sim \bar{L}_i H e_{Rj} \left(\frac{\phi}{\Lambda}\right)^{n_{ij}},$$

(11.7)

where Λ is the cutoff scale of the theory, and n_{ij} are integers determined by the $U(1)$ charge conservation:

$$n_{ij} = q_{L_i} + q_{e_{R_j}} + q_H.$$

(11.8)

The Froggatt-Nielsen mechanism explains the hierarchical structure of fermion masses through the spontaneous breaking of the $U(1)$ flavor symmetry. The flavon field ϕ acquires a VEV, breaking the $U(1)$ symmetry. The VEV is typically much smaller than the cutoff scale Λ:

$$\langle\phi\rangle = \epsilon\Lambda, \quad \epsilon \ll 1.$$

(11.9)

Thus, the Yukawa couplings are suppressed by powers of the small parameter ϵ:

$$y_{ij} \sim \epsilon^{n_{ij}}.$$

(11.10)

This generates a hierarchical structure in the fermion mass matrices. For example, the charged lepton mass matrix takes the form:

$$M_e \sim v_H \begin{pmatrix} \epsilon^{n_{11}} & \epsilon^{n_{12}} & \epsilon^{n_{13}} \\ \epsilon^{n_{21}} & \epsilon^{n_{22}} & \epsilon^{n_{23}} \\ \epsilon^{n_{31}} & \epsilon^{n_{32}} & \epsilon^{n_{33}} \end{pmatrix},$$

(11.11)

where v_H is the VEV of the Higgs field.

One can demonstrate that the $U(1)$ flavor symmetry helps construct the correct fermion masses by generating hierarchical Yukawa couplings. For example, the charged lepton mass matrix is diagonalized by the hierarchy $\epsilon^{n_{11}} \ll \epsilon^{n_{22}} \ll \epsilon^{n_{33}}$, which naturally leads to the observed mass hierarchy $m_e \ll m_\mu \ll m_\tau$.

The quark mass matrices exhibit similar hierarchies, explaining the smallness of the up, charm, and top quark masses relative to each other. For example:

$$M_u \sim v_H \begin{pmatrix} \epsilon^{n_{11}} & \epsilon^{n_{12}} & \epsilon^{n_{13}} \\ \epsilon^{n_{21}} & \epsilon^{n_{22}} & \epsilon^{n_{23}} \\ \epsilon^{n_{31}} & \epsilon^{n_{32}} & \epsilon^{n_{33}} \end{pmatrix}.$$

(11.12)

In the neutrino sector, the $U(1)$ symmetry can be combined with the seesaw mechanism to generate small neutrino masses. The Dirac mass matrix M_D and the Majorana mass matrix M_R take the form:

$$M_D \sim v_H \begin{pmatrix} \epsilon^{n_{11}} & \epsilon^{n_{12}} & \epsilon^{n_{13}} \\ \epsilon^{n_{21}} & \epsilon^{n_{22}} & \epsilon^{n_{23}} \\ \epsilon^{n_{31}} & \epsilon^{n_{32}} & \epsilon^{n_{33}} \end{pmatrix}, \quad M_R \sim \Lambda \begin{pmatrix} \epsilon^{m_{11}} & \epsilon^{m_{12}} & \epsilon^{m_{13}} \\ \epsilon^{m_{21}} & \epsilon^{m_{22}} & \epsilon^{m_{23}} \\ \epsilon^{m_{31}} & \epsilon^{m_{32}} & \epsilon^{m_{33}} \end{pmatrix}.$$

(11.13)

The effective light neutrino mass matrix M_ν is then given by:

$$M_\nu = M_D^T M_R^{-1} M_D.$$

(11.14)

It has been shown that the $U(1)$ flavor symmetry also influences the mixing patterns in both the quark and lepton sectors. For quarks, the

hierarchical structure of the mass matrices leads to small mixing angles in the CKM matrix, consistent with experimental observations. In the lepton sector, the $U(1)$ symmetry can predict specific patterns in the PMNS matrix, depending on the charge assignments and symmetry-breaking mechanism, such as generating the large mixing angles observed in neutrino experiments.

While the $U(1)$ flavor symmetry offers a compelling framework for explaining fermion masses and mixing patterns, it faces several challenges. For instance, the introduction of additional parameters, such as charges and vacuum expectation values (VEVs), reduces the model's predictive power. Additionally, precision measurements of flavor-changing processes place strict constraints on the parameter space of $U(1)$ models. Furthermore, the symmetry must align with other BSM phenomena, such as neutrino masses, dark matter, and baryogenesis. Despite these challenges, the $U(1)$ flavor symmetry remains a valuable tool for understanding the origins of fermion masses and mixing. Future experiments, including those studying rare decays and neutrino oscillations, will play a crucial role in testing $U(1)$ models and advancing our understanding of flavor physics.

11.4 FLAVOR AND CP VIOLATION BEYOND THE SM

BSM theories introduce new particles and interactions that can significantly alter the flavor structure and CP-violating mechanisms of the SM. These extensions aim to address unresolved questions in the SM, such as the origin of fermion mass hierarchies, the smallness of neutrino masses, and the matter-antimatter asymmetry in the universe. In this context, we focus on three key examples: the Two-Higgs-Doublet Model (2HDM), described in detail in Chapter 2; the Left-Right Symmetric Model (LRSM), discussed in Chapters 4 and 5; and the Minimal Supersymmetric Standard Model (MSSM), explored in Chapter 8. These models demonstrate how BSM physics can reshape our understanding of flavor and CP violation, offering testable predictions for current and future experiments.

11.4.1 Flavor and CP Violation in 2HDM

The flavor structure of the 2HDM depends on how the Higgs doublets couple to fermions, leading to different types of 2HDMs (Type I, II, and III) [48]. In particular, Type III models allow for tree-level flavor-changing

neutral currents (FCNCs), which are tightly constrained by experimental data [189]. In the 2HDM, the Yukawa Lagrangian for the quark sector can be written as:

$$\mathscr{L}_Y = -\bar{Q}_L Y_1^u \tilde{\Phi}_1 u_R - \bar{Q}_L Y_2^u \tilde{\Phi}_2 u_R - \bar{Q}_L Y_1^d \Phi_1 d_R - \bar{Q}_L Y_2^d \Phi_2 d_R + \text{h.c.},$$

(11.15)

where Q_L is the left-handed quark doublet, u_R and d_R are the right-handed up- and down-type quark singlets, Φ_1 and Φ_2 are the two Higgs doublets (with $\tilde{\Phi}_i = i\sigma_2 \Phi_i^*$), and Y_1^u, Y_2^u, Y_1^d, and Y_2^d are the Yukawa coupling matrices. In Type I and Type II models, a Z_2 symmetry is imposed to eliminate tree-level FCNCs by coupling each type of fermion to only one Higgs doublet. However, in Type III models, this symmetry is relaxed, allowing both Higgs doublets to couple to all fermions, leading to tree-level FCNCs. The flavor-violating interactions can be parameterized as:

$$\mathscr{L}_{\text{FCNC}} = -\frac{\sqrt{2}}{v} \left(\bar{d}_L X_d d_R \phi + \bar{u}_L X_u u_R \phi + \text{h.c.} \right),$$

(11.16)

where ϕ represents the neutral Higgs bosons (h, H, A), X_d and X_u are the flavor-violating coupling matrices for down-type and up-type quarks, respectively, and $v = \sqrt{v_1^2 + v_2^2} \approx 246\,\text{GeV}$ is the SM Higgs VEV. These couplings lead to flavor-violating processes such as $K^0 - \bar{K}^0$ mixing, $B^0 - \bar{B}^0$ mixing, and rare decays like $B \to X_s \gamma$.

The flavor-violating couplings in the 2HDM are tightly constrained by experimental data. For example, the mass difference Δm_K and the CP-violating parameter ϵ_K in $K^0 - \bar{K}^0$ mixing provide stringent constraints on the off-diagonal elements of X_d [190]. The contribution to Δm_K is given by:

$$\Delta m_K \sim \frac{1}{m_H^2} |(X_d)_{12}|^2,$$

(11.17)

where m_H is the mass of the mediating Higgs boson. Similarly, the mass differences Δm_{B_d} and Δm_{B_s} in $B^0 - \bar{B}^0$ mixing constrain the off-diagonal

elements $(X_d)_{13}$ and $(X_d)_{23}$. The contribution to Δm_{B_d} is:

$$\Delta m_{B_d} \sim \frac{1}{m_H^2} |(X_d)_{13}|^2.$$

(11.18)

Rare decays such as $B \to X_s\gamma$ and $B_s \to \mu^+\mu^-$ provide additional constraints. For instance, the branching ratio of $B \to X_s\gamma$ is sensitive to the charged Higgs contribution:

$$\text{BR}(B \to X_s\gamma) \propto \left| \frac{(X_d)_{23}}{m_{H^\pm}^2} \right|^2,$$

(11.19)

where $m_{H^\pm}$ is the mass of the charged Higgs boson.

In the alignment limit, the light CP-even Higgs boson *h* behaves like the SM Higgs, suppressing FCNCs [191]. This limit is achieved when the mixing angle α between the CP-even Higgs states satisfies $\alpha \approx \beta - \pi/2$. In this limit, the flavor-violating couplings are suppressed, and the model becomes consistent with experimental constraints. The charged Higgs bosons $H^\pm$ can also mediate flavor-changing processes, such as $B \to X_s\gamma$. The contribution to the decay amplitude is proportional to:

$$\mathscr{A}(B \to X_s\gamma) \propto \frac{(X_d)_{23}}{m_{H^\pm}^2}.$$

(11.20)

This imposes constraints on the charged Higgs mass and the flavor-violating couplings. It is worth stressing that experimental constraints on significant flavor violation in 2HDM Type III necessitate either a precise alignment of the Higgs couplings or severe fine-tuning to suppress tree-level FCNCs.

In addition, CP violation can arise in the 2HDM from complex phases in the Higgs potential, Yukawa couplings, or interactions involving the additional Higgs bosons [192]. These new sources of CP violation can have significant implications for flavor physics, electric dipole moments (EDMs), and cosmology.

In Type III 2HDM, where both Higgs doublets couple to all fermions, complex Yukawa couplings can introduce new sources of CP violation.

These phases can contribute to CP-violating observables, such as $B^0 - \bar{B}^0$ mixing and electric dipole moments (EDMs). The contribution to the electron EDM, for example, can be written as:

$$d_e \propto \text{Im}\left(\frac{(Y_e)_{11}}{m_H^2}\right),$$

(11.21)

where $(Y_e)_{11}$ is the Yukawa coupling of the electron to the Higgs bosons, and m_H is the mass of the mediating Higgs boson. Current experimental limits on EDMs place stringent constraints on the CP-violating phases in the 2HDM.

The 2HDM can also contribute to CP violation in meson mixing, such as $K^0 - \bar{K}^0$ and $B^0 - \bar{B}^0$ mixing. The contribution to the CP-violating parameter ϵ_K in $K^0 - \bar{K}^0$ mixing can be written as:

$$\epsilon_K \propto \text{Im}\left(\frac{(X_d)_{12}^2}{m_H^2}\right).$$

(11.22)

The experimental value of the CP-violating parameter is precisely measured, with $|\epsilon_K| \approx 2.228 \times 10^{-3}$. This stringent constraint severely limits the imaginary part of the flavor-changing couplings in the down-quark sector, particularly $\text{Im}[(X_d)_{12}^2]$, thus placing strong bounds on new sources of CP violation within the 2HDM framework. As a result, any viable model must ensure that such contributions remain sufficiently suppressed, either through flavor alignment or by pushing the mass scale m_H to higher values.

11.4.2 Flavor and CP Violation in LRSM

The LRSM introduces new sources of flavor violation through the interactions of the right-handed gauge bosons $W_R^\pm$ and the additional Higgs fields. The right-handed gauge boson $W_R^\pm$ mediates flavor-changing interactions between right-handed quarks, described by the interaction Lagrangian:

$$\mathscr{L}_{W_R} = \frac{g_R}{\sqrt{2}} \bar{u}_R \gamma^\mu V_R d_R W_{R\mu}^+ + \text{h.c.},$$

(11.23)

where g_R is the $SU(2)_R$ gauge coupling, and V_R is the right-handed analog of the CKM matrix [193]. The bidoublet Higgs field Φ can also induce tree-level flavor-changing neutral currents (FCNCs) through its Yukawa couplings. The Yukawa Lagrangian for the quark sector is:

$$\mathscr{L}_Y = \bar{Q}_L (Y_1 \Phi + Y_2 \tilde{\Phi}) Q_R + \text{h.c.},$$

(11.24)

where $\tilde{\Phi} = \sigma_2 \Phi^* \sigma_2$, and Y_1, Y_2 are Yukawa coupling matrices. These couplings can lead to flavor-violating processes such as $K^0 - \bar{K}^0$ mixing and $B^0 - \bar{B}^0$ mixing. The LRSM contributions to FCNCs are tightly constrained by experimental data. For example, the contribution to $K^0 - \bar{K}^0$ mixing is given by:

$$\Delta m_K \propto \frac{(V_R)_{12}^2}{m_{W_R}^2},$$

(11.25)

where $(V_R)_{12}$ is the flavor-violating coupling between the first and second generations of right-handed quarks, and m_{W_R} is the mass of the right-handed gauge boson [194].

The LRSM also introduces new sources of CP violation through complex phases in the right-handed CKM matrix V_R and the Higgs sector. The right-handed CKM matrix V_R can have complex phases that contribute to CP-violating observables. For example, the phase of $(V_R)_{13}$ can affect $B^0 - \bar{B}^0$ mixing. The bidoublet Higgs field Φ can have complex Yukawa couplings, leading to CP-violating interactions. The contribution to the CP-violating parameter ϵ_K in $K^0 - \bar{K}^0$ mixing is given by:

$$\epsilon_K \propto \text{Im} \left(\frac{(Y_1)_{12} (Y_2^*)_{12}}{m_H^2} \right),$$

(11.26)

where m_H is the mass of the mediating Higgs boson. The LRSM can also contribute to electric dipole moments (EDMs) of particles such as the electron, neutron, and atoms through CP-violating interactions involving the right-handed gauge bosons and Higgs fields. The contribution to the electron EDM is given by:

$$d_e \propto \text{Im}\left(\frac{(Y_e)_{11}}{m_{W_R}^2}\right), \tag{11.27}$$

where $(Y_e)_{11}$ is the Yukawa coupling of the electron to the Higgs fields [190].

11.4.3 Flavor and CP Violation in the MSSM

In the MSSM, the soft SUSY breaking terms, such as sfermion masses and trilinear couplings, can introduce new sources of flavor-changing neutral currents (FCNCs) and CP-violating phases [118]. These terms must be carefully constrained to avoid large contributions to FCNCs and CP-violating observables, which are tightly constrained by precision experimental data.

For example, transitions like $\tilde{d}_L \to \tilde{s}_L$, arising from off-diagonal elements in the down-type squark mass matrix, can contribute to processes such as $K^0 - \bar{K}^0$ mixing [118]. The key observables in the neutral kaon system are the mass difference Δm_K and the CP-violating parameter ϵ_K. It is essential that SUSY contributions to Δm_K and ϵ_K remain smaller than the SM predictions and do not exceed the difference between experimental results and SM predictions. This requirement imposes the following stringent constraint on the off-diagonal elements of the squark mass matrices $(\tilde{m}^2_{Q,D})_{12}$:

$$\left|\frac{(\tilde{m}^2_{Q,D})_{12}}{\tilde{m}^2}\right| \lesssim 10^{-3} \quad \text{for} \quad \tilde{m} \sim 1\,\text{TeV}. \tag{11.28}$$

Moreover, the neutral B-meson system also imposes significant constraints on the SUSY parameter space [118]. The $B^0 - \bar{B}^0$ mixing

observables, Δm_{B_d} and Δm_{B_s}, require that the off-diagonal elements in the squark mass matrices $(\tilde{m}^2_{Q,D})_{13}$ and $(\tilde{m}^2_{Q,D})_{23}$ satisfy:

$$\left| \frac{(\tilde{m}^2_{Q,D})_{13}}{\tilde{m}^2} \right|, \left| \frac{(\tilde{m}^2_{Q,D})_{23}}{\tilde{m}^2} \right| \lesssim 10^{-2} \quad \text{for} \quad \tilde{m} \sim 1\,\text{TeV}.$$

(11.29)

In addition, rare decays such as $B \to X_s \gamma$ and $B_s \to \mu^+ \mu^-$, with their SM predictions, impose stringent constraints on SUSY parameters. Specifically, the trilinear coupling A_t and the charged Higgs mass $m_{H^\pm}$ must satisfy:

$$|A_t| \lesssim 2\,\text{TeV}, \quad m_{H^\pm} \gtrsim 500\,\text{GeV}.$$

(11.30)

On the other hand, the CP-violating parameter ϵ_K and $\sin 2\beta$ (B-meson system), with their SM predictions, imply that the off-diagonal elements in the squark mass matrices and the CP-violating phases in SUSY must satisfy:

$$\left| \frac{(\tilde{m}^2_{Q,D})_{12}}{\tilde{m}^2} \right| \lesssim 10^{-3}, \quad \phi_{\text{SUSY}} \lesssim 10^{-2}.$$

(11.31)

The Electric Dipole Moments (EDMs) of the electron (d_e), neutron (d_n), and atoms (e.g., d_{Hg}) impose stringent constraints on SUSY CP-violating phases. Their current experimental limits are:

$$|d_e| \quad < 1.1 \times 10^{-29}\, e \cdot \text{cm},$$

(11.32)

$$|d_n| \quad < 1.8 \times 10^{-26}\, e \cdot \text{cm},$$

(11.33)

$$|d_{\text{Hg}}| \quad < 6.3 \times 10^{-30}\, e \cdot \text{cm}.$$

(11.34)

The CP-violating phases in the SUSY soft terms (e.g., ϕ_μ, ϕ_{A_t}) must satisfy:

$$\phi_\mu, \phi_{A_t} \lesssim 10^{-2} \quad \text{for} \quad \tilde{m} \sim 1\,\text{TeV}.$$

(11.35)

These constraints highlight the stringent limits on SUSY parameter space imposed by flavor and CP-violating observables. Future experiments will further test these constraints and guide the development of SUSY models.

11.5 SCALAR LEPTOQUARK FLAVOR VIOLATION IN *SU*(5)

As advocated above, the scalar triplets contained in the $\mathbf{45}_H$ Higgs representation decompose under the Standard Model gauge group as:

$$(3^*,2)^{ij}_{-7/6} \quad \equiv (\mathbf{45}_H)^{ij}_{c} \equiv \Phi^{ij}_{c},$$

(11.36)

$$(3^*,1)^{ab}_{4/3} \quad \equiv (\mathbf{45}_H)^{ab}_{k} \equiv \Phi^{ab}_{k},$$

(11.37)

$$[(3,1)\oplus(3,3)]^{ib}_{-1/3} \quad \equiv (\mathbf{45}_H)^{ib}_{c} \equiv \Phi^{ib}_{c}.$$

(11.38)

As emphasized in [195], while Φ^{ab}_k and Φ^{ib}_c mediate proton decay and must therefore be superheavy, the scalar triplet Φ^{ij}_c does not couple to baryon number violating operators and hence does not contribute to proton decay. Writing Φ^{ij}_c as a weak doublet $\Phi^{ij}_c = (\phi^i_1, \phi^i_2)^T$, its relevant interactions with matter fields are:

$$\begin{aligned}\mathscr{L} \;&= 2Y^2_{AB}\, e^T_A C u^c_{Bi}\, \phi^{i1*} + 4(Y^4_{AB} - Y^4_{BA})\, u^{iT}_A C e^c_B\, \phi_{i1} \\ &\quad -2Y^2_{AB}\, \nu^T_A C u^c_{Bi}\, \phi^{i2*} + 4(Y^4_{AB} - Y^4_{BA})\, d^{iT}_A C e^c_B\, \phi_{i2}.\end{aligned}$$

(11.39)

The first two terms induce $b \to s\ell^+\ell^-$ transitions via ϕ^{i1} exchange, while the last two account for $b \to c\tau\nu$ through ϕ^{i2} [196]. These interactions can be rewritten using Dirac notation and antisymmetric coupling definitions:

$$\mathscr{L} = 2Y^{2}_{AB}\,\bar{u}_{Bi}P_L\nu_A\,\phi^{i2*} - 4Y^{4'}_{AB}\,\bar{e}_B P_L d^i_A\,\phi_{i2} + \text{h.c.},$$

(11.40)

where $Y^{4'}_{AB} \equiv Y^{4}_{AB} - Y^{4}_{BA}$ and we used the identities $C^T = -C$ and $\bar{\Psi} = \Psi^{cT}_L$. In the mass eigenstate basis:

$$d_A \to V^{\text{CKM}}_{AK} d'_K, \quad \nu_A \to V^{\text{PMNS}}_{AK}\nu'_K, \quad u_A \to u'_A, \quad e_A \to e'_A,$$

the Lagrangian becomes:

$$\mathscr{L} \quad = 2Y^{2}_{AB}\,\bar{u}'_{Bi}P_L V^{\text{PMNS}}_{AK}\nu'_K\,\phi^{i2*} - 4Y^{4'}_{AB}\,\bar{e}'_B P_L V^{\text{CKM}}_{AK} d'_K\,\phi_{i2} + \text{h.c.}$$

(11.41)

Consequently, the amplitude for the process $b \to c\tau\nu$ is given by[196]:

$$\begin{aligned}\mathscr{M} = \quad & -\frac{8Y^{4'}_{13}V^{\text{CKM}}_{13}}{M^2_\phi}\left[\frac{1}{2}\left(\bar{u}_\tau P_L v_{\nu_\tau}\right)\left(\bar{u}_c P_L u_b\right) + \frac{1}{8}\left(\bar{u}_\tau \sigma^{\mu\nu} P_L v_{\nu_\tau}\right)\right. \\ & \left.\times\left(\bar{u}_c P_L \sigma_{\mu\nu} u_b\right)\left(Y^2_{12}V^{\text{PMNS}}_{13} + Y^2_{22}V^{\text{PMNS}}_{23} + Y^2_{32}V^{\text{PMNS}}_{33}\right)\right] \\ & + \left(Y^{4'}_{13}V^{\text{CKM}}_{13} \to Y^{4'}_{23}V^{\text{CKM}}_{23}\right).\end{aligned}$$

(11.42)

Since $V^{\text{CKM}}_{13} \sim 10^{-3}$ and $V^{\text{CKM}}_{23} \sim 10^{-2}$, the amplitude is predominantly controlled by the leptoquark mass M_ϕ, the couplings Y^2_{22}, Y^2_{32}, and $Y^{4'}_{13}$. The general expression of the effective Hamiltonian for the transition $b \to c\ell\bar{\nu}_\ell$ reads [197]:

$$\begin{aligned}\mathscr{H}_{\text{eff}} = \quad & \frac{4G_F V_{cb}}{\sqrt{2}}\Big[(1+g_{V_L})[\bar{c}\gamma_\mu P_L b][\bar{\ell}\gamma^\mu P_L \nu_\ell] + g_{V_R}[\bar{c}\gamma_\mu P_R b][\bar{\ell}\gamma^\mu P_L\nu_\ell] \\ & + g_{S_L}[\bar{c}P_L b][\bar{\ell}P_L\nu_\ell] + g_{S_R}[\bar{c}P_R b][\bar{\ell}P_L\nu_\ell] + g_T[\bar{c}\sigma^{\mu\nu}P_L b][\bar{\ell}\sigma_{\mu\nu}P_L\nu_\ell]\Big],\end{aligned}$$

(11.43)

where $P_{L,R} = (1 \mp \gamma_5)/2$ and $g_i = C_i^{\text{NP}}/C^{\text{SM}}$ with $C^{\text{SM}} = \frac{4G_F V_{cb}}{\sqrt{2}}$.

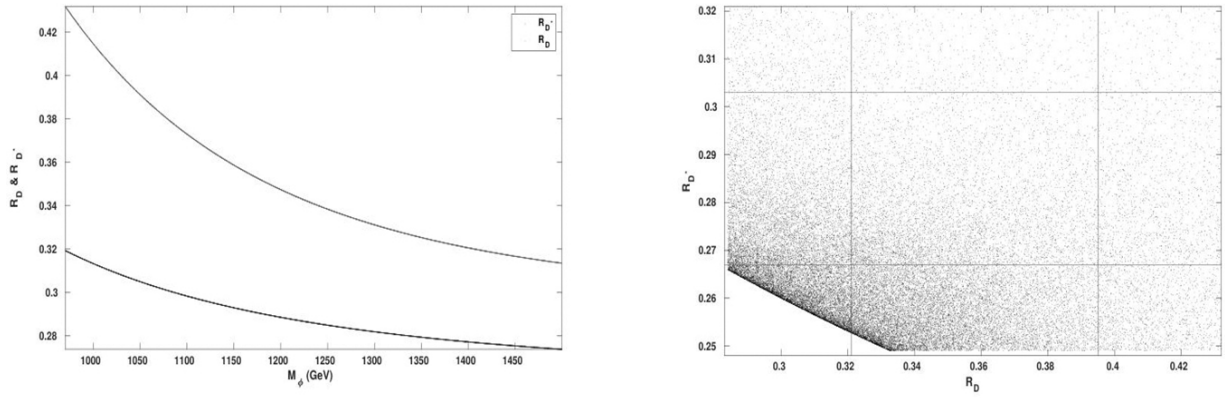

Figure 11.1 R_D and R_{D^*} as function of the Leptoquark mass and The correlation between R_D and R_{D^*}.

In our model, $g_{V_L} = g_{V_R} = g_{S_R} = 0$, while:

$$g_{S_L} = -\frac{\sqrt{2}Z}{M_\phi^2 G_F}, \qquad g_T = \frac{g_{S_L}}{4} = -\frac{Z}{2\sqrt{2}M_\phi^2 G_F},$$

(11.44)

with

$$Z = \left(Y_{12}^2 V_{13}^{\text{PMNS}} + Y_{22}^2 V_{23}^{\text{PMNS}} + Y_{32}^2 V_{33}^{\text{PMNS}}\right)\left(\frac{Y_{13}^{4'} V_{13}^{\text{CKM}}}{V_{23}^{\text{CKM}}} + Y_{23}^{4'}\right).$$

(11.45)

Using SM inputs and central form factor values [198], the observables $R(D)$ and $R(D^*)$ are given by:

$$R(D) \quad = R(D)^{\text{SM}}\left[1 + 1.02|g_{S_L}|^2 + 0.9|g_T|^2 + 1.49\,\text{Re}(g_{S_L}^*) + 1.14\,\text{Re}(g_T^*)\right].$$

(11.46)

$$R(D^*) \quad = R(D^*)^{\text{SM}}\left[1 + 0.04|g_{S_L}|^2 + 16.07|g_T|^2 - 0.11\,\text{Re}(g_{S_L}^*) - 5.12\,\text{Re}(g_T^*)\right].$$

(11.47)

A numerical scan shows that for TeV-scale leptoquarks, the model can accommodate the current values of $R(D)$ and $R(D^*)$ [196], while

respecting bounds from B_c decays and polarization observables (see Fig. 11.1).

CHAPTER 12

BSM Cosmological Implications

DOI: 10.1201/9781003457701-12

12.1 INTRODUCTION

We now turn our attention to the cosmological implications of BSM physics. As emphasized throughout this work, the SM of particle physics has been extraordinarily successful in describing the fundamental particles and forces that make up the universe. However, we have also highlighted its limitations, gaps that strongly suggest the existence of new physics beyond the SM. These limitations are not just theoretical curiosities; they are intimately tied to some of the most profound questions in cosmology, including the nature of dark matter, the origin of dark energy, the generation of neutrino masses, and the baryon asymmetry of the universe. In this chapter, we will explore how BSM physics addresses these questions and enriches our understanding of the universe [199].

As emphasized earlier, one of the most compelling examples of the SM's limitations is dark matter, which makes up approximately 27% of the universe's energy density. Astronomical observations, such as galaxy rotation curves, gravitational lensing, and the cosmic microwave background (CMB), provide robust evidence for the existence of dark matter. However, the SM lacks a viable candidate particle to account for it. Neutrinos, the only weakly interacting particles in the SM, are far too light to explain the observed dark matter density [200]. This significant gap has driven the search for BSM candidates.

Another profound puzzle is dark energy, the mysterious force responsible for the accelerated expansion of the universe. Observations of distant supernovae [201, 202] and the large-scale structure of the cosmos have firmly established the presence of dark energy, which constitutes approximately 68% of the universe's total energy content. Despite its dominance, the SM offers no explanation for dark energy. While the cosmological constant in Einstein's equations could, in principle, account for it, the predicted value is orders of magnitude larger than what is observed, a glaring inconsistency known as the “cosmological constant problem” [203, 204]. To address this enigma, BSM theories propose alternative explanations, such as dynamic scalar fields (quintessence) [205], modifications to general relativity [206], or contributions from extra dimensions [139].

The baryon asymmetry of the universe, the observed dominance of matter over antimatter, is another profound mystery that the SM cannot resolve. While the SM includes processes that violate baryon number, such as sphaleron transitions, these mechanisms are insufficient to generate the observed asymmetry [207]. Furthermore, the SM fails to satisfy all three Sakharov conditions: baryon number violation, C and CP violation, and departure from thermal equilibrium, required to explain the matter-antimatter imbalance [40]. To address this puzzle, BSM theories propose compelling mechanisms, such as leptogenesis [208, 209] and electroweak baryogenesis [210]. These frameworks introduce new sources of CP violation, additional particles, or cosmological phase transitions, providing viable explanations for the origin of the baryon asymmetry and its role in the evolution of the universe. In this context, cosmology plays a pivotal role in testing and constraining BSM theories.

12.2 DARK MATTER AND BSM PHYSICS

Despite profound implications of dark matter (DM) for cosmology and fundamental physics, the nature of DM remains one of the most significant unsolved mysteries in modern science. Although its existence was first suggested over seven decades ago, we still lack a definitive understanding of its composition or interactions beyond gravitational effects. The first strong evidence for DM emerged in 1933 when Swiss astrophysicist Fritz Zwicky studied the Coma galaxy cluster. He observed that the visible, luminous matter in the cluster accounted for only a fraction of the total

mass required to explain the gravitational motions of its member galaxies. This discrepancy suggested the presence of an unseen mass component, which he referred to as DM [211]. However, for decades, this idea remained largely speculative. It was not until the 1970s, through the work of Vera Rubin and others on the anomalous rotation curves of spiral galaxies, that dark matter began to be seriously considered as a necessary component of the Universe. The observed rotational speeds of galaxies could not be explained by visible matter alone, reinforcing the hypothesis that a dominant, yet invisible, form of matter must be present to account for these observations [212].

The concept of inferring unseen masses based on gravitational effects is not new. A historical analogy can be drawn from the discovery of Neptune in 1846, which was guided by irregularities in Uranus' orbit. These deviations could not be explained by known celestial bodies, leading astronomers to predict the existence of an unknown planet, later confirmed through direct observation. Similarly, the unexplained gravitational effects in galaxies and clusters suggest the presence of DM, even though it has yet to be directly detected.

While the dark matter hypothesis is widely accepted, a small number of researchers argue that it may not be necessary to explain observed galactic rotation curves. Instead, they propose modifications to Newtonian dynamics at galactic scales, suggesting that deviations from expected motion could result from an incomplete understanding of gravity rather than the presence of an unseen mass component. The most well-known alternative in this regard is Modified Newtonian Dynamics (MOND), which introduces adjustments to Newton's laws at extremely low accelerations to account for the observed rotational speeds of galaxies without invoking DM [213]. However, these approaches are generally considered ad hoc and lack a strong theoretical foundation within a broader physical framework. Moreover, while such modifications may offer an explanation for galaxy rotation curves, they fail to account for the full range of astrophysical and cosmological evidence supporting DM, including gravitational lensing effects, cosmic microwave background anisotropies [31], and large-scale structure formation [214]. The necessity of dark matter extends far beyond individual galaxies, as its presence is also inferred from observations of galaxy clusters and the evolution of the Universe on cosmological scales, reinforcing the view that a fundamental, non-luminous component must exist [215].

12.2.1 What is DM made of?

The nature of DM remains one of the most compelling mysteries in modern physics. Observations from CMB radiation, galaxy rotation curves, and large-scale structure formation strongly suggest the existence of dark matter, which interacts primarily through gravity and possibly weakly via other forces [211, 212]. However, its exact composition is unknown. Constraints from Big Bang nucleosynthesis indicate that DM cannot be baryonic, as the abundance of baryonic matter in the universe is insufficient to account for the observed gravitational effects [216]. A viable DM candidate must satisfy several essential properties:

- It must be stable on cosmological timescales, suggesting either absolute stability or a lifetime much longer than the age of the universe.
- It is non-baryonic, as the observed baryonic matter is insufficient to explain the total gravitational effects attributed to DM.
- It interacts very weakly with SM particles, at least through non-electromagnetic forces, to remain undetected in direct searches.
- It is cold and non-relativistic at the time of structure formation, as required by large-scale structure observations.
- It does not emit, absorb, or reflect light and does not participate in strong interactions.
- It must produce a relic density consistent with cosmological observations ($\Omega_{\mathrm{DM}} \approx 0.27$) [31].

The SM of particle physics does not provide a suitable DM candidate, as all known particles either interact too strongly or fail to match the required relic density [217]. Extensions beyond the SM propose new particles, which may fulfill the above criteria. DM is broadly classified based on its velocity dispersion and interaction properties in the early Universe. The main types of dark matter include:

- Cold Dark Matter (CDM), which consists of particles that were non-relativistic (moving at sub-relativistic speeds) at the time of their decoupling from the thermal bath. These particles clump under gravitational attraction, leading to the formation of large-scale

structures in the Universe. Weakly Interacting Massive Particles (WIMPs) [218] and axions [219] are prominent CDM candidates.

- Warm Dark Matter (WDM), which had a relativistic speed at early times but became non-relativistic later. Their intermediate velocity suppresses small-scale structure formation compared to CDM, making them a possible solution to certain discrepancies in standard structure formation models [220]. Sterile neutrinos are a leading candidate for WDM [221].
- Hot Dark Matter (HDM), which consists of particles that remained relativistic for a significant period after their decoupling. Due to their high velocities, HDM particles do not easily cluster, suppressing the formation of small-scale structures. A classic example is the standard neutrino [222].

Each of these DM types has distinct implications for cosmology and structure formation. Observational evidence, such as measurements from the CMB, galaxy distributions, and large-scale structure evolution, strongly favors a cold dark matter-dominated Universe, as predicted by the ΛCDM model [31]. WIMPs are among the most compelling candidates for CDM in the Universe. These hypothetical particles are expected to interact only through the weak nuclear force and gravity, making their direct detection extremely challenging [218].

In the early Universe, WIMPs were in thermal equilibrium with SM particles. Frequent interactions kept their number density comparable to that of photons. As the Universe expanded and cooled, the interaction rate between WIMPs and SM particles diminished. When the temperature dropped below the WIMP mass ($T \ll M_{\mathrm{WIMP}}$), annihilation processes became inefficient at maintaining thermal equilibrium, resulting in the decoupling of WIMPs from the thermal plasma. This freeze-out process left behind a relic abundance of WIMPs, which persists today as a substantial component of the dark matter [215]. The decoupling of WIMPs is a key aspect of their cosmological evolution. At high temperatures ($T \gg M_{\mathrm{WIMP}}$), WIMPs and SM particles maintained equilibrium through frequent interactions. As the Universe cooled, the WIMP number density underwent an exponential suppression, with their abundance freezing out at a characteristic value. Today, these relic WIMPs form a dominant, non-relativistic component of dark matter, with their number density significantly lower than that of photons [217].

This thermal production mechanism, often referred to as the "WIMP miracle," naturally leads to a relic abundance that aligns with observations from CMB measurements and large-scale structure formation [31]. Despite their strong theoretical motivation, WIMPs have yet to be detected experimentally, making their search a major goal of ongoing direct and indirect detection experiments, as well as collider studies [223].

12.2.2 Experimental Evidence for Dark Matter

Multiple lines of astronomical and cosmological observations provide compelling evidence for the existence of DM:

1. Galaxy Cluster Rotation Curves:

   Early signs of dark matter were suggested by mass discrepancies in galaxy clusters, but strong empirical support came in the 1970s through observations of spiral galaxy rotation curves [212]. These studies showed that stars and gas in the outer regions of galaxies orbit at nearly constant velocities, inconsistent with the distribution of visible matter.

   According to Newtonian dynamics, the rotational velocity $v(r)$ at a radius r should satisfy:

$$M(r) = \frac{Gv(r)^2}{r}, \tag{12.1}$$

   where $M(r)$ is the mass enclosed within radius r, and G is Newton's gravitational constant. If only luminous matter contributed, $v(r)$ would decrease with increasing r. Instead, observations show that $v(r)$ remains flat at large radii, as shown in Fig. 12.1, indicating the presence of additional unseen mass.

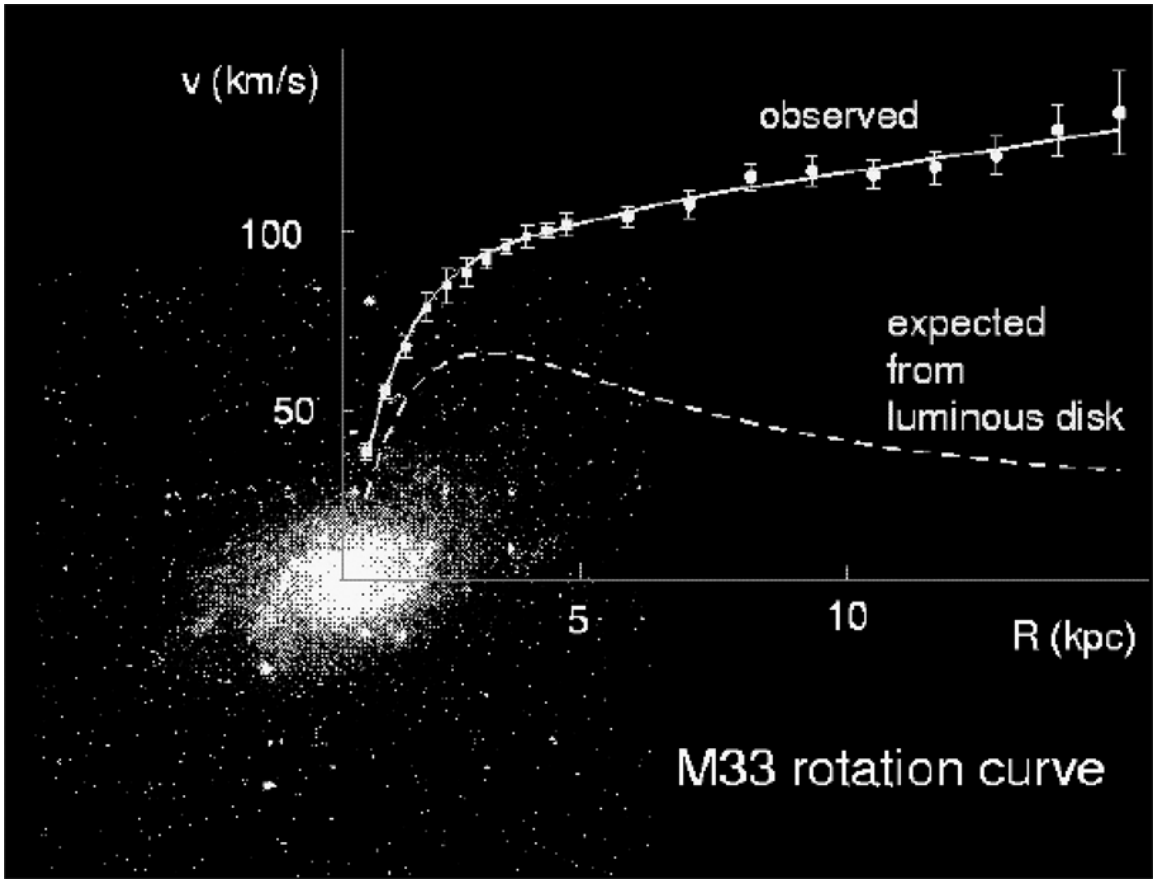

Figure 12.1 Rotation curve of the dwarf spiral galaxy M33 overlaid on its optical image [28]. ⏎

This phenomenon has been observed in hundreds of spiral galaxies, supporting the idea that they are embedded in extended dark matter halos. These halos dominate the mass distribution at large distances and provide the gravitational influence needed to sustain the flat rotation curves, reinforcing the dark matter hypothesis.

2. Gravitational Lensing:

   When light from distant galaxies passes through a massive foreground object like a galaxy cluster, its path is bent by gravity, a phenomenon known as gravitational lensing. This effect distorts the images of background galaxies, allowing astronomers to map the mass distribution of the lensing object. In many cases, the mass inferred from lensing far exceeds that of visible matter, providing strong evidence for the presence of DM [224].

3. The Bullet Cluster:

The Bullet Cluster (1E0657-558) [30] offers one of the most compelling pieces of evidence for the existence of dark matter. X-ray observations from the Chandra satellite reveal a shock front in the hot gas resulting from the collision of two galaxy clusters. Meanwhile, weak gravitational lensing maps derived from Hubble Space Telescope data show that most of the mass is located in regions offset from the luminous matter. This spatial separation between the baryonic matter and the gravitational potential strongly indicates the presence of non-luminous, collisionless dark matter halos. The Bullet Cluster thus serves as a striking, direct observational demonstration of DM's gravitational influence (see Fig. 12.2).

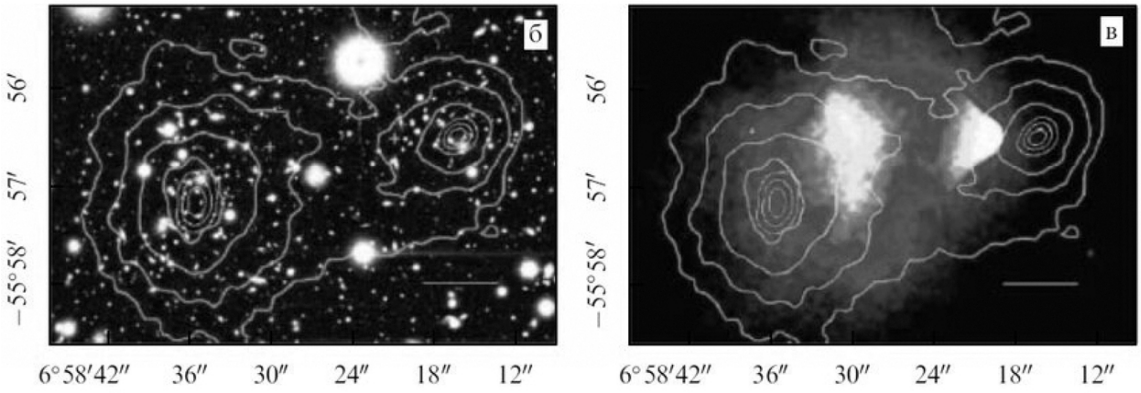

Figure 12.2 Optical (left) and X-ray (right) images of the Bullet Cluster with gravitational lensing contours, showing that most of the mass is offset from the luminous matter [30]. ⏎

4. Cosmic Microwave Background

While various observations provide compelling evidence for dark matter (DM), they do not directly determine its total abundance or composition. In contrast, the analysis of the Cosmic Microwave Background (CMB) offers crucial insights into these fundamental properties. The CMB, a relic radiation from the early universe, was discovered in 1965 by Arno Penzias and Robert Wilson. Since then, experiments such as WMAP and Planck have mapped its anisotropies with remarkable precision, providing a wealth of cosmological data. In the 2018 data release, the Planck collaboration reported the following values for the total matter and baryonic matter density parameters [31]:

$$\Omega_{\mathrm{m}}h^2 = 0.1430 \pm 0.0011, \quad \Omega_{\mathrm{b}}h^2 = 0.02237 \pm 0.00015.$$

(12.2)

The significant gap between the total matter density Ω_m and the baryonic matter density Ω_b indicates that most of the matter in the universe is non-baryonic, that is, DM. These results are also consistent with predictions from Big Bang nucleosynthesis (BBN), lending additional support to the inferred value of Ω_b [32].

CMB observations have significantly advanced our understanding of DM's role in cosmic evolution. The precise measurements of temperature fluctuations reveal the composition of the universe as follows (see Fig. 12.3):

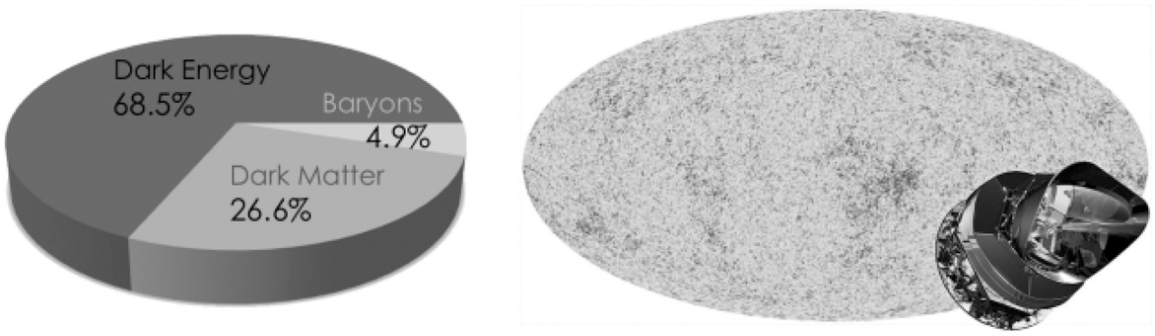

Figure 12.3 Left: Energy density distribution among different components of the universe. Right: Temperature fluctuations in the CMB as observed by the Planck satellite. ⏎

- 4.9%: Ordinary (baryonic) matter, atoms that make up stars, planets, and visible structures.
- 26.6%: Dark matter, non-luminous matter detectable only through its gravitational effects.
- 68.5%: Dark energy, responsible for the accelerated expansion of the universe.

These results provide one of the most robust confirmations of dark matter's existence, underscoring its essential role in the formation and structure of the universe.

12.2.3 DM Relic Abundance

In this framework, we assume that χ, a DM candidate, was initially in thermal equilibrium with SM particles in the early universe and decoupled when it became non-relativistic. The annihilation rate of χ, given by $\Gamma_\chi = \langle \sigma_\chi^{\text{ann}} v \rangle n_\chi$, eventually became smaller than the expansion rate of the universe ($\Gamma_\chi \leq H$), at which point χ ceased to annihilate and fell out of equilibrium [199]. The relic density of χ was then frozen and has remained constant ever since [225]. Here, $\langle \sigma_\chi^{\text{ann}} v \rangle$ represents the thermally averaged cross-section for annihilation.

The relic density is determined by solving the Boltzmann equation for the number density n_χ, coupled with the law of entropy conservation [225]:

$$\frac{dn_\chi}{dt} = -3Hn_\chi - \langle \sigma_\chi^{\text{ann}} v \rangle \left[n_\chi^2 - (n_\chi^{\text{eq}})^2 \right], \tag{12.3}$$

$$\frac{ds}{dt} = -3Hs, \tag{12.4}$$

where n_χ^{eq} is the equilibrium number density, which depends on the temperature T, and is given by:

$$n_\chi^{\text{eq}} = g_\chi \left(\frac{m_\chi T}{2\pi} \right)^{3/2} e^{-m_\chi/T}. \tag{12.5}$$

The Hubble parameter H is related to the temperature T as [215]:

$$H(T) = 2\pi \sqrt{\frac{\pi g_*}{45}} \frac{T^2}{M_{Pl}}, \tag{12.6}$$

where M_{Pl} is the Planck mass, and g_* is the number of relativistic degrees of freedom at the time. For the MSSM, $g_* \simeq 228.75$.

To simplify the Boltzmann equation, it is convenient to introduce the dimensionless variable $x = m_\chi / T$ and the comoving number density $Y = n_\chi / s$, where s is the entropy density. The equation then becomes:

$$\frac{dY}{dx} = \frac{1}{3H}\frac{ds}{dx}\langle\sigma^{\rm ann}_{\chi} v\rangle \left(Y^2 - Y^2_{\rm eq}\right).$$

(12.7)

During the radiation-dominated era, the entropy density is approximately:

$$s(x) = \frac{2\pi^2}{45}\, g_{*_s}(x)\, m_{\chi}^3\, x^{-3},$$

(12.8)

with its derivative given by:

$$\frac{ds}{dx} = -\frac{3s}{x}.$$

(12.9)

Assuming $g_* \simeq g_{*_s}$, the Boltzmann equation simplifies to:

$$\frac{dY}{dx} = -\sqrt{\frac{\pi g_*}{45}}\, M_{Pl}\, m_{\chi}\, \frac{\langle\sigma^{\rm ann}_{\chi} v\rangle}{x^2}\left(Y^2 - Y^2_{\rm eq}\right).$$

(12.10)

If the DM candidate annihilates predominantly via s-wave and p-wave processes, the thermally averaged cross-section can be approximated as [226]:

$$\langle\sigma^{\rm ann}_{\chi} v\rangle \simeq a_{\chi} + \frac{6 b_{\chi}}{x},$$

(12.11)

where a_{χ} and b_{χ} correspond to the s-wave and p-wave contributions, respectively. The present-day relic abundance of DM is given by:

$$\Omega h^2 = \frac{m_{\chi} s_0 Y_{\chi}(\infty)}{\rho_c/h^2},$$

(12.12)

where $Y_{\chi}(\infty)$ is the asymptotic value of the comoving number density, s_0 is the current entropy density, and ρ_c is the critical density of the universe. Solving the Boltzmann equation yields:

$$Y_\chi(\infty) = \frac{1}{\lambda_\chi}\left(\frac{a_\chi}{x_f} + \frac{3b_\chi}{x_f^2}\right)^{-1},$$

(12.13)

where $x_f = m_\chi/T_f$ is the freeze-out parameter and $\lambda_\chi = s(m_\chi)/H(m_\chi)$. The value of x_f is obtained from the transcendental equation:

$$x_f = \ln\left[\frac{\alpha_\chi \lambda_\chi c(c+2)}{\sqrt{x_f}}\left(a_\chi + \frac{6b_\chi}{x_f}\right)\right],$$

(12.14)

with $\alpha_\chi = \frac{45}{2\pi^4}\sqrt{\frac{\pi}{8}}\frac{g_\chi}{g_{*s}(T_f)}$, and $c \approx 0.5$ is a fitting parameter that yields sufficient accuracy for most cosmological applications.

12.2.4 Lightest Neutralino as DM in SUSY Theories

The lightest neutralino (χ) in supersymmetric (SUSY) theories is among the most compelling dark matter (DM) candidates. In the Minimal Supersymmetric Standard Model (MSSM), it naturally arises as a linear combination of the bino ($\tilde{B}$), wino ($\tilde{W}^0$), and the neutral higgsinos ($\tilde{H}_1^0, \tilde{H}_2^0$) [33]. The mass eigenstate is given by:

$$\chi = N_{11}\tilde{B} + N_{12}\tilde{W}^0 + N_{13}\tilde{H}_1^0 + N_{14}\tilde{H}_2^0,$$

(12.15)

where N_{ij} are elements of the neutralino mixing matrix. The specific composition of the lightest neutralino determines its couplings and annihilation mechanisms.

Depending on its nature, the neutralino can annihilate into various final states such as fermion-antifermion pairs ($f\bar{f}$), W^+W^-, ZZ, Zh, ZH, ZA, H^+H^-, and others involving Higgs bosons. For a bino-like LSP (i.e., $N_{11} \simeq 1$, $N_{1i} \simeq 0$ for $i = 2, 3, 4$), the dominant annihilation channels are into fermion-antifermion pairs, as shown in Fig. 12.4, while all other channels are suppressed.

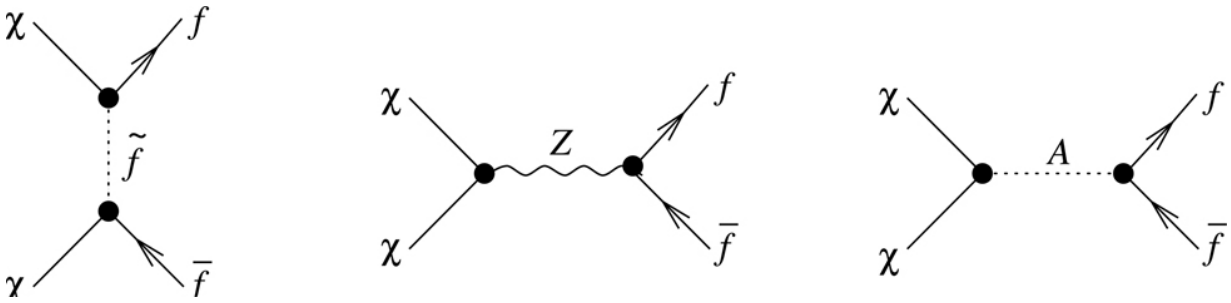

Figure 12.4 Feynman diagrams contributing to early-universe neutralino χ annihilation into fermions through sfermions, Z-gauge boson, and Higgs.

In this scenario, annihilation via Z-boson exchange is typically negligible due to the small $Z\chi\chi$ coupling, which is proportional to $N_{13}^2 - N_{14}^2$, unless the process occurs near the Z-resonance ($m_\chi \approx m_Z/2$). However, such a mass range is excluded by current experimental bounds.

The dominant annihilation proceeds through t-channel exchange of sleptons, particularly into lepton pairs via $\tilde{l}_L, \tilde{l}_R$ (with $l = e, \mu, \tau$), as shown in the first diagram of Fig. 12.4. Annihilation via squark exchange is generally suppressed due to their heavier masses.

In Fig. 12.5, we illustrate the constraints from the observed relic abundance Ωh^2 in the $(m_0, m_{1/2})$ plane for two values of the trilinear coupling, $A_0 = 0$ and $2000\,\text{GeV}$, and for $\tan\beta = 10$ and 50, with $\mu > 0$ [227]. The relic abundance of the lightest neutralino was computed using the micrOMEGAs package [62], which includes all relevant annihilation and coannihilation channels. In particular, coannihilation with the next-to-lightest supersymmetric particle (NLSP), typically the lightest stau, $\tilde{\tau}_1$, is fully accounted for [228].

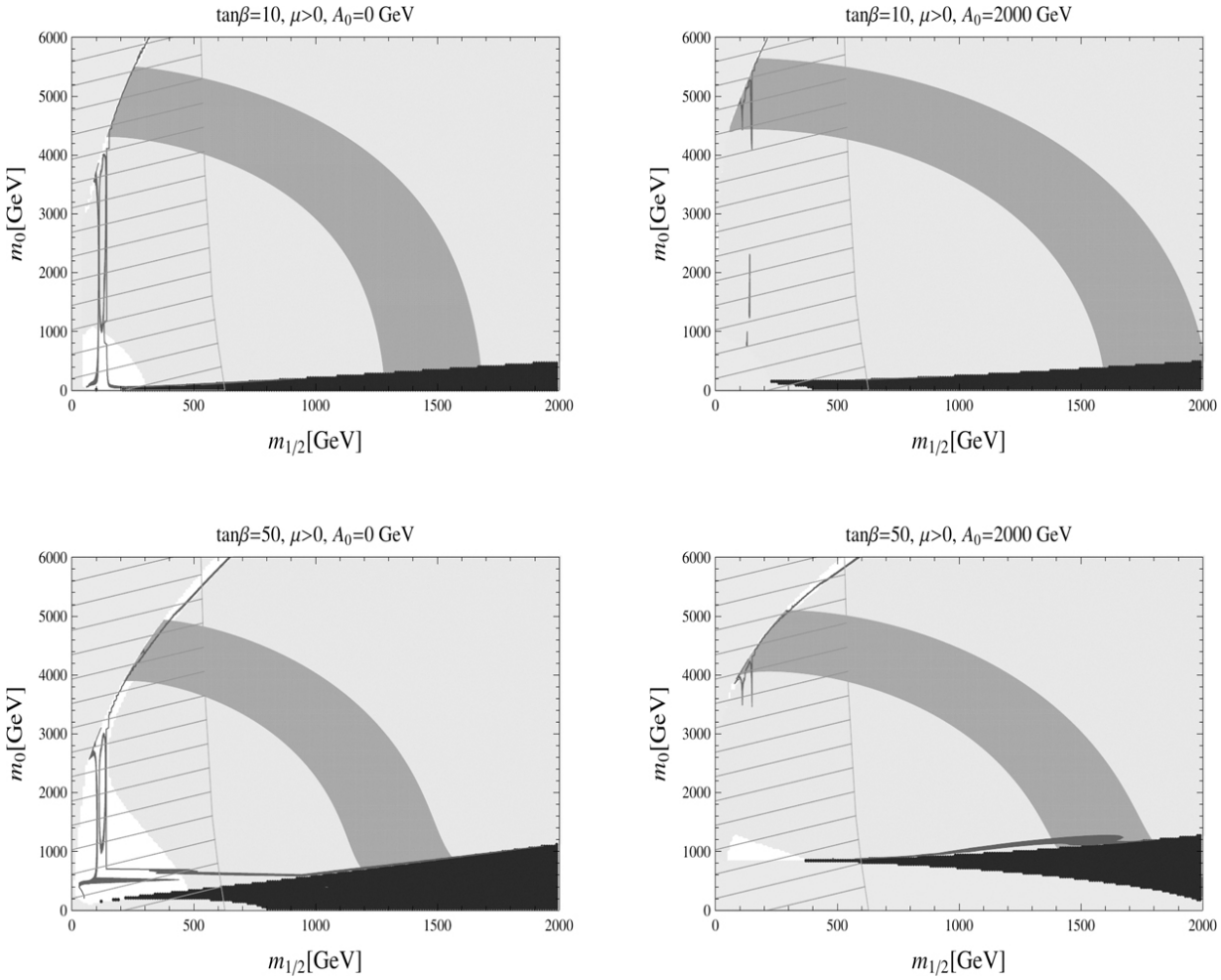

Figure 12.5 LSP relic–abundance constraints shown as differently shaded regions in the $(m_0 - m_{1/2})$ plane. The LUX constraint corresponds to the light–shaded region. The parameter points yielding the correct neutralino relic abundance, $0.09 < \Omega h^2 < 0.14$, appear as the *medium–shaded curved band*. The *dark–shaded* and hatched areas denote parameter points excluded by experimental or theoretical constraints. ⏎

It is important to note that these coannihilation effects are not captured by the simplified analytic expressions in Eqs. (12.11)–(12.14). In the figure, the *medium-shaded region* corresponds to points where the computed relic abundance falls within the experimentally allowed range, [229]:

$$0.09 < \Omega h^2 < 0.14. \tag{12.16}$$

The LUX constraint is satisfied in the *light–shaded region*.

It is noticeable that for low values of $\tan\beta$ (around 10), the allowed region corresponds to light $m_{1/2}$ values (below 500 GeV), where efficient coannihilation between the LSP and the lightest stau occurs. However, this region is now excluded due to current constraints on the Higgs and gluino masses [230]. At large $\tan\beta$, an additional viable region appears, corresponding to a resonance in the s-channel annihilation of DM pairs into fermion-antifermion final states via the pseudoscalar Higgs boson A, when $M_A \simeq 2m_\chi$. For $A_0 = 0$, only a small part of this region satisfies the Higgs mass constraint, while for larger A_0 values (around 2 TeV), a modest enhancement of the allowed region can be achieved.

12.3 BARYON ASYMMETRY OF THE UNIVERSE

The baryon asymmetry of the universe refers to the observed imbalance between matter and antimatter, where matter vastly dominates. This asymmetry is quantified by the baryon-to-photon ratio, η, defined as [31]:

$$\eta \equiv \frac{n_B - n_{\bar{B}}}{n_\gamma} \approx 6 \times 10^{-10}, \tag{12.17}$$

where n_B and $n_{\bar{B}}$ denote the number densities of baryons and antibaryons, respectively, and n_γ is the photon number density. The small but non-zero value of η implies that, despite the near-equal creation of matter and antimatter in the early universe, an imbalance emerged, leaving a surplus of matter [231].

In the hot, dense conditions of the early universe, matter and antimatter were produced in almost equal amounts and subsequently annihilated into photons as the universe cooled. In the absence of any asymmetry, this process should have left a universe devoid of matter. However, the presence of a substantial matter component today, with negligible amounts of primordial antimatter, indicates that a fundamental asymmetry developed during the early stages of cosmic evolution. This leads to one of the most profound open questions in modern physics: Why does the universe exhibit a preference for matter over antimatter? Understanding the origin of this asymmetry is essential to comprehending the conditions and mechanisms that shaped the early universe.

12.3.1 Sakharov Conditions

In 1967, Andrei Sakharov identified three essential conditions required to generate the baryon asymmetry of the universe [40]. These conditions, known as the Sakharov conditions, provide the minimal ingredients for a matter-dominated universe:

1. Baryon Number Violation: Interactions that violate baryon number (B) must exist to allow a net excess of baryons over antibaryons.
2. C and CP Violation: Charge conjugation (C) and charge-parity (CP) symmetries must be violated so that baryons and antibaryons behave differently, enabling an imbalance in their production rates.
3. Departure from Thermal Equilibrium: The universe must have undergone periods out of thermal equilibrium; otherwise, any generated asymmetry would be washed out by inverse processes.

Although the SM includes mechanisms that partially satisfy these conditions, they fall short of explaining the observed asymmetry. This limitation motivates extensions of the SM and ongoing research into the early universe.

12.3.2 Leptogenesis

Leptogenesis is one of the most compelling mechanisms proposed to explain the observed baryon asymmetry of the universe. It provides a natural connection between the matter-antimatter imbalance and neutrino physics, relying on processes beyond the SM. The core idea is that a lepton asymmetry is first generated and subsequently converted into a baryon asymmetry via electroweak sphaleron transitions [232]. This elegantly links the baryon asymmetry to the properties of neutrinos, which are already known to possess non-zero masses and mixing angles not accounted for in the SM.

In the SM extended by three right-handed neutrinos ν_{R_i}, the relevant Lagrangian involving these fields is given by

$$\begin{aligned}\mathscr{L} &= \sum_i M_i \left(\bar{\nu}^c_{Ri}\nu_{Ri} + \bar{\nu}_{Ri}\nu^c_{Ri}\right) + \sum_{ij} \lambda^*_{ji}\, \bar{\nu}_{Ri}\phi L_j + \sum_{ij} \lambda_{ji}\, \bar{L}_j\bar{\phi}\nu_{Ri} \\ &\quad + \sum_{ij} \lambda^*_{ji}\bar{L}^c_j\phi\nu^c_{Ri} + \sum_{ij} \lambda_{ji}\bar{\nu}^c_{Ri}\bar{\phi}L^c_j,\end{aligned}$$

(12.18)

where L denotes the lepton doublet, ϕ the Higgs doublet, and $\psi^c = C\gamma^0\psi^* = i\gamma^2\psi^* = C\bar{\psi}^T$ is the charge-conjugated spinor.

Asymmetry ε_i arises from the CP-violating decays of the heavy Majorana right-handed neutrinos N_i into the Higgs doublet ϕ and lepton doublets L_α, where $\alpha = e, \mu, \tau$, i.e., $N_i \to \phi + L_\alpha$. In most scenarios, the resulting lepton asymmetry is dominated by the decay of the lightest right-handed neutrino N_1. The N_i are Majorana fermions, representing the mass eigenstates of the right-handed neutrinos, and are defined as:

$$N_i = \nu_{Ri} + \nu_{Ri}^c, \qquad N^c = N.$$

(12.19)

The chiral components relate to N via the projection operators:

$$\nu_R = P_R N, \qquad \nu_R^c = P_L N,$$

(12.20)

where $P_L = \frac{1}{2}(1 - \gamma^5)$ and $P_R = \frac{1}{2}(1 + \gamma^5)$ are the standard left- and right-handed helicity projectors.

The CP asymmetry ε_1 generated by the decay of the lightest right-handed neutrino N_1 is defined as

$$\varepsilon_1 = \frac{\sum_\alpha \left(|A(N_1 \to \phi L_\alpha)|^2 - \left|A(N_1 \to \bar{\phi} L_\alpha)\right|^2 \right)}{\sum_\alpha \left(|A(N_1 \to \phi L_\alpha)|^2 + \left|A(N_1 \to \bar{\phi} L_\alpha)\right|^2 \right)},$$

(12.21)

where $A(N_1 \to \phi L_\alpha)$ denotes the total decay amplitude, including both tree-level and one-loop contributions:

$$A(N_1 \to \phi L_\alpha) = A_0(N_1 \to \phi L_\alpha) + A_1(N_1 \to \phi L_\alpha).$$

(12.22)

The CP asymmetry arises from the interference between the tree-level amplitude and the loop corrections. In the SM extended by right-handed neutrinos, the decay of N_1 proceeds via the tree-level process, as well as

through one-loop vertex and self-energy diagrams, as illustrated in Fig. 12.6.

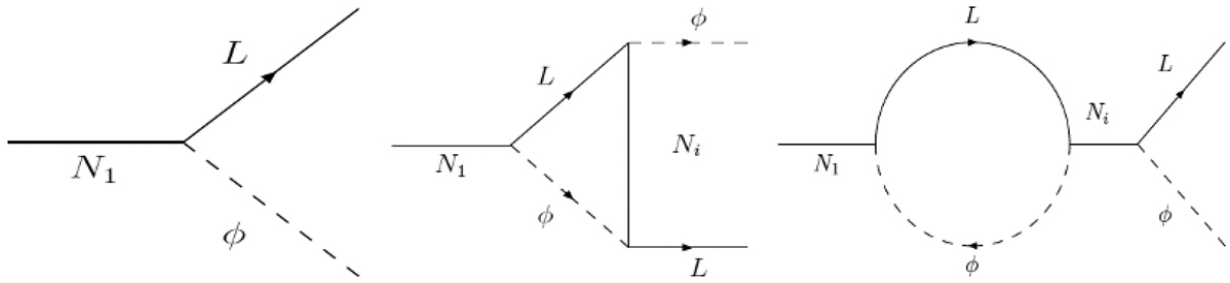

Figure 12.6 Feynman diagrams in SM with right-handed neutrinos that contribute to the decay $N_1 \to \phi L_\alpha$.

The tree-level decay amplitude of ν_{R_1} into the Higgs doublet ϕ and lepton doublet L_α is given by:

$$A_0(N_1 \to \phi L_\alpha) = -(\lambda_\nu)_{\alpha 1}\,(\bar{u}(p) P_R u^c(q)),$$

(12.23)

where $\bar{u}(p)$ is the Dirac spinor of the outgoing lepton l_α, $u^c(q)$ is the spinor of the incoming Majorana neutrino N_1, and P_R is the right-handed projection operator.

The one-loop vertex correction contributes:

$$A_{1V}(N_1 \to \phi L_\alpha) = \frac{1}{16\pi} \sum_i (\lambda_\nu)_{\alpha i} (\lambda_\nu^\dagger \lambda_\nu)_{1i}\,(\bar{u}(p) P_R u^c(q)) F_V\left(\frac{M_i^2}{M_1^2}\right),$$

(12.24)

where the loop function $F_V(x)$ has the imaginary and real parts:

$$\mathrm{Im}\, F_V(x) = \sqrt{x}\left[1 - (1+x)\ln\left(\frac{1+x}{x}\right)\right],$$

(12.25)

$$\mathrm{Re}\, F_V(x) = -\sqrt{x}\left[1 + \ln(x)\left(1 - (1+x)\ln\left(\frac{1+x}{x}\right)\right)\right].$$

(12.26)

The self-energy contribution to the decay amplitude is:

$$A_{1S}(N_1 \to \phi L_\alpha) = \frac{1}{16\pi} \sum_i (\lambda_\nu)_{\alpha i} (\lambda_\nu^\dagger \lambda_\nu)_{1i} \, (\bar{u}(p) P_R u^c(q)) F_S \left(\frac{M_i^2}{M_1^2} \right),$$

(12.27)

where $F_S(x) = \operatorname{Re} F_S(x) + i \operatorname{Im} F_S(x)$, and in the limit $|M_i - M_1| \gg |\Gamma_i - \Gamma_1|$, the imaginary part simplifies to:

$$\operatorname{Im} F_S(x) = \frac{\sqrt{x}}{1-x}.$$

(12.28)

The CP asymmetry in $N_1 \to \phi L_\alpha$ decays arises from complex phases in the Yukawa couplings λ_ν, which violate CP symmetry. These phases change sign under CP conjugation, leading to differences in the decay amplitudes of particles and antiparticles. In contrast, the phases of the loop functions $F_V(x)$ and $F_S(x)$ are CP-conserving, i.e., they remain unchanged under CP.

To analyze the asymmetry, the decay amplitudes can be factorized into CP-violating and CP-conserving components. Specifically, we write:

$$A_0(N_1 \to \phi L_\alpha) = A_{\text{tree}}, \quad \bar{A}_0(N_1 \to \bar{\phi} \bar{L}_\alpha) = A_{\text{tree}}^*,$$

(12.29)

$$A_1(N_1 \to \phi L_\alpha) = A_{\text{loop}} \cdot F, \quad \bar{A}_1(N_1 \to \bar{\phi} \bar{L}_\alpha) = A_{\text{loop}}^* \cdot F.$$

(12.30)

Here, F represents the loop function (from vertex and self-energy corrections), which is CP-even, while A_{tree} and A_{loop} carry the CP-odd phases from the Yukawa couplings.

The CP asymmetry then follows from the interference between tree and loop amplitudes:

$$\varepsilon = \frac{\operatorname{Im}\left[A_{\text{tree}} A_{\text{loop}}^* \right] \cdot \operatorname{Im}[F]}{|A_{\text{tree}}|^2 + |A_{\text{loop}} F|^2 + 2 \operatorname{Re}[F] \operatorname{Re}\left[A_{\text{tree}} A_{\text{loop}}^* \right]}.$$

(12.31)

Since the tree-level amplitude typically dominates, this simplifies to:

$$\varepsilon_1 \simeq \frac{1}{|A_{\rm tree}|^2}\,\mathrm{Im}\left[A_{\rm tree}A^*_{\rm loop}\right]\cdot \mathrm{Im}[F].$$

(12.32)

In the SM with right-handed neutrinos, the resulting CP asymmetry becomes:

$$\varepsilon_1 \simeq \frac{1}{8\pi}\frac{1}{(\lambda_\nu^\dagger\lambda_\nu)_{11}}\sum_{i=2,3}\mathrm{Im}\left[(\lambda_\nu^\dagger\lambda_\nu)^2_{1i}\right]\left[\mathrm{Im}F_V\left(\frac{M^2_{R_i}}{M^2_{R_1}}\right)+\mathrm{Im}F_S\left(\frac{M^2_{R_i}}{M^2_{R_1}}\right)\right].$$

(12.33)

Several key points follow from this expression: (i) A non-zero lepton asymmetry requires $\mathrm{Im}[(\lambda_\nu^\dagger\lambda_\nu)_{1i}]\neq 0$, which translates to

$$\mathrm{Im}\left(\sqrt{M_R}\,R\,m_\nu^{\rm diag}\,R^\dagger\sqrt{M_R}\right)\neq 0,\quad \text{for}\, i=2,3.$$

(ii) Leptogenesis is independent of the phases in the PMNS matrix due to its unitarity. (iii) If both R and M_R are real, then $\varepsilon_1=0$, and leptogenesis cannot proceed. (iv) In the case of quasi-degenerate right-handed neutrino masses, the CP asymmetry can be resonantly enhanced due to the near-zero denominator in the loop function $g(x)$, a scenario known as resonant leptogenesis [233]. This becomes particularly relevant for models with suppressed Yukawa couplings.

Once a lepton asymmetry is generated, it can be partially converted into a baryon asymmetry via electroweak sphaleron processes. Sphalerons are non-perturbative configurations in the Standard Model that violate baryon number (B) and lepton number (L) individually, but preserve their difference, $B-L$. Active during the electroweak phase transition in the early universe, these processes convert part of the lepton asymmetry into a baryon asymmetry.

The final baryon asymmetry η_B is related to the initial lepton asymmetry $\eta_L\sim\kappa\,\varepsilon$, where ε is the CP asymmetry from heavy neutrino decays, and κ is an efficiency factor accounting for washout processes and the thermal history. In typical thermal leptogenesis scenarios, κ ranges from 10^{-3} to 10^{-1}, depending on the model parameters [209]. The conversion between lepton and baryon asymmetries can be approximated as:

$$\eta_B \simeq -\frac{1}{3}\eta_L,$$

with the factor $-1/3$ arising from the equilibrium conditions of sphaleron interactions and the Standard Model particle content.

12.4 INFLATION AND BSM

The SM of cosmology, grounded in the cosmological principle, has successfully predicted key phenomena such as the universe's expansion and the existence of the CMB. However, it originally faced several challenges related to initial conditions. To resolve these, the theory of inflation was introduced [234, 235], providing a mechanism that explains the observed homogeneity, isotropy, and large-scale structure of the universe. Inflation thereby addresses many of the initial value problems inherent in the classical Big Bang framework.

The theoretical foundation of cosmology rests on General Relativity (GR), formulated by Einstein in 1915 [236], with field equations:

$$R_{\mu\nu} - \frac{1}{2} g_{\mu\nu} R = 8\pi G T_{\mu\nu}.$$

(12.34)

In the 1920s, Friedmann used these equations to derive a solution for a homogeneous and isotropic universe [237, 238], leading to the Friedmann-Lemaitre-Robertson-Walker (FLRW) metric:

$$ds^2 = dt^2 - a^2(t) \left[\frac{dr^2}{1 - \kappa r^2} + r^2 \left(d\theta^2 + \sin^2 \theta \, d\phi^2 \right) \right],$$

(12.35)

where $\kappa = -1, 0, 1$ corresponds to open, flat, and closed geometries, respectively. The evolution of the scale factor $a(t)$ is governed by the Friedmann equations:

$$\ddot{a} = -\frac{4\pi G}{3} (\rho + 3p) a,$$

(12.36)

$$H^2 + \frac{\kappa}{a^2} = \frac{8\pi G}{3} \rho,$$

(12.37)

with the Hubble parameter defined as $H = \dot{a}/a$. For a spatially flat universe ($\kappa = 0$), two distinct eras emerge: Radiation domination, with $a(t) \propto t^{1/2}$, $\rho \propto a^{-4}$, and Matter (dust) domination, with $a(t) \propto t^{2/3}$, $\rho \propto a^{-3}$. In both cases, if $\rho + 3p > 0$, the expansion is decelerating ($\ddot{a} < 0$).

The Friedmann equation can also be recast as:

$$\Omega - 1 = \frac{\kappa}{a^2 H^2},$$

(12.38)

where $\Omega = \rho/\rho_c$ and the critical density is given by $\rho_c = \frac{3H^2}{8\pi G}$. Present observations, particularly those from the Planck satellite, indicate that the density parameter Ω is very close to unity ($\Omega \sim \mathcal{O}(1)$), implying that the universe is nearly flat [31]. This near-flatness today suggests that in the early universe, Ω must have been extraordinarily fine-tuned to be even closer to one. For instance, at the Planck time ($t \sim 10^{-43}$ s), the deviation from exact flatness would have had to satisfy:

$$|\Omega - 1| < \mathcal{O}(10^{-64}).$$

(12.39)

This extreme sensitivity to initial conditions is known as the flatness problem [239], and it poses a major challenge to the standard Big Bang model, which lacks a dynamical mechanism to explain why Ω should be so close to one.

Closely related is the horizon problem, which concerns the causal structure of the early universe. Observations of the CMB reveal that regions of the sky separated by large angular distances have nearly identical temperatures, as shown in Fig. 12.7, differing by less than one part in 10^5. However, under standard Big Bang evolution, these regions should have been causally disconnected, meaning they could not have exchanged information or energy due to the finite speed of light [240]. The observed uniformity suggests that these regions were once in thermal equilibrium, a state that cannot be explained without invoking a mechanism that allows causal contact over large distances.

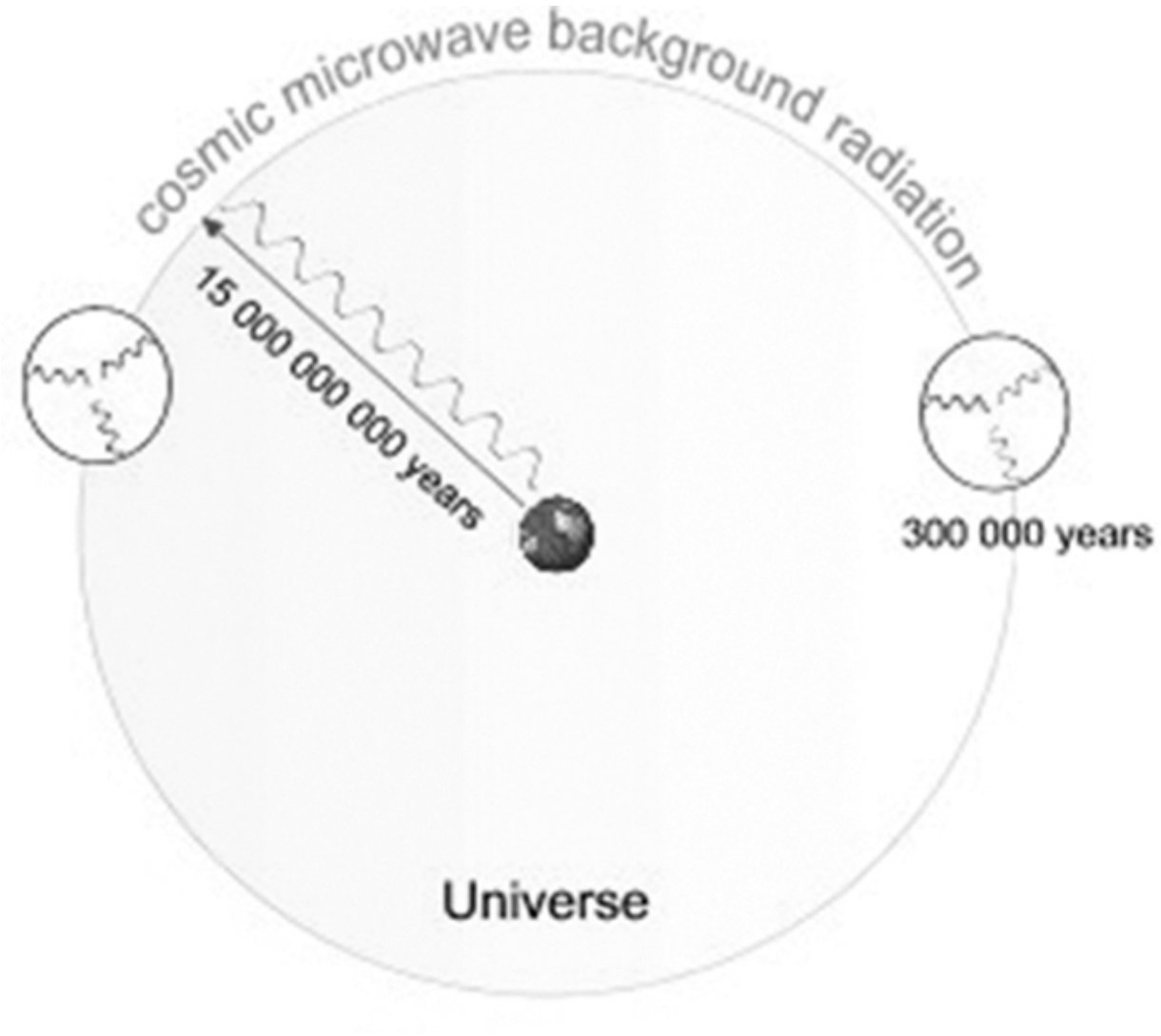

Figure 12.7 The CMB temperature map shows uniform temperatures across causally disconnected regions, highlighting the horizon problem and motivating cosmic inflation. ⏎

Alan Guth proposed that at $t \sim 10^{-37}$ seconds, the universe underwent a brief period of exponential expansion, known as inflation, increasing in size by over 25 orders of magnitude within 10^{-34} seconds [234]. After inflation ended, the universe resumed a slower expansion over the next 13.7 billion years. Inflation requires accelerated expansion, $\ddot{a} > 0$, which from the Friedmann equations implies negative pressure:

$$p < -\frac{\rho}{3}.$$

(12.40)

This yields exponential growth of the scale factor:

$$a(t) \propto e^{Ht}, \quad t \in [t_i, t_f].$$

(12.41)

A scalar field with potential $V(\phi)$ provides a natural mechanism for this behavior [241]. Its Lagrangian is:

$$\mathscr{L} = \frac{1}{2} g^{\mu\nu} \partial_\mu \phi \partial_\nu \phi - V(\phi),$$

(12.42)

with energy density and pressure:

$$\rho_\phi = \frac{1}{2}\dot{\phi}^2 + V(\phi), \quad p_\phi = \frac{1}{2}\dot{\phi}^2 - V(\phi).$$

(12.43)

When the potential dominates, $\dot{\phi}^2 \ll V(\phi)$, the condition for inflation is met [242]. This requires a flat potential for slow-roll and a minimum to end inflation [243].

The dynamics of a homogeneous scalar field in an expanding universe are governed by the following equations:

$$H^2 = \frac{8\pi G}{3}\left[V(\phi) + \frac{1}{2}\dot{\phi}^2\right],$$

(12.44)

$$\ddot{\phi} + 3H\dot{\phi} = -V'(\phi),$$

(12.45)

which describe the evolution of the scalar field and the expansion during inflation, as shown in Fig. 12.8 [244]. Scalar fields, fundamental in many physical theories, are characterized by their potential forms. Notable examples include:

- The Higgs potential:

$$V(\phi) = \lambda\left(\phi^2 - M^2\right)^2,$$

(12.46)

central to the Higgs mechanism and spontaneous symmetry breaking [7],

- The massive scalar field potential:

$$V(\phi) = \frac{1}{2}m^2\phi^2,$$

(12.47)

describing a scalar field with mass m [241],

- The self-interacting scalar field potential:

$$V(\phi) = \lambda\phi^4,$$

(12.48)

modeling a scalar field with quartic self-interactions [245].

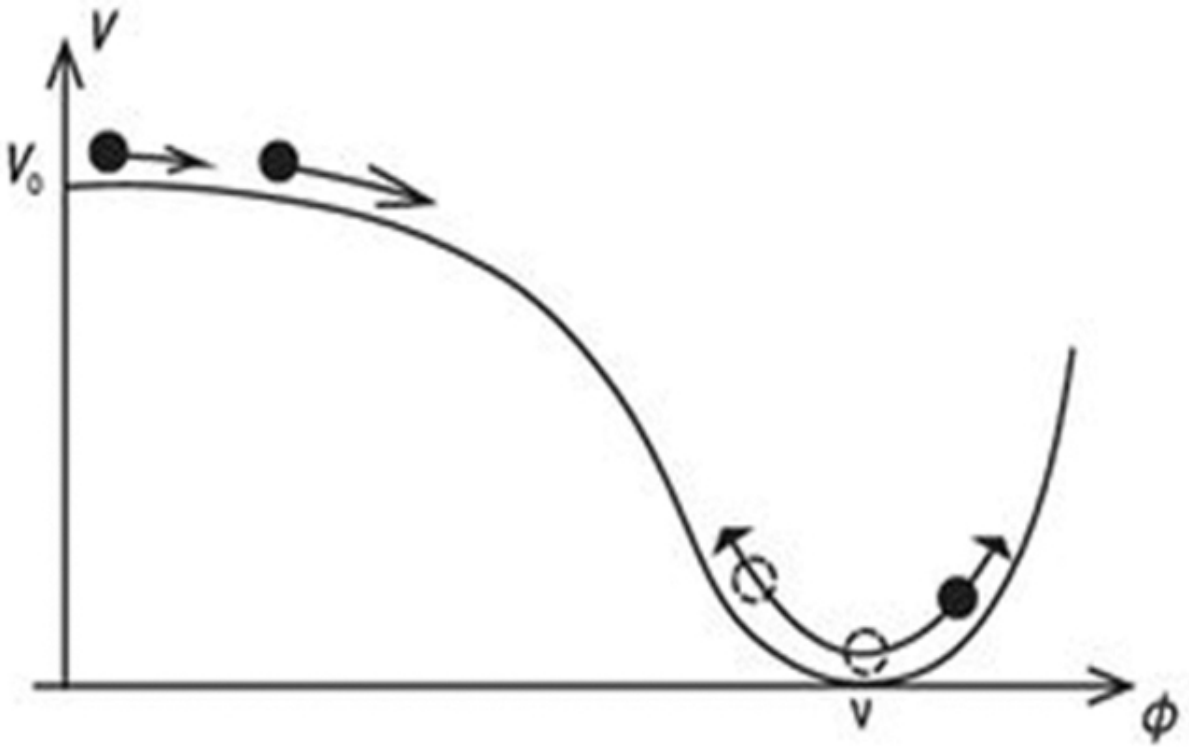

Figure 12.8 The flat region of the potential allows for slow-roll inflation, while the minimum provides a natural endpoint for the inflationary phase. ⏎

In inflationary cosmology, the slow-roll approximation describes when a scalar field ϕ induces exponential expansion. This is quantified by two slow-roll parameters:

$$\epsilon = \frac{m_{\text{pl}}^2}{16\pi}\left(\frac{V'(\phi)}{V(\phi)}\right)^2, \quad \eta = \frac{m_{\text{pl}}^2}{8\pi}\frac{V''(\phi)}{V(\phi)},$$

(12.49)

where $V(\phi)$ is the potential, $V'(\phi)$ and $V''(\phi)$ are its first and second derivatives, and m_{pl} is the Planck mass. The slow-roll condition holds when:

$$\epsilon \ll 1, \quad |\eta| \ll 1,$$

(12.50)

allowing for prolonged accelerated expansion [246]. Inflation ends when either ϵ or $|\eta|$ approaches unity [247].

The amount of inflation required to address the horizon and flatness problems of the Big Bang model is quantified by the number of e-foldings, denoted by N. The number of e-foldings is defined as:

$$N(\phi) = \ln\left(\frac{a_f}{a_i}\right) = \int_{t_i}^{t_f} H\, dt = -\frac{8\pi}{m_{\text{pl}}^2}\int_{\phi_i}^{\phi_f}\frac{V(\phi)}{V'(\phi)}\, d\phi,$$

(12.51)

where:

- a_i and a_f are the initial and final scale factors,
- H is the Hubble parameter,
- ϕ_i and ϕ_f are the initial and final values of the scalar field.

This formulation provides a detailed description of inflationary dynamics and the conditions necessary to resolve cosmological issues.

12.5 DARK ENERGY AND BSM

Dark energy, which accounts for approximately 68% of the total energy density of the universe [31], is one of the most profound mysteries in modern cosmology. It is responsible for the observed accelerated late expansion of the universe, first discovered through observations of Type Ia supernovae in the late 1990s. Despite its dominance, the nature of dark energy remains unknown, and its explanation often requires physics beyond the BSM. This section explores the dark energy problem, BSM explanations, and observational constraints.

12.5.1 Observational Evidence for Cosmic Acceleration

The accelerated expansion of the universe is strongly supported by multiple independent lines of observational evidence:

- Type Ia Supernovae (SN Ia): Observations of distant Type Ia supernovae provided the first direct evidence for cosmic acceleration, showing that the universe's expansion is speeding up over time [248, 249].
- CMB: Measurements of temperature anisotropies in the CMB, particularly by the Wilkinson Microwave Anisotropy Probe (WMAP), have confirmed the presence of dark energy and its influence on the universe's large-scale structure [31].
- Baryon Acoustic Oscillations (BAO): The detection of BAO in the distribution of galaxies has provided additional evidence for cosmic acceleration, serving as a “standard ruler” for measuring the expansion history of the universe.

12.5.2 The Nature of Dark Energy

Dark energy is a mysterious form of energy that plays a crucial role in the dynamics of the universe. It is believed to be the driving force behind the accelerated expansion, acting as a repulsive force that counteracts gravity on cosmic scales. Unlike matter, dark energy does not clump or cluster but is uniformly distributed throughout space, making it homogeneous. This uniformity ensures that its density remains constant across different regions of the universe, in contrast to visible matter and dark matter, which tend to cluster due to gravitational attraction.

The exact nature of dark energy remains one of the most profound questions in modern cosmology. Several theories have been proposed to explain its origin, including:

- Cosmological Constant (Λ): A constant energy density that fills space homogeneously, representing the simplest explanation for dark energy [203].
- Dynamical Fields (e.g., Quintessence): A time-varying scalar field that provides a dynamic explanation for dark energy [250], potentially addressing some of the theoretical challenges associated with the cosmological constant.

12.5.3 Cosmological Constant

The dark energy problem arises from the observed acceleration of the universe's expansion, as described by the Friedmann equation:

$$H^2 = \frac{8\pi G}{3}(\rho_m + \rho_r + \rho_\Lambda), \tag{12.52}$$

where H is the Hubble parameter, ρ_m and ρ_r represent the energy densities of matter and radiation, respectively, and ρ_Λ is the energy density associated with dark energy.

The concept of dark energy originates from Einstein's cosmological constant (Λ), introduced in 1916 to describe a static universe. He proposed Λ as a repulsive force to counteract gravity, ensuring a non-expanding universe. However, after Edwin Hubble's discovery of the expansion of the universe in the 1920s, Einstein discarded the cosmological constant, calling it his “biggest mistake.”

Modern cosmology has revived the cosmological constant, driven by the observed acceleration of the universe's expansion, first confirmed in 1998 through Type Ia supernova measurements [248, 249]. In this context, the cosmological constant corresponds to a constant energy density:

$$\rho_\Lambda = \frac{\Lambda}{8\pi G}. \tag{12.53}$$

This energy density is uniform in space and time, providing a simple explanation for the accelerated expansion.

Despite its success, the cosmological constant faces two significant theoretical challenges.

- Cosmological Constant Problem: The observed value of ρ_Λ is exceedingly small ($\sim 10^{-47}\,\mathrm{GeV}^4$), and is very different from theoretical predictions from quantum field theory, suggesting a value many orders of magnitude larger. This discrepancy highlights the difficulty in reconciling the observed dark energy density with quantum physics [203].
- Coincidence Problem: The energy densities of dark energy and matter are comparable in the present epoch, even though they evolve differently over the universe's history. Matter density decreases with expansion, while dark energy remains constant. This raises the question of why the two densities are so similar today, challenging our understanding of the timing and nature of dark energy's dominance, as shown in Fig. 12.9 [251, 252].

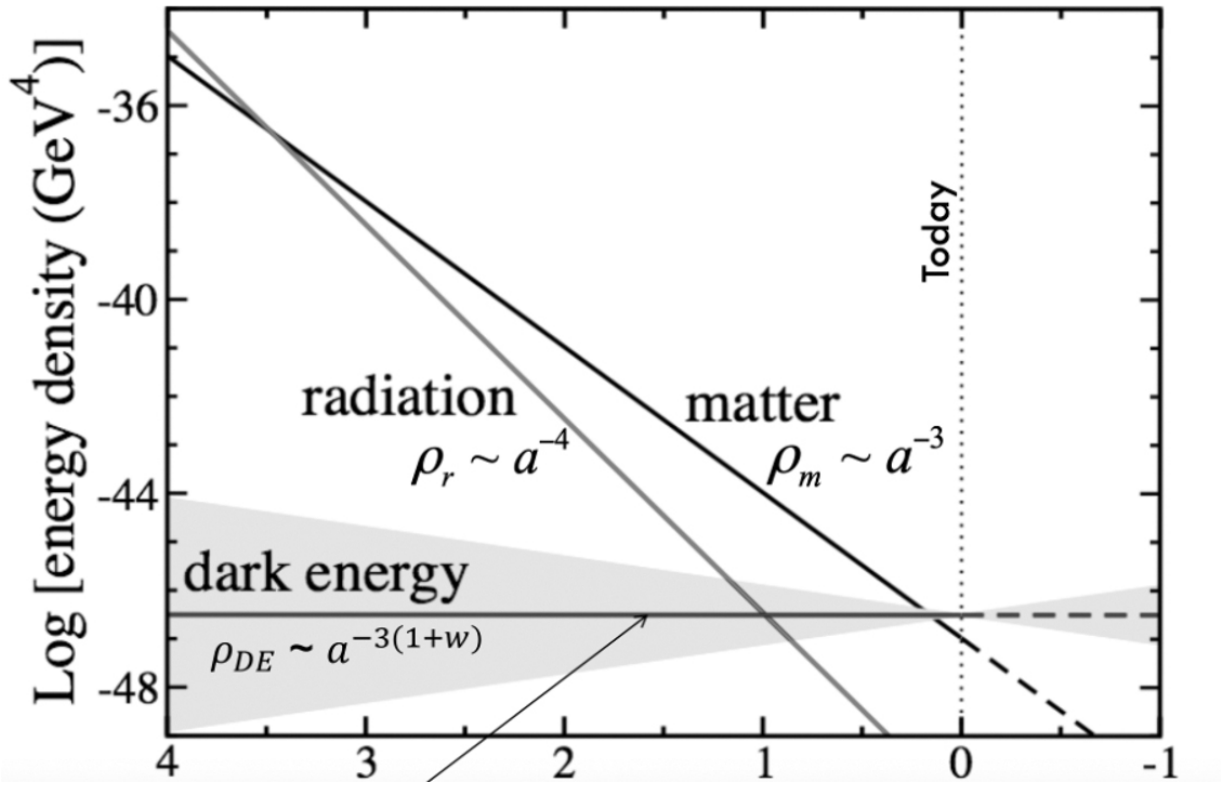

Figure 12.9 Energy density evolution in the universe as a function of scale factor a, showing logarithmic densities (in GeV^4) for radiation, matter, and dark energy. The vertical axis represents log density, and the horizontal axis the scale factor, with "Today" marking the present. Source: [253]. ⏎

These challenges highlight the elusive nature of dark energy and its deep implications for cosmology and fundamental physics. Addressing them may require new theoretical frameworks, such as modifications to general relativity, dynamical fields like quintessence, or more radical extensions beyond the SM. Observations from the CMB, large-scale structure surveys, and supernova data continue to offer essential insights, guiding the quest to understand dark energy and its role in the universe.

12.5.4 Quintessence

To address the limitations of the cosmological constant, several BSM explanations have been proposed. One prominent idea is that dark energy arises from a dynamical field, known as quintessence, which differs from the cosmological constant by varying over time and space. Unlike matter and radiation, which slow down the expansion through gravitational attraction, quintessence generates a repulsive force that accelerates the universe's expansion [250].

Quintessence is described by a dynamical scalar field ϕ that evolves over time, providing a time-varying dark energy density. The energy density ρ_ϕ and pressure p_ϕ of the quintessence field are:

$$\rho_\phi = \frac{1}{2}\dot{\phi}^2 + V(\phi), \tag{12.54}$$

$$p_\phi = \frac{1}{2}\dot{\phi}^2 - V(\phi), \tag{12.55}$$

where $V(\phi)$ is the scalar field potential [254].

A key feature of quintessence is the time-varying equation of state $w_\phi = p_\phi/\rho_\phi$, distinguishing it from the cosmological constant, which has a fixed equation of state $w_\Lambda = -1$. This dynamism may help resolve the

coincidence problem, which questions why dark energy and matter densities are similar in the present epoch [255].

However, the specific form of the potential $V(\phi)$ remains unknown, and various models have been proposed, each with distinct implications for the evolution of the universe. Common choices for $V(\phi)$ include exponential, power-law, and tracker potentials, each leading to different cosmological behaviors [256]. Despite this diversity, none of these models have been conclusively supported by observational data.

A classic example of a quintessence potential is the exponential form:

$$V(\phi) = V_0 e^{-\lambda \kappa \phi},$$

(12.56)

where V_0 is a constant with dimensions of energy density, λ is a dimensionless parameter controlling the slope of the potential, and $\kappa = \sqrt{8\pi G}$ is the gravitational coupling constant. The equation of state parameter w_ϕ for the quintessence field is given by:

$$w_\phi = \frac{p_\phi}{\rho_\phi} = \frac{\frac{1}{2}\dot{\phi}^2 - V(\phi)}{\frac{1}{2}\dot{\phi}^2 + V(\phi)}.$$

(12.57)

The evolution of the field depends on λ: for small λ, the field rolls slowly down the potential, leading to $w_\phi \approx -1$, mimicking a cosmological constant. For large λ, the field rolls faster, and w_ϕ deviates from -1, potentially resulting in a time-varying equation of state.

12.5.5 Modified Gravity

Modified gravity theories propose that dark energy is not a new form of energy but rather a manifestation of deviations from general relativity on cosmological scales [257, 258]. The action for $f(R)$ gravity, an arbitrary function of the Ricci scalar R, is given by:

$$S = \frac{1}{2\kappa^2} \int \mathrm{d}^4x \, \sqrt{-g} \, f(R) + \int \mathrm{d}^4x \, \mathscr{L}_M(g_{\mu\nu}, \Psi_M),$$

(12.58)

where $\kappa^2 = 8\pi G$ is the gravitational coupling constant, G is the Newtonian coupling constant, g is the determinant of the metric tensor $g_{\mu\nu}$, and $\mathscr{L}_M$ is the matter Lagrangian depending on the metric $g_{\mu\nu}$ and matter fields Ψ_M. Varying the action (12.58) with respect to the metric $g_{\mu\nu}$ leads to the field equations for $f(R)$ gravity [259]:

$$F(R)R_{\mu\nu}(g) - \frac{1}{2}f(R)g_{\mu\nu} - \nabla_\mu\nabla_\nu F(R) + g_{\mu\nu}\Box F(R) = \kappa^2 T_{\mu\nu},$$

(12.59)

where $F(R) \equiv \partial f/\partial R$ is the derivative of $f(R)$ with respect to R, $R_{\mu\nu}$ is the Ricci tensor, and $T_{\mu\nu} = -\frac{2}{\sqrt{-g}}\frac{\delta \mathscr{L}_M}{\delta g^{\mu\nu}}$ is the energy-momentum tensor of matter [258].

In $f(R)$ gravity, the modified Friedmann equations for a flat Friedmann-Robertson-Walker (FRW) universe with the metric

$$ds^2 = -dt^2 + a(t)^2 dx^2,$$

are:

$$3FH^2 \quad = \kappa^2(\rho_m + \rho_r) + \frac{FR - f}{2} - 3H\dot{F},$$

(12.60)

$$-2F\dot{H} \quad = \kappa^2\left(\rho_m + \frac{4}{3}\rho_r\right) + \ddot{F} - H\dot{F}.$$

(12.61)

Here, ρ_m and ρ_r are the energy densities of matter and radiation, respectively, and $H = \frac{\dot{a}}{a}$ is the Hubble parameter [257].

The total energy density ρ_{tot} and pressure p_{tot} in $f(R)$ gravity include contributions from matter, radiation, and the effective dark energy component arising from the modification of gravity. The conservation equation for the total energy-momentum tensor is:

$$\dot{\rho}_{\text{tot}} + 3H(\rho_{\text{tot}} + p_{\text{tot}}) = 0.$$

(12.62)

This equation can be split into separate conservation equations for matter and radiation:

$$\dot{\rho}_m + 3H\rho_m = 0, \quad \text{(matter)}$$

(12.63)

$$\dot{\rho}_r + 4H\rho_r = 0. \quad \text{(radiation)}$$

(12.64)

In $f(R)$ gravity, the dark energy component arises from the modification of the gravitational action. The effective dark energy density ρ_{DE} and pressure p_{DE} are defined as:

$$\rho_{\mathrm{DE}} = \frac{1}{\kappa^2}\left(\frac{FR - f}{2} - 3H\dot{F}\right),$$

(12.65)

$$p_{\mathrm{DE}} = \frac{1}{\kappa^2}\left(\frac{f - FR}{2} + \ddot{F} + 2H\dot{F}\right).$$

(12.66)

These definitions ensure that the Friedmann equations can be written in the standard form:

$$3H^2 \quad = \kappa^2(\rho_m + \rho_r + \rho_{\mathrm{DE}}),$$

(12.67)

$$-2\dot{H} \quad = \kappa^2\left(\rho_m + \frac{4}{3}\rho_r + \rho_{\mathrm{DE}} + p_{\mathrm{DE}}\right).$$

(12.68)

The effective equation of state parameter w_{eff} is defined as the ratio of the total pressure to the total energy density of the universe:

$$w_{\mathrm{eff}} = \frac{p_{\mathrm{tot}}}{\rho_{\mathrm{tot}}}.$$

(12.69)

From Friedmann equations, one can express $\dot{H}$ as follows:

$$\dot{H} = -\frac{3}{2} H^2 \left(1 + w_{\text{eff}}\right).$$

(12.70)

Solving for w_{eff}, we arrive at:

$$w_{\text{eff}} = -1 - \frac{2\dot{H}}{3H^2}.$$

(12.71)

The effective equation of state w_{eff} describes the overall behavior of the universe's expansion:

- If $w_{\text{eff}} < -\frac{1}{3}$, the universe undergoes accelerated expansion (dark energy domination).
- If $w_{\text{eff}} = -1$, the expansion mimics a cosmological constant (ΛCDM).
- If $w_{\text{eff}} > -\frac{1}{3}$, the expansion decelerates (matter or radiation domination).

It is worth mentioning that w_{eff} depends on the functional form of $f(R)$ [257, 259].

Bibliography

[1] Shaaban Khalil and Stefano Moretti. *Standard Model Phenomenology*. CRC Press, 6 2022.

[2] Sheldon L. Glashow. Partial-symmetries of weak interactions. *Nucl. Phys.*, 22:579–588, 1961.

[3] Steven Weinberg. A Model of Leptons. *Phys. Rev. Lett.*, 19:1264–1266, 1967.

[4] Abdus Salam. Weak and electromagnetic interactions. In Nils Svartholm, editor, *Elementary Particle Theory: Relativistic Groups and Analyticity (Nobel Symposium No. 8)*, pages 367–377, Stockholm, 1968. Almqvist & Wiksell.

[5] David J. Gross and Frank Wilczek. Ultraviolet Behavior of Non-Abelian Gauge Theories. *Phys. Rev. Lett.*, 30:1343–1346, 1973.

[6] H. David Politzer. Reliable Perturbative Results for Strong Interactions? *Phys. Rev. Lett.*, 30:1346–1349, 1973.

[7] Peter W. Higgs. Broken Symmetries and the Masses of Gauge Bosons. *Phys. Rev. Lett.*, 13:508–509, 1964.

[8] Francois Englert and Robert Brout. Broken Symmetry and the Mass of Gauge Vector Mesons. *Phys. Rev. Lett.*, 13:321–323, 1964.

[9] Gerald S. Guralnik, C. R. Hagen, and T. W. B. Kibble. Global Conservation Laws and Massless Particles. *Phys. Rev. Lett.*, 13:585–587, 1964.

[10] Nicola Cabibbo. Unitary Symmetry and Leptonic Decays. *Phys. Rev. Lett.*, 10:531–533, 1963.

[11] Makoto Kobayashi and Toshihide Maskawa. CP Violation in the Renormalizable Theory of Weak Interaction. *Prog. Theor. Phys.*, 49:652–657, 1973.

[12] Particle Data Group and R. L. et al. Workman. Review of Particle Physics. *PTEP*, 2022(8):083C01, 2022.

[13] Y. et al. [Super-Kamiokande Collaboration] Fukuda. Evidence for oscillation of atmospheric neutrinos. *Phys. Rev. Lett.*, 81:1562–1567, 1998.

[14] Q. R. et al. [SNO Collaboration] Ahmad. Direct evidence for neutrino flavor transformation from neutral current interactions in the Sudbury Neutrino Observatory. *Phys. Rev. Lett.*,

89:011301, 2002.

[15] B. et al. [Muon g-2 Collaboration] Abi. Measurement of the Positive Muon Anomalous Magnetic Moment to 0.46 ppm. *Phys. Rev. Lett.*, 126:141801, 2021.

[16] T. et al. Aoyama. The anomalous magnetic moment of the muon in the Standard Model. *Phys. Rept.*, 887:1–166, 2020.

[17] R. et al. [LHCb Collaboration] Aaij. Test of Lepton Universality Using $B^+ \to K^+\ell^+\ell^-$ Decays. *Phys. Rev. Lett.*, 113:151601, 2014.

[18] R. et al. [LHCb Collaboration] Aaij. Test of lepton universality with $B^0 \to K^{*0}\ell^+\ell^-$ decays. *JHEP*, 08:055, 2017.

[19] Tsutomu Yanagida. Horizontal gauge symmetry and masses of neutrinos. *Conf. Proc. C*, 7902131:95–99, 1979.

[20] Rabindra N. Mohapatra and Goran Senjanović. Neutrino mass and spontaneous parity nonconservation. *Phys. Rev. Lett.*, 44:912–915, 1980.

[21] M. Magg and C. Wetterich. Neutrino Mass Problem and Gauge Hierarchy. *Phys. Lett. B*, 94:61–64, 1980.

[22] Rabindra N. Mohapatra and Goran Senjanovic. Neutrino Masses and Mixings in Gauge Models with Spontaneous Parity Violation. *Phys. Rev. D*, 23:165, 1981.

[23] Robert Foot, H. Lew, X. G. He, and Girish C. Joshi. Seesaw Neutrino Masses Induced by a Triplet of Leptons. *Z. Phys. C*, 44:441, 1989.

[24] R. N. Mohapatra and J. W. F. Valle. Neutrino Mass and Baryon Number Nonconservation in Superstring Models. *Phys. Rev. D*, 34:1642, 1986.

[25] D. Wyler and L. Wolfenstein. Massless Neutrinos in Left-Right Symmetric Models. *Nucl. Phys. B*, 218:205–214, 1983.

[26] S. M. Barr. A Different seesaw formula for neutrino masses. *Phys. Rev. Lett.*, 92:101601, 2004.

[27] V. C. Rubin, N. Thonnard, and W. K. Ford, Jr. Rotational properties of 21 SC galaxies with a large range of luminosities and radii, from NGC 4605/R = 4kpc/to UGC 2885/R = 122 kpc/. *Astrophys. J.*, 238:471, 1980.

[28] Edvige Corbelli and Paolo Salucci. The Extended Rotation Curve and the Dark Matter Halo of M33. *Mon. Not. Roy. Astron. Soc.*, 311:441–447, 2000.

[29] A. N. Taylor, S. Dye, Thomas J. Broadhurst, N. Benitez, and E. van Kampen. Gravitational lens magnification and the mass of Abell 1689. *Astrophys. J.*, 501:539, 1998.

[30] Douglas Clowe, Marusa Bradac, Anthony H. Gonzalez, Maxim Markevitch, Scott W. Randall, Christine Jones, and Dennis Zaritsky. A direct empirical proof of the existence of

dark matter. *Astrophys. J. Lett.*, 648:L109–L113, 2006.

[31] N. Aghanim et al. Planck 2018 results. VI. Cosmological parameters. *Astron. Astrophys.*, 641:A6, 2020. [Erratum: Astron. Astrophys. 652, C4 (2021)].

[32] Gianfranco Bertone, Dan Hooper, and Joseph Silk. Particle dark matter: Evidence, candidates and constraints. *Phys. Rept.*, 405:279–390, 2005.

[33] Gerard Jungman, Marc Kamionkowski, and Kim Griest. Supersymmetric dark matter. *Phys. Rept.*, 267:195–373, 1996.

[34] Paolo Gondolo and Graciela Gelmini. Cosmic abundances of stable particles: Improved analysis. *Nucl. Phys. B*, 360:145–179, 1991.

[35] Leonard Susskind. Dynamics of Spontaneous Symmetry Breaking in the Weinberg-Salam Theory. *Phys. Rev. D*, 20:2619–2625, 1979.

[36] Steven Weinberg. Implications of Dynamical Symmetry Breaking. *Phys. Rev. D*, 13:974–996, 1976. [Addendum: Phys.Rev.D 19, 1277–1280 (1979)].

[37] Eldad Gildener. Gauge Symmetry Hierarchies. *Phys. Rev. D*, 14:1667, 1976.

[38] Riccardo Barbieri and G. F. Giudice. Upper Bounds on Supersymmetric Particle Masses. *Nucl. Phys. B*, 306:63–76, 1988.

[39] Steven Weinberg. Anthropic Bound on the Cosmological Constant. *Phys. Rev. Lett.*, 59:2607, 1987.

[40] A. D. Sakharov. Violation of CP Invariance, C asymmetry, and baryon asymmetry of the universe. *Pisma Zh. Eksp. Teor. Fiz.*, 5:32–35, 1967.

[41] N. Aghanim et al. Planck 2018 results. vi. cosmological parameters. *Astron. Astrophys.*, 641:A6, 2020.

[42] M. Fukugita and T. Yanagida. Baryogenesis Without Grand Unification. *Phys. Lett. B*, 174:45–47, 1986.

[43] T. D. Lee. A Theory of Spontaneous T Violation. *Phys. Rev. D*, 8:1226–1239, 1973.

[44] Sheldon L. Glashow and Steven Weinberg. Natural Conservation Laws for Neutral Currents. *Phys. Rev. D*, 15:1958, 1977.

[45] Junjie Cao, Peihua Wan, Lei Wu, and Jin Min Yang. Lepton-Specific Two-Higgs Doublet Model: Experimental Constraints and Implication on Higgs Phenomenology. *Phys. Rev. D*, 80:071701, 2009.

[46] Heather E. Logan and Deanna MacLennan. Charged Higgs phenomenology in the flipped two Higgs doublet model. *Phys. Rev. D*, 81:075016, 2010.

[47] T. P. Cheng and Marc Sher. Mass Matrix Ansatz and Flavor Nonconservation in Models with Multiple Higgs Doublets. *Phys. Rev. D*, 35:3484, 1987.

[48] G.C. Branco, P.M. Ferreira, L. Lavoura, M.N. Rebelo, M. Sher, and Joao P. Silva. Theory and phenomenology of two-Higgs-doublet models. *Phys. Rept.*, 516:1–102, 2012.

[49] John F. Gunion and Howard E. Haber. The CP conserving two Higgs doublet model: The Approach to the decoupling limit. *Phys. Rev. D*, 67:075019, 2003.

[50] Shinya Kanemura, Koji Tsumura, Kei Yagyu, and Hiroshi Yokoya. Fingerprinting nonminimal Higgs sectors. *Phys. Rev. D*, 90:075001, 2014.

[51] J.F. Gunion, H.E. Haber, G.L. Kane, and S. Dawson. *The Higgs Hunter's Guide*. Addison-Wesley, 1990.

[52] G. Passarino and M. J. G. Veltman. One Loop Corrections for e+ e- Annihilation Into mu+ mu- in the Weinberg Model. *Nucl. Phys. B*, 160:151–207, 1979.

[53] Vernon D. Barger, King-man Cheung, A. Djouadi, Bernd A. Kniehl, and P. M. Zerwas. Higgs bosons: Intermediate mass range at e+ e- colliders. *Phys. Rev. D*, 49:79–90, 1994.

[54] Tao Han and Danny Marfatia. h —>mu tau at hadron colliders. *Phys. Rev. Lett.*, 86:1442–1445, 2001.

[55] Albert M Sirunyan et al. Search for additional neutral MSSM Higgs bosons in the $\tau\tau$ final state in proton-proton collisions at $\sqrt{s} = 13$ TeV. *JHEP*, 09:007, 2018.

[56] Georges Aad et al. Search for heavy Higgs bosons decaying into two tau leptons with the ATLAS detector using pp collisions at $\sqrt{s} = 13$ TeV. *Phys. Rev. Lett.*, 125(5):051801, 2020.

[57] D. J. Miller, S. Moretti, D. P. Roy, and W. James Stirling. Detecting heavy charged Higgs bosons at the CERN LHC with four b quark tags. *Phys. Rev. D*, 61:055011, 2000.

[58] Athanasios Dedes and Howard E. Haber. Can the Higgs sector contribute significantly to the muon anomalous magnetic moment? *JHEP*, 05:006, 2001.

[59] Stephen M. Barr and A. Zee. Electric Dipole Moment of the Electron and of the Neutron. *Phys. Rev. Lett.*, 65:21–24, 1990. [Erratum: Phys.Rev.Lett. 65, 2920 (1990)].

[60] Darwin Chang, We-Fu Chang, Chung-Hsien Chou, and Wai-Yee Keung. Large two loop contributions to g-2 from a generic pseudoscalar boson. *Phys. Rev. D*, 63:091301, 2001.

[61] Riccardo Barbieri, Lawrence J. Hall, and Vyacheslav S. Rychkov. Improved naturalness with a heavy Higgs: An Alternative road to LHC physics. *Phys. Rev. D*, 74:015007, 2006.

[62] G. Belanger, F. Boudjema, A. Pukhov, and A. Semenov. micromegas_3: A program for calculating dark matter observables. *Comput. Phys. Commun.*, 185:960–985, 2014.

[63] Rabindra N. Mohapatra and R. E. Marshak. Local B-L Symmetry of Electroweak Interactions, Majorana Neutrinos and Neutron Oscillations. *Phys. Rev. Lett.*, 44:1316–1319, 1980. [Erratum: Phys.Rev.Lett. 44, 1643 (1980)].

[64] Shaaban Khalil. Low scale $B - L$ extension of the Standard Model at the LHC. *J. Phys. G*, 35:055001, 2008.

[65] W. Emam and S. Khalil. Higgs and Z-prime phenomenology in B-L extension of the standard model at LHC. *Eur. Phys. J. C*, 52:625–633, 2007.

[66] Lorenzo Basso, Alexander Belyaev, Stefano Moretti, and Claire H. Shepherd-Themistocleous. Phenomenology of the minimal B-L extension of the Standard Model: Z' and neutrinos. *Phys. Rev. D*, 80:055030, 2009.

[67] S. Khalil and S. Moretti. Heavy neutrinos, Z' and Higgs bosons at the LHC: new particles from an old symmetry. *J. Mod. Phys*., 4(1):7–10, 2013.

[68] A. Leike. The Phenomenology of extra neutral gauge bosons. *Phys. Rept*., 317:143–250, 1999.

[69] J. A. Casas and A. Ibarra. Oscillating neutrinos and $\mu \to e\gamma$. *Nucl. Phys. B*, 618:171–204, 2001.

[70] M. Carena, A. Daleo, B. A. Dobrescu, and T. M. P. Tait. Z' gauge bosons at the Tevatron. *Phys. Rev. D*, 70:093009, 2004.

[71] Lorenzo Basso, Alexander Belyaev, Stefano Moretti, and Claire H. Shepherd-Themistocleous. Phenomenology of the minimal B-L extension of the Standard model: Z' and neutrinos. *Phys. Rev. D*, 80:055030, 2009.

[72] Shaaban Khalil and Stefano Moretti. Heavy neutrinos, Z' and Higgs bosons at the LHC: new particles from an old symmetry. *J. Mod. Phys*., 3:1302–1314, 2012.

[73] S. Khalil and A. Masiero. Radiative B-L symmetry breaking in supersymmetric models. *Phys. Lett. B*, 665:374–377, 2008.

[74] Jogesh C. Pati and Abdus Salam. Lepton Number as the Fourth Color. *Phys. Rev. D*, 10:275–289, 1974.

[75] Rabindra N. Mohapatra and Jogesh C. Pati. A Natural Left-Right Symmetry. *Phys. Rev. D*, 11:2558, 1975.

[76] N. G. Deshpande, J. F. Gunion, Boris Kayser, and Fredrick I. Olness. Left-right symmetric electroweak models with triplet Higgs. *Phys. Rev. D*, 44:837–858, 1991.

[77] P. S. Bhupal Dev, Rabindra N. Mohapatra, and Yongchao Zhang. Probing the higgs sector of the minimal left-right symmetric model at future hadron colliders. *Phys. Rev. D*, 93(11):115001, 2016.

[78] Paul Langacker. The physics of heavy z' gauge bosons. *Rev. Mod. Phys*., 81:1199–1228, 2009.

[79] P. Langacker and S. Uma Sankar. Bounds on the mass of w_r and the $w_l - w_r$ mixing angle ξ in general $su(2)_l \times su(2)_r \times u(1)$ models. *Phys. Rev. D*, 40:1569, 1989.

[80] Joydeep Chakrabortty, Partha Konar, and Tirtha Sankar Ray. Constraining a class of $b - l$ extended models from vacuum stability and perturbativity. *JHEP*, 08:008, 2012.

[81] M. Ashry and Shaaban Khalil. Phenomenological aspects of a tev-scale alternative left-right model. *Phys. Rev. D*, 91:015009, 2015.

[82] Shaaban Khalil, Hye-Sung Lee, and Ernest Ma. Generalized lepton number and dark left-right gauge model. *Phys. Rev. D*, 79:041701, 2009.

[83] Ernest Ma. Variants of the dark left-right gauge model: Neutrinos and scotinos. *Phys. Rev. D*, 79:117701, 2009.

[84] Ernest Ma and Utpal Sarkar. Radiative left-right dirac neutrino mass. *Phys. Rev. D*, 96:095017, 2017.

[85] K. Ezzat, M. Ashry, and S. Khalil. Search for a heavy neutral higgs boson in a left-right model with an inverse seesaw mechanism at the lhc. *Phys. Rev. D*, 104(1):015016, 2021.

[86] M. T. Arun, T. Mandal, S. Mitra, A. Mukherjee, L. Priya, and A. Sampath. Testing left-right symmetry with an inverse seesaw mechanism at the lhc. *Phys. Rev. D*, 105(11):115007, 2022.

[87] W. Abdallah, A. Awad, S. Khalil, and H. Okada. Muon Anomalous Magnetic Moment and mu -> e gamma in B-L Model with Inverse Seesaw. *Eur. Phys. J. C*, 72:2108, 2012.

[88] Ziro Maki, Masami Nakagawa, and Shoichi Sakata. Remarks on the unified model of elementary particles. *Prog. Theor. Phys.*, 28:870–880, 1962.

[89] M. Ashry, K. Ezzat, and S. Khalil. Muon g-2 anomaly in a left-right model with an inverse seesaw mechanism. *Phys. Rev. D*, 107(5):055044, 2023.

[90] P. Osland, A. A. Pankov, and I. A. Serenkova. Bounds on the mass and mixing of Z' and W' bosons decaying into different pairings of W, Z, or Higgs bosons using CMS data at the LHC. 6 2022.

[91] S. L. Glashow, J. Iliopoulos, and L. Maiani. Weak Interactions with Lepton-Hadron Symmetry. *Phys. Rev. D*, 2:1285–1292, 1970.

[92] S. Antusch, C. Biggio, E. Fernandez-Martinez, M. B. Gavela, and J. Lopez-Pavon. Unitarity of the Leptonic Mixing Matrix. *JHEP*, 10:084, 2006.

[93] Michal Malinsky, Tommy Ohlsson, Zhi-zhong Xing, and He Zhang. Non-unitary neutrino mixing and CP violation in the minimal inverse seesaw model. *Phys. Lett. B*, 679:242–248, 2009.

[94] K. Ezzat, M. Ashry, and S. Khalil. Search for a heavy neutral Higgs boson in a left-right model with an inverse seesaw mechanism at the LHC. *Phys. Rev. D*, 104(1):015016, 2021.

[95] Angela Papa. Towards a new generation of Charged Lepton Flavour Violation searches at the Paul Scherrer Institut: The MEG upgrade and the Mu3e experiment. *EPJ Web Conf.*, 234:01011, 2020.

[96] Howard Georgi and Sheldon L. Glashow. Unity of All Elementary Particle Forces. *Phys. Rev. Lett.*, 32:438–441, 1974.

[97] Richard Slansky. Group Theory for Unified Model Building. *Phys. Rept.*, 79:1–128, 1981.

[98] Paul Langacker. Grand Unified Theories and Proton Decay. *Phys. Rept.*, 72:185, 1981.

[99] Pran Nath and Pavel Fileviez Perez. Proton stability in grand unified theories, in strings and in branes. *Phys. Rept.*, 441:191–317, 2007.

[100] John R. Ellis, Mary K. Gaillard, and Dimitri V. Nanopoulos. Fermion Masses and Higgs Representations in SU(5). *Phys. Lett. B*, 88:320–324, 1979.

[101] Graham G. Ross. Grand Unified Theories. 1985.

[102] Howard Georgi and Cecilia Jarlskog. A New Lepton - Quark Mass Relation in a Unified Theory. *Phys. Lett. B*, 86:297–300, 1979.

[103] S. Raby. Grand unified theories. *Rept. Prog. Phys.*, 67:755–811, 2004.

[104] S. Dimopoulos and F. Wilczek. Incomplete multiplets in supersymmetric unified models. Preprint NSF-ITP-82-07 (unpublished).

[105] R. N. Mohapatra. *Unification and Supersymmetry: The Frontiers of Quark-Lepton Physics*. Springer, 3rd edition, 2003.

[106] Particle Data Group and R.L. et al. Workman. Review of Particle Physics. *Prog. Theor. Exp. Phys.*, 2022:083C01, 2022.

[107] K. Abe et al. (Super-Kamiokande Collaboration). Search for proton decay via $p \to e^+\pi^0$ and $p \to \mu^+\pi^0$ in 0.31 megaton·years exposure of the super-kamiokande water cherenkov detector. *Phys. Rev. D*, 95(1):012004, 2017.

[108] H. Murayama and A. Pierce. Not even decoupling can save minimal supersymmetric su(5). *Phys. Rev. D*, 65:055009, 2002.

[109] J. Hisano. Proton decay in grand unified theories. *Lect. Notes Phys.*, 939:483–508, 2017.

[110] P. Eckert, J. M. Gerard, H. Ruegg, and Thomas Schucker. Minimization of the SU(5) Invariant Scalar Potential for the Fortyfive-dimensional Representation. *Phys. Lett. B*, 125:385–388, 1983.

[111] Ilja Dorsner and Pavel Fileviez Perez. Unification versus proton decay in SU(5). *Phys. Lett. B*, 642:248–252, 2006.

[112] Pavel Fileviez Perez. Renormalizable adjoint SU(5). *Phys. Lett. B*, 654:189–193, 2007.

[113] K. Abe et al. Search for proton decay via $p \to k^+\nu$ using 260 kiloton·year data of super-kamiokande. *Phys. Rev. D*, 90(7):072005, 2014.

[114] S. Khalil and S. Salem. Enhancement of $H \to \gamma\gamma$ in $SU(5)$ model with $45H^1$ plet. *Nucl. Phys. B*, 876:473–492, 2013.

[115] S. Khalil, S. Salem, and M. Allam. SU(5) Octet Scalar at the LHC. *Phys. Rev. D*, 89:095011, 2014. [Erratum: Phys.Rev.D 91, 119908 (2015)].

[116] Toru Goto, Satoshi Mishima, and Tetsuo Shindou. Flavor physics in SU(5) GUT with scalar fields in the 45 representation. *Phys. Rev. D*, 108(9):095012, 2023.

[117] Julius Wess and Jonathan Bagger. *Supersymmetry and Supergravity*. Princeton University Press, 2nd edition, 1992.

[118] Stefano Moretti and Shaaban Khalil. *Supersymmetry Beyond Minimality: From Theory to Experiment*. CRC Press, 2019.

[119] S. Dimopoulos, S. Raby, and Frank Wilczek. Supersymmetry and the Scale of Unification. *Phys. Rev. D*, 24:1681–1683, 1981.

[120] Ugo Amaldi, Wim de Boer, and Hermann Furstenau. Comparison of grand unified theories with electroweak and strong coupling constants measured at LEP. *Phys. Lett. B*, 260:447–455, 1991.

[121] Paul Langacker and Nir Polonsky. Uncertainties in coupling constant unification. *Phys. Rev. D*, 47:4028–4045, 1993.

[122] Yu. A. Golfand and E. P. Likhtman. Extension of the Algebra of Poincare Group Generators and Violation of p Invariance. *JETP Lett.*, 13:323–326, 1971.

[123] J. Wess and B. Zumino. Supergauge Transformations in Four-Dimensions. *Nucl. Phys. B*, 70:39–50, 1974.

[124] Sidney R. Coleman and J. Mandula. All Possible Symmetries of the S Matrix. *Phys. Rev.*, 159:1251–1256, 1967.

[125] Steven Weinberg. *The Quantum Theory of Fields. Vol. 3: Supersymmetry*. Cambridge University Press, 2000.

[126] Stephen P. Martin. A supersymmetry primer. 1997. [*Adv. Ser. Direct. High Energy Phys*. 21 (2010) 1–153].

[127] L. Girardello and M. T. Grisaru. Soft breaking of supersymmetry. *Nucl. Phys. B*, 194:65–76, 1982.

[128] Steven Weinberg. Supersymmetry at Ordinary Energies. 1. Masses and Conservation Laws. *Phys. Rev. D*, 26:287, 1982.

[129] Yasuhiro Okada, Masahiro Yamaguchi, and Tsutomu T. Yanagida. Upper bound of the lightest higgs boson mass in the minimal supersymmetric standard model. *Prog. Theor. Phys.*, 85:1–6, 1991.

[130] John R. Ellis, Giovanni Ridolfi, and Fabio Zwirner. Radiative corrections to the masses of supersymmetric higgs bosons. *Phys. Lett. B*, 257:83–91, 1991.

[131] Howard E. Haber and Ralf Hempfling. Can the mass of the lightest higgs boson of the minimal supersymmetric model be larger than m_z? *Phys. Rev. Lett.*, 66:1815–1818, 1991.

[132] ATLAS Collaboration. Search for supersymmetry in final states with missing transverse momentum and multiple b-jets in proton–proton collisions at $\sqrt{s} = 13$ tev with the atlas detector. *JHEP*, 04:084, 2019.

[133] CMS Collaboration. Search for new physics in final states with jets and missing transverse momentum in proton-proton collisions at 13 tev. *JHEP*, 10:005, 2017.

[134] ATLAS and CMS Collaborations. Searches for supersymmetry at the high-luminosity lhc: a summary of current status and prospects. *Nature Phys.*, 18:1326–1337, 2022.

[135] ATLAS Collaboration. Search for squarks and gluinos in final states with jets and missing transverse momentum using 139 fb^{-1} of $\sqrt{s} = 13$ tev pp collision data with the atlas detector. *Phys. Rev. D*, 101(5):052005, 2020.

[136] Fabiola Gianotti et al. Supersymmetry prospects at the hl-lhc and he-lhc. *Eur. Phys. J. C*, 78:110, 2018.

[137] Th. Kaluza. Zum Unitätsproblem der Physik. *Sitzungsber. Preuss. Akad. Wiss. Berlin (Math. Phys.)*, 1921:966–972, 1921.

[138] Oskar Klein. Quantum Theory and Five-Dimensional Theory of Relativity. (In German and English). *Z. Phys.*, 37:895–906, 1926.

[139] Nima Arkani-Hamed, Savas Dimopoulos, and Gia Dvali. The Hierarchy Problem and New Dimensions at a Millimeter. *Phys. Lett. B*, 429:263–272, 1998.

[140] Lisa Randall and Raman Sundrum. A Large Mass Hierarchy from a Small Extra Dimension. *Phys. Rev. Lett.*, 83:3370–3373, 1999.

[141] Lisa Randall and Raman Sundrum. An Alternative to Compactification. *Phys. Rev. Lett.*, 83:4690–4693, 1999.

[142] Joseph Polchinski. *String Theory: Volume 1, An Introduction to the Bosonic String*. Cambridge University Press, 1998.

[143] Edward Witten. String theory and m-theory at strong coupling. *Nuclear Physics B*, 443:85–126, 1995.

[144] Shamit Kachru, Renata Kallosh, Andrei D. Linde, and Sandip P. Trivedi. De sitter vacua in string theory. *Physical Review D*, 68:046005, 2003.

[145] G. R. Dvali and G. Gabadadze. Gravity on a brane in anti-de sitter space. *Physical Review D*, 63:065007, 2001.

[146] J. M. Overduin and P. S. Wesson. Kaluza-klein gravity. *Phys. Rept.*, 283:303–378, 1997.

[147] T. Appelquist, A. Chodos, and P. G. O. Freund. Modern kaluza-klein theories. *Front. Phys.*, 65, 1987. Originally published in 1983 by Benjamin/Cummings.

[148] Ignatios Antoniadis, Nima Arkani-Hamed, Savas Dimopoulos, and Gia Dvali. New dimensions at a millimeter to a Fermi and superstrings at a TeV. *Phys. Lett. B*, 436:257–263, 1998.

[149] C. D. Hoyle, U. Schmidt, B. R. Heckel, E. G. Adelberger, J. H. Gundlach, D. J. Kapner, and H. E. Swanson. Submillimeter tests of the gravitational inverse square law: a search for large extra dimensions. *Phys. Rev. Lett.*, 86:1418–1421, 2001.

[150] Petr Horava and Edward Witten. Heterotic and Type I string dynamics from eleven dimensions. *Nucl. Phys. B*, 460:506–524, 1996.

[151] Walter D. Goldberger and Mark B. Wise. Modulus stabilization with bulk fields. *Phys. Rev. Lett.*, 83:4922–4925, 1999.

[152] Y. S. Myung, Gungwon Kang, and H. W. Lee. Randall-Sundrum gauge in the brane world. *Phys. Lett. B*, 478:294–298, 2000.

[153] X. Cid Vidal et al. Beyond the Standard Model Physics at the HL-LHC and HE-LHC. *CERN Yellow Rep. Monogr.*, 7:585–865, 2019.

[154] Daniel Abercrombie et al. Dark Matter Benchmark Models for Early LHC Run-2 Searches: Report of the ATLAS/CMS Dark Matter Forum.

[155] O. Buchmueller, S.A. Malik, A. Saavedra, A. Weiler, and T. Weiler. Simplified models for displaced dark matter signatures. *Phys. Lett. B*, 771:100–106, 2017.

[156] Nathaniel Craig, Hou Keong Lou, Matthew McCullough, and Jesse Thaler. The Higgs Portal Above Threshold. *JHEP*, 02:127, 2016.

[157] Jonathan L. Feng. Dark matter candidates from particle physics and methods of detection. *Annual Review of Astronomy and Astrophysics*, 48:495–545, 2010.

[158] ATLAS Collaboration. Summary of the searches for squarks and gluinos using $\sqrt{s} = 8$ tev pp collisions with the atlas experiment at the lhc. *JHEP*, 10:054, 2015.

[159] CMS Collaboration. Search for long-lived particles using nonprompt jets and missing transverse momentum with proton-proton collisions at $\sqrt{s} = 13$ tev. *Phys. Lett. B*, 797:134876, 2019.

[160] Search for squarks and gluinos with the ATLAS detector in final states with jets and missing transverse momentum and 20.3 fb^{-1} of $\sqrt{s} = 8$ TeV proton-proton collision data. 5 2013.

[161] Serguei Chatrchyan et al. Inclusive search for squarks and gluinos in pp collisions at $\sqrt{s} = 7$ TeV. *Phys. Rev. D*, 85:012004, 2012.

[162] Georges Aad et al. Observation of a new particle in the search for the Standard Model Higgs boson with the ATLAS detector at the LHC. *Phys. Lett. B*, 716:1–29, 2012.

[163] Serguei Chatrchyan et al. Search for Top-Squark Pair Production in the Single-Lepton Final State in pp Collisions at $\sqrt{s}$ = 8 TeV. *Eur. Phys. J. C*, 73(12):2677, 2013.

[164] Search for direct top squark pair production in final states with one isolated lepton, jets, and missing transverse momentum in $sqrts = 8$,TeV pp collisions using 21 fb^{-1} of ATLAS data. 3 2013.

[165] Search for direct top squark pair production and dark matter production in final states with two leptons in $\sqrt{s} = 13$ TeV pp collisions using 13.3 fb^{-1} of ATLAS data. 8 2016.

[166] Search for direct top squark pair production in the single lepton final state at $\sqrt{s}$= 13Tev. 2016.

[167] Search for electroweak production of charginos, neutralinos, and sleptons using leptonic final states in pp collisions at 8 TeV. 2013.

[168] Search for direct-slepton and direct-chargino production in final states with two opposite-sign leptons, missing transverse momentum and no jets in 20/fb of pp collisions at sqrt(s) = 8 TeV with the ATLAS detector. 5 2013.

[169] Search for electroweak SUSY production in multilepton final states in pp collisions at sqrt(s)=13 TeV with 12.9/fb. 2016.

[170] Morad Aaboud et al. Search for new high-mass phenomena in the dilepton final state using 36 fb^{-1} of proton-proton collision data at $\sqrt{s} = 13$ TeV with the ATLAS detector. *JHEP*, 10:182, 2017.

[171] Albert M Sirunyan et al. Search for high-mass resonances in dilepton final states in proton-proton collisions at $\sqrt{s} = 13$ TeV. *JHEP*, 06:120, 2018.

[172] Search for a narrow resonance in high-mass dilepton final states in proton-proton collisions using 140fb^{-1} of data at $\sqrt{s}$= 13Tev. 2019.

[173] Search for high-mass dilepton resonances using 139fb^{-1} of pp collision data collected at $\sqrt{s}$= 13Tev with the ATLAS detector. 2 2019.

[174] Vardan Khachatryan et al. Search for heavy gauge W' boson in events with an energetic lepton and large missing transverse momentum at $\sqrt{s} = 13$ TeV. *Phys. Lett. B*, 770:278–301, 2017.

[175] Abdelhak Djouadi. The Anatomy of electro-weak symmetry breaking. I: The Higgs boson in the standard model. *Phys. Rept.*, 457:1–216, 2008.

[176] Aram Hayrapetyan et al. Dark sector searches with the CMS experiment. *Phys. Rept.*, 1115:448–569, 2025.

[177] Georges Aad et al. Search for new phenomena in events with an energetic jet and missing transverse momentum in pp collisions at $\sqrt{s}$ =13 TeV with the ATLAS detector. *Phys. Rev. D*, 103(11):112006, 2021.

[178] LHCb Collaboration. Updated constraints on rare decays and flavor observables. *LHCb-PAPER-2022-XXX*, 2022. CERN preprint, in preparation.

[179] The MEG Collaboration. Search for the lepton flavour violating decay $\mu^+ \to e^+\gamma$ with the full dataset of the meg experiment. *Eur. Phys. J. C*, 76:434, 2016.

[180] Super-Kamiokande Collaboration. Evidence for oscillation of atmospheric neutrinos. *Phys. Rev. Lett.*, 81:1562–1567, 1998.

[181] Gino Isidori, Yosef Nir, and Gilad Perez. Flavor physics constraints for physics beyond the standard model. *Ann. Rev. Nucl. Part. Sci.*, 60:355–389, 2010.

[182] Ferruccio Feruglio. Pieces of the flavor puzzle. *Eur. Phys. J. C*, 75:373, 2015.

[183] Guido Altarelli and Ferruccio Feruglio. Discrete flavor symmetries and models of neutrino mixing. *Rev. Mod. Phys.*, 82:2701–2729, 2010.

[184] Hiroshi Ishimori, Tatsuo Kobayashi, Hiroshi Ohki, Yusuke Shimizu, and Morimitsu Tanimoto. Non-abelian discrete symmetries in particle physics. *Prog. Theor. Phys. Suppl.*, 183:1–163, 2010.

[185] Stephen F. King and Christoph Luhn. Neutrino mass and mixing with discrete symmetry. *Rept. Prog. Phys.*, 76:056201, 2013.

[186] Guido Altarelli and Ferruccio Feruglio. Tri-bimaximal neutrino mixing from discrete symmetry in extra dimensions. *Nucl. Phys. B*, 720:64–88, 2005.

[187] C. D. Froggatt and H. B. Nielsen. Hierarchy of Quark Masses, Cabibbo Angles and CP Violation. *Nucl. Phys. B*, 147:277, 1979.

[188] M. Leurer, Y. Nir, and N. Seiberg. Mass matrix models: The sequel. *Nucl. Phys. B*, 420:468–504, 1994.

[189] A. Crivellin, C. Greub, and A. Kokulu. Explaining $B \to D\tau\nu$, $B \to D^*\tau\nu$ and $B \to \tau\nu$ in a 2HDM of type III. *Phys. Rev. D*, 86:054014, 2012.

[190] A. J. Buras and D. Guetta. The standard model and beyond: Implications for cp violation. *Phys. Lett. B*, 688(1):55–64, 2010.

[191] Martin Jung, Antonio Pich, and Paula Tuzon. Charged-Higgs phenomenology in the Aligned two-Higgs-doublet model. *JHEP*, 11:003, 2010.

[192] S. Inoue, M. J. Ramsey-Musolf, and Y. Zhang. CP-violating phenomenology of flavor conserving two Higgs doublet models. *Phys. Rev. D*, 89:115023, 2014.

[193] R. N. Mohapatra and J. C. Pati. A gauge theory of grand unification of electromagnetic, weak and strong interactions. *Phys. Rev. D*, 10(5):1507–1514, 1974.

[194] Goran Senjanović and Vladimir Tello. Right Handed Quark Mixing in Left-Right Symmetric Theory. *Phys. Rev. Lett.*, 114(7):071801, 2015.

[195] Ilja Dorsner and Pavel Fileviez Perez. Unification without supersymmetry: Neutrino mass, proton decay and light leptoquarks. *Nucl. Phys. B*, 723:53–76, 2005.

[196] A. Ismael and S. Khalil. Resolving R_D and R_{D^*} anomalies in adjoint SU(5). *JHEP*, 11:143, 2023.

[197] Minoru Tanaka and Ryoutaro Watanabe. New physics in the weak interaction of $b^- \to d^{(*)}\tau\nu^-$. *Phys. Rev. D*, 87(3):034028, 2013.

[198] Syuhei Iguro, Teppei Kitahara, Yuji Omura, Ryoutaro Watanabe, and Kei Yamamoto. d^* polarization vs. $r_D^{(*)}$ anomalies in the leptoquark models. *JHEP*, 02:194, 2019.

[199] Edward W. Kolb and Michael S. Turner. *The Early Universe*, volume 69. Taylor and Francis, 5 2019.

[200] Julien Lesgourgues and Sergio Pastor. Massive neutrinos and cosmology. *Phys. Rept.*, 429:307–379, 2006.

[201] Adam G. Riess et al. Observational evidence from supernovae for an accelerating universe and a cosmological constant. *Astron. J.*, 116:1009–1038, 1998.

[202] S. Perlmutter et al. Measurements of Ω and Λ from 42 High Redshift Supernovae. *Astrophys. J.*, 517:565–586, 1999.

[203] Steven Weinberg. The Cosmological Constant Problem. *Rev. Mod. Phys.*, 61:1–23, 1989.

[204] Jerome Martin. Everything You Always Wanted To Know About The Cosmological Constant Problem (But Were Afraid To Ask). *Comptes Rendus Physique*, 13:566–665, 2012.

[205] R. R. Caldwell, Rahul Dave, and Paul J. Steinhardt. Cosmological imprint of an energy component with general equation of state. *Phys. Rev. Lett.*, 80:1582–1585, 1998.

[206] Tim Clifton, Pedro G. Ferreira, Antonio Padilla, and Constantinos Skordis. Modified gravity and cosmology. *Physics Reports*, 513(1):1–189, 2012.

[207] Andrew G. Cohen, D. B. Kaplan, and A. E. Nelson. Progress in electroweak baryogenesis. *Ann. Rev. Nucl. Part. Sci.*, 43:27–70, 1993.

[208] Masanori Fukugita and Tsutomu Yanagida. Baryogenesis without grand unification. *Physical Letters B*, 174(1):45–47, 1986.

[209] W. Buchmüller, P. Di Bari, and M. Plumacher. Leptogenesis for pedestrians. *Annals of Physics*, 315(1):305–351, 2005.

[210] David E. Morrissey and Michael J. Ramsey-Musolf. Electroweak baryogenesis. *New J. Phys.*, 14:125003, 2012.

[211] Fritz Zwicky. Die rotverschiebung von extragalaktischen nebeln. *Helvetica Physica Acta*, 6:110–127, 1933.

[212] Vera C. Rubin and W. Kent Ford, Jr. Rotation of the Andromeda Nebula from a Spectroscopic Survey of Emission Regions. *Astrophys. J.*, 159:379–403, 1970.

[213] Mordehai Milgrom. A modification of the newtonian dynamics as a possible alternative to the hidden mass hypothesis. *The Astrophysical Journal*, 270:365–370, 1983.

[214] Masataka Fukugita and P. James E. Peebles. The Cosmic energy inventory. *Astrophys. J.*, 616:643–668, 2004.

[215] Giovanni Bertone, Dan Hooper, and Joao Silk. Particle dark matter: Evidence, candidates, and constraints. *Physics Reports*, 405(5):279–390, 2005.

[216] Keith A. Olive and P. Shaver. Big bang nucleosynthesis and the problem of dark matter. *Review of Modern Physics*, 86(4):1063–1099, 2014.

[217] Jonathan L. Feng. Dark matter candidates from particle physics and methods of detection. *Annual Review of Astronomy and Astrophysics*, 48:495–545, 2010.

[218] Mark Kamionkowski Gary Jungman and Kent A. Olive. Supersymmetric dark matter. *Physics Reports*, 267(5):195–373, 1996.

[219] Michael B. Wise John Preskill and Frank Wilczek. Cosmology of the axion. *Physical Review Letters*, 51:1231–1234, 1983.

[220] Scott D. H. Dodelson Peter Bode and Alex Kehayias. Warm dark matter. *Astrophysical Journal*, 556:93–105, 2001.

[221] Kevork Abazajian, George M. Fuller, and Mitesh Patel. Sterile neutrino hot, warm, and cold dark matter. *Phys. Rev. D*, 64:023501, 2001.

[222] Scott Dodelson and Lawrence M. Widrow. Sterile neutrinos as dark matter. *Phys. Rev. Lett.*, 72:17–20, 1994.

[223] M. Aaboud et al. Search for supersymmetry with the atlas detector at the lhc. *Nature*, 563:345–348, 2018.

[224] A. N. Taylor et al. Gravitational lens magnification and the mass of abell 1689. *The Astrophysical Journal*, 501(2):539–553, 1998.

[225] B. W. Lee and Steven Weinberg. Cosmological Lower Bound on Heavy-Neutrino Masses. *Phys. Rev. Lett.*, 39:165–168, 1977.

[226] J. Edsjö and P. Gondolo. Neutralino relic density including co-annihilations. *Physics Review D*, 56:1879–1894, 1997.

[227] Jalal Abdallah et al. Simplified models for dark matter searches at the lhc. *Physics of the Dark Universe*, 9-10:8–23, 2015.

[228] Kim Griest and David Seckel. Three exceptions in the calculation of relic abundances. *Phys. Rev. D*, 43:3191–3203, 1991.

[229] P. A. R. Ade and others [Planck Collaboration]. Planck 2013 results. xvi. cosmological parameters. *Astronomy & Astrophysics*, 571:A16, 2014.

[230] S. Chakraborti, A. Ray, N. Chandra, S. S. S. V. Cheela, and R. S. Barniol Duran. Radio detection of a type ia supernova: Implications for the single degenerate scenario. *Astrophysical Journal*, 805:187, 2015.

[231] Gary Steigman. Primordial Nucleosynthesis in the Precision Cosmology Era. *Ann. Rev. Nucl. Part. Sci.*, 57:463–491, 2007.

[232] V. A. Kuzmin, V. A. Rubakov, and M. E. Shaposhnikov. On the Anomalous Electroweak Baryon Number Nonconservation in the Early Universe. *Phys. Lett. B*, 155:36, 1985.

[233] Apostolos Pilaftsis. Resonant cp violation induced by particle mixing in transition amplitudes. *Nucl. Phys. B*, 504:61–107, 1997.

[234] Alan H. Guth. Inflationary universe: A possible solution to the horizon and flatness problems. *Phys. Rev. D*, 23:347–356, 1981.

[235] A. A. Starobinsky. A new type of isotropic cosmological models without singularity. *Phys. Lett. B*, 91:99–102, 1980.

[236] Albert Einstein. The foundation of the general theory of relativity. *Annalen der Physik*, 49:769–822, 1916.

[237] A. Friedmann. Über die krümmung des raumes. *Zeitschrift für Physik*, 10:377–386, 1922.

[238] A. Friedmann. Über die möglichkeit einer welt mit konstanter negativer krümmung des raumes. *Zeitschrift für Physik*, 21:326–332, 1924.

[239] R. H. Dicke and P. J. E. Peebles. The big bang cosmology and the microwave background. *The Astrophysical Journal*, 192:E1–E5, 1979.

[240] P. J. E. Peebles. *Principles of Physical Cosmology*. Princeton University Press, Princeton, NJ, 1993.

[241] A. D. Linde. Chaotic inflation. *Physics Letters B*, 129:177–181, 1983.

[242] A. Albrecht and P. J. Steinhardt. Cosmology for grand unified theories with radiatively induced symmetry breaking. *Physical Review Letters*, 48:1220–1223, 1982.

[243] David H. Lyth and Antonio Riotto. Particle physics models of inflation and the cosmological density perturbation. *Physics Reports*, 314:1–146, 1999.

[244] Viatcheslav F. Mukhanov, H. A. Feldman, and Robert H. Brandenberger. Theory of cosmological perturbations. part 1. classical perturbations. part 2. quantum theory of perturbations. part 3. extensions. *Physics Reports*, 215:203–333, 1992.

[245] S. R. Coleman and E. J. Weinberg. Radiative corrections as the origin of spontaneous symmetry breaking. *Physical Review D*, 7:1888–1910, 1973.

[246] A. R. Liddle and D. H. Lyth. The cold dark matter density perturbation. *Physics Reports*, 231:1–105, 1993.

[247] Paul J. Steinhardt and Michael S. Turner. A prescription for successful new inflation. *Phys. Rev. D*, 29:2162, 1984.

[248] A. G. Riess et al. Observational evidence from supernovae for an accelerating universe and a cosmological constant. *The Astronomical Journal*, 116:1009–1038, 1998.

[249] S. Perlmutter et al. Discovery of a supernova explosion at half the age of the universe. *Nature*, 391:51–54, 1998.

[250] B. Ratra. Cosmological implications of a rolling scalar field. *Physical Review D*, 35:232–235, 1987.

[251] Ivaylo Zlatev, Li-Min Wang, and Paul J. Steinhardt. Quintessence, cosmic coincidence, and the cosmological constant. *Phys. Rev. Lett.*, 82:896–899, 1999.

[252] R. R. Caldwell, Romesh Dave, and Paul J. Steinhardt. Cosmological Imprint of an Energy Component with Generalized Equation of State. *Phys. Rev. Lett.*, 80:1582–1585, 2002.

[253] Galaxies Cosmology. History of the universe, 2015. Accessed: 2025-04-07.

[254] R. R. Caldwell, R. Dave, and P.J. Steinhardt. Cosmological imprint of an energy component with general equation of state. *Physical Review Letters*, 80:1582–1585, 2002.

[255] I. Zlatev, L. Wang, and P.J. Steinhardt. Quintessence, cosmic coincidence, and the cosmological constant. *Physical Review Letters*, 82:896–899, 1999.

[256] P.J. Steinhardt, L. Wang, and I. Zlatev. Cosmological consequences of a rolling homogeneous scalar field. *Physics Letters B*, 459:1–10, 1999.

[257] S. Capozziello et al. Curvature quintessence from modified gravity. *International Journal of Modern Physics D*, 12(6):1073–1088, 2003.

[258] S. Nojiri and S. D. Odintsov. Modified gravity with the help of the scalar field and the fate of the universe. *Phys. Lett. B*, 639:144–152, 2006.

[259] A. A. Starobinsky. Disappearing cosmological constant in f(R) gravity. *J. Exp. Theor. Phys. Lett.*, 86:157–163, 2007.

Index